

DEPARTAMENT DE QUIMICA ANALITICA

NEW INSTRUMENTAL AND CHEMOMETRIC
DEVELOPMENTS FOR THE ON-LINE HYPHENATION OF
LIQUID CHROMATOGRAPHY AND INFRARED
SPECTROSCOPY.

JULIA KULIGOWSKI

UNIVERSITAT DE VALÈNCIA
Servei de Publicacions
2011

Aquesta Tesi Doctoral va ser presentada a València el dia 14 de desembre de 2011 davant un tribunal format per:

- Dra. María José Ayora Cañada
- Dr. Egon Erwin Rosenberg
- Dr. Boris Mizaikoff
- Dr. Bartolomé Simonet Suau
- Dra. Yolanda Pico García

Va ser dirigida per:

Dr. Miguel de la Guardia Cirugeda

Dr. Guillermo Quintás Soriano

©Copyright: Servei de Publicacions
Julia Kuligowski

I.S.B.N.: 978-84-370-8816-7

Edita: Universitat de València

Servei de Publicacions

C/ Arts Gràfiques, 13 baix

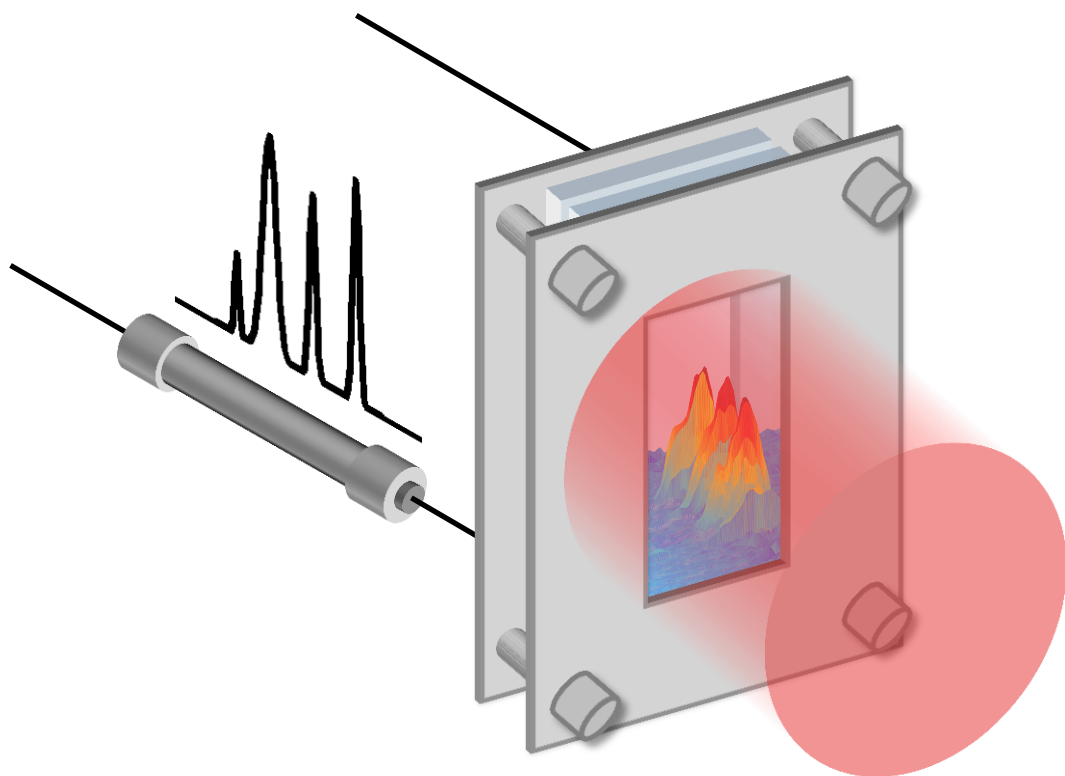
46010 València

Spain

Telèfon:(0034)963864115

New Instrumental and Chemometric Developments for the on-line Hyphenation of Liquid Chromatography and Infrared Spectroscopy

Julia Kuligowski



PhD Thesis
Department of Analytical Chemistry
University of Valencia
Valencia - 2011

VNIVERSITAT
DE VALÈNCIA

PhD Thesis

New Instrumental and Chemometric Developments for the on-line Hyphenation of Liquid Chromatography and Infrared Spectroscopy

Julia Kuligowski

Supervisors:

Prof. Dr. Miguel de la Guardia Cirugeda

Dr. Guillermo R. Quintás Soriano

PhD Program: 560 310E - Técnicas Experimentales en Química

Department of Analytical Chemistry

University of Valencia

Valencia - 2011

LOS DIRECTORES DE TESIS

el **Dr. Guillermo R. Quintás Soriano** y el **Dr. Miguel de la Guardia Cirugeda**

CERTIFICAN QUE

Julia Kuligowski ha realizado el trabajo sobre “New Instrumental and Chemometric Developments for the on-line Hyphenation of Liquid Chromatography and Infrared Spectroscopy”, bajo su dirección y autorizan su presentación para optar al Grado de Doctor en Química.

Burjassot, octubre del 2011

Miguel de la Guardia Cirugeda

Guillermo R. Quintás Soriano

Acknowledgements

Am Ende eines jeden Projektes hat man es sich verdient, sich für einen Moment zurückzulehnen und es zu genießen, auf die getane Arbeit zurück zu schauen. Über die letzten vier Jahre hinweg habe ich viele interessante Erfahrungen gemacht und viel Neues kennen gelernt. All das hat zum Gelingen dieser Arbeit beigetragen und deswegen möchte ich mich an dieser Stelle bedanken....

....bei meinen Betreuern Guillermo Quintás Soriano und Miguel de la Guardia für die tatkräftige Unterstützung, Hilfe und Motivation.

....bei Guillermo Quintás Alonso für seine Hilfe bei der Bewältigung (und Bezwingung) des universitären Papierkriegs.

....bei meinen Arbeitskollegen an der Universidad de Valencia. Mein Dank geht insbesondere an David Pérez, Luis Juan, Dani San Juan, Yelko Rodriguez und Manuela Ruiz die sowohl für einen konstanten Ideenaustausch in diversen Kaffeepausen als auch für die notwendige Ablenkung gesorgt haben.

....bei Bernhard Lendl und der gesamten Arbeitsgruppe CAVS and der TU Wien bei denen ich mich bei meinen diversen Kurzaufenthalten aufgrund des guten Arbeitsklimas immer herzlichst willkommen gefühlt habe. In dieser Zeit ist ein wesentlicher Teil dieser Dissertation entstanden und auch außerhalb der Aufenthalte hat die Zusammenarbeit trotz der großen geographischen Distanz immer gut funktioniert.

....bei Peter Schoenmakers und der restlichen Arbeitsgruppe an der Universiteit van Amsterdam bei denen ich ebenfalls für einen Kurzaufenthalt Unterschlupf gefunden habe, um mein Wissen auf dem Gebiet der Flüssigchromatographie zu vervollständigen.

....bei sämtlichen Co-Autoren und helfenden Händchen:

bei Salvador Garrigues und Bernhard Lendl für ihr Mitwirken in zahlreichen Publikationen

bei Romà Tauler für seine Hilfe und die praktischen Tipps bei der Anwendung von MCR auf LC-IR Datensätze

bei David Carrión für die Aufarbeitung unendlich vieler Proben

bei Javier Moros, Paco Esteve-Turrillas und Aaron Breivogel für die Zusammenarbeit in der Anfangsphase meiner Dissertation

bei Wolfgang Tomischko, Wolfgang Ritter und Bernhard Zachhuber für die Hilfe mit dem dual-QC-laser set-up und dem daraus entstandenen Poster

bei Ralph Marbach für die hilfreichen Kommentare bezüglich der Anwendung der SBC Methode

bei Erwin Rosenberg für die Idee, LC-IR für die Analyse von Nitrophenolen zu verwenden

bei Christoph Herwig für die Bereitstellung der Hefe Proben und die Unterstützung im Zusammenhang mit dem daraus entstehenden Paper

bei Mercedes Cascant für die gute Zusammenarbeit

bei Alison Hobro für die gute Zusammenarbeit bei der Analyse verschiedenster biologischer Proben und ihrer Hilfe bei der Perfektionierung des Englisch in einigen Publikationen

bei Eva Aguilera Herrador für viel positives Denken bei unseren gemeinsamen LC-IR Experimenten

bei Christoph Wagner und Markus Brandstetter, die immer für einen hilfreichen Kommentar oder auch ein kühles Bier zu haben waren

bei Wim Th. Kok, Hans-Gerd Janssen, Filippo Bedani und Eva Reingruber für die gute Zusammenarbeit in Amsterdam

bei Berber van der Veen für die nette Aufnahme in die WG in Amsterdam

bei María Martínez Galera, María Dolores Gil García, María J. Culzoni und Héctor C. Goicoechea die mir ihre Daten zur Verfügung gestellt haben

....bei all meinen Freunde, meiner Familie und besonders meinen Eltern, ohne die ich nicht so wäre wie ich bin.

....bei Guillermo, der meine Arbeit mit so viel Einsatz unterstützt hat, als wäre es seine eigene. Danke für die viele Hilfe, die viele Motivation und die Geduld, die mir des öfteren gefehlt hätte.

Am Ende möchte ich mich außerdem noch sowohl für die finanzielle Unterstützung des Ministerio de Educación y Ciencia (Projekte CTQ205-05604, CTQ2008-05719, FEDER, AGL2007-64567 und CTQ2008-05719/BQU), der Direcció General d'Investigació i Transferència Tecnològica de la Generalitat Valenciana (Projekt ACOMP/2007/131), der Conselleria d'Educació de la Generalitat Valenciana (Projekt PROMETEO 2010-055) und der Generalitat Valenciana (Projekt GVA-PRE-2008-301) im Rahmen diverser Projekte als auch bei der Universidad de Valencia für mein Stipendium ("V Segles") bedanken, die es mir ermöglicht haben dieses Projekt zu verwirklichen.

*Zu pflanzen einen schönen Baum
braucht's eine halbe Stunde kaum.
Zu wachsen, bis man ihn bewundert,
braucht er - bedenk' es - ein Jahrhundert.*

Eugen Roth

Resumen

1. Introducción

La cromatografía líquida (*liquid chromatography*, LC) es una de las técnicas de separación más empleadas en la actualidad. El campo de aplicaciones de la LC abarca desde el análisis industrial hasta el bioquímico. Por otra parte, la espectrometría infrarroja (IR) es una técnica de detección no destructiva, que proporciona información molecular específica de un gran número de analitos, desde pequeños iones a macromoléculas como las proteínas y que puede ser utilizada tanto para el análisis cualitativo como cuantitativo.

El acoplamiento efectivo entre la LC y la espectrometría IR (LC-IR) presenta una serie de importantes ventajas que justifican el interés que existe en su desarrollo. Por un lado, la alta resolución que proporciona la LC aumenta la aplicabilidad y la exactitud de los procedimientos basados en el empleo de la espectrometría IR, al reducir el número de posibles interferentes y, por otro lado, la detección IR puede ser una alternativa al uso de detectores utilizados actualmente, como el *evaporative light scattering detector* (ELSD) o el *refractive index detector* (RID) que proporcionan baja o ninguna información estructural sobre los analitos.

Sin embargo, el acoplamiento LC-IR tiene dos importantes limitaciones derivadas de la intensa absorción que presentan los eluyentes utilizados como componentes de las fases móviles, como se muestra en la Figura R-1. Este efecto, especialmente relevante en el caso de la cromatografía en fase reversa, limita la sensibilidad del acoplamiento *on-line* LC-IR al requerir el empleo de pasos ópticos reducidos para garantizar una transparencia adecuada del disolvente en el infrarrojo medio y, por otro lado, dificulta la extracción exacta de la señal del analito en el caso de separaciones en régimen de gradiente.

Existen dos formas de acoplamiento LC-IR: i) el acoplamiento fuera de línea (*off-line*) y ii) en línea (*on-line*). El primero supone el empleo de un interfaz para la eliminación física del disolvente antes de registrar la señal de los analitos depositados sobre una ventana transparente a la radiación IR (p.ej. CaF_2 , BaF_2 , ZnSe o Ge). La eliminación del disolvente antes de la medida IR ha sido el tipo de acoplamiento más utilizado hasta

ahora por su mejor sensibilidad y el acceso al espectro completo de los analitos en ausencia de absorción IR debida a los componentes de la fase móvil.

No obstante, las principales desventajas de este tipo de acoplamiento son: menor resolución cromatográfica; mayor tiempo de análisis debido a la obtención de las medidas posteriormente a la separación; posible pérdida de analitos volátiles durante la etapa de eliminación del disolvente, así como otras dificultades derivadas del uso de fases móviles no volátiles y del mantenimiento del interfaz.

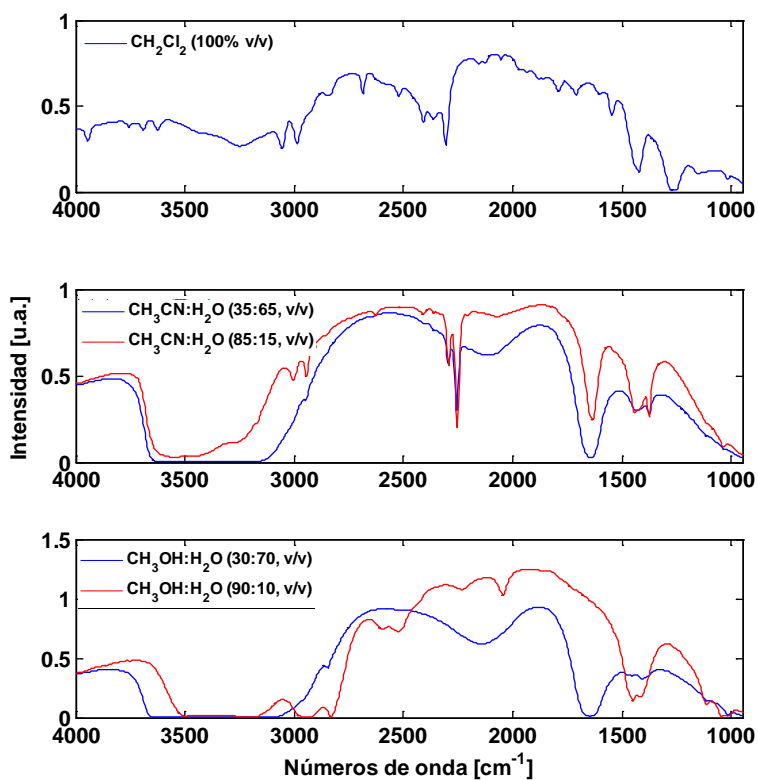


Figure R-1. Señales adquiridas en modo *single channel* de diferentes disolventes, obtenidas utilizando una celda de flujo con ventanas de selenuro de zinc y fluoruro de calcio y un paso óptico de 150 μm para el diclorometano y de 16.5 μm para mezclas de acetonitrilo:agua y metanol:agua.

El acoplamiento *on-line* es técnicamente una opción más sencilla ya que utiliza celdas de flujo para la medida en tiempo real de la señal cromatográfica. Utilizando celdas de flujo, la adquisición de la señal se puede llevar a cabo en modo transmisión, reflectancia o reflectancia total atenuada (*Attenuated Total Reflectance*, ATR). El intervalo espectral que se puede utilizar para la detección de los analitos depende, principalmente, de la absorción de los materiales ópticos del sistema IR y de la absorbancia de la fase móvil.

El acoplamiento *on-line* presenta una serie de ventajas como son una mejor resolución cromatográfica, bajo coste, la posibilidad de utilizar fases móviles no volátiles y tamponadas, un fácil desarrollo de aplicaciones cuantitativas, menor mantenimiento y permite la medida de los espectros IR de los analitos sin efectos de cristalización, degradación u oxidación que pueden producirse cuando se utilizan interfaces para la eliminación del disolvente. Las dos principales desventajas del acoplamiento *on-line* en LC-IR son: i) una baja sensibilidad y ii) la intensa absorbancia de la fase móvil.

Los avances en los últimos años en el desarrollo de láseres de cascada cuántica (*quantum cascade-laser*, QC-laser), tanto respecto a la intensidad de la luz emitida como a las regiones accesibles del espectro infrarrojo medio, hacen que la sustitución de fuentes de tipo *global* de uso general en sistemas IR, por QC-láseres sea una opción prometedora para la mejora de los niveles de sensibilidad. Una estrategia adicional para la mejora de la sensibilidad de sistemas *on-line* LC-IR se basa en el empleo de sistemas de separación y detección miniaturizados. La dispersión radial causa la distribución del analito después de su inyección en la columna cromatográfica. Reduciendo el diámetro interno (*inner diameter*, ID) de la columna, la dispersión disminuye permitiendo una mejora de la sensibilidad de la detección en una relación inversamente proporcional al cuadrado del ID, manteniendo el mismo volumen de inyección. Sin embargo, el uso de columnas con un ID reducido requiere el desarrollo de sistemas de detección adaptados con celdas de flujo de muy bajo volumen.

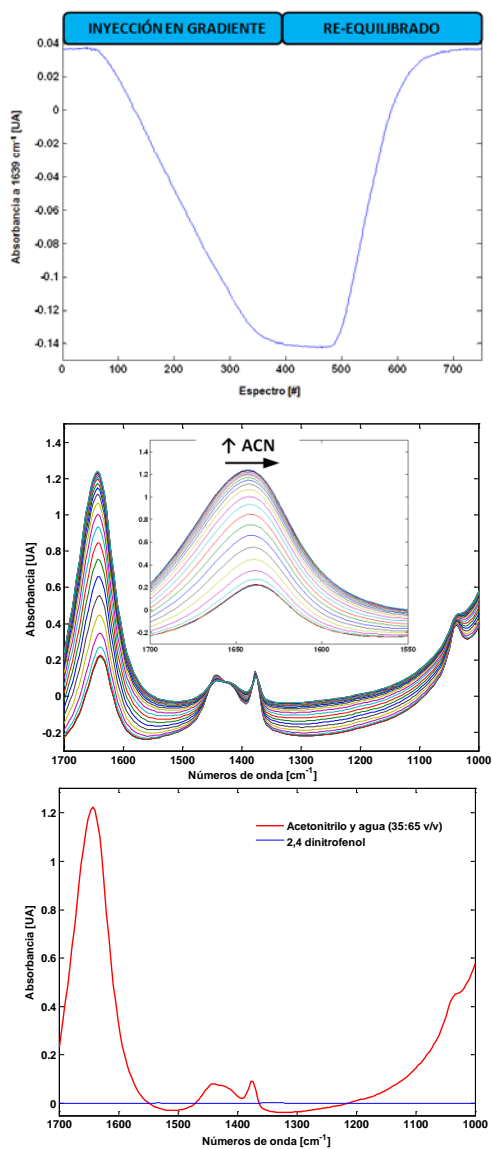


Figure R-2. arriba: Cambios en la absorbancia a 1639 cm^{-1} observados durante un gradiente acetronitrilo:agua del 35 al 85% de acetronitrilo y el re-equilibrado del sistema; en medio: espectros adquiridos durante un gradiente de acetronitrilo:agua del 35 al 85% de acetronitrilo; abajo: espectro de una disolución de acetronitrilo:agua 35:65 v/v y espectro de una disolución de 2,4-dinitrofenol (1.5 mg mL^{-1}) medidos ambos utilizando una celda de flujo con un paso óptico de $10\text{ }\mu\text{m}$.

La corrección de la señal debida a la absorción de la fase móvil (*background absorption*) en régimen isocrático se realiza mediante la resta del espectro de la fase móvil registrado al inicio del cromatograma o antes de la elución de los analitos. No obstante, este sencillo procedimiento presenta dos importantes limitaciones: i) la intensa absorción de la fase móvil provoca que ligeros cambios de la composición del eluyente puedan modificar sensiblemente la señal de fondo, afectando a la exactitud de la corrección incluso en régimen isocrático, y ii) no es aplicable en régimen de gradiente. El cambio de composición de la fase móvil durante un gradiente provoca que la absorción debida a la fase móvil cambie de forma muy intensa. Los cambios en la absorción de la fase móvil pueden llegar a ser varios órdenes superiores a los debidos a la elución de los analitos; por lo que para poder recuperar el espectro de los analitos se requiere una corrección quimiométrica muy exacta de la señal de fondo. Ambos efectos se ilustran en la Figura R-2. La falta de métodos quimiométricos capaces de corregir con exactitud los cambios en la absorción de los distintos componentes de la fase móvil durante una separación en régimen de gradiente ha limitado el uso del acoplamiento *on-line* LC-IR a separaciones en régimen isocrático.

Con estos precedentes, el objetivo de esta Tesis ha sido el desarrollo de herramientas instrumentales y quimiométricas que proporcionen una mejora en los niveles de sensibilidad y aplicabilidad del acoplamiento *on-line* LC-IR, con el fin de demostrar la capacidad de la espectrometría IR como herramienta alternativa o complementaria a otros sistemas de detección como ELSD o RID, entre otros. Para ello, en esta tesis se ha evaluado el uso de QC-láseres para sustituir fuentes de IR convencionales y celdas de flujo miniaturizadas en combinación con sistemas LC capilar. Adicionalmente se ha desarrollado un conjunto de métodos quimiométricos, tanto univariantes como multivariantes, dirigidos a la eliminación de la contribución espectral de la fase móvil en sistemas cromatográficos LC-IR.

Esta Tesis se divide en tres partes:

- 1.- Mejoras en el campo de las aplicaciones isocráticas (Capítulo 2)
- 2.- Desarrollo y aplicación de métodos quimiométricos para la corrección de la absorción debida a la fase móvil (*background correction*) aplicables tanto en régimen isocrático como en gradiente, y para el aumento de la sensibilidad y selectividad de la señal en *on-line* LC-IR (Capítulos 3 a 6).

3.- Desarrollo de mejoras instrumentales dirigidas a una mejora significativa de los niveles de sensibilidad del acoplamiento *on-line* LC-IR (Capítulo 7).

Con el fin de mostrar la aplicabilidad de los métodos quimiométricos y mejoras instrumentales propuestos en esta Tesis, éstos se emplearon en el desarrollo de aplicaciones en diversos campos incluyendo el análisis de polímeros y productos cosméticos y alimentarios.

2. Desarrollo de aplicaciones basadas en el empleo de *on-line* GPC-IR y LC-IR en régimen isocrático

*2.1 Análisis cualitativo y cuantitativo de suplementos alimenticios mediante *on-line* GPC-ATR-IR: determinación del contenido total en lecitina y aceite de soja*

Se ha propuesto el empleo de un sistema *on-line* GPC-ATR-FTIR para la cuantificación del contenido total de fosfolípidos y aceite de soja en suplementos dietéticos. La resolución cromatográfica obtenida entre los dos grupos de analitos, combinada con el uso de la primera derivada (*first derivative*, FD) de los espectros FTIR medidos durante la elución de los analitos, proporcionó un aumento significativo de la selectividad de la medida.

El sistema experimental estaba compuesto por un sistema GPC equipado con dos columnas Envirolgel (19×150 mm, 19×300 mm) y una celda de flujo de ATR acoplada *on-line*. Se utilizó diclorometano como fase móvil. La corrección de la señal debida al disolvente se realizó mediante la sustracción de un espectro de referencia medido al inicio de cada cromatograma.

El uso de espectros FD, calculados empleando el algoritmo de Savitzky-Golay, permitió reducir el grado de solapamiento espectral entre analitos y corregir variaciones en la línea base. Sin embargo, los espectros de los fosfolípidos y del aceite de soja presentes en las muestras analizadas siguieron presentando un alto grado de solapamiento. Debido a esto, y a que la resolución cromatográfica no era completa, se propuso un método simple para la selección de las condiciones óptimas para la extracción de cromatogramas específicos que permitiera maximizar la sensibilidad, minimizando al mismo tiempo la interferencia entre los analitos.

El método se basa en el cálculo de un factor (F_i) definido como:

$$F_i = |A_{i,analito} - A_{i,interferente}| \cdot \left| \frac{A_{i,analito}}{A_{i,interferente}} \right| \quad (\text{Ecuación R-1})$$

El valor de F_i depende de la altura del pico del analito y del grado de solapamiento con el interferente, siendo $A_{i,analito}$ y $A_{i,interferente}$ las intensidades de los picos cromatográficos del analito de interés y del interferente medidas en los cromatogramas extraídos utilizando cada número de onda (i) en los espectros FD.

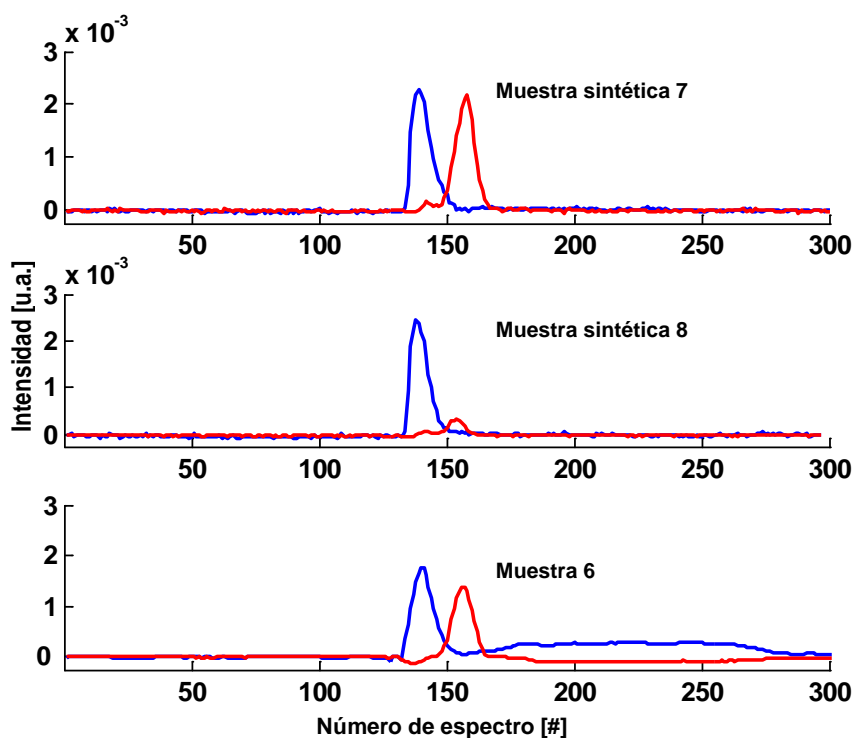


Figure R-3. Cromatogramas *on-line* GPC-ATR-(FD)-FTIR de muestras sintéticas y reales extraídos empleando las condiciones seleccionadas (1034 cm^{-1} y 1138 cm^{-1} para lecitina y aceite de soja, respectivamente).

Este sencillo procedimiento permite la localización del número de onda al que la influencia del interferente es mínima y la intensidad del analito es máxima. De este modo se eligieron los números de onda en 1034 y 1138 cm^{-1} para la extracción de los cromatogramas de lecitina y aceite de soja, respectivamente (ver Figura R-3).

Los niveles de sensibilidad (LOD de 2 y 4 mg mL⁻¹ para lecitina y aceite de soja, respectivamente) y repetibilidad (2.5 y 3.4% RSD para lecitina y aceite de soja, respectivamente) son adecuados para el análisis de muestras reales. Por otra parte, el análisis del espectro IR de los picos cromatográficos permitió la identificación cualitativa de lecitina y aceite de soja en las muestras analizadas.

2.2 Determinación del contenido en triglicéridos polimerizados del aceite de oliva calentado mediante on-line GPC-FTIR y un método multivariante (SBC)

En este estudio se demostró la aplicabilidad de un método multivariante reciente (SBC) en *on-line* GPC-IR para mejorar los niveles de sensibilidad y selectividad de las determinaciones. El método SBC, desarrollado por Ralph Marbach, se basa en la estimación (que puede ser física o quimiométrica) de la señal (en este caso, espectro) del analito de interés g y en la estimación estadística del 'ruido' espectral (Σ). Empleando esta información, se puede llegar – cumpliendo una serie de condiciones descritas en el Capítulo 2 de esta Tesis – a calcular un vector de regresión (b):

$$b = \frac{\Sigma^{-1}g}{g^T \Sigma^{-1}g} \quad (\text{Ecuación R-2})$$

Ese vector de regresión se puede utilizar para calcular la concentración del analito en cada punto del cromatograma (y_{pred}), de acuerdo con la ecuación R-3.

$$y_{pred} = \bar{y} + (x_{pred} - \bar{x}) b \quad (\text{Ecuación R-3})$$

dónde \bar{y} es la concentración promedio de analito y \bar{x} la concentración promedio del ruido.

Se escogió como sistema modelo un problema analítico real como es la monitorización del contenido de triglicéridos polimerizados en aceite de oliva. La experimentación se llevó a cabo con un sistema GPC equipado con columnas Envirogel (19mm×150 mm, 19mm×300 mm), una celda de flujo con un paso óptico de 150 μ m acoplada *on-line* y empleando diclorometano como fase móvil. La corrección de la señal debida al disolvente se realizó mediante la resta de un espectro de referencia medido al inicio de cada cromatograma.

Comparando los cromatogramas obtenidos durante el análisis de una muestra de aceite de oliva virgen antes y después de un proceso de polimerización por calentamiento a 180°C durante 25 h (*deep frying*), se pudo apreciar que la resolución

cromatográfica obtenida entre el triacilglicérido monomérico (TG, *retention time* RT=10.1 min) y los triacilglicéridos poliméricos (PTGs, RT=7.7-938 min, dímeros, trímeros y oligómeros) formados durante el proceso del calentamiento era insuficiente. Por otra parte, en algunas muestras analizadas se observó la elución de un contaminante (RT=7.9 min), con un espectro IR que solapaba con el de los TG y PTGs.

Debido a que los espectros de TG y PTG presentan una correlación muy elevada ($r > 0.99$), se empleó un único espectro de TG extraído durante el análisis de una muestra de aceite sin calentar como espectro de referencia (vector g en la ecuación R-2) para el cálculo del vector de regresión b en el método SBC. Por lo tanto, los cromatogramas extraídos se consideraron específicos para una familia de compuestos con espectros altamente correlacionados, en este caso TG y PTG. Para el cálculo de Σ , se utilizó el conjunto de espectros obtenidos durante el análisis de un blanco.

La Figura R-4 (arriba) muestra los cromatogramas, obtenidos a partir del análisis de una muestra de aceite degradado a 180°C durante 25 h, calculados empleando SBC y utilizando diferentes intervalos espectrales. Además, la Figura R-4 (abajo) muestra los cromatogramas obtenidos a partir de la integración de los mismos intervalos espectrales empleando una corrección de línea base a 1900 cm^{-1} .

Los resultados obtenidos empleando SBC para la extracción de los cromatogramas mostraron una mayor especificidad de la señal, al no detectarse en ningún caso la presencia de un pico interferente a 7.9 min. Por otra parte, empleando el intervalo entre 1900 y 1600 cm^{-1} , los valores de LOD [mg mL^{-1}] y de RSD [%] fueron 8 y 7.2 veces inferiores, respectivamente, a los alcanzados mediante la integración directa de la señal en ese mismo intervalo espectral.

Finalmente, el método se empleó para la monitorización de tres procesos de degradación de aceite de oliva a 180°C, uno de ellos llevado a cabo introduciendo patatas en el aceite durante el calentamiento. Aunque se observaron diferentes velocidades de polimerización debido a variables experimentales no controladas, no se pudieron observar diferencias espectrales entre los experimentos de degradación con patatas y sin ellas.

A partir de estos resultados, se pudo concluir que el empleo de SBC en este tipo de sistemas proporciona mejores niveles de sensibilidad, selectividad y precisión en comparación con los niveles obtenidos mediante la integración de la señal

cromatográfica en regiones específicas en las que el analito presenta bandas de absorción.

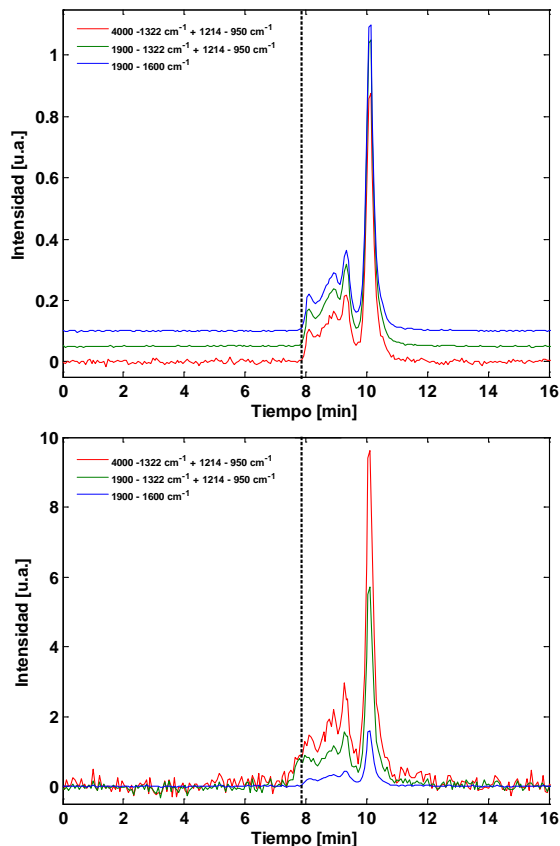


Figure R-4. Cromatogramas GPC-FTIR extraídos de la inyección de un aceite de oliva después de calentarlo durante 25 h a 180°C empleando SBC (arriba) e integrando diferentes áreas espectrales (abajo). La línea indica la elución de un compuesto desconocido.

2.3 Determinación del contenido en ácido glicólico en productos cosméticos mediante on-line LC-FTIR

Uno de los objetivos de esta Tesis, es la mejora en los niveles de sensibilidad del acoplamiento on-line LC-IR. En el caso de llevarse a cabo la detección mediante espectrometría FTIR, una forma de incrementar la relación señal-ruido (*signal-to-noise*, SNR) de la medida es mediante la acumulación de un mayor número de barridos. Esto,

sin embargo, aumenta el tiempo de adquisición, por lo que es necesario establecer un compromiso entre el nivel de SNR y la frecuencia de adquisición de datos. En este estudio, se evaluó la utilidad de un modo de adquisición (*rapid scan*) que reduce el efecto que tiene el número de barridos (*scans*) por espectro sobre la frecuencia de adquisición de datos.

Se desarrolló un método para la determinación de ácido glicólico en muestras de productos cosméticos. El método se basó en la aplicación de un sistema de LC-IR *on-line*, empleando una columna cromatográfica de fase reversa y una fase móvil compuesta por acetonitrilo y tampón fosfato (25 mM, pH 2.7) con una composición constante de 3:97 v/v. El acoplamiento se llevó a cabo empleando una celda de flujo con un paso óptico de 14 μm . Para la adquisición espectral se empleó el modo *rapid scan* que permite una frecuencia de registro más alta ya que, en un primer paso, se registran los interferogramas y, al acabar el cromatograma, se transforman a la dimensión espectral. En comparación con el modo de adquisición habitual, el uso de *rapid scan* permitió un aumento de la frecuencia de adquisición de 15 a 38 espectros min^{-1} acumulando el mismo número de *scans* por espectro.

Para la extracción de los cromatogramas se seleccionó la medida de la absorbancia entre 1288 y 1215 cm^{-1} empleando una línea base entre 1319 y 1150 cm^{-1} , que corresponde a la *coupling vibration* de los grupos CH_2 y C=O del ácido glicólico. La Figura R-5 muestra un cromatograma obtenido durante el análisis del extracto de una muestra comercial.

Los valores de LOD obtenidos a partir del análisis de 5 inyecciones de un patrón con una concentración de ácido glicólico de 0.174 mg mL^{-1} , fueron de 47 y 34 mg mL^{-1} , midiendo la altura y el área del pico, respectivamente. Tanto la precisión como la sensibilidad fueron adecuadas para el análisis de muestras comerciales. Adicionalmente, se llevó a cabo un estudio de recuperación analizando muestras adicionadas con cantidades conocidas de ácido glicólico. Los niveles de recuperación obtenidos variaron entre el 82.8 y el 94.7% midiendo la altura del pico y entre el 99.6 y el 101.0% midiendo el área del pico.

El análisis de diferentes productos comerciales empleando el método desarrollado proporcionó niveles de ácido glicólico coincidentes con lo declarado por los fabricantes.

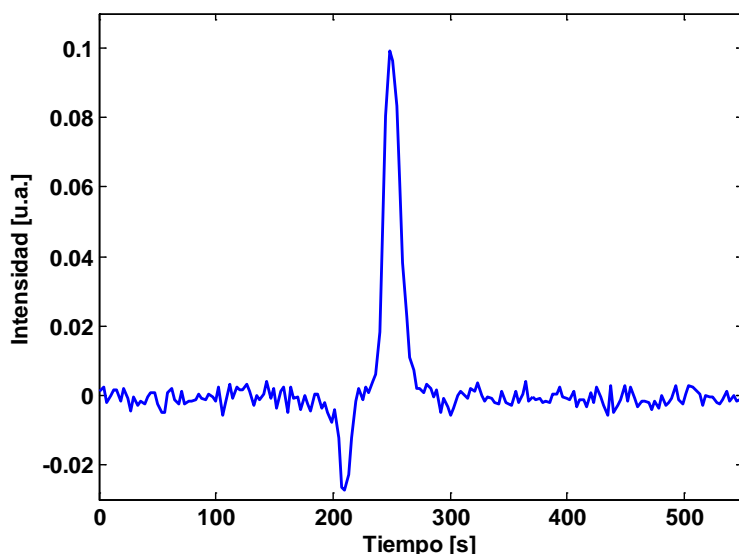


Figura R-5. Cromatograma obtenido durante la inyección de un extracto de muestra con un contenido de ácido glicólico declarado por el fabricante del 8% w/w.

3.- Desarrollo y aplicación de nuevos métodos quimiométricos en on-line LC-IR para la corrección de la absorción debida a la fase móvil (*background correction*)

En 2008, se propuso un método para la corrección del *background* aplicable a sistemas *on-line* LC-IR, tanto en régimen isocrático como en gradiente, que dio acceso a un aumento de la aplicabilidad del acoplamiento *on-line* LC-IR. Este método (*Univariate background correction based on the use of a reference spectra matrix, BGC-RSM*) se basa en el empleo de una matriz espectral de referencia (*reference spectra matrix, RSM*) que se puede obtener fácilmente midiendo un gradiente LC-IR en el mismo intervalo de composición de fase móvil que el utilizado durante el análisis cromatográfico de la muestra (*sample matrix, SM*).

La corrección del *background* en cada punto (espectro IR) del cromatograma **SM** se lleva a cabo mediante la selección, empleando un 'parámetro de identificación' (*identification parameters, IP*), del espectro de referencia más adecuado dentro de la matriz de referencia **RSM** para su posterior sustracción. El IP debe ser un parámetro espectral característico de la composición de la fase móvil durante todo el intervalo de composiciones del gradiente, libre de interferencias durante la elución de los analitos

presentes en la muestra analizada. En esta Tesis se propusieron y evaluaron diferentes IPs para la selección del espectro de referencia más adecuado, de manera que este tipo de *background correction* fuera aplicable en un amplio intervalo de situaciones.

El método BGC-RSM requiere el cumplimiento de las siguientes condiciones: i) estabilidad instrumental del equipo, ii) medida de una matriz de referencia adecuada, iii) que el espectro de la fase móvil presente, por lo menos, una región espectral característica de su composición y libre de solapamiento espectral con los analitos presentes en la muestra.

Para facilitar la aplicación de los métodos de corrección del *background* a usuarios no habituados a trabajar en entorno Matlab, así como para visualizar e interpretar los resultados obtenidos de forma rápida, se desarrolló una interfaz gráfica (*Graphical User-friendly Interface*, GUI-File) en Matlab. La interfaz se puede obtener en http://www.iac.tuwien.ac.at/cavs/lc_ftir_toolbox.php.



Figura R-6. Ventana inicial de la interfaz gráfica en entorno Matlab.

Se incluyeron distintas funciones para la corrección del *background*, basadas en el uso de una **RSM** (AR-, RW-, p2p-, PLS-BGC-RSM o Polyfit-RSM, entre otras), desarrolladas a partir de 2008. Además se han incorporado una serie de herramientas sencillas para facilitar su uso, como funciones para importar/exportar espectros desde/a OPUS

(Bruker Optics), herramientas para la corrección de línea base, derivatización o normalización de espectros, selección de condiciones para la corrección del *background*, y visualización de los resultados, entre otras. La Figura R-6 muestra la ventana principal de la interfaz.

3.1 Empleo de la absorbancia relativa a dos números de onda como IP en BGC-RSM: determinación de las condiciones críticas en LC para polietilenglicol utilizando un sistema metanol:agua como fase móvil

El objetivo de este estudio fue demostrar la utilidad de la detección IR para la determinación de las condiciones críticas en LC (*liquid chromatography under critical conditions, LCCC*) en el análisis de polímeros. Para ello se escogió como ejemplo representativo el análisis de polietilenglicol (PEG) en un sistema LC en fase reversa empleando un gradiente compuesto por metanol y agua.

Este estudio se puede dividir en dos etapas: i) *background correction* de los cromatogramas obtenidos a partir de la inyección de PEGs utilizando diferentes gradientes, y ii) determinación de la composición de la fase móvil durante el desarrollo del cromatograma mediante *Partial Least Squares* (PLS).

En este estudio, se utilizó la absorbancia relativa (AR) entre dos números de onda, como IP para la selección del espectro de referencia más adecuado para la corrección de la señal debida a la fase móvil en cada punto del cromatograma. La selección de los números de onda utilizados para el cálculo del AR es, obviamente, un parámetro crítico del que depende la exactitud de la corrección. El valor del AR debe ser característico de la composición de la fase móvil durante todo el intervalo de composiciones empleado en el gradiente y, además, debe estar libre de interferencias espectrales de los analitos. La selección de los dos números de onda empleados para el cálculo del AR, se realizó utilizando los espectros adquiridos durante el análisis de un blanco de muestra. Una vez escogida una región espectral libre de solapamiento espectral con los analitos, se evaluó la exactitud de la corrección empleando todos los posibles pares de números de onda. El parámetro 'respuesta' escogido para la evaluación de la exactitud de la corrección fue la señal residual a un determinado número de onda en el que la fase móvil presenta una banda de absorción muy intensa (p. ej. 1640 cm^{-1}). A partir de los

resultados obtenidos, se seleccionaron los números de onda 2086.7 y 1893.9 cm^{-1} para el cálculo del AR en el sistema metanol:agua evaluado.

Se analizó PEG con un peso molecular de 40000 g mol^{-1} en un sistema cromatográfico empleando una columna Kromasil 100 C_{18} y diferentes gradientes lineales de metanol:agua entre el 5 y el 100% v/v de metanol. El acoplamiento se llevó a cabo empleando una celda de flujo con un paso óptico de 10 μm .

Después de llevar a cabo la corrección de la absorbancia debida a la fase móvil, se extrajeron cromatogramas específicos para el PEG mediante la medida de la absorción a 1091.6 cm^{-1} utilizando una línea base a 1273 cm^{-1} .

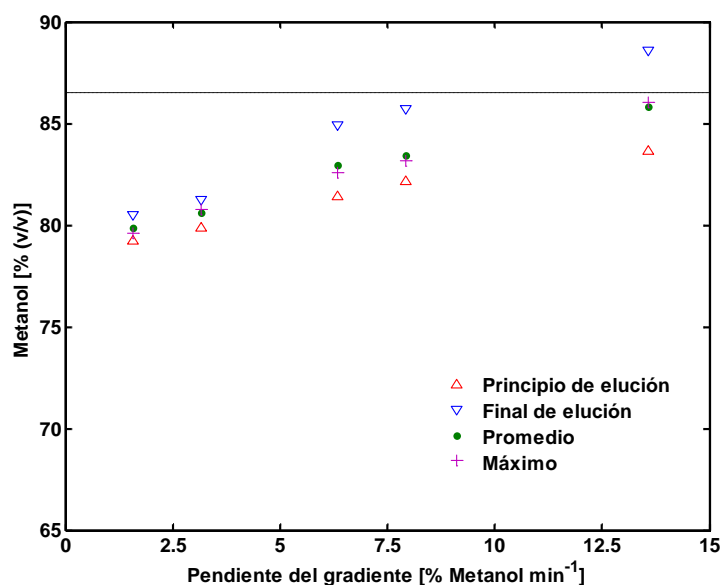


Figura R-7. Composición de la fase móvil durante la elución de un patrón de PEG 40000 en función de la pendiente del gradiente. La línea discontinua muestra el punto crítico de adsorción (*critical point of adsorption*, CAP) encontrado en la bibliografía para el sistema investigado.

La corrección del *background*, por un lado, mejoró significativamente la sensibilidad del acoplamiento LC-FTIR en régimen de gradiente cuando se emplearon gradientes de composición rápidos. Por otro lado, permitió el uso del espectro IR de los analitos para la confirmación de los resultados cuantitativos obtenidos.

Para el cálculo de la composición del eluyente a partir del espectro IR, se empleó un modelo PLS después de seleccionar el intervalo espectral y el número de variables latentes óptimos mediante validación cruzada.

Finalmente, empleando distintos gradientes lineales, se determinó la composición de la fase móvil durante la elución del polímero y se pudo comprobar que, al emplear gradientes con una mayor pendiente, esta composición se aproxima a la composición crítica (ver Figura R-7). En este caso, la composición crítica estimada corresponde a 86.5% v/v metanol, siendo comparable a resultados previos encontrados en la bibliografía. Adicionalmente, este resultado se comprobó mediante el análisis de PEG de diferentes masas moleculares (12000, 20000 y 40000 g mol⁻¹) en régimen isocrático empleando las condiciones críticas previamente determinadas.

3.2 Empleo de la absorbancia relativa a dos números de onda como IP en BGC-RSM para el desarrollo de un método cuantitativo: determinación de hidratos de carbono en muestras acuosas utilizando un sistema acetonitrilo:agua como fase móvil

Este estudio tuvo como objetivo demostrar la capacidad que ofrece el método AR-BGC-RSM para el desarrollo de aplicaciones cuantitativas en *on-line* LC-FTIR en régimen de gradiente. Con este objetivo, se desarrolló un método para la cuantificación de cuatro azúcares (glucosa, fructosa, sacarosa y maltosa) en muestras acuosas, que implicara una mínima manipulación de la muestra (dilución y filtración) y permitiera una identificación basada en el tiempo de retención y en la comparación de los espectros obtenidos durante la elución de los analitos con espectros de referencia.

Para llevar a cabo el estudio, se utilizó un sistema cromatográfico empleando una columna Kromasil 100 NH₂, gradientes lineales de acetonitrilo:agua entre 75 y 55% acetonitrilo en 15 min, y una celda de flujo con un paso óptico de 10 μm. Utilizando el mismo método de selección que en estudios anteriores de esta Tesis, se seleccionó la absorbancia relativa a 2256.5 y 2252.6 cm⁻¹ para llevar a cabo la corrección del gradiente.

La Figura R-8 muestra los cromatogramas obtenidos a partir del análisis de un patrón de fructosa, glucosa, sacarosa y maltosa, antes (arriba) y después (abajo) de aplicar la corrección de la señal de fondo. Una simple inspección visual de los resultados permite comprobar que la corrección de la señal de fondo elimina una gran parte de la

contribución de la absorbancia del eluyente y permite la detección e identificación de los cuatro azúcares con tiempos de retención de 11.8 ± 0.2 , 12.7 ± 0.2 , 15.0 ± 0.2 y 16.5 ± 0.2 min para fructosa, glucosa, sacarosa y maltosa, respectivamente. Los cromatogramas de fructosa se obtuvieron a partir de la medida del área del espectro entre 1108 y 1069 cm^{-1} , corregida usando una línea base a 1203 cm^{-1} . Los cromatogramas para glucosa, sacarosa y maltosa se obtuvieron a partir de la medida del área del espectro entre 1177 y 1025 cm^{-1} , corregida con una línea base establecida a 1177 cm^{-1} .

Las características analíticas del método (linealidad, límite de detección, repetibilidad) encontradas resultaron adecuadas para el análisis de los carbohidratos seleccionados. Los coeficientes de regresión de las rectas de calibrado obtenidas a partir de medidas de altura del pico cromatográfico variaron entre 0.9962 y 0.9995 ; los límites de detección encontrados variaron entre 0.4 mg ml^{-1} para fructosa y maltosa y 0.6 mg ml^{-1} para glucosa y la precisión del procedimiento de medida, calculada a partir de seis inyecciones independientes de un patrón de 3 mg ml^{-1} , varió entre el 3.3 y el 4.1% de desviación de estándar relativa (*relative standard deviation*, RSD) para la glucosa y fructosa, respectivamente.

Se determinó el coeficiente de correlación entre espectros de referencia y espectros extraídos, tanto de inyecciones de patrones como de muestras, después de realizar la corrección de la señal de fondo. Usando la región espectral entre 1250 y 1060 cm^{-1} , se obtuvieron valores entre el 96.25 y el 98.73% .

Se analizó un conjunto de muestras de refrescos, adquiridos en el mercado español, utilizando las condiciones experimentales descritas, y se obtuvieron unas concentraciones coincidentes con las indicadas por los fabricantes. Finalmente, se llevó a cabo un estudio de recuperación con el fin de evaluar la exactitud del procedimiento. Usando concentraciones añadidas de entre 0.97 y $2.54 \text{ g } 100 \text{ ml}^{-1}$, 0.90 y $2.36 \text{ g } 100 \text{ ml}^{-1}$, 0.97 y $3.13 \text{ g } 100 \text{ ml}^{-1}$ y 1.10 y $3.34 \text{ g } 100 \text{ ml}^{-1}$ para fructosa, glucosa, sacarosa y maltosa, respectivamente, se encontraron recuperaciones medias entre el 92.5 y el 105.1% .

A partir de los resultados obtenidos, se pudo concluir que la corrección quimiométrica de la señal de la fase móvil permite el empleo de sistemas *on-line* LC-FTIR en régimen de gradiente para el desarrollo de aplicaciones cuantitativas y cualitativas.

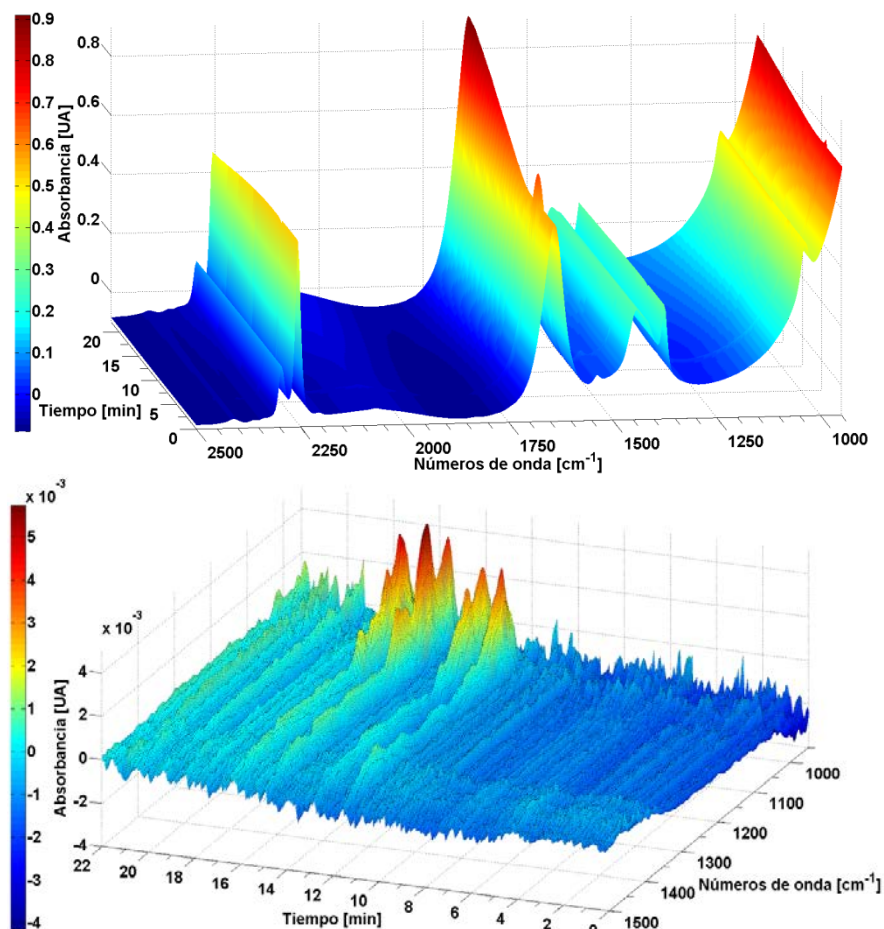


Figura R-8. Espectros obtenidos durante la inyección de una mezcla de patrones de fructosa, glucosa, sacarosa y maltosa a un nivel de concentración de 2.5 mg mL⁻¹ antes (arriba) y después (abajo) de aplicar la corrección de la señal de fondo.

3.3 Empleo del valor de absorbancia a 1639 cm⁻¹ calculado mediante PLS, como IP en BGC-RSM

En este estudio, se desarrolló y evaluó un nuevo IP para la corrección de la señal debida a una fase móvil conteniendo agua mediante el método BGC-RSM. Como nuevo IP se estudió la posibilidad de emplear la absorbancia a 1639 cm⁻¹. La absorbancia a ese número de onda se puede correlacionar con la concentración de agua y, por tanto, en sistemas binarios, con la composición de la fase móvil. Sin embargo, el uso de la

absorbancia en esta región presenta como dificultad el frecuente solapamiento con bandas de absorción de analitos presentes en la muestra. Debido a esto, en este estudio se propuso la predicción de este valor mediante un modelo PLS, empleando regiones del espectro con un menor grado de solapamiento con bandas de absorción de los analitos. En este caso, se seleccionó la región entre 2345 y 2145 cm^{-1} para el cálculo del modelo PLS.

Se utilizaron cromatogramas obtenidos a partir del análisis de patrones de cafeína empleando una fase móvil acetonitrilo:agua (1% v/v ácido acético) a 60:40 v/v en régimen isocrático y, a partir del análisis de patrones de atracina y diurón empleando un gradiente acetonitrilo:agua con porcentajes de acetonitrilo entre el 60 y el 100% v/v. Las separaciones se llevaron a cabo utilizando una columna C_{18} .

En el caso del análisis de patrones de cafeína en régimen isocrático, los niveles de relación señal-ruido obtenidos fueron comparables a los obtenidos utilizando un espectro de referencia medido al principio del cromatograma. La Figura R-9 muestra espectros extraídos durante la elución de la cafeína, corregidos utilizando ambos métodos. En esta figura se puede comprobar que los espectros presentaron elevados coeficientes de correlación (>0.99) en la región espectral entre 1700 y 1050 cm^{-1} .

La corrección de la señal proporcionó resultados satisfactorios en el caso del análisis de patrones de atracina y diurón en régimen de gradiente. En este caso, la exactitud de la corrección de la señal se evaluó comparando los espectros recuperados después de aplicar la corrección de la señal de fondo con espectros de referencia, obteniendo coeficientes de correlación de 0.94 y 0.93 para atracina y diurón, respectivamente. Adicionalmente, se utilizó la corrección de la señal de fondo del cromatograma de un blanco para la comprobación de la exactitud de la corrección. De nuevo, los niveles de ruido en el cromatograma corregido, a números de onda en los que los componentes de la fase móvil presentan máximos en su espectro de absorción, fueron comparables a los obtenidos en régimen isocrático. Además, la ausencia de pendiente y la distribución aleatoria de los residuales, junto con los resultados anteriores, permitieron concluir que el IP propuesto proporciona resultados exactos tanto en régimen isocrático, como en gradiente y puede utilizarse para el desarrollo de aplicaciones basadas en el empleo de *on-line* LC-FTIR.

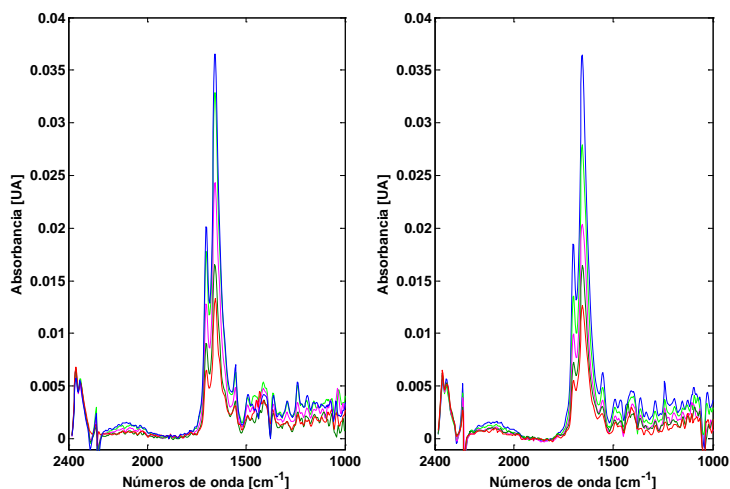


Figura R-9. Espectros extraídos durante la elución de cafeína, analizada en un régimen isocrático, empleando el método de corrección propuesto (izquierda) y un espectro de referencia constante medido al principio del cromatograma (derecha).

3.4 Empleo de 'point-to-point matching algorithms' como IP en BGC-RSM

En estudios anteriores realizados durante esta Tesis, se pudo comprobar que el uso de AR o el valor de absorbancia calculada mediante PLS a un determinado número de onda, son procedimientos válidos para la selección de espectros incluidos en la RSM. En este estudio, se evaluó el uso de una serie de IPs basados en el uso de algoritmos de corrección punto a punto (*point to point matching algorithms*, p2p) para la corrección de la señal debida a la fase móvil mediante el método BGC-RSM.

Se evaluaron las características de los métodos de corrección de la señal de la fase móvil empleados, utilizando datos obtenidos durante el análisis de patrones de 4-nitrofenol (4-NP), 2,4-dinitrofenol (2,4-dNP), 2-nitrofenol (2-NP) y 3-metil-4-nitrofenol (3m4-NP), empleando una columna C₁₈ y gradientes de fase móvil entre 65:35 v/v agua (0.08% v/v TFA):acetonitrilo (0.08% v/v TFA) y 15:85 v/v agua (0.08% v/v TFA):acetonitrilo (0.08% v/v TFA) en 20 minutos. El acoplamiento se llevó a cabo con una celda de flujo con un paso óptico de 16.5 μm .

En este trabajo, el '*point to point matching algorithm*' seleccionado para su uso como IP en BGC-RSM fue el coeficiente de correlación (COR). El COR entre dos espectros (S_A y S_B) se define como:

$$COR = \frac{z_A^T z_B}{\|z_A\| \|z_B\|} \quad (\text{Ecuación R-4})$$

donde z_A y z_B son los espectros S_A y S_B centrados: $z_n = S_n - \overline{S_n}$, donde $\overline{S_n}$ es el valor de absorbancia promedio en el espectro S_n ($n = A, B$).

El estudio efectuado para la selección del intervalo espectral utilizado para calcular el índice de similitud 'COR' demostró que, para el sistema estudiado, se obtuvieron los mejores resultados para la corrección de la señal de fondo empleando la región espectral de la banda de CN *stretching* en el intervalo espectral entre 2318 y 2237 cm^{-1} . La corrección de la señal llevada a cabo en los cromatogramas obtenidos a partir de la inyección de 4-NP, 2,4-dNP, 2-NP y 3m4-NP en régimen de gradiente proporcionó resultados satisfactorios y no se vio afectada durante la elución de los analitos. Los picos de 4-NP, 3m4-NP, 2,4-dNP y 2 NP se identificaron a tiempos de retención de 10.4, 12.1, 13.0 y 14.1 min, respectivamente.

La Figura R-10 muestra los espectros recuperados de los cuatro analitos junto a su correspondiente espectro de referencia. A pesar de la baja intensidad (<5 mAU), los espectros recuperados mostraron una alta correlación con los espectros de referencia obteniendo valores de 91.7, 98.6, 97.8 y 98.4% para 4-NP, 3m4-NP, 2,4-dNP y 2-NP, respectivamente, en la región entre 1200 y 1550 cm^{-1} . Los resultados indicaron que este método de corrección de la señal se puede considerar como una opción adicional válida para el desarrollo de aplicaciones cualitativas y cuantitativas basadas en el empleo de *on-line* LC-FTIR.

Los resultados obtenidos empleando el índice COR se compararon con los obtenidos utilizando un AR como IP, obteniendo resultados comparables. Sin embargo, una característica relevante del método propuesto es que, para la selección de las condiciones óptimas para la corrección de la señal del eluyente, únicamente es necesario definir el intervalo espectral utilizado para calcular los valores de correlación; lo que representa una ventaja relevante frente a otros métodos de corrección (p.ej. PLS-BGC-RSM), ya que simplifica el proceso de selección de las condiciones óptimas y minimiza la interacción del usuario.

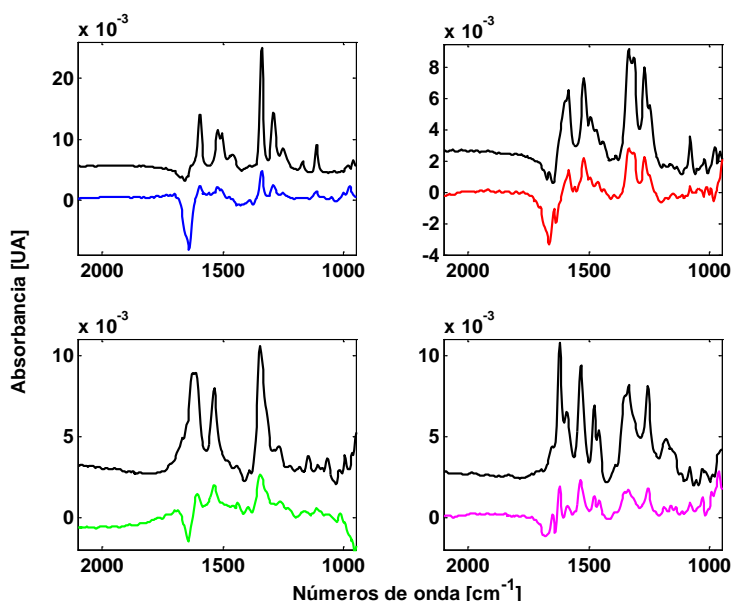


Figura R-10. Espectros de nitrofenoles obtenidos después de aplicar la corrección de la señal de fondo, extraídos de la inyección de una mezcla de patrones de 1.25 mg mL^{-1} de 4-NP (arriba, izquierda), 2 mg mL^{-1} de 3m4-NP (arriba, derecha), 2.25 mg mL^{-1} de 2,4-dNP (abajo, izquierda) y 4.5 mg mL^{-1} de 2-NP (abajo, derecha). Las figuras incluyen los correspondientes espectros de referencia (líneas negras) medidos en condiciones de flujo parado.

4. Compensación de la señal de fondo en LC-IR on-line empleando técnicas quimiométricas 'column-wise'

Anteriormente, se han descrito y evaluado diferentes métodos para la compensación de la señal de fondo empleando una matriz de referencia (*reference spectra matrix*, **RSM**) y una selección utilizando diferente IPs, del espectro de referencia más adecuado para la corrección de la señal de fondo para cada espectro incluido en el cromatograma LC-IR. En esta Tesis se propuso también una estrategia alternativa, basada en una corrección de la señal debida a la fase móvil llevada a cabo de forma independiente para cada variable (número de onda) utilizada. En esta estrategia alternativa, se propusieron dos métodos: uno basado en el uso de ajustes polinómicos y una matriz de referencia (Polyfit-RSM), y otro basado en el empleo de *cubic smoothing splines* (CSS) para el cálculo y la eliminación de la señal debida al eluyente.

4.1 Empleo de funciones polinómicas y matrices de referencia para la eliminación de la señal de la fase móvil en on-line LC-FTIR

El método se puede dividir en varias etapas diferenciadas: en la primera se lleva a cabo la adquisición del cromatograma de la muestra (*sample matrix*, **SM**) y de una matriz de referencia (*reference spectra matrix*, **RSM**). A continuación, empleando la **RSM**, se calcula una función polinómica de grado n que relaciona el valor de absorbancia (y) de cada variable j durante el gradiente, con un valor de referencia característico de la fase móvil (x), por ejemplo un AR:

$$P(x)_j^n = y_j = p_1x^n + p_2x^{n-1} + \dots + p_nx + p_{n+1} \quad (\text{Ecuación R-5})$$

El orden de la función se selecciona utilizando como parámetro estadístico de calidad del ajuste el valor del *adjusted R-square*. Se seleccionó este parámetro porque, a diferencia del *R-square*, el *adjusted R-square* puede disminuir cuando la contribución a la varianza explicada, obtenida al incrementar el orden del polinomio, es menor que su efecto sobre los grados de libertad. En este estudio se propuso aceptar un incremento del orden del polinomio siempre que incrementara el valor del *adjusted R-square* en más de un 0.1%.

A continuación, empleando el conjunto de polinomios óptimos y los valores del parámetro de referencia característico de la fase móvil (x) obtenidos durante la medida de la muestra (**SM**), se calcula el valor de la absorbancia debida a la fase móvil para cada variable mediante interpolación en los polinomios. Finalmente, una vez calculada la contribución de la fase móvil a la absorbancia medida en la **SM**, se resta para obtener el cromatograma corregido.

Para demostrar el funcionamiento del método, se emplearon datos obtenidos para el análisis de azúcares en bebidas con una columna Kromasil 100 NH₂ y un gradiente de acetonitrilo:agua del 75 al 55% de acetonitrilo en 15 min. El acoplamiento se llevó a cabo utilizando una celda de flujo con un paso óptico de 10 μm. En este estudio, se utilizaron dos parámetros de referencia característicos de la composición de la fase móvil: la absorbancia a un número de onda, 2210 cm⁻¹ (SW-Polyfit), y la absorbancia relativa de dos números de onda, 2256.5 y 2248.7 cm⁻¹ (AR-Polyfit).

La Figura R-11 muestra los espectros corregidos, empleando SW-Polyfit y AR-Polyfit y los parámetros de referencia anteriormente descritos, obtenidos a partir del análisis de

un blanco y de una muestra de una bebida con un contenido conocido de glucosa y fructosa, convenientemente diluida. Aunque se detectó presencia de bandas de absorción residuales características de los componentes de la fase móvil en los espectros corregidos, su intensidad fue muy baja, en el intervalo de ± 1.5 mAU (aprox.), por lo que se consideró que el procedimiento resultaba adecuado para la corrección de la señal en muestras reales.

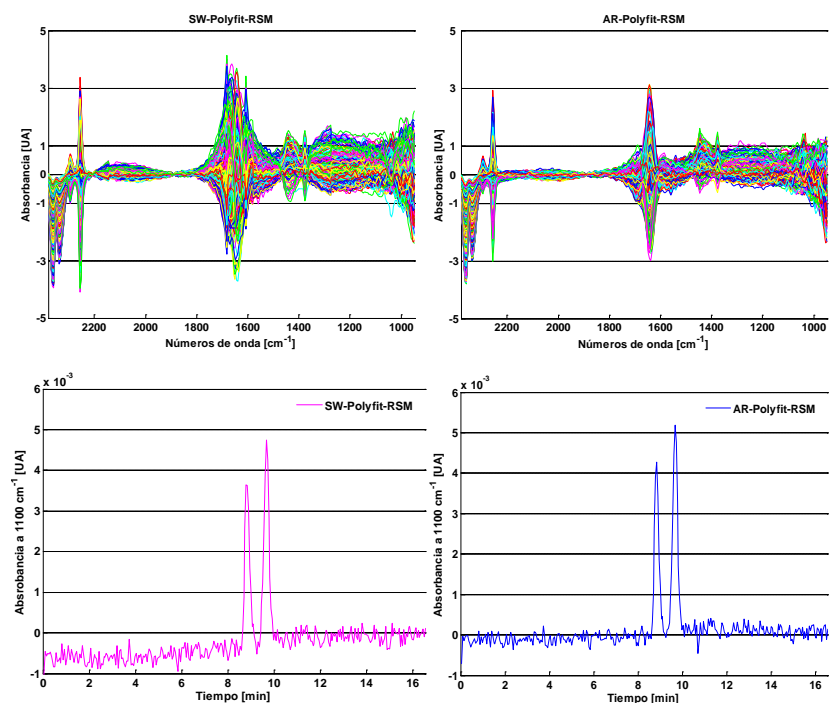


Figure R-11. Arriba: Espectros obtenidos a partir del análisis de un blanco, corregidos empleando AR-Polyfit y SW-Polyfit, abajo: Cromatogramas obtenidos a partir del análisis de una muestra de bebida azucarada diluida, corregidos empleando AR-Polyfit y SW-Polyfit.

Como se puede ver en la Figura R-11, los dos picos correspondientes a glucosa (8.5 min) y fructosa (9.7 min) fueron fácilmente identificables en el cromatograma corregido.

Se comparó la exactitud del procedimiento de corrección de la señal con otros propuestos anteriormente (AR-BGC-RSM, PLS-BGC-RSM) empleando los niveles de ruido en cromatogramas extraídos a números de onda en los que los componentes de

la fase móvil presentan bandas de absorbancia. Los resultados obtenidos indicaron que tanto la calidad de los cromatogramas como de los espectros recuperados fue ligeramente mejor empleando el método Polyfit. Sin embargo, la diferencia entre los valores obtenidos fue muy reducida, por lo que resultó difícil asegurar que los resultados son estadísticamente diferentes.

No obstante, el estudio del efecto del tamaño de la **RSM** en los diferentes métodos evaluados permitió comprobar que los métodos propuestos, basados en el empleo de funciones polinómicas, se ven afectados en menor manera por una reducción del tamaño de la **RSM**; lo que facilita la adquisición de matrices de referencia y reduce la importancia de la estabilidad instrumental en el proceso de corrección de la señal.

4.2. Empleo de 'cubic smoothing splines' para la eliminación de la señal de la fase móvil en on-line LC-FTIR

El método desarrollado en este estudio para la corrección de la señal debida a la fase móvil, prescinde del uso de una **RSM**. El método se basa en la aplicación de *cubic smoothing splines* (CSS), siguiendo una estrategia univariante que se aplica a cada variable (número de onda) por separado ('column-wise').

Los espectros registrados antes y después de cada agrupación de picos se utilizan como nodos (*knots*) para la modelización de la variación de la intensidad de la absorbancia del eluyente con el tiempo empleando funciones CSS. El método se puede dividir en varias etapas diferenciadas: en la primera, se lleva a cabo la adquisición del cromatograma de la muestra (*sample matrix*, **SM**). A continuación, se seleccionan los puntos del cromatograma que se utilizarán como *knots* para el ajuste de las funciones CSS. Después, se calculan las funciones CSS y se interpola el valor de la absorbancia debida a la fase móvil en los puntos no utilizados como *knots*. Una vez calculados estos valores, se restan del cromatograma original para obtener la señal corregida.

La selección de los *knots* puede hacerse de distintas formas: manual mediante simple observación del cromatograma original, utilizando algoritmos para la detección de picos, o incluso en dos etapas, utilizando una primera 'corrección' que emplee *knots* distribuidos regularmente a lo largo del cromatograma, comprobando en el cromatograma corregido la idoneidad de los *knots* utilizados y modificando, si fuera

necesario, su posición dentro del cromatograma para una nueva corrección del cromatograma original.

Para evaluar el método CSS, se utilizaron datos simulados y datos reales obtenidos durante el análisis de mezclas de patrones de PEGs con diferentes pesos moleculares. Para la separación se utilizaron un sistema LC con una columna C₄ y gradientes lineales de fases móviles compuestas de metanol:agua, 2-propanol:agua y etanol:agua entre 30 y 90, 10 y 25 y 10 y 40% v/v de disolvente orgánico en 10, 15 y 10 min, respectivamente. El registro de los espectro IR se llevó a cabo empleando una celda de flujo con un paso óptico de 10 μm. Cabe destacar que el uso de estas fases móviles es especialmente complicado; ya que, por una parte, los alcoholes muestran una intensa absorbancia en el IR y, por otra parte, la región de su absorbancia más intensa es similar a la región de máxima absorbancia de los analitos investigados, dificultando de esta manera la compensación de la señal de fondo. Además, es de interés el uso de 2-propanol y etanol como disolventes orgánicos en LC ya que se trata de dos alcoholes con una toxicidad reducida, por lo que su uso es aconsejable para el desarrollo de métodos de análisis más respetuosos con el medio ambiente.

Al aplicar el método CSS para la corrección de la señal de fondo en datos simulados, los picos de los 'analitos' pudieron identificarse fácilmente en los cromatogramas, obteniendo una línea base muy buena del cromatograma con un nivel de ruido muy bajo distribuido alrededor de cero. Además, la altura y el área de los picos en los cromatogramas corregidos fueron comparables a los teóricos. De la misma manera, los espectros recuperados mostraron alta calidad sin presentar distorsiones de las bandas características de los componentes de la fase móvil simulada. El análisis de los datos simulados confirmó que la selección de los *knots* es un paso crítico. Por otro lado, este método puede automatizarse empleando algoritmos de detección de picos que, en parte, reducen la interacción del usuario.

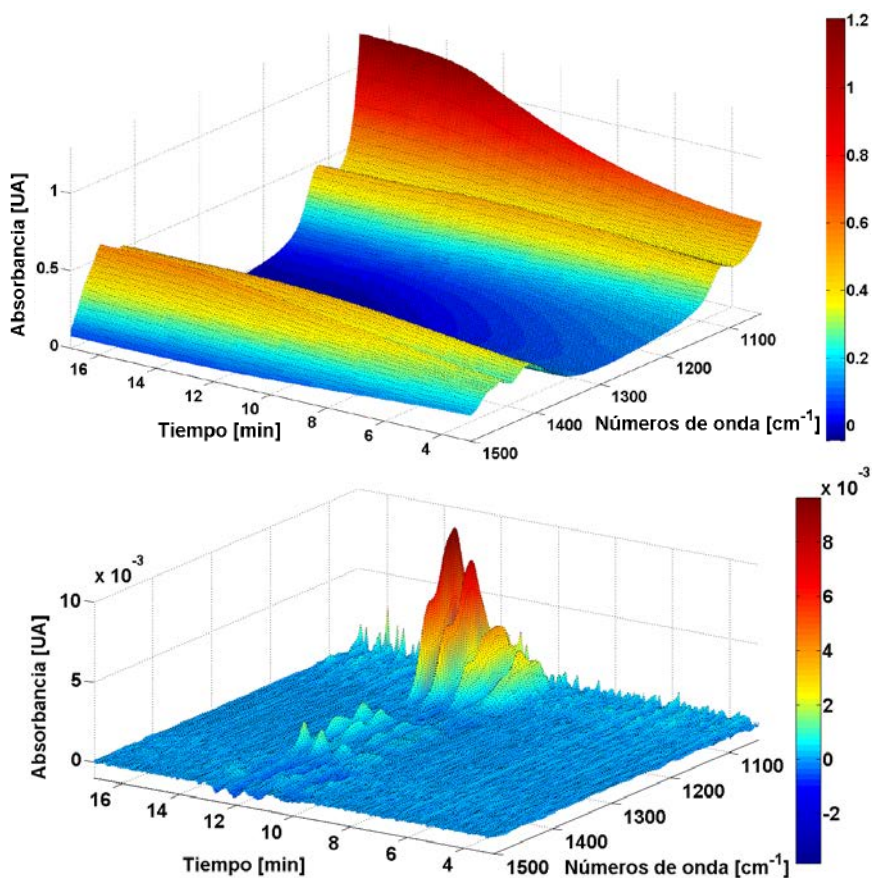


Figure R-12. Representación gráfica del cromatograma antes (arriba) y después (abajo) de aplicar la corrección CSS. Los espectros entre 1500 y 950 cm^{-1} se registraron durante la inyección de una mezcla de patrones de 5.1 mg mL^{-1} de PEG 2000, 5.3 mg mL^{-1} de PEG 4000, 5.6 mg mL^{-1} de PEG 8000 y 5.1 mg mL^{-1} de PEG 40000.

La Figura R-12 muestra el cromatograma obtenido durante el análisis de un patrón de PEGs con diferentes masas moleculares empleando un gradiente metanol:agua del 30 al 90% de metanol antes (arriba) y después (abajo) de aplicar la corrección CSS. Se puede observar que, antes de aplicar la corrección, la identificación de los analitos se ve enormemente dificultada por los intensos cambios en la absorción del eluyente producidos como consecuencia del gradiente. Aplicando una corrección CSS, la

contribución debida a la fase móvil se pudo eliminar de forma cuantitativa y todos los analitos se pudieron identificar correctamente.

A continuación, se evaluó la posibilidad de utilizar este tipo de corrección para el desarrollo de métodos cuantitativos. Las características analíticas obtenidas empleando los tres sistemas de fases móviles fueron adecuadas para el análisis de PEGs mostrando una alta linealidad ($R^2 > 0.98$) y LODs, LOQs y repetibilidades muy buenas en todos los casos evaluados. En el caso del sistema etanol:agua, los valores de ruido obtenidos fueron ligeramente más elevados por el alto solapamiento espectral entre la fase móvil y los analitos.

Por último, se compararon las exactitudes en la corrección de las señales proporcionadas por los métodos CSS y AR-BGC-RSM. A partir de los resultados obtenidos, se concluyó que el método CSS, al no emplear una **RSM**, es más robusto al eliminar prácticamente la importancia de la estabilidad instrumental y no depender del tamaño y distribución de espectros y composiciones de fase móvil de la **RSM**. En resumen, el método CSS proporciona los mejores niveles de exactitud en la corrección del efecto de la fase móvil, aunque esta exactitud se puede ver afectada si la separación entre *knots* no es adecuada o si la resolución cromatográfica es reducida.

5. Corrección multivariante de la señal de fondo en on-line LC-IR empleando factor analysis, MCR-ALS y matrices de espectros de referencia

Los sistemas *on-line* LC-IR son capaces de proporcionar matrices de datos bidimensionales y, por tanto, una aproximación de tipo multivariante para el tratamiento de un problema, como la corrección de la señal debida al eluyente, debe ser, en principio, factible. En este sentido, en los últimos años se han desarrollado una serie de estrategias basadas en *Principal Component Analysis* (PCA), *Evolving Factor Analysis* (EFA) o *Parallel Factor Analysis* (PARAFAC) dirigidas a la eliminación quimiométrica de la señal del eluyente. Sin embargo, los métodos encontrados en la bibliografía sólo eran aplicables cuando la separación se llevaba a cabo en régimen isocrático, y presentan una serie de limitaciones muy importantes.

Debido a esto, en este estudio se desarrolló una nueva estrategia de eliminación de la señal de la fase móvil basada en el empleo de una matriz de referencia (**RSM**) y

diferentes métodos de análisis multivariante (p.ej. SIMPLISMA y PCA). Un objetivo adicional de este estudio consistió en comprobar que la eliminación previa de la señal debida a la fase móvil permite el empleo de MCR-ALS en *on-line* LC-IR.

Los métodos de corrección que se han desarrollado se pueden dividir en cuatro etapas: i) adquisición de la **SM** y la **RSM** durante la separación cromatográfica y el re-equilibrio del sistema, respectivamente; ii) selección del número de componentes (k_{opt} , *chemical rank*) debidos al gradiente de la fase móvil. Para ello, se propone el uso de los *eigenvalues* obtenidos mediante PCA, o la medida del error de corrección promedio de un cromatograma empleando diferentes componentes; iii) cálculo de los perfiles de concentración de los k_{opt} componentes en la matriz de **SM** empleando *simple-to-use interactive self modeling analysis* (SIMPLISMA) o *Principal Component Analysis* (PCA); y iv) cálculo y sustracción de la contribución de la señal de fondo en la **SM** empleando *Classical Least Squares regression* (CLS) y la matriz de espectros de los k_{opt} componentes.

Los métodos se evaluaron empleando dos sets de datos de un sistema *on-line* LC-FTIR. El primero se obtuvo a partir del análisis de un patrón de azúcares empleando gradientes lineales de acetonitrilo:agua entre el 75 y el 55% v/v de acetonitrilo. El segundo set de datos se adquirió durante el análisis de un patrón de 4-nitrofenol (4-NP), 2,4-dinitrofenol (2,4-dNP), 2-nitrofenol (2-NP) y 3-methyl-4-nitrofenol (3m4-NP) empleando gradientes lineales de 65:35 v/v agua (0.08% v/v TFA):acetonitrilo (0.08% v/v TFA) a 15:85 v/v agua (0.08% v/v TFA):acetonitrilo (0.08% v/v TFA). Para el acoplamiento se utilizó una celda de flujo con un paso óptico de 16.5 μm .

Al aplicar ambos métodos de corrección comentados anteriormente a los datos, se observó que tanto los espectros de los componentes puros calculados mediante SIMPLISMA, como los *loadings* calculados mediante PCA, reflejaron los cambios espectrales observados en la fase móvil durante el gradiente. Después de la corrección, se observó en todos casos una alta correlación entre los espectros de los analitos recuperados y espectros de referencia previamente adquiridos.

Se evaluó el uso de MCR-ALS en *on-line* LC-IR en régimen de gradiente. Los resultados obtenidos analizando la matriz antes de la corrección de la señal debida al disolvente fueron claramente insatisfactorios. Por el contrario, el empleo de una corrección previa al análisis MCR-ALS permitió la recuperación de los perfiles de concentración y

espectrales de todos los analitos. Además, el análisis mediante MCR-ALS permitió la eliminación de contribuciones espectrales residuales de la fase móvil y derivadas de la señal del detector MCT empleado, que no habían sido corregidas en la etapa anterior.

A modo de ejemplo representativo de los resultados obtenidos tras el análisis mediante MCR-ALS de un cromatograma corregido, la Figura R-13 (arriba), muestra los perfiles de concentración de los cuatro nitrofenoles presentes en una muestra analizada. Los dos componentes restantes indican la presencia de cambios residuales en la absorción debida al disolvente y producidos durante el gradiente. Un ejemplo de la elevada exactitud de los perfiles espectrales obtenidos mediante MCR-ALS se muestra en la Figura R-13 (abajo).

En resumen, a partir de los resultados presentados se pudo concluir que: i) los dos métodos multivariantes propuestos, basados en el empleo de SIMPLISMA y PCA, son muy efectivos y permiten la corrección de la señal debida a la fase móvil en régimen de gradiente; y ii) el uso de MCR-ALS en *on-line* LC-IR se facilita debido a la eliminación previa de la contribución espectral de la fase móvil. Por otra parte, el uso de MCR-ALS permite una mejor recuperación de los perfiles espectrales y de concentración obtenidos tras la corrección inicial de la señal de *background*.

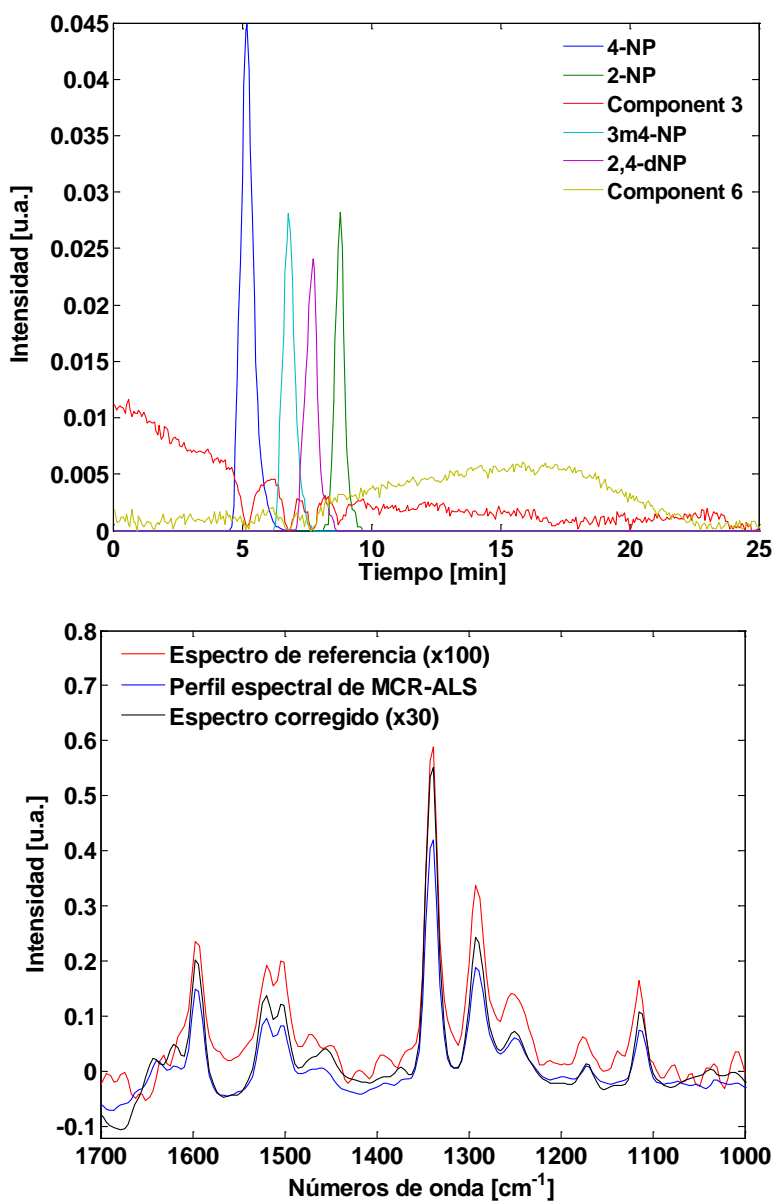


Figura R-13. Aplicación de MCR-ALS al conjunto de datos de nitrofenoles después de corregir la señal de fondo; arriba: Perfiles de concentración para los seis componentes calculados empleando MCR-ALS; abajo: espectro de referencia, perfil espectral calculado empleando MCR-ALS y espectro extraído después de aplicar la corrección de la señal de fondo de 4-NP.

6. Extracción quimiométrica de cromatogramas específicos para un analito en on-line LC-IR

Los procedimientos descritos anteriormente desarrollados durante esta Tesis, tuvieron como objetivo la corrección de los cambios en la señal debida a la fase móvil producidos durante una elución en gradiente. En este estudio, se aplicó un método multivariante para la extracción de cromatogramas específicos de un analito sin necesidad de llevar a cabo una corrección previa del *background* buscando, simultáneamente, un aumento significativo de la sensibilidad y selectividad de la señal. Para evaluar la utilidad de SBC en *on-line* LC-IR para la extracción de cromatogramas específicos para un analito, se investigaron diferentes inyecciones de mezclas de patrones de 2-nitrofenol (2-NP), 3-methyl-4-nitrofenol (3m4-NP), 2,4-dinitrofenol (2,4-dNP) y 4-nitrofenol (4-NP). Estos analitos se caracterizan por la gran semejanza entre sus espectros IR. Además, se seleccionaron unas condiciones experimentales que proporcionaran un alto solapamiento cromatográfico entre los picos de 3m4-NP y 2,4-dNP. Se utilizó un sistema de separación con una columna C₁₈ y un gradiente de acetonitrilo:agua de 35:65 a 85:15 v/v en 20 minutos. El acoplamiento se llevó a cabo empleando una celda de flujo con un paso óptico de 16.5 µm. En este estudio, se evaluó el funcionamiento del algoritmo en dos situaciones que se diferenciaban en el contenido de información disponible para la extracción del cromatograma.

En la primera situación (A), la extracción del cromatograma de 2,4-dNP se llevo a cabo sin el uso de información acerca de los interferentes presentes en la matriz de la muestra. Para ello, se utilizó para el cálculo del vector de regresión (*b*) un conjunto de espectros adquiridos durante el re-equilibrado del sistema cromatográfico. Como se puede ver en los cromatogramas mostrados en la Figura R-14, la presencia de los interferentes no incluidos en el modelo afectó la especificidad de la determinación de 2,4-dNP. Por otra parte, es muy significativo que se compensó la intensa contribución del eluyente obteniendo una línea base sin pendiente con el ruido distribuido aleatoriamente alrededor de cero.

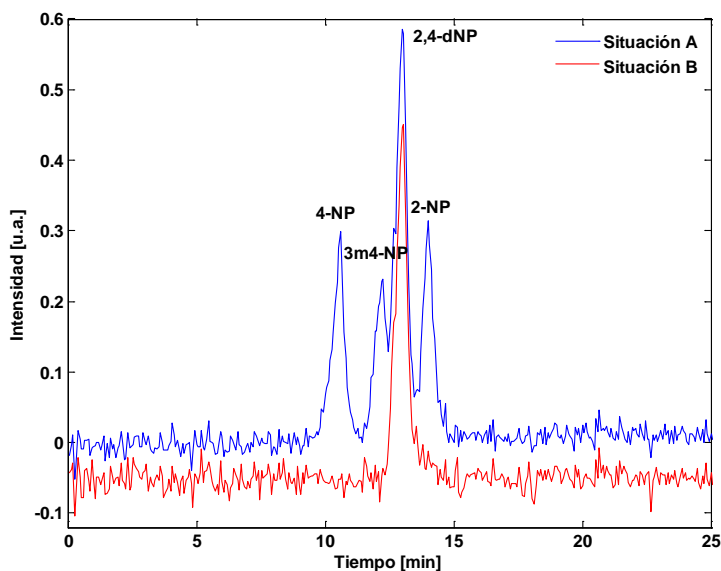


Figura R-14. Comparación de cromatogramas de 2,4-dNP extraídos utilizando espectros registrados durante el re-equilibrio del sistema LC después del gradiente (Situación A) y espectros medidos durante la inyección de un 'blanco de muestra' (Situación B) para el cálculo de la matriz de covarianza. Nota: el cromatograma B se desplazó a un valor igual a -0.05.

En la segunda situación investigada (B), se utilizó información espectral acerca de los otros componentes de la muestra en el cálculo del vector de regresión (b). Para ello, se empleó como matriz de 'ruido' un 'blanco de muestra', es decir, se utilizó un cromatograma obtenido a partir del análisis de una disolución de patrones de los analitos interferentes (4-NP, 3m4-NP y 2-NP). Por lo tanto, esta matriz de datos incluyó el ruido instrumental, la variación de la señal de fondo debido al cambio de la absorbancia del eluyente y los espectros de los compuestos interferentes. En este caso, el cromatograma obtenido fue altamente específico para el analito de interés como se puede apreciar en la Figura R-14.

Los resultados obtenidos demostraron la aplicabilidad directa de un método multivariante (*Science Based Calibration*, SBC) en *on-line* LC-IR en régimen de gradiente. Una selección apropiada del vector 'respuesta' (en este caso, el espectro de absorbancia) del analito y de la matriz espectral empleada para el cálculo del vector de regresión b permiten una mejora muy importante en los niveles de sensibilidad y selectividad obtenidos.

7.- Desarrollo de mejoras instrumentales dirigidas a una mejora significativa de los niveles de sensibilidad del acoplamiento on-line LC-IR

Como se ha descrito previamente, una de las principales limitaciones del acoplamiento *on-line* de LC-IR es una baja sensibilidad. Debido a esto, uno de los objetivos principales de esta Tesis fue continuar con el desarrollo de instrumentación capaz de mejorar sensiblemente esta limitación con el fin de aumentar el uso de este acoplamiento.

7.1 Desarrollo del acoplamiento on-line capillary LC-FTIR mediante el empleo de micro-celdas de flujo

En este estudio, se acoplaron por primera vez de forma *on-line* un espectrómetro FTIR y un sistema de LC capilar. Para ello, se empleó una micro-celda de flujo con ventanas de CaF₂ transparentes al IR y unas dimensiones de (2 x 150 mm), un paso óptico de 25 μm y un volumen interno de 7.5 nL. Además, esta micro-celda se instaló en un sistema de condensación del haz (*beam condenser*) necesario para la focalización del haz de IR a través del canal de la micro-celda.

Se utilizó como sistema modelo la separación mediante LC en fase reversa de nitrofenoles descrita en estudios anteriores empleando gradientes lineales de agua (0.05% TFA):acetonitrilo con un contenido de acetonitrilo entre el 50 y el 65% en 15 minutos. La separación se realizó empleando una columna C₁₈ (300 μm ID x 150 mm, 3 μm, 100 Å), un flujo de 3 μL min⁻¹ y un volumen de inyección de 1 μL.

En la Figura R-15 se pueden ver los espectros obtenidos durante la inyección de 1 μL de una disolución de patrones de 4-NP (270 ng μL⁻¹), 3m4-NP (230 ng μL⁻¹), 2,4-dNP (230 ng μL⁻¹) y 2-NP (230 ng μL⁻¹) después de aplicar la corrección de la señal de fondo. En la figura se aprecian la elución del disolvente a 4 min y la ventana de elución de los analitos entre 8 y 11 min. Los cambios en la señal de fondo debida a la elución en gradiente se compensaron de forma exacta mediante el empleo de BGC-RSM, pudiendo recuperar espectros de los analitos seleccionados obteniendo valores de coeficientes de correlación con espectros de referencia previamente adquiridos, entre el 89 y el 95.8%. Bajo estas condiciones experimentales se obtuvieron límites de detección entre 35 y 94 ng *on-column*, mejorando significativamente los LODs que se encuentran en la bibliografía.

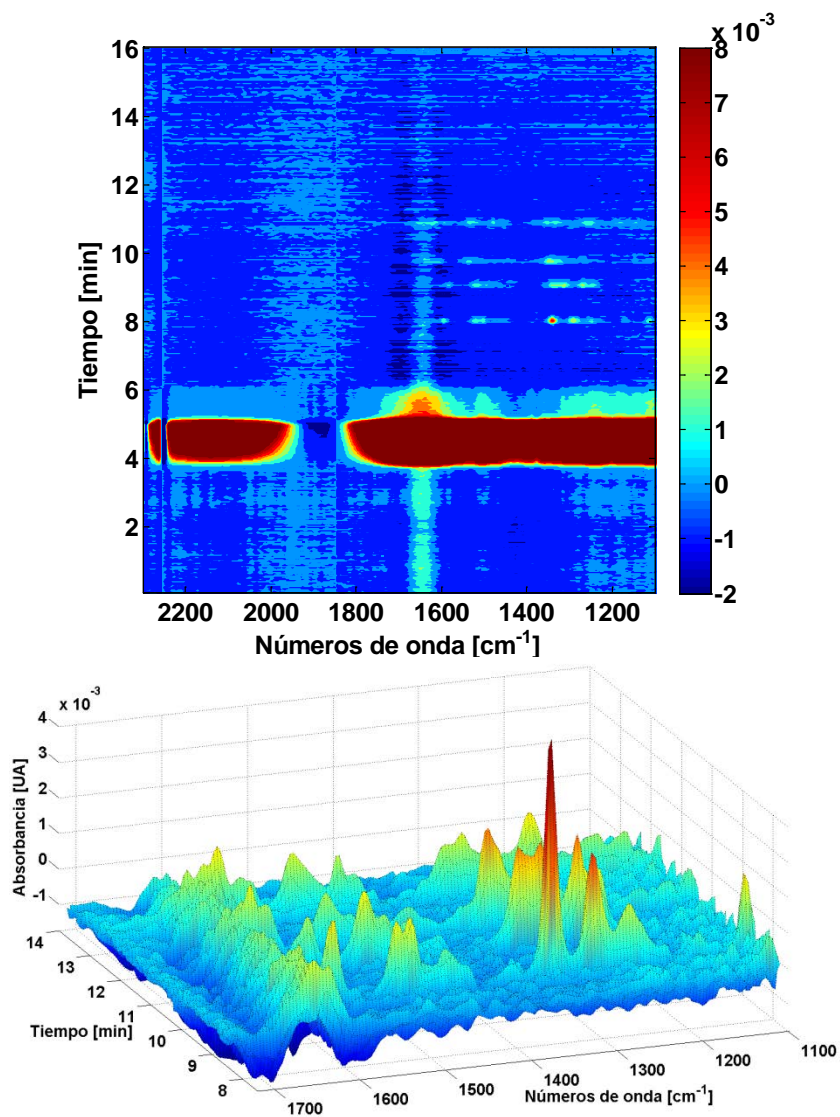


Figura R-15. Espectros corregidos registrados durante la inyección de 1 μL de una disolución de 4-NP (270 $\text{ng } \mu\text{L}^{-1}$), 3m4-NP (230 $\text{ng } \mu\text{L}^{-1}$), 2,4-dNP (230 $\text{ng } \mu\text{L}^{-1}$) y 2-NP (230 $\text{ng } \mu\text{L}^{-1}$) (arriba) y representación gráfica en tres dimensiones de la ventana de elución de los analitos (abajo).

7.2 Desarrollo de un sistema on-line LC-IR con detección dual-QC-laser

Como se ha indicado al principio de este resumen, el gran avance tecnológico sufrido por los QC-láseres en los últimos años, tanto respecto a la intensidad de la luz emitida como a las regiones accesibles del espectro IR, hacen que su uso en sistemas IR sea una opción realista para la mejora de los niveles de sensibilidad. Debido a esto, en este estudio se desarrolló un sistema LC-IR que incorporó el uso simultáneo de dos QC-láseres para la detección *on-line*. Con el objetivo de evaluar las características del acoplamiento, se analizó el contenido en muestras de vino y zumos de uva de ácidos cítrico, tartárico, acético y málico, glucosa, fructosa, glicerol y etanol.

La Figura R-16 muestra una fotografía de la óptica del *set-up* experimental. Se emplearon dos QC-láseres con máximos de emisión a 1080 cm^{-1} y 1393 cm^{-1} y una celda de flujo con un paso óptico de $52\text{ }\mu\text{m}$. El *set-up* experimental incluyó unidades de control de la temperatura y generación de señal y sistemas de adquisición de datos. La separación cromatográfica se llevó a cabo empleando una columna de intercambio aniónico y agua desionizada como fase móvil en régimen isocrático.

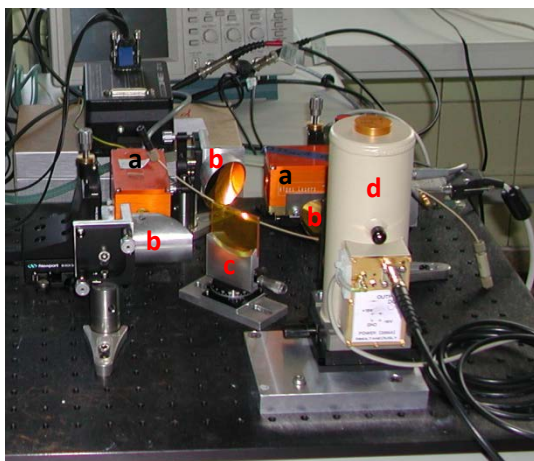


Figura R-16. Montaje experimental incluyendo dos QC-láseres (a), tres espejos de oro (b), un divisor de haz de ZnSe (c) y un detector MCT (d).

Bajo estas condiciones experimentales, se pudieron resolver los picos de los ocho analitos investigados. Los picos de los analitos mostraron una alta simetría a excepción de los picos de ácido cítrico y ácido tartárico que mostraron una forma distorsionada

(*fronting*). Los coeficientes de regresión lineal obtenidos a partir del análisis de una serie de patrones mostraron alta linealidad ($R^2 > 0.99$). Se evaluó el nivel de precisión de las concentraciones obtenidas mediante el análisis, por triplicado, de las muestras reales, obteniendo valores de RSD entre el 0.1 y el 10% para todas las muestras y todos los analitos.

A modo de ejemplo, la Figura R-17 muestra la señal registrada durante el análisis de una muestra en la que se cuantificó el contenido de glucosa, ácido tartárico, fructosa, glicerol y etanol. Finalmente se llevó a cabo un estudio de recuperaciones obteniendo valores entre el 95 y el 109%, confirmando la exactitud del método.

Este estudio demostró que el uso de QC-láseres permite mejorar la sensibilidad del acoplamiento LC-IR, ya que facilitó el uso de una celda de flujo con un paso óptico elevado en comparación con las celdas utilizadas empleando fuentes *globalar*. Además, la frecuencia de adquisición de puntos del cromatograma puede ser aumentada a valores del orden de 2 puntos s^{-1} o superior, lo que supone un aumento considerable si se compara con la frecuencia de adquisición de (aproximadamente) 0.5 puntos s^{-1} que se suele emplear utilizando espectrómetros FTIR convencionales.

Sin embargo, a pesar de los buenos resultados obtenidos en este estudio, la relación señal-ruido podría verse aumentada significativamente con pequeñas modificaciones del *set-up*, entre las que se encuentran: i) mejora en la adquisición de datos, ii) emplear QC-láseres más estables y iii) adaptar el sistema cromatográfico, por ejemplo utilizando columnas con un menor diámetro interno.

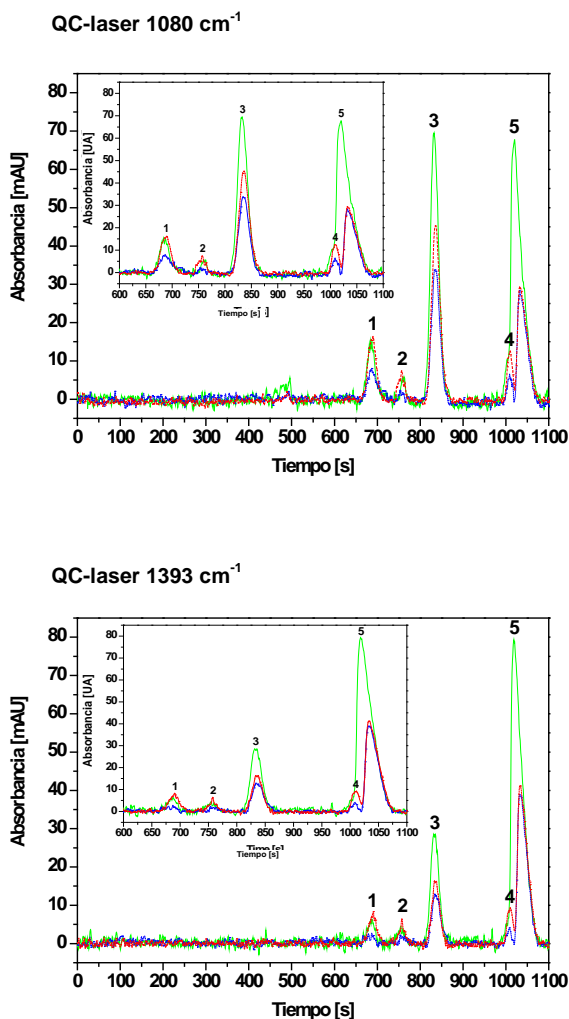


Figura R-17. Cromatogramas de una muestra de vino blanco (muestra 1); cromatogramas registrados con el QC-laser que emite a 1080 cm^{-1} (arriba) y cromatogramas registrados con el QC-laser que emite a 1393 cm^{-1} (abajo); línea verde entera: muestra 1, línea punteada azul: muestra 1 diluida 1:2, línea roja punteada: muestra 1 con patrón adicionado conteniendo glucosa, ácido tartárico, fructosa, glicerol y etanol; la ampliación muestra la región entre 600 y 1100 s; (1) glucosa - 686 s, (2) ácido tartárico - 761 s, (3) fructosa - 830 s, (4) glicerol - 1006 s, (5) etanol - 1033 s.

8. Conclusiones

El acoplamiento *on-line* LC-IR proporciona información molecular específica y dispone de unas prestaciones de sensibilidad, velocidad de respuesta y selectividad adecuadas para el desarrollo de aplicaciones en diferentes campos. Por otra parte, este tipo de acoplamiento presenta dos importantes limitaciones derivadas de la intensa absorción que presentan los componentes de las fases móviles: la baja sensibilidad de la técnica IR y la necesidad de una eliminación de la señal de la fase móvil, especialmente problemática en el caso de separaciones en régimen de gradiente.

Con el objetivo final de extender el empleo de este tipo de acoplamiento, esta Tesis Doctoral se enfocó hacia el desarrollo de herramientas quimiométricas e instrumentales que permitieran superar las limitaciones anteriormente descritas. A partir de los trabajos desarrollados durante la realización de esta Tesis, se pueden extraer las siguientes conclusiones:

Mejoras en régimen isocrático

1. Los métodos isocráticos desarrollados han demostrado su utilidad en diferentes campos de aplicaciones utilizando tanto diclorometano como mezclas de acetonitrilo:agua como fases móviles. Su rendimiento ha podido ser mejorado al aplicar métodos multivariantes (SBC) para la extracción de la señal cromatográfica y un modo diferente de adquisición de datos (*rapid scan*).

Nuevas herramientas quimiométricas

2. Las nuevas estrategias y métodos quimiométricos desarrollados para la corrección de la absorbancia debida a los componentes de la fase móvil han demostrado su utilidad para el desarrollo de métodos cuantitativos y cualitativos, tanto en régimen isocrático como en gradiente, empleando fases móviles compuestas por acetonitrilo:agua, metanol:agua, etanol:agua y 2-propanol:agua.

Los métodos desarrollados se pueden clasificar en dos grandes grupos, en función de la necesidad o no de utilizar una matriz espectral de referencia (**RSM**), para llevar a cabo la corrección. Entre los métodos quimiométricos que utilizan este tipo de matrices de referencia se puede hacer una segunda subdivisión. Por un lado, se encuentran los

métodos basados en la selección del espectro óptimo de referencia en la **RSM** de acuerdo con diferentes parámetros de identificación (IP). En este sub-grupo, se encuentran los siguientes métodos desarrollados durante esta Tesis: AR-BGC-RSM, RW-BGC-RSM, PLS-BGC-RSM y p2p-BGC-RSM. Por otro lado, se encuentran los métodos que utilizan la **RSM** para establecer un ajuste polinómico entre la absorbancia a cada número de onda y un parámetros de identificación (IP) para, posteriormente, predecir y corregir la absorbancia debida a la fase móvil durante la medida del cromatograma de la muestra (**SM**). En este sub-grupo, se encuentran los siguientes métodos desarrollados durante esta Tesis: AR-Polyfit, SW-Polyfit. En un tercer sub-grupo, se encuentran los dos métodos multivariantes basados en el empleo de SIMPLISMA o PCA, en combinación con CLS y matrices espectrales de referencia.

El otro grupo incluye el método basado en el empleo de *cubic smoothing splines* (CSS), que no utiliza una matriz de referencia para llevar a cabo la corrección, así como la resolución de curvas multivariante (MCR-ALS).

3. No se puede seleccionar un único método de corrección de la señal debida a la absorción de la fase móvil como óptimo y válido para cualquier situación experimental, ya que el rendimiento de cada uno de los métodos desarrollados en esta Tesis depende de diferentes parámetros experimentales. A pesar de esto, distintos métodos pueden proporcionar resultados estadísticamente comparables sobre los mismos datos. Debido a esto, el usuario tiene que conocer las capacidades y limitaciones del sistema instrumental para poder seleccionar el método de corrección óptimo para cada situación.

En resumen, la selección del método óptimo de corrección de *background* vendrá determinada tanto por las características de los métodos de corrección como por las condiciones experimentales específicas de cada situación. Por ejemplo, factores como el tipo de fase móvil y de gradiente, la frecuencia de adquisición de datos, el espectro IR de los analitos, la estabilidad del detector o la necesidad de llevar a cabo una corrección *on-the-fly*, entre otros, se han de tener en cuenta a la hora de seleccionar el método de corrección. Como regla empírica, los métodos más simples son más robustos y por lo tanto deben aplicarse de forma prioritaria si los resultados obtenidos son comparables a los obtenidos con métodos más complejos.

De forma general, los métodos AR-, SW-, p2p-, PLS-BGC-RSM y Polyfit-RSM sólo deben aplicarse cuando se dispone de una región espectral característica de la composición de la fase móvil libre de interferencias espectrales por los componentes de la muestra. Por otra parte, un número y/o una distribución de espectros en la **RSM** inadecuada, o la falta de estabilidad instrumental afecta de forma muy negativa a la exactitud de estos métodos de corrección.

El método CSS presenta la ventaja de no utilizar una **RSM** y de minimizar al máximo el efecto de la falta de estabilidad instrumental sobre la exactitud de la corrección. Además, es de fácil uso ya que el número de parámetros o variables que el usuario tiene que elegir es mínimo. Sin embargo, presenta el inconveniente de que la exactitud de la corrección puede depender de la distribución de los *knots* y ésta, a su vez, de la presencia de un mayor o menor número de picos en el cromatograma y de su resolución cromatográfica.

En el caso de los métodos multivariantes, basados en el uso de SIMPLISMA o PCA en combinación con CLS, la relación entre el tamaño de la **RSM** y la exactitud de la corrección es menor que en otros métodos (p.ej. AR-BGC-RSM). Además, el uso de estas potentes herramientas quimiométricas facilita la corrección de la señal de fondo en situaciones de mayor dificultad (p. ej. tamaño reducido de la **RSM** y co-elución de un gran número de analitos).

El diagrama de flujo mostrado en la Figura R-18 incluye algunas de las consideraciones más relevantes a tener en cuenta para la selección del método de corrección de la señal de fondo; a la vez ofrece una visión de conjunto de los métodos desarrollados en esta Tesis.

4. El uso de *Multivariate Curve Resolution – Alternating Least Squares* (MCR-ALS) en sistemas *on-line* LC-IR en régimen de gradiente se ve facilitado por la eliminación previa de la contribución de la fase móvil. El análisis mediante MCR-ALS de cromatogramas corregidos mejora la recuperación de los perfiles de concentración y espectrales de los analitos. Además, el análisis mediante MCR-ALS permite la eliminación de contribuciones espectrales residuales de la fase móvil presentes en cromatogramas previamente corregidos.

5. El uso de *Science Based Calibration* en *on-line* LC-IR permite la extracción de cromatogramas específicos de los analitos sin necesidad de llevar a cabo una corrección previa del *background*. Este procedimiento proporciona, simultáneamente, un aumento significativo de la sensibilidad y especificidad de la señal tanto en régimen isocrático como en gradiente. Por otra parte, debe tenerse en cuenta que el método SBC no corrige la señal, por lo que, en el caso de eluciones en gradiente no se recuperan los espectros corregidos.

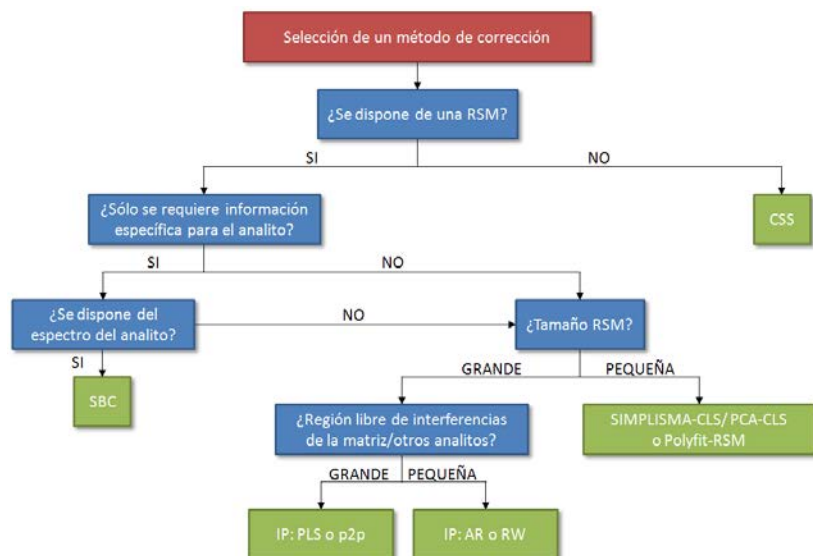


Figura R-18. Diagrama de flujo para la selección del método de corrección de fondo más adecuado.

Desarrollos instrumentales

6. El uso de micro-celdas de flujo con un volumen del orden de nL, en combinación con un sistema LC capilar ha demostrado ser una vía para una mejora muy importante de la sensibilidad del acoplamiento *on-line*.

7. Los láseres de cascada cuántica (QC-láseres) reúnen todas las características necesarias para ser utilizados en sistemas *on-line* LC-IR: alta potencia de emisión, tamaño reducido, respuesta rápida, funcionamiento a temperatura ambiental y bajo consumo de energía.

El uso simultáneo de dos QC-láseres en *on-line* LC-IR facilita la detección y la mejora la sensibilidad permitiendo el empleo de celdas de flujo con un mayor paso óptico. En esta Tesis, a pesar de emplear una fase móvil acuosa, permitió el uso de una celda de flujo estándar con un paso óptico de 52 μm . Considerando que utilizando una fuente Global, el paso óptico en esas condiciones está limitado a un máximo de 7-8 μm , representa una ganancia en sensibilidad por un factor de ~ 7 .

Otra ventaja que presenta el uso de QC-láseres en *on-line* LC-IR es su reducido tiempo de respuesta, lo que facilita una alta frecuencia de registro de datos y, por lo tanto, mejora los niveles de precisión en el desarrollo de métodos cuantitativos.

Perspectivas para el futuro

A partir de los resultados obtenidos en esta Tesis, se pueden identificar una serie de posibilidades que permitirían una mejora de los desarrollos presentados.

8. En sistemas *on-line* LC-QC-laser, el desarrollo de las siguientes modificaciones proporcionaría muy probablemente, importantes mejoras en sensibilidad: i) modificación del sistema de adquisición de datos; ii) mejora de la estabilidad de los *laser drivers* para disminuir el ruido y las derivas observadas en el *set-up* utilizado en esta Tesis; y iii) el empleo de QC-láseres sintonizables (*tunable QC-lasers*) desarrollados muy recientemente, con una potencia de emisión más alta lo que facilitaría el uso de pasos ópticos mayores e intervalos espectrales más amplios.

En resumen, tal como se había planteado al definir los objetivos iniciales, esta Tesis Doctoral ha aportado soluciones quimiométricas e instrumentales a las dos limitaciones más importantes que venían restringiendo el empleo de *on-line* LC-IR: baja sensibilidad y falta de métodos para la eliminación de la señal del eluyente en régimen de gradiente. Las herramientas instrumentales y quimiométricas descritas en esta Tesis pueden ser aplicadas en futuros desarrollos como, por ejemplo, en el desarrollo de sistemas que combinen QC-láseres sintonizables, celdas de flujo miniaturizadas, sistemas LC capilares y nuevos métodos quimiométricos para la corrección de la señal del eluyente facilitando así la aplicación de *on-line* LC-IR para la resolución de nuevos retos analíticos.

Abstract

The coupling of Liquid Chromatography (LC) to infrared (IR) spectrometry is an interesting analytical tool, because high resolution provided by LC is combined with the non-destructive and molecular specific information of IR spectrometry. However, the potential of on-line LC-IR employing a flow cell interface, characterized by its technical simplicity, cannot yet be fully exploited due to the limited sensitivity of IR detection and difficulties in on-line measurements arising from the dominating absorption of most of the commonly used mobile phase components. Accordingly, the objective of this thesis can be divided into three parts: Innovations in the field of isocratic separations are discussed in Chapter 2. New methods for chemometric background correction, especially focusing on gradient LC applications, are described in Chapters 3 to 6. The last chapter (Chapter 7) deals with instrumental developments of LC-IR set-ups. In summary, on-line LC-IR instrumentation as well as new chemometric tools for user-friendly background compensation, both necessary for enabling new applications of this analysis technique, should be improved or developed.

Chapter 2 describes latest improvements in the field of isocratic separations with on-line IR detection. A method for the determination of lecithin and soybean oil in dietary supplements using on-line Gel Permeation Chromatography – Attenuated Total Reflectance – Infrared (GPC-ATR-IR) was developed including a simple procedure to select the optimum wavenumber used for the extraction of characteristic elution profiles of each analyte. Another method was developed for the monitoring of polymerized triglycerides in deep-frying oil by on-line GPC-IR spectrometry using the Science Based Calibration (SBC) multivariate approach for the extraction of chromatograms improving both, sensitivity and selectivity of the technique as compared to the use of the ‘classical’ univariate approach consisting of the monitoring of the change in absorption in a defined spectral interval with time. Finally, for the determination of glycolic acid in cosmetics a simple on-line LC-IR procedure was developed employing the rapid scan data acquisition mode.

Chapter 3 deals with different methods for background correction in on-line LC-IR using reference spectra matrices (**RSM**). In the course of this, the determination of the

critical eluent composition for polyethylene glycols using methanol as organic modifier was discussed employing the absorbance ratio as identification parameter for background correction. Results found for the estimation of the chromatographic critical conditions of PEG correspond to a methanol:water composition of 86.5:13.5% v/v and were in good agreement with previously published results. For the determination of sugars in beverages employing acetonitrile as organic modifier, again the absorbance ratio was used as identification parameter. Fructose, glucose, sucrose and maltose could be separated, identified and quantified in commercial samples with limits of detection between 0.4 and 0.6 mg mL⁻¹. Moreover, a Partial Least Squares (PLS) procedure for automated background correction was introduced. Its applicability for the measurement of the analyte spectra in isocratic and gradient LC has been tested, achieving accurate results in both experimental conditions. Finally, the application of point-to-point matching algorithms for background correction was discussed. The proposed background correction process has been used in on-line LC-IR using acetonitrile (0.08% v/v TFA):water (0.08% v/v TFA) gradients between 35 and 85% acetonitrile for the determination of nitrophenols as model compounds, obtaining accurate results.

Chapter 4 deals with the compensation of the background contribution employing column-wise techniques. On the one hand side, polynomial regressions modelling the background absorbance at each wavenumber throughout the gradient run were used. The proposed method has been tested on real reversed-phase on-line LC-IR data sets using a mobile phase composed by acetonitrile and water. This approach reduces the influence of the size of the **RSM** on the accuracy of the background correction process, thus allowing the use of reduced size **RSMs**. On the other hand, cubic smoothing splines were used for background correction. This method works without the need of a **RSM** and it was tested and evaluated by means of simulated as well as real data sets obtained employing different alcoholic organic modifiers (methanol, 2-propanol and ethanol).

In Chapter 5, background correction based on factor analysis, multivariate curve resolution and reference spectra matrices was discussed. The contribution of the background absorption to overall LC-IR signals could be compensated using two

approaches based on Principal Component Analysis (PCA) and simple-to-use interactive self modeling analysis (SIMPLISMA), obtaining good results. multivariate curve resolution-alternating least squares (MCR-ALS) was applied to background-corrected data improving peak and spectral resolution and eliminating remaining signal variation due to background absorption and detector drift.

The chemometric extraction of 'analyte-specific' chromatograms in on-line LC-IR was discussed in Chapter 6. Obtained results confirm that the SBC method is particularly well suited for recovering an 'analyte-specific' signal from on-line LC-IR chromatograms. The usefulness of this method could be confirmed even when the analyte was injected in the presence of unknown interfering compounds and no deep knowledge of the sample constituents was needed.

The last chapter describes instrumental developments in on-line LC-IR. First, on-Line IR detection in gradient capillary liquid chromatography using micromachined nanoliter-flow cells was discussed. Four model compounds were separated and identified using an acetonitrile:H₂O gradient with limits of detection in the concentration range of 35-94 ng μL^{-1} , representing an increase in mass sensitivity by a factor of approximately 30 as compared to LC systems employing a 4.6 mm ID column. In spite of using a gradient technique, high quality analyte spectra could be recovered by employing background correction using a reference spectra matrix and the relative absorbance as an identification parameter. The last chapter also focuses on the development of LC with on-line dual Quantum Cascade Laser (QC-laser) detection. Compared to the use of state-of-the-art FTIR spectrometers, the use of the developed QC-laser based system provided a significant improvement in both, sensitivity and data acquisition frequency.

List of Impact Factors

List of impact factors of the scientific journals where papers were published in the course of this thesis:

TrAC, Trends in Analytical Chemistry: 6.602 (2010)

Analytical Chemistry: 5.874 (2010)

Analytica Chimica Acta: 4.311 (2010)

Journal of Chromatography A: 4.194 (2010)

Analytical and Bioanalytical Chemistry: 3.841 (2010)

Talanta: 3.722 (2010)

Food Chemistry: 3.458 (2010)

Journal of Separation Science: 2.631 (2010)

Applied Physics B: Lasers and Optics: 2.240 (2010)

Applied Spectroscopy: 1.729 (2010)

Chromatographia: 1.075 (2010)

List of Publications

CHAPTER 1

Recent advances in on-line liquid chromatography - infrared spectrometry, J. Kuligowski, G. Quintás, S. Garrigues, B. Lendl, M. de la Guardia, **Trends in Analytical Chemistry**, 29 (2010) 544-552.

Analytical potential of mid infrared detection in capillary electrophoresis and liquid chromatography: A review. J. Kuligowski, G. Quintás, M. de la Guardia, B. Lendl, **Analytica Chimica Acta**, 679 (2010) 31-42.

CHAPTER 2

On-line gel permeation chromatography–attenuated total reflectance–Fourier transform infrared determination of lecithin and soybean oil in dietary supplements, J. Kuligowski, G. Quintás, F.A. Esteve-Turrillas, S. Garrigues, M. de la Guardia, **Journal of Chromatography A**, 1185 (2008) 71-77.

Monitoring of Polymerized Triglycerides in Deep-frying Oil by on-line Gel Permeation Chromatography–Fourier Transform Infrared Spectrometry using the Science Based Calibration Multivariate Approach, J. Kuligowski, G. Quintás, S. Garrigues, M. de la Guardia, **Chromatographia**, 71 (2010) 201-209.

Determination of glycolic acid in cosmetics by on-line liquid chromatography–Fourier transform infrared spectrometry, J. Kuligowski, A. Breivogel, G. Quintás, S. Garrigues and M. de la Guardia, **Analytical and Bioanalytical Chemistry**, 392 (2008) 1383-1389.

CHAPTER 3

Determination of critical eluent composition for polyethyleneglycols using on-line liquid chromatography–Fourier transform infrared spectrometry, J. Kuligowski, G. Quintás, S. Garrigues, M. de la Guardia, **Analytica Chimica Acta**, 624 (2008) 278-285.

On-line gradient liquid chromatography–Fourier transform infrared spectrometry determination of sugars in beverages using chemometric background correction, J. Kuligowski, G. Quintás, S. Garrigues, M. de la Guardia, **Talanta**, 77 (2008) 779-785.

Procedure for automated background correction in flow systems with IR spectroscopic detection and changing liquid phase composition, G. Quintás, J. Kuligowski, B. Lendl, **Applied Spectroscopy**, 63 (2009) 1363-1369.

Application of point-to-point matching algorithms for background correction in on-line liquid chromatography–Fourier transform infrared spectrometry (LC–FTIR), J. Kuligowski, G. Quintás, S. Garrigues, M. de la Guardia, **Talanta**, 80 (2010) 1771-1776.

CHAPTER 4

New background correction approach for on-line liquid chromatography - Fourier transform infrared spectrometry based on polynomial regressions, J. Kuligowski, G. Quintás, S. Garrigues, M. de la Guardia, **Journal of Chromatography A**, 1216 (2009) 3122-3130.

Cubic smoothing splines background correction in on-line liquid chromatography - Fourier transform infrared spectrometry, J. Kuligowski, D. Carrión, G. Quintás, S. Garrigues, M. de la Guardia, **Journal of Chromatography A**, 1217 (2010) 6733-6741.

CHAPTER 5

Background correction and multivariate curve resolution in hyphenated liquid chromatography infrared using factor analysis and alternating least squares, J. Kuligowski, G. Quintás, R. Tauler, B. Lendl, M. de la Guardia, **Analytical Chemistry**, (2011) DOI: 10.1021/ac2004407.

CHAPTER 6

Chemometric extraction of analyte-specific chromatograms in on-line gradient LC-infrared spectrometry, J. Kuligowski, G. Quintás, S. Garrigues, M. de la Guardia, **Journal of Separation Science**, 32 (2009) 1-7.

CHAPTER 7

On-Line Fourier Transform Infrared Spectrometric Detection in Gradient Capillary Liquid Chromatography Using Nanoliter-Flow Cells, G. Quintás, J. Kuligowski, B. Lendl, **Analytical Chemistry**, 81 (2009) 3746-3753.

High performance liquid chromatography with on-line dual quantum cascade laser detection for the determination of carbohydrates, alcohols and organic acids in wine and grape juice, J. Kuligowski, G. Quintás, B. Lendl, **Applied Physics B: Laser and Optics**, 99 (2010) 833-840.

Other publications not included in this thesis

Determination of lecithin and soybean oil in dietary supplements using partial least squares–Fourier transform infrared spectroscopy, J. Kuligowski, G. Quintás, S. Garrigues, M. de la Guardia, **Talanta**, 77 (2008) 229-234.

New cut-off criterion for uninformative variable elimination in multivariate calibration of near-infrared spectra for the determination of heroin in illicit street drugs, J. Moros, J. Kuligowski, G. Quintás, S. Garrigues, M. de la Guardia, **Analytica Chimica Acta**, 630 (2008) 150-160.

Direct determination of polymerized triglycerides in deep-frying olive oil by Attenuated Total Reflectance–Fourier Transform Infrared Spectrometry using Partial Least Squares regression, J. Kuligowski, G. Quintás, S. Garrigues, M. de la Guardia, **Analytical and Bioanalytical Chemistry**, 397 (2010) 861-869.

Differentiation of walnut wood species and steam treatment using ATR-FTIR and partial least squares discriminant analysis (PLS-DA), A.J. Hobro, J. Kuligowski, M. Döll, B. Lendl, **Analytical and Bioanalytical Chemistry**, 398 (2010) 2713-2722.

Science Based Calibration for the extraction of ‘analyte-specific’ high performance liquid chromatography - diode array chromatograms in environmental analysis, J. Kuligowski, M. Martínez Galera, M.D. Gil García, M.J. Culzoni, H.C. Goicoechea, S. Garrigues, G. Quintás, M. de la Guardia, **Talanta**, 83 (2011), 1158-1165.

Sample classification for improved performance of PLS models applied to the quality control of deep frying oils of different botanic origins analyzed using ATR-FTIR spectroscopy, J. Kuligowski, D. Carrión, G. Quintás, S. Garrigues, M. de la Guardia, **Analytical and Bioanalytical Chemistry**, 399 (2011) 1305-1314.

Determination of sugars in depilatory formulations: A green analytical method employing infrared detection and Partial Least Squares regression, M. Cascant, J. Kuligowski, S. Garrigues, M. de la Guardia, **Talanta**, 85 (2011), 1721-1729.

Direct determination of polymerized triacylglycerides in deep-frying vegetable oil by near infrared spectroscopy using Partial Least Squares regression, J. Kuligowski, D. Carrión, G. Quintás, S. Garrigues, M. de la Guardia, **Food Chemistry**, 131 (2012), 353-359.

A rapid method for the differentiation of yeast cells grown under carbon and nitrogen-limited conditions by means of partial least squares discriminant analysis employing infrared micro-spectroscopic data of entire yeast cells, J. Kuligowski, Ch. Herwig, B. Lendl, **Analyst**, (2011), sent for publication.

A novel approach for assessing injection volume limits: application to one- and two-dimensional liquid chromatography with gradient elution, F. Bedani, E. Reingruber, J. Kuligowski, W. Th. Kok, H.G. Janssen, (2011), in preparation.

List of Scientific Communications

CHAPTER 2

Infrared Spectroscopy for the Determination of Polymerized Triglycerides in Deep-frying Vegetable oils, **poster**, Euroanalysis XVI, 11.09. – 15.09.2011, Belgrade, Serbia.

Determination of glycolic acid in cosmetics by on-line liquid chromatography – Fourier transform infrared spectrometry, **oral presentation**, XII Jornadas de Análisis Instrumental (JAI), 21. – 23.10.2008, Barcelona, Spain.

CHAPTER 3

A MATLAB graphical user-friendly interface for background correction in continuous liquid flow systems, **poster**, XXI Reunión Nacional de Espectroscopía, V Congreso Ibérico de Espectroscopía, 09. – 11.09.2008, Murcia, Spain.

Determination of critical eluent composition for Polyethylenglycols using on-line gradient liquid chromatography- Fourier transform infrared spectrometry, **poster**, XXI Reunión Nacional de Espectroscopía, V Congreso Ibérico de Espectroscopía, 09. – 11.09.2008, Murcia, Spain.

Application of on-line gradient liquid chromatography – Fourier transform infrared spectrometry for the determination of sugars in beverages using chemometric background correction, **oral presentation**, XII Jornadas de Análisis Instrumental (JAI), 21. – 23.10.2008, Barcelona, Spain.

Chemometric background correction in on-line liquid chromatography - Fourier transform infrared spectrometry (LC-FTIR) applying a point-to-point matching algorithm, **poster**, Euroanalysis XV, 06.09. – 10.09.2009, Innsbruck, Austria.

CHAPTER 4

New method for background correction in on-line gradient liquid chromatography – Fourier transform infrared spectrometry based on polynomial regressions, **oral presentation**, XII Jornadas de Análisis Instrumental (JAI), 21. – 23.10.2008, Barcelona, Spain.

New Background Correction Based on Cubic Smoothing Splines in On-Line Liquid Chromatography - Fourier Transform Infrared Spectrometry, **poster**, Eleventh International Symposium on Hyphenated Techniques in Chromatography and Hyphenated Chromatographic Analyzers (HTC-11), 27.01. – 29.01.2010, Bruges, Belgium.

CHAPTER 5

Multivariate Approaches for Background Correction of Data obtained from on-line Liquid Chromatography with Infrared Spectrometric Detection, **oral presentation**, Euroanalysis XVI, 11.09. – 15.09.2011, Belgrade, Serbia.

CHAPTER 6

Science Based Calibration for the extraction of 'analyte-specific' chromatograms in LC, **oral presentation**, 28th International Symposium on Chromathography (ISC), 12.09. – 16.09.2010, Valencia, Spain.

CHAPTER 7

Nuevos desarrollos instrumentales y quimiométricos para el acoplamiento en línea de la CL y la espectroscopia IR, **oral presentation**, I Simposio de Jóvenes Investigadores en Espectroscopia Aplicada, 06. – 09.07.2011, Madrid, Spain.

On-line Fourier Transform Infrared Spectrometric Detection in Gradient Capillary Liquid Chromatography Using nL-flow Cells, **oral presentation**, HPLC 2009, 28.06. – 02.07.2009, Dresden, Germany.

Simultaneous use of two QCLs for on-line mid-IR detection with HPLC for wine analysis, **poster**, International Conference on Advanced Vibrational Spectrometry (ICAVS V), 12.07. – 17.07.2009, Melbourne, Australia.

Other Scientific Communications not included in this thesis

Estimating the effect of chance correlations in variable subset selection using UVE-PLS-DA in metabolomic datasets, poster, International Workshop on Metabolomics "Technology and Applications", CIC bioGUNE, 12.09. – 14.09.2011, Bilbao, Spain.

A Green Analytical Method for the Determination of Sugars in Depilatory formulations employing Infrared Detection and Partial Least Squares Regression, poster, International Conference on Materials and Technologies for Green Chemistry, 05.09. – 09.09.2011, Tallinn, Estonia.

Metal contents in Iberian bones ashes, poster, XXXIII Reunión Bienal de la Real Sociedad Española de la Química (RSEQ), 25.07. – 28.07.2011, Valencia, Spain.

Differentiation of walnut wood species and steam treatment using ATR-FTIR and partial least squares discriminant analysis (PLS-DA), poster, Sixth International Conference on Advanced Vibrational Spectroscopy (ICAVS-6), 17.06. – 12.06.2011, Sonoma County, California, USA.

Nuevas estrategias quimiométricas e instrumentales para el empleo de detección IR en sistemas de separación cromatográficos, poster, VIII Edición de los Premios Lilly de Investigación para Alumnos de Doctorado, 24.09.2010, Lilly en Alcobendas, Madrid, Spain.

A Novel Approach for Assessing Injection Volume Limits when Using Comprehensive Two-Dimensional Liquid Chromatography with Gradient Elution, poster, Eleventh International Symposium on Hyphenated Techniques in Chromatography and Hyphenated Chromatographic Analyzers (HTC-11), 27.01. – 29.01.2010, Bruges, Belgium.

Improved tool for the elimination of uninformative variables applied on simulated spectra and NIR spectra of real heroine samples, poster, XII Jornadas de Análisis Instrumental (JAI), 21. – 23.10.2008, Barcelona, Spain.

Determination of soybean oil in dietary supplements using Partial Least Squares – Fourier Transform infrared spectroscopy, poster, XXI Reunión Nacional de Espectroscopía, V Congreso Ibérico de Espectroscopía, 09. – 11.09.2008, Murcia, Spain.

List of Abbreviations

2DCoS	2D correlation spectroscopy
2D-LC	two dimensional liquid chromatography (LC x LC)
a.u.	arbitrary units
AR	absorbance ratio
ATR	attenuated total reflectance
AU	absorbance units
BGC-RSM	background correction based on the use of a reference spectra matrix
CAP	critical point of adsorption
CLS	classical least squares
COR	correlation coefficient on the mean centered absorbances
CSS	cubic smoothing splines
CW	continuous wave
CZE	capillary zone electrophoresis
DAD	diode array detection
DFB	distributed feedback
dRID	differential refractive index detector
DTGS	deuterated tri-glycine sulfate
EBS	eluent background subtraction
EC	external cavity
EFA	evolving factor analysis
ELSD	evaporative light scattering detector
EPA	US Environmental Protection Agency
FA	factor analysis
F-P	Fabry-Pérot
FD	first derivative
FFT	Fast Fourier Transform
FIR	far-IR
FLD	fluorescence detection

FTIR	Fourier Transform infrared
GPC	gel permeation chromatography
GUI	Graphical User-friendly Interface
HEPT	height equivalent to a theoretical plate
HCS	highly correlated spectrum
HPLC	High Performance Liquid Chromatography
ID	internal diameter
IP	identification parameter
iPLS	interval PLS
IR	infrared
IRE	internal reflection element
KF	correction factor
LCCC	liquid chromatography under critical conditions
LOD	limit of detection
LOI	limit of identification
LO-phonon	longitudinal optical phonon
LOQ	limit of quantification
MCR-ALS	multivariate curve resolution-alternating least squares
MCT	Mercury-Cadmium-Telluride
MIR	mid-IR
MS	mass spectrometry
NIR	near-IR
NEP	noise equivalent power
D*	normalized detectivity
NP	normal-phase
OSSS-IU-PARAFAC	objective subtraction of solvent spectrum with iterative use of PARAFAC
p2p	Point-to-point
PARAFAC	parallel factor analysis
PCA	principal component analysis
PEEK	polyetheretherketone
PEG	polyethylene glycol

PLS	Partial Least Squares
PRESS	predicted residual error sum of squares
PTFE	polytetrafluoroethane
PTGs	polymer triacylglycerides
QC-laser	Quantum Cascade laser
RI	refractive index
RID	refractive index detector
RMS	root mean square
RMSEC	root mean square error of calibration
RMSECV	root mean square error of cross validation
RMSEP	root mean square error of prediction
RP	reversed-phase
RSD	relative standard deviation
RSM	reference spectra matrix
RW	relative wavenumber
SBC	Science Based Calibration
SFC	supercritical fluid chromatography
SIMPLISMA	simple-to-use interactive self modeling analysis
SM	sample matrix
SVD	singular value decomposition
SW	single wavenumber
TGs	triacylglycerides
TLC	thin-layer chromatography
UPLC	ultra performance liquid chromatography
UV	ultraviolet

Table of Contents

CHAPTER 1. INTRODUCTION	1
1.1 Infrared Spectroscopy	1
1.1.1 Principles of Infrared Spectroscopy	
1.1.2 Qualitative analysis	
1.1.3 Quantitative analysis	
1.1.4 Fourier Transform Infrared Spectroscopy	
1.1.5 Mid-IR sources	
1.1.6 Mid-IR detectors	
1.1.7 Sampling devices	
1.2 Liquid Chromatography	16
1.2.1 Separation principles	
1.2.2 Basic concepts	
1.2.3 Latest trends in instrumentation	
1.3 Infrared detection in LC systems	24
1.3.1 Why hyphenate?	
1.3.2 On-line vs. off-line hyphenation: State-of-the-art in LC-IR	
1.3.3 Potential and limitations of on-line LC-IR	
1.4 Motivation	39
1.5 References for Chapter 1	41
CHAPTER 2. IMPROVEMENTS IN ISOCRATIC ON-LINE GPC-IR AND ON-LINE LC-IR	47
2.1 On-line GPC-ATR-IR determination of lecithin and soybean oil in dietary supplements	49
2.1.1 Introduction	
2.1.2 Material and methods	
2.1.3 Results and discussion	
2.1.4 Conclusions	

2.2 Monitoring of polymerized triglycerides in deep-frying olive oil by on-line GPC-IR spectrometry using the Science Based Calibration multivariate approach	62
2.2.1 Introduction	
2.2.2 Material and methods	
2.2.3 Results and discussion	
2.2.4 Conclusions	
2.3 Determination of glycolic acid in cosmetics	80
2.3.1 Introduction	
2.3.2 Material and methods	
2.3.3 Results and discussion	
2.3.4 Conclusions	
2.4 References for Chapter 2	90

CHAPTER 3. BACKGROUND CORRECTION IN ON-LINE LC-IR USING REFERENCE SPECTRA MATRICES 93

3.1. Determination of critical eluent conditions for polyethylene glycols using univariate chemometric background correction	100
3.1.1 Introduction	
3.1.2 Material and methods	
3.1.3 Results and discussion	
3.1.4 Conclusions	
3.2. Quantification of sugars in beverages using univariate chemometric background correction	118
3.2.1 Introduction	
3.2.2 Material and methods	
3.2.3 Results and discussion	
3.2.4 Conclusions	

3.3. A Partial Least Squares procedure for background correction	136
3.3.1 Introduction	
3.3.2 Material and methods	
3.3.3 Results and discussion	
3.3.4 Conclusions	
3.4. Application of point-to-point matching algorithms for background correction	146
3.4.1 Introduction	
3.4.2 Material and methods	
3.4.3 Results and discussion	
3.4.4 Conclusions	
3.5. References for Chapter 3	156

CHAPTER 4. BACKGROUND CORRECTION IN ON-LINE LC-IR USING 'COLUMN-WISE' CHEMOMETRIC TECHNIQUES..... 159

4.1. Background correction based on polynomial regressions	160
4.1.1 Introduction	
4.1.2 Theoretical background	
4.1.3 Material and methods	
4.1.4 Results and discussion	
4.1.5 Conclusions	
4.2. Cubic smoothing splines background correction	177
4.2.1 Introduction	
4.2.2 Theoretical background	
4.2.3 Material and methods	
4.2.4 Results and discussion	
4.2.5 Conclusions	
4.3. References for Chapter 4	197

**CHAPTER 5. BACKGROUND CORRECTION IN ON-LINE LC-IR
BASED ON FACTOR ANALYSIS, MULTIVARIATE CURVE
RESOLUTION AND REFERENCE SPECTRA MATRICES 199**

- 5.1 Introduction
- 5.2 Theoretical background
- 5.3 Material and methods
- 5.4 Results and discussion
- 5.5 Conclusions
- 5.6 References for Chapter 5

**CHAPTER 6. CHEMOMETRIC EXTRACTION OF 'ANALYTE-
SPECIFIC' CHROMATOGRAMS IN ON-LINE LC-IR..... 223**

- 6.1 Introduction
- 6.2 Material and methods
- 6.3 Results and discussion
- 6.4 Conclusions
- 6.5 References for Chapter 6

**CHAPTER 7. INSTRUMENTAL DEVELOPMENTS IN ON-LINE LC-
IR..... 239**

**7.1. On-Line Fourier transform infrared spectrometric detection
in gradient capillary LC using nanoliter-flow cells240**

- 7.1.1 Introduction
- 7.1.2 Material and methods
- 7.1.3 Results and discussion
- 7.1.4 Conclusions

7.2. High performance liquid chromatography with on-line dual Quantum Cascade Laser detection	254
7.2.1 Introduction	
7.2.2 Material and methods	
7.2.3 Results and discussion	
7.2.4 Conclusions	
7.3. References for Chapter 7	268
CHAPTER 8. CONCLUSIONS AND OUTLOOK.....	271
APPENDIX	277
MATLAB® Functions.....	277
• Science Based Calibration Multivariate Approach for its use in on-line LC-IR	
• Univariate Background Correction using a Reference Spectra Matrix and the Absorbance Ratio as Identification Parameter (AR-BGC-RSM)	
• Background Correction using a Reference Spectra Matrix and a point-to-point matching algorithm (p2p-BGC-RSM)	
• Background correction based on polynomial regressions	
• Cubic smoothing splines background correction	
• Background Correction in on-line LC-IR based on PCA, SIMPLISMA, CLS and Reference Spectra Matrices	

CHAPTER 1. INTRODUCTION

1.1 Infrared Spectroscopy

1.1.1 Principles of Infrared Spectroscopy

Spectroscopy is based on interactions of matter and electromagnetic radiation, thereby changing the energetic state of the matter. The measurement of the absorbance or emission of radiation, as well as luminescence effects such as fluorescence and phosphorescence, allows identifying and quantifying the analyte under investigation. Hence, any spectroscopic measurement can be described as the measurement of a wavelength (qualitative measurements) and its intensity (quantitative measurements) of electromagnetic radiation [1.1]. The energy E associated with the electromagnetic radiation of light follows the expression:

$$E = h\nu \quad (\text{Equation 1.1.1})$$

where h is the Planck's constant and ν the frequency. Electromagnetic radiation can be characterized either by its frequency or its wavelength (λ). In IR spectroscopy frequently instead of the wavelength, the wavenumber ($\tilde{\nu}$) expressed as the number of waves per unit length and measured in cm^{-1} , is used. All three measures are related to each other by the speed of light (c) according to:

$$\lambda = \frac{c}{\nu} = \frac{1}{\tilde{\nu}} \quad (\text{Equation 1.1.2})$$

The electromagnetic radiation can be classified into several regions according to its frequency. The infrared spectral region adjoins the visible light region to the higher energy side and the microwave region to the lower energy side as shown in Figure 1.1.1. The range of infrared radiation is located between 0.7 and 1000 μm corresponding to the range between 14300 and 10 cm^{-1} .

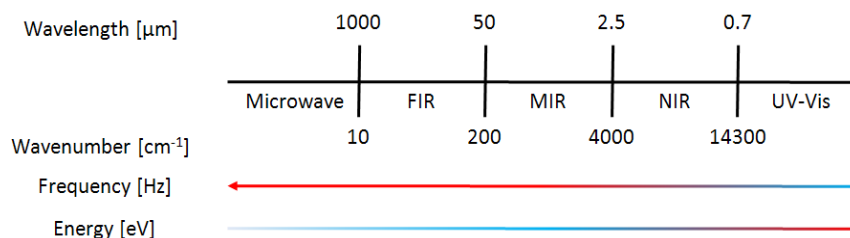


Figure 1.1.1. Electromagnetic spectrum.

The principle of IR spectroscopy is the measurement of wavelengths and intensities of absorption of infrared light by a molecule. The energy of the absorbed wavelength causes the excitation of the molecule and its resulting vibration. The IR spectral range can be divided into three regions associated with different transitions. The mid-IR (MIR) region is ranging from 2.5 to 50 μm (4000 to 200 cm^{-1}) and in this range fundamental intramolecular vibrations are excited. In the near IR (NIR) region ranging from 0.7 to 2.5 μm (14300 to 4000 cm^{-1}) overtone vibrations and combinations of fundamental vibrational modes are observed. Adjacent to the mid-IR region, the far infrared (FIR) region ranging from 50 to 1000 μm (200 to 10 cm^{-1}) is located. Here, bands due to low frequency bonds, skeletal vibrations, crystalline phonon vibrations and intermolecular vibrations are induced [1.2].

IR light can excite vibrations in molecules that show a permanent dipole. A vibration is IR active as long as the absorption process induces a vibrational excitation that causes a change in the dipole moment. Thus, almost all molecules absorb in the IR region. Only homonuclear molecules as for example N_2 , O_2 or Cl_2 do not have such a dipolar moment and therefore do not show bands in the IR region [1.3]. Infrared spectra result from transitions between quantized vibrational energy states. Molecules with N atoms show $3N$ degrees of freedom, three of which represent translational motion in the x , y and z directions and three represent rotational motion about the x , y and z axes. Hence, the remaining $3N - 6$ degrees of freedom give the number of vibrational modes in non-linear molecules and $3N - 5$ degrees of freedom in linear molecules [1.4].

The absorption frequency or band position in an IR spectrum is dependent on the mass of the involved atoms and the strength of the bond. Applying the model of the harmonic oscillator (see Figure 1.1.2) to two atoms holding together through atomic binding strength, the quantization leads to different permitted vibrational states. This

means that energy only appears in discrete steps of $h\nu$. The solution of the Schrödinger equation for the harmonic oscillator gives the following energy levels:

$$E = h \cdot \nu_{osc} \left(n + \frac{1}{2} \right) = \frac{h}{2\pi} \sqrt{\frac{k}{m_r}} \left(n + \frac{1}{2} \right) \quad (\text{Equation 1.1.3})$$

where k is the atomic binding strength, ν_{osc} is the oscillator frequency, m_r is the reduced mass calculated as the product of both atomic masses divided by the sum of the atomic masses and n is the vibrational quantum number. Band positions are therefore dependent on the atomic binding strength of the molecules as well as the mass of the atoms. In this model Δn can only be ± 1 . Whereas using this model, the fundamental vibrations observed in the mid-IR region can be explained, the extension to the anharmonic oscillator is necessary to understand the occurrence of overtones and combination vibrations as observed in the NIR region (see Figure 1.1.2). This is caused by the decreasing binding strength when the atoms show a bigger distance between each other. In this model, the allowed energy levels are not equidistant, but decrease with increasing n [1.1, 4].

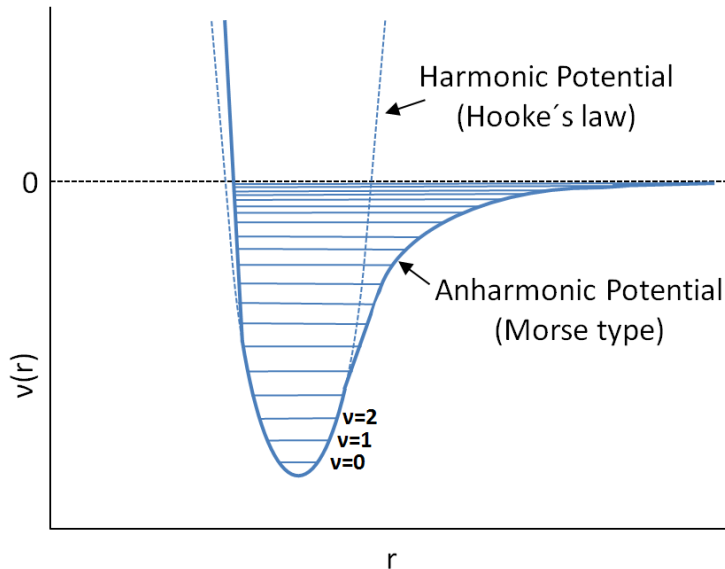


Figure 1.1.2. Harmonic and anharmonic oscillator. Potential energy of a diatomic molecule as a function of the atomic displacement during a vibration for a harmonic oscillator (dashed line) and an anharmonic oscillator (solid line) [1.4].

The observed vibrations can be divided into stretching and deformation vibrations. A stretching vibration involves a change in the bond-length between two atoms. If the bond-angle of the group is affected, the vibration is called deformation vibration. Stretching vibrations are usually observed at higher wavenumbers, as the binding force directly opposes the vibrational changes and a lot of energy is required [1.3]. In case of a three atomic, non-linear molecule as it is the case of CH₂ groups, already six different vibrations can be observed as described in Table 1.1.1.

Table 1.1.1. Vibrations observed in a CH₂ group.

Name	Vibration type	
Stretching vibration	Symmetric stretching vibration	
	Asymmetric stretching vibration	
Deformation vibrations	Bending/Scissoring vibration	In-plane
	Rocking vibration	In-plane
	Twisting vibration	Out-of-plane
	Wagging vibration	Out-of-plane

1.1.2 Qualitative analysis

For many vibrational modes, only a few atoms show large displacements whereas the rest of the molecule remains almost stationary. In this sense, the resonance frequency of such modes is characteristic of the specific functional group almost without being affected by the nature of the other atoms in the molecule [1.3]. Extensive spectra-structure correlation tables have been developed and can be consulted in specific textbooks on the interpretation of infrared spectra [1.5, 6]. With the help of these tables, it is possible to assign one or more absorption bands in a given infrared spectrum to the vibrational mode(s) associated with a certain functional group. With the exception of enantiomers, every IR active molecule shows a slightly different pattern, allowing its identification [1.4].

In the region between 4000 and 1400 cm⁻¹, stretching vibrations can be observed. Between 3700 and 2500 cm⁻¹, bands are attributed to vibrational modes of O-H and N-H and between 3300 and 2800 cm⁻¹ to C-H groups. Bands between 2700 and 1850 cm⁻¹

arise due to triple bonds ($C\equiv C$, $C\equiv N$, $N\equiv N$) as well as Si-H, P-H and S-H vibrations. From 1950 to 1450 cm^{-1} , double bonds ($C=O$, $C=C$) show bands. The region between 1400 and 900 cm^{-1} is called fingerprint region, where single bonds that show strong coupling can be observed. This region is characteristic for each molecule. Below 900 cm^{-1} characteristic bands of aromatic rings (C-H out-of-plane) as well as of C-X show up.

1.1.3 Quantitative analysis

In IR spectroscopy, quantitative measurements follow the Lambert-Beer law [1.4]. The transmittance of a sample at wavenumber $T(\tilde{\nu})$ is given by the ratio of the radiant power acquiring the background signal at that wavenumber ($I(\tilde{\nu})$) to the power of the radiation acquired during the sample measurement ($I_o(\tilde{\nu})$) as:

$$T(\tilde{\nu}) = \frac{I(\tilde{\nu})}{I_o(\tilde{\nu})} \quad (\text{Equation 1.1.4})$$

The absorbance of the sample ($A(\tilde{\nu})$) is given by the base 10 logarithm of $\frac{1}{T(\tilde{\nu})}$ as:

$$A(\tilde{\nu}) = -\log \frac{I(\tilde{\nu})}{I_o(\tilde{\nu})} = -\log(T(\tilde{\nu})) = \alpha \cdot b \cdot c \quad (\text{Equation 1.1.5})$$

where α stands for the molar absorption coefficient of the analyte, b stands for the optical pathlength and c stands for the concentration of the analyte. It has to be remarked that only the absorbance of a component is proportional to its concentration in the sample if the measurement is carried out within the linear concentration range of the instrument and, because of that, the use of IR spectra in absorbance and not in transmittance units is mandatory for analytical purposes.

1.1.4 Fourier Transform Infrared Spectroscopy

The working principle of early IR spectrometers was based on the use of monochromators such as prisms or gratings to disperse the light and sequentially acquire the signal at different wavelengths of a spectrum. The introduction of the mathematical principle of Fast Fourier transform (FFT) as well as advances in calculating capacities gave rise to a new era in infrared spectroscopy, leading to the development of Fourier transform infrared (FTIR) spectrometers. The first commercially available FTIR spectrometer with a spectral resolution $<2\text{ cm}^{-1}$ was developed in 1969. Since then, dispersive instruments were successively replaced by

FTIR spectrometers. Yet they still find application in dedicated systems because of their low price and ruggedness.

Michelson interferometer

The design of FTIR instruments used today is based on that of the two-beam interferometer introduced by Michelson in 1891, which is schematically shown in Figure 1.1.3.

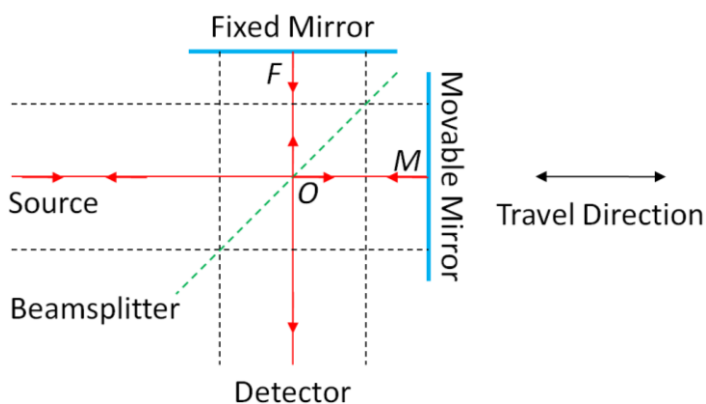


Figure 1.1.3. Working principle of a Michelson interferometer.

The interferometer consists of two perpendicular plane mirrors, one of which can move along an axis that is perpendicular to its plane and a beamsplitter. The radiation of a collimated beam of an external light source is partially reflected to the fixed mirror (at position F) and partially transmitted to the movable mirror (at position M). Both beams return to the beamsplitter, they interfere and are again partially reflected and partially transmitted. Approximately 50% of the total light intensity is returned to the source and although this light beam contains the same information as the output beam travelling in the direction perpendicular to the input beam, it is rarely measured because of the difficulty of separating the output beam returning to the source from the input beam [1.4].

Generation of an interferogram

To explain the generation of an interferogram, ideal conditions are assumed. The path difference between both beams that travel to the mirrors and back to the beamsplitter is $2(OM-OF)$. This optical path difference is called retardation (δ). At zero retardation, the two beams are perfectly in phase and interfere constructively. The sum of the intensity of the beam passing to the detector is the sum of the intensities of both beams. If the beamsplitter is displaced a distance of $\frac{1}{4}\lambda$, the retardation is now $\frac{1}{2}\lambda$. On recombination at the beamsplitter, the beams are out of phase and destructive interference occurs. For a displacement of $\frac{1}{2}\lambda$, the retardation is λ and again constructive interference takes place. If instead of a broadband light source, a monochromatic light source is used and the mirror is moved continuously, the signal at the detector will be seen to vary sinusoidally and a maximum is registered each time that the retardation is a multiple of λ . For a polychromatic light source, instead of a sinusoidal signal, an interferogram will be obtained. Due to the constant velocity of the mirror, the intensity of the interferogram registered at the detector is time-dependent. To obtain a spectrum, Fourier transformation is employed to convert the time-dependent signal into a frequency-dependent signal [1.4]. The process is illustrated in Figure 1.1.4.

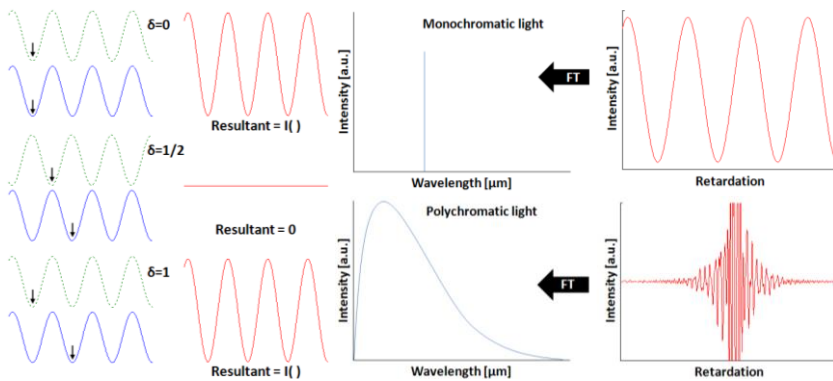


Figure 1.1.4. Illustration of the signal processing in an FTIR spectrometer. Left: Phase of the electromagnetic waves from fixed (dashed line) and movable (solid line) mirrors at different values of the optical retardation and right: spectra and interferograms from an infinitesimally narrow line and a polychromatic light source.

Advantages of FTIR instruments

Three main advantages of FTIR instruments can be identified:

1. The high light throughput due to the measurement of the whole spectral range at the same time increases the sensitivity (Fellgett or multiplex advantage).
2. A fast spectrum acquisition is achieved due to the simultaneous detection of the whole spectrum during one single scan (Jaquinot or throughput advantage).
3. A high wavenumber precision is achieved, because of the HeNe laser incorporated in the interferometer, used as an internal wavelength calibration standard controlling the mirror-displacement (Connes or calibration advantage).

The latter two advantages are responsible for the fast and precise signal averaging improving the signal-to-noise-ratio (S/N) by the square root of the number of co-added scans.

1.1.5 Mid-IR sources

The ideal source of continuous mid-IR radiation is a high temperature black-body. The Planck's law defines the spectral energy density at a defined wavenumber as a function of the temperature. Typical plots of the spectral energy density are shown in Figure 1.1.5. From a practical point of view, the spectral energy density of a given infrared source is the product of its emissivity and the black body spectral energy density. Besides temperature, lifetime and stability are relevant factors that limit the intensity provided by incandescent mid-IR sources.

The *Nernst glower* consists of a mixture of yttrium and zirconium oxides and used to be the most popular mid-IR light source. As the Nernst glower is an insulator at room temperature, it has to be pre-heated in order to become a conductor. Once reaching working conditions, its emission spectrum is similar to that of a black body radiator at 1800 K. However, the Nernst glower is mechanically unstable and has a short lifetime. Nowadays, the most commonly used source in mid-IR instruments is the *Globar* source. It is a resistively heated silicon carbide rod (6-8 mm length) which typically works at

1400 K heated by a high current at low voltage, providing a peak value at 2.1 μm and not requiring pre-heating.

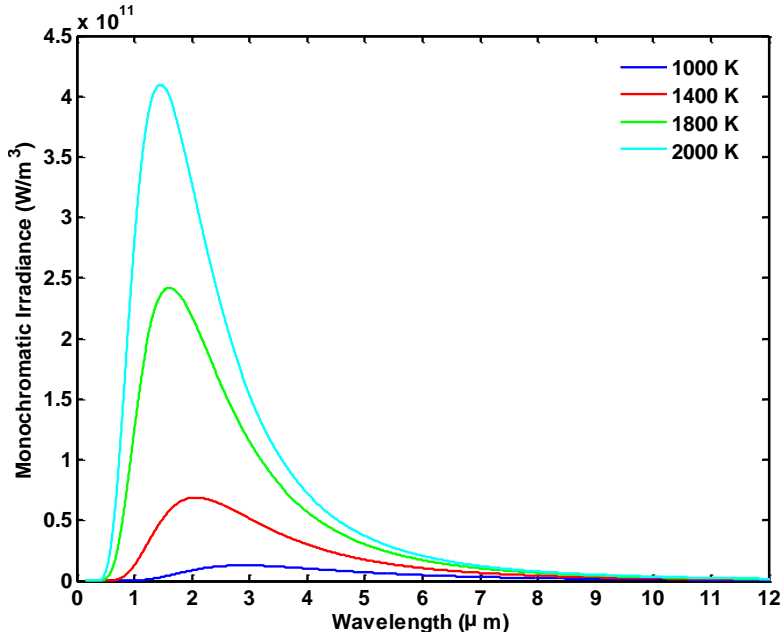


Figure 1.1.5. Spectral intensities of black bodies at different temperatures.

The intensity of the IR radiation is one of the limiting factors of the achievable sensitivity in IR spectroscopy. Therefore the recent introduction of Quantum Cascade Lasers (QC-lasers) as powerful mid-IR light sources is of interest [1.7]. The theoretical concept of QC-lasers was first described in 1971 by R. F. Kazarinov and R. A. Suris [1.8] and the first experimental realization was reported in 1994 by Faist et al. [1.9]. QC-lasers are unipolar semiconductor lasers that differ fundamentally from diode lasers. They are built out of quantum semiconductor structures (GaAs/AlGaAs and InGaAs/InAlAs) that are grown by molecular beam epitaxy. The emission wavelength of the QC-laser can be tailored over a wide spectral range from the mid-IR to the submillimeter wave region ($\sim 100 \mu\text{m}$), a portion of the spectrum not easily accessible with diode lasers, using the same heterostructure material [1.9]. Other advantages of QC-lasers are their small dimensions, converting them into the ideal light source for portable sensing systems and that they work at room temperature without the need of

cryogenic [1.10] or water cooling. In general, laser light shows certain characteristics: it is usually strongly parallel, monochrome, tunable and shows high emission intensity. The basic principles on which the light emission of a laser is based are stimulated emission, population inversion and resonance [1.11].

In the case of bipolar lasers a transition takes place between energy bands where conduction electrons and band holes recombine across the band gap (p and n structure). In contrast to bipolar diode lasers, QC-lasers are unipolar semiconductor lasers composed of heterostructures. In unipolar lasers, the light is generated based on intersubband transitions within the conduction band [1.10].

Between the valence band and the conduction band the so-called band gap is located, which is a forbidden region for electrons. The size of the band gap is material dependent and usually corresponds to several electron volts ($1 \text{ eV} = 1,602 \times 10^{-19} \text{ Joule}$). In a semiconductor composed by two different semiconductor materials, a step in the valence and conduction band is formed. This construction is called "heterostructure". If a thin layer of one semiconductor is surrounded by two thicker layers of a different semiconductor material, a two dimensional quantum well is formed and in this configuration, a quantization of the energy levels takes place and the conduction band is divided into a certain number of defined energy states [1.12]. A schematic view of the conduction band edges of the two materials forming a step structure is shown in Figure 1.1.6. The spacing between the energetic states depends on the thickness of the well layers and the used semiconductor materials [1.11, 12].

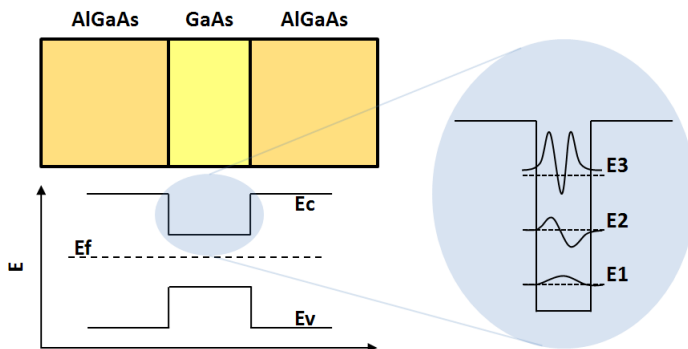


Figure 1.1.6. Schematic energy diagram of the conduction band in a heterostructure consisting of barrier layers and well layers and the quantization of the energy states.

If the barrier layer that separates the well layers is thin enough, a phenomenon called tunneling can occur. This is the case when wave functions overlap and form a hybrid state resulting in electrons that physically move from one well layer to the adjacent one, even if they do not have enough energy to pass the barrier (see Figure 1.1.7) [1.11].

Transitions between the different energy states in a quantum well can occur based on different mechanisms. One of those mechanisms is based on the emission of an electromagnetic wave, the so-called photon. This process takes place in the range of pico-seconds and is therefore relatively slow. A much more efficient process for the emission of energy is the transition of an impulse of an electron to the crystal lattice of the semiconductor. This process is called the emission of a longitudinal optical phonon (LO-phonon). The life-time of this transition is approximately ten times smaller than the one of a photon emission [1.12].

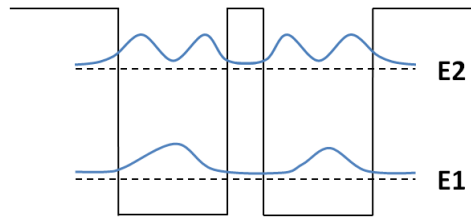


Figure 1.1.7. Hybrid state formed by overlapping wave functions of electrons in two adjacent well layers separated by a thin barrier layer.

In a quantum cascade laser a sequence of several barrier and well layers is assembled. An active cell consists of three quantum wells, containing three energy states. Varying the layer thickness, a pair of injection region and active region generates three coupled energetic levels. This energy diagram is shown in Figure 1.1.8. An electrical current is used to inject the electrons into the third energy level to achieve population inversion. During the radiant transition, taking place between the third and the second level, a photon is emitted. Its wavelength depends on the energy difference between both energy states. A subsequent transition from level 2 to level 1 is tailored to be in resonance with the longitudinal optical phonon energy, following the mechanism of a LO-Phonon – emission. The second transition is several orders of magnitude faster than the transition for photon emission. During this process, the electrons are removed

from level 2 and therefore population inversion between level 3 and 2 is re-established. Moreover, the extraction of electrons from level 2 and 1 into the next injection region takes place (very fast), whereas the extraction of electrons from level 3 is a forbidden transition [1.11, 12]. When one electron passes through a cascade of quantum wells with 25 active cells, theoretically 25 photons are excited for emission [1.9].

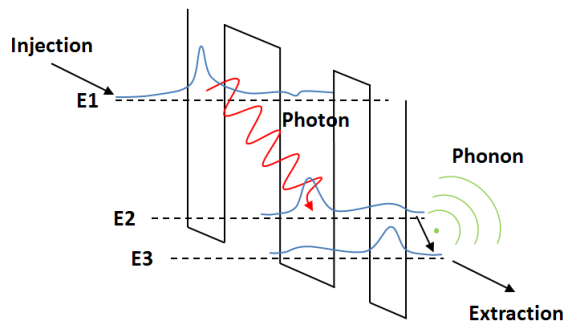


Figure 1.1.8. Energy diagram of an active region.

By means of a Fabry-Pérot resonator (F-P resonator), based on the use of two parallel mirrors or a distributed feedback resonator (DFB resonator), based on the use of an integrated grating, photons are re-injected into the medium and stimulated emission is achieved. The emitted light of a QC-laser working with F-P resonators is multimodal – the spectral width is about 30 cm^{-1} . Using DFB resonators, a certain wavenumber with a small spectral width can be obtained [1.10]. During a laser pulse the laser gets warmer leading to a widening of the spectral width. For example, using a pulse width of 10 ns, the spectral width of the emission is 0.3 cm^{-1} [1.13, 14]. A typical laser pulse is depicted in Figure 1.1.9. The newest development are broadly tunable external cavity (EC) QC-lasers, reducing the laser emission to a single wavelength and allowing to tune the radiation while covering high spectral power densities. In contrast to DFB QC-lasers, wavelength selection is not carried out by a grating placed directly on the QC-laser, but separated from the laser by an external cavity. This permits to scan through a broad spectral range of about 250 cm^{-1} [1.14, 15]. Furthermore these EC QC-lasers are available as tunable continuous wave (CW) EC-QC-lasers, permitting operation in continuous wave emission mode [1.15].

The development of QC-lasers is of great importance for the IR spectroscopy to achieve lower limits of detection which opens a big field of possible applications. Nowadays QC-lasers are used for the analysis of trace gases [1.16], process analysis and environmental applications [1.17, 18], medical diagnostics [1.19] and for the measurement of samples in the liquid phase [1.14, 20, 21]. Especially for on-line LC-IR these new light sources are a promising device to overcome challenges concerning limits of detection, which in the past strongly restricted the applicability of this hyphenation.

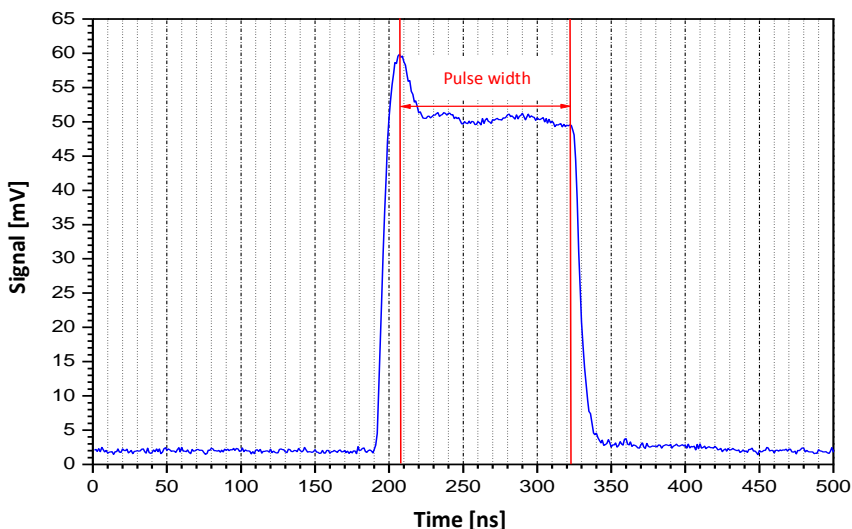


Figure 1.1.9. Typical Laser pulse of a 7.26 μm DFB-QC-laser from Nano Plus GmbH; the red line indicates the pulse width.

1.1.6 Mid-IR detectors

The detector is an essential part of every IR spectrometer. Employing different processes an input, like for example the radiant power (W), irradiance (W cm^{-2}) or radiant energy (W s), is transformed into an output, usually an electric charge, current or potential. The responsivity of a detector is defined by the ratio between the detector output and detector input. The smallest signal that can be determined by a detector is limited by the noise. The noise equivalent power (NEP) is defined as the incident radiant power (W) resulting in a signal-to-noise ratio of 1 within a given

bandwidth of 1 Hz and at a given wavelength. Its reciprocal is called detectivity (D). To facilitate the comparison of detectors, it is useful to normalize the detectivity by referring it to the sensitive area of the detector and to the frequency bandwidth of the measurement, resulting in the normalized detectivity (D^*).

Basically, among the detectors employed in the mid-IR region, two types of detectors can be distinguished. Those who directly produce an electrical signal by the quantum effect (e.g. semiconductor detectors) and those who record a temperature increase through radiation and convert this into an electrical signal (thermal detectors). Whereas semiconductor detectors have a larger detectivity, within a limited spectral range, the response of thermal detectors is proportional to the flux of absorbed radiant power, independent of the wavelength.

The most commonly used thermal detector in mid-IR spectroscopy is the DTGS (deuterated tri-glycine sulfate) detector. Photons that hit the DTGS element cause a change in temperature that alters the surface polarization. The resulting capacity change is measured as a voltage. DTGS detectors are robust, simple, low cost detectors with a long lifetime and a wide dynamic range. Another advantage is that they are operated at room temperature. However, due to their slow response time and their relatively low detectivity, they are not suitable for on-line hyphenation to liquid chromatography.

Mercury-Cadmium-Telluride (MCT) detectors are semiconductor detectors making use of the photoconductive effect which is based on the decrease of the resistance value of the detector element when exposed to light. Photons in the mid-IR region with energy bigger than the band-gap excite electrons from the valence band into the conduction band, thereby increasing the conductivity of the material. The band gap of the MCT crystals depends on the alloy composition. This means that changing the composition ratio, infrared detectors having their maximum sensitivity at different wavelengths can be produced. Furthermore the band gap is sensitive to temperature changes, needing photons with higher energy to excite electrons from the valence band into the conduction band at raising temperatures. Standard MCT detectors for laboratory instruments have to be cooled with liquid nitrogen (-196°C), although thermoelectrically cooled MCT detectors employing Peltier elements working at room temperatures are already commercially available [1.22]. MCT detectors are adequate

for their use for detection of analytes in a moving stream as the detectivity is higher and their response time is short, allowing for increased scan speeds of the interferometer [1.7, 23].

1.1.7 Sampling devices

In principle, using standard IR spectrometers, liquid, gaseous and solid samples can be measured. Of special interest for the analysis of liquid samples in a moving stream are standard flow cells and attenuated total reflectance (ATR) flow cells. Two examples are shown in Figure 1.1.10. Working in the mid-IR region, it has to be taken into account that the used window materials have to be transparent to the IR radiation, being CaF_2 , ZnSe, KBr and KRS-5 (thallium bromoiodide) the most commonly used crystals. To guide and collimate light in optical set-ups and instruments, typically gold mirrors are employed.

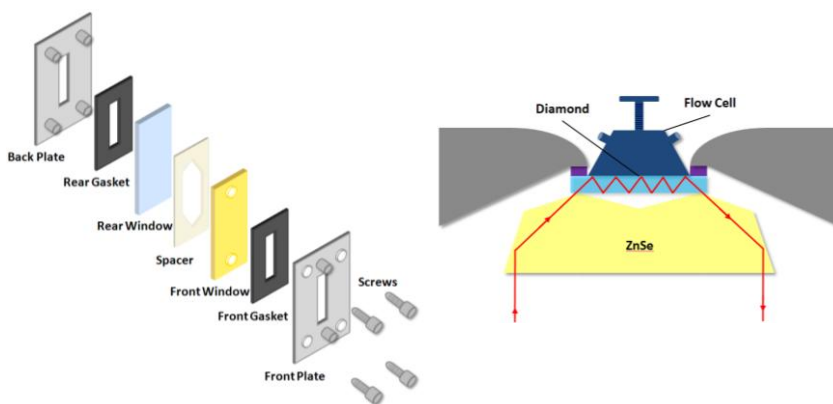


Figure 1.1.10. Schematic view of a standard flow cell and a nine reflection diamond ZnSe ATR flow cell.

1.2 Liquid Chromatography

Liquid chromatography started to be developed in the early 1900s. A glass cylinder was packed with a finely divided powder, a sample was applied to the top of the column and a solvent was poured onto the column. The solvent flew down the column by gravity, the components of the sample began to move through the column at different speeds and finally became separated. High performance liquid chromatography (LC), also called high pressure liquid chromatography, follows the same principle representing the modern culmination of liquid chromatography. It is a chromatographic technique for the separation and analysis of chemical mixtures. The sample is injected (automatically) onto the column. When a substance is injected onto the column, it forms a narrow band on its top. This band becomes broader as the analyte migrates through the column. Assuming uniform column packing, the peak width increases with the square root of the length that the band has traveled inside the column. If a mixture of two compounds that show a different affinity to the packing material inside the column is injected onto the column, they will travel at different speeds through the column and the distance between both bands increases in direct proportion to the length that the bands have traveled and at some point both substances will be separated completely. Solvent is continually pumped through the column and the separated compounds are detected as they elute from the column. The resulting signal plotted against time is called chromatogram. A chromatographic band recorded at the detector can be seen as the statistical distribution of molecules, described by its variance σ^2 , which increases linearly as a function of the traveled distance.

LC is characterized by the use of high pressure pumps for fast separations, re-usable and efficient columns and the control of the overall separation process to achieve precise and reproducible results. LC is exceptional, because it is almost universally applicable to any type of samples, a wide range of equipment, columns and other materials is commercially available and most laboratories that are dealing with the analysis of mixtures are using LC [1.24, 25].

1.2.1 Separation principles

Different separation mechanisms are used in LC. The most popular ones are described subsequently. *Normal-phase (NP) chromatography* employs polar adsorbents such as silica or alumina as a stationary phase and a non-polar mobile phase, typically consisting of hydrocarbons. Retention is based on the interaction of the polar functional groups of the analytes with polar sites on the surface of the packing material. *Hydrophilic interaction chromatography* is an extension of NP chromatography and is utilized for the analysis of very polar analytes using aqueous mobile phases. In *reversed-phase (RP) chromatography* a non-polar stationary phase is used in combination with polar (frequently mainly aqueous) mobile phases. *Hydrophobic interaction chromatography* is based on the use of stationary phases with reduced hydrophobicity and the analytes are typically adsorbed onto the packing in a buffer with high salt concentration and eluted with a buffer of low ionic strength. This technique can be seen as an extension of RP chromatography. *Ion-exchange chromatography* is based on the interaction of charged analytes with oppositely charged functional groups on the stationary phase. To achieve the elution of the analytes, either an increase of the ionic strength of the buffer (thus increasing the concentration of the competing counterions) or a change of pH (which can modify the charge of the analyte or of the ion exchanger) is necessary. In *size-exclusion chromatography (SEC)*, also called *gel permeation chromatography (GPC)*, separation is based on the partial exclusion of analytes from the pores of the packing due to differences in size [1.25].

1.2.2 Basic concepts

Isocratic and gradient chromatography

In isocratic chromatography during a run all conditions and settings of the separation are held constant. In contrast, referring to gradient chromatography, parameters are varied during the sample analysis. Typically, the mobile phase composition is (continuously) varied from low elution strength to high elution strength. Other employed gradients are temperature gradients, implying the change of the temperature or flow gradients, varying the flow rate during the run [1.25].

Height equivalent to a theoretical plate, efficiency and plate count

In the plate model, the chromatographic column is divided into a number of adjoining separation zones N , with each zone having such a length that there can be complete equilibrium of the solute between the mobile phase and the stationary phase within the zone. Each zone is called theoretical plate and its length in the column is called the plate height (H) or the height equivalent to a theoretical plate ($HETP$) [1.26].

The terms efficiency and plate count are synonyms. The column efficiency is a measure of the quality of the separations, taking into account only the peak dispersion. The number of plates in the column, the so-called plate count N is calculated dividing the column length L by the height equivalent to a theoretical plate:

$$N \equiv \frac{L}{HETP} \quad (\text{Equation 1.2.1})$$

Since $HETP$ is a function of many parameters, the plate count or column efficiency is not a physical property of a column and is therefore not a measure for column quality. The plate count can be determined from a chromatogram obtained under isocratic conditions. It is a dimensionless parameter that can be calculated from the peak width and the retention time (assuming that the migration velocity of the peak has been constant during the recording of the chromatogram) [1.25].

In summary, the predictions resulting from the general plate theory are [1.26]:

1. The peak shape is Gaussian.
2. The peak width increases linearly with the retention volume.
3. Each peak in a chromatogram has approximately the same values of N and H .
4. N increases linearly with the column length.

The van Deemter Equation

The curved relation obtained by plotting the $HETP$ against a linear velocity, can be described by the van Deemter equation (see Equation 1.2.2). It is assumed that the $HETP$ is composed of three independent contributions adding up and thus forming the observed curvilinear relationship shown in Figure 1.2.1.

$$H = A + \frac{B}{v} + Cv \quad (\text{Equation 1.2.2})$$

The dispersion process due to eddy diffusion (term A) is not expected to vary with changing flow rates and is largely dependent on particle size and the homogeneity of

the packed column bed. The second term (B) is inversely proportional to the flow velocity v . It accounts for band broadening due to simple molecular diffusion in the long axis of the column (longitudinal diffusion) and decreases with increasing flow rate because less time is available for longitudinal diffusion in a faster chromatographic separation. C is directly proportional to the flow velocity and contains all terms related to mass transfer: from the flowing solvent to the particle through the stationary mobile phase to the retentive phase and back again (rate of diffusion of solute in and out of the pore structure), as well as terms related to sorption kinetics (lateral diffusion). For term C , an increase in flow rate emphasizes the velocity differences between flow streams, which results in an increase in plate height. The solid line in Figure 1.2.1 shows the sum of all three dispersion processes where the minimum in plate height corresponds to the optimum flow rate, because at this velocity, the column has maximum efficiency [1.25, 26].

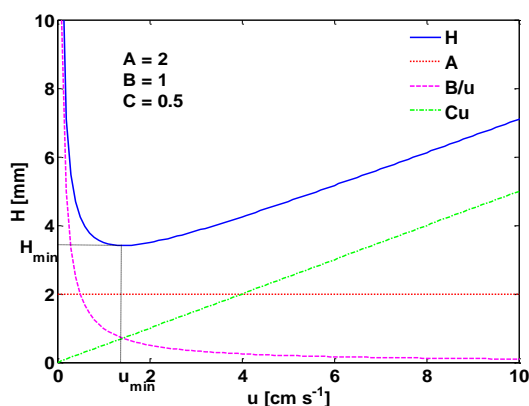


Figure 1.2.1. Van Deemter plot and graphical explanation of terms A, B and C.

Retention

Sample components migrate through the column at different velocities and elute separately from the column at different times. A solute that travels along with the mobile phase is at times held back momentarily either by the surface, by the stationary phase or by both. Since solutes move only when they are in the mobile phase, the distribution of solute molecules between the mobile phase and the stationary phase determines the average solute migration velocity and the retention time. In general, all

forms of chromatography are therefore simply differential migration separation processes where sample components are selectively retained to different degrees by a stationary phase.

There are four ways of describing conventional LC peak retention: retention time, retention volume, retention factor and solute distribution coefficient. The retention time is measured by the time required for a peak to elute from the column following sample injection and is useful for comparing peaks that have appeared in the same chromatogram. As it varies when experimental conditions are changed (e.g. the flow rate) and depends on the specific column used, it is not suitable to define sample components. The retention volume is obtained multiplying the retention time by the flow rate and accounts therefore, in contrast to the retention time, for differences in the flow rate, but is still sensitive to changes in column size or instrumental dead volume. Such variations are compensated using a more basic retention parameter, the retention factor k' . This parameter represents the ratio of the weight of solute in the stationary phase to that in the mobile phase and thus, the weight fraction of solute remaining in the mobile phase is $1/(1+k')$ [1.26].

Since solutes only migrate when in the mobile phase, the retention factor can be defined as follows:

$$k' = \frac{t_R - t_0}{t_0} \quad (\text{Equation 1.2.3})$$

where t_R is the retention time of an analyte and t_0 is the retention time of an unretained peak [1.25]. Still, this parameter does not compensate for differences in the stationary phase concentration and increases with increasing stationary phase loading. To account for differences in the stationary phase loading, the solute distribution coefficient should be used which is defined as the ration of solute concentration in the stationary phase to that in the mobile phase [1.24, 26].

Resolution

Resolution R_s is a dimensionless parameter used to characterize the amount of separation between two peaks. The most common form to calculate the resolution is using the chromatogram, where the distance between peaks and their width are recorded in time units. The resolution is defined as the ratio of the distance between the peaks to their peak width:

$$Rs \equiv \frac{\Delta t_R}{\frac{1}{2}(w_{t,1} + w_{t,2})} \quad (\text{Equation 1.2.4})$$

where Δt_R is the retention time difference between the peaks and w_t is the width of the peaks, both measured in time units.

As described before, the distance between the centers of two peaks increases with the length that they have migrated, whereas the width of the peaks increases only with the square root of this length. This means that the resolution increases with the square root of the distance traveled by the analytes [1.25].

Resolution is a more meaningful column performance parameter than the plate count, accounting for peak broadening as well as the selectivity of the column. It shows how well peaks are resolved (assuming symmetrical Gaussian peak shapes): the evidence of a double peak begins at $Rs = 0.5$, at $Rs = 1$ the peaks are reasonably well resolved and at $Rs = 1.5$ complete peak separation to baseline resolution occurs [1.26].

For LC the resolution can be also expressed as:

$$Rs = \frac{(\alpha-1)}{\alpha} \cdot \frac{\sqrt{N}}{4} \cdot \frac{k'}{1+k'} \quad (\text{Equation 1.2.5})$$

where α is the separation factor, that equals the k' ratio of two adjacent peaks; the plate count is assumed to be constant. This equation is very useful for the design and optimization of LC methods, since the resolution of LC peaks can be controlled by independently changing the separation selectivity α , efficiency N and capacity k' [1.26].

1.2.3 Latest trends in instrumentation

Industry and R+D laboratories strongly focus on making chromatography work robustly, reliable, rapidly and automatically, also new technologies are widely implemented. Hyphenated systems and multidimensional separation methods find numerous applications. Moreover, there is a trend towards the development of strategies aimed at speeding up the analysis for high throughput analysis. It is of great interest to achieve enhanced separation performance. One strategy is the use of ultraperformance liquid chromatography (UPLC) using columns with small particles [1.27].

The gain in efficiency using small particles is mainly linked to the A and C terms of the van Deemter equation, as their contribution decreases with decreasing particle size,

resulting in a reduced band broadening within the column by utilizing smaller particles. Consequently, the optimum flow rate shifts to higher values, at the same time reducing the contribution of the B term, and the backpressure increases. Pressure results to be a significant limitation when small particles are used and this often results in a restriction of column length or operating at sub-optimum flow rates. Attempts to compensate the higher pressure produced by small particles working at elevated temperatures fail as the mobile phase viscosity decreases at increasing temperatures leading to a lower backpressure, but also creating the need of a flow rate increase in order to maintain performance [1.28].

In summary, employing UPLC systems and small particles, the following changes in comparison to conventional LC can be identified:

1. Improved resolution by improved efficiency
2. Higher optimum flow rates
3. Reduction of analysis time
4. Increased sample throughput
5. Decreased peak widths (higher sensitivity)

With regard to on-line hyphenation of UPLC systems to (IR) detectors, it has to be remarked that due to the reduced peak width, the data acquisition rate has to be adequate to record sufficient data points across the peak and achieve reproducible results. This can be troublesome using standard FTIR equipment with MCT detectors, providing spectrum acquisition frequencies of about 18 spectra min^{-1} .

In comparison to sub-2- μm particles, monolithic columns are used less often [1.27]. Providing good efficiencies, using monolithical columns the permeability is much higher than that of comparable micro-particulate columns, leading to much lower pressure drops for the same eluent at the same flow rate [1.29].

Recently the use of columns packed with superficially porous particles (Poroshell columns) has gained importance. The stationary phase of those columns consists of a solid core and a porous shell. In comparison to conventional totally porous particles, Poroshell particles show improved mass-transfer kinetic properties that permit more rapid separations of macromolecules [1.30]. Poroshell columns present an attractive alternative to alleviate the ultra-high backpressures generated with sub-2- μm particle-

packed columns maintaining efficiencies comparable to those found with the sub-2 μm columns [1.31].

Apart from innovations achieved in the field of stationary phases, improved performances are achieved by downsizing LC systems, helping at the same time to save solvents and enabling the analysis of smaller sample volumes. The gain in sensitivity achieved by the use of capillary-LC systems is caused by a reduction of the radial dispersion in the chromatographic column by diminishing its internal diameter. Concerning on-line IR measurements, the combination with e.g. capillary-LC systems is appealing, because of the flow rate reduction and the improved sensitivity [1.32]. However, special attention has to be paid to limit extra-column band broadening, as its contribution to the over-all band broadening is comparatively high using capillary-LC. Extra-column sources for band broadening include the injection volume, tubings (from the injector to the column and from the column to the detector), connections and detector flow cells and special attention should be paid when setting up the system. Tubings should be as short as possible and have a small inner diameter to avoid extra column band broadening [1.28]. Adequate flow cells are substantial to reduce dispersion effects and maintain sensitivity.

In summary, nowadays still speed and efficiency are important parameters, constantly intended to be improved. If robust, reliable and easy to use systems can be developed, the demand for automated as well as hyphenated systems for sample preparation and hyphenated detection systems is expected to increase. Sometimes high-throughput experimentation is desirable including fast chromatographic separations and more rapid sample preparation as well as parallel sample processing [1.27].

1.3 Infrared detection in LC systems

1.3.1 Why hyphenate?

Vibrational spectrometry is accepted to be a versatile tool in research as well as in dedicated systems as molecular specific information of a vast amount of molecules can be obtained. Dealing with complex samples containing multiple analytes, this property can be increasingly disadvantageous as the obtained spectra will frequently provide strongly overlapping signals. Although in the last decade methods based on the direct determination of analytes using ATR or NIR spectrometry in combination with multivariate chemometric techniques are emerging [1.33], in many cases the use of a separation system prior to detection is still necessary to handle problems associated to the analysis of multiple analytes and/or complex sample matrices.

The potential of coupling LC to IR spectrometry combines the high resolution provided by LC with the non-destructive and molecular specific information of IR spectrometry and allows the development of qualitative as well as quantitative applications. In this respect, IR spectrometry used for detection in LC can provide much more information than conventional detectors such as ultraviolet (UV), refractive index (RI) or evaporative light scattering (ELS) detectors. Despite the frequent use of IR detection in liquid flow systems for routine analysis of a broad variety of samples [1.34, 35], its hyphenated use with LC is still rarely exploited.

Raman spectroscopy, often mentioned as complementary technique together with IR spectroscopy, also provides molecular specific fingerprints and structural information. In contrast to IR spectroscopy, Raman spectroscopy is affected less by background absorption of typical solvents used in LC systems. However, the application of Raman spectroscopy for on-line detection is not feasible due to the low concentration sensitivity of this technique. Using the off-line approach, this lack of sensitivity is compensated, as the number of accumulated scans can be augmented. Using this strategy, Raman spectroscopy has found application. Due to the non-destructive character, Raman spectroscopic detection can be combined with other detection strategies. Although of interest in some applications, Raman spectroscopic detection was not the scope of the present thesis. The topic was, however, recently reviewed [1.36].

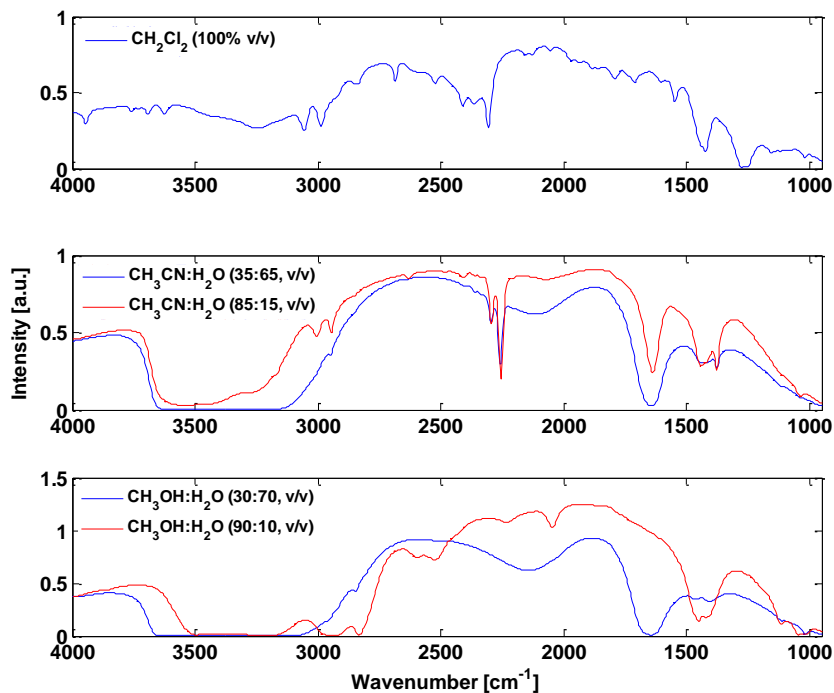


Figure 1.3.1. Single Channel signals from different solvents systems acquired using a flow cell with ZnSe and CaF₂ windows and an optical pathlength of 150 μm for CH₂Cl₂ and 16.5 μm for CH₃CN:H₂O and CH₃OH:H₂O.

In principle, infrared detection can be applied to the detection of a vast amount of molecules. However, its broad detection capabilities also represent an important drawback as a result of the intense background absorption arising from common eluents and solvents used in LC. This is exemplified in Figure 1.3.1, where single channel signals of three commonly used mobile phase systems are depicted. It can be observed that the transparency is reduced in determinate spectral regions of all three systems and that especially mobile phase systems with high water content are troublesome because the regions between ~ 2900 and 3700 cm^{-1} (symmetric and anti-symmetric O-H stretching vibration), around 1640 cm^{-1} (O-H bending vibration) as well as the region around 950 cm^{-1} (libration modes) are (almost) completely obscured as no light passes through the flow cell. Hence, those regions cannot be used for the analysis in LC-IR systems without solvent removal. However, the remaining spectral regions can be used for identification and quantification purposes providing different

noise levels throughout the spectral range in dependence of the eluent transparency and the optical pathlength.

1.3.2 On-line vs. off-line hyphenation: State-of-the-art in LC-IR

Basically, two strategies for an effective coupling of FTIR spectrometry can be distinguished: i) off-line and ii) on-line, presenting specific features, advantages and drawbacks. IR spectral acquisition in off-line hyphenated systems is normally carried out in transmission mode using an IR microscope. On-line measurements can be carried out using both, transmission and attenuated total reflectance (ATR) approaches, providing the limitations and characteristics specific for each detection method.

Detailed descriptions of the general features of the above mentioned off-line and on-line approaches have been reported in previous works. In 1989 Fujimoto et al. [1.37] described the main drawbacks and the potential of the LC-IR coupling and presented and described the advantages of using micro-columns to overcome some of these limitations. In 1999 Somsen et al. [1.38] reviewed the state of the art of the on-line LC-IR coupling approach discussing its restrictions and making a detailed description of five early solvent elimination interfaces: thermospray, particle beam and electrospray interfaces as well as pneumatic and ultrasonic nebulizers. Lendl et al. [1.39, 40] reviewed the range of applications of LC-IR in aqueous systems. In 2003 using commercially available interfaces, Kok et al. [1.41] assessed both, on- and off-line approaches for their application in chromatography with respect to the chromatographic features as well as to quantitative and qualitative aspects.

Off-line LC-IR

Employing the off-line approach involves the elimination of the solvent prior to IR detection using an interface which evaporates the solvent and deposits the analytes onto an IR-transparent substrate such as CaF_2 , BaF_2 , ZnSe or Ge , for a subsequent spectral analysis of the dried spots. Solvent removal interfaces are developed to minimize the spot area maintaining the chromatographic resolution. Major advantages of this approach are the reduction or elimination of spectral interferences originating from the eluent and the improved signal-to-noise ratios. The main drawbacks of the

off-line coupling procedures are band broadening, a limited sample throughput due to the post separation measurement, the loss of volatile analytes, spectral interferences arising due to the use of non-volatile buffers and the handling and maintenance of the interface.

Some interfaces for solvent removal in LC-IR are commercially available. Although several thermospray and pneumatic nebulizer interfaces have been proposed, careful and time-consuming optimization is still needed. Some examples of applications of different types of solvent elimination interfaces are listed in Table 1.3.1.

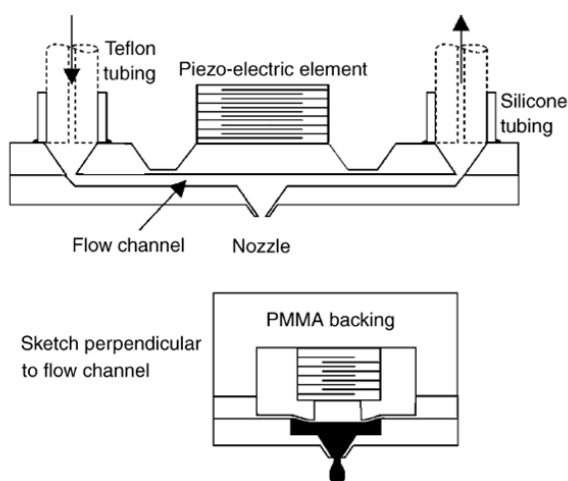


Figure 1.3.2. Top: cross section of a flow-through microdispenser, bottom: schematic view of the electrically induced deformation of the piezo-element which causes droplet ejection from the main flow stream [1.43].

Lendl et al. [1.42, 43] introduced a fully automatic on-line piezoactuated flow-through microdispenser as a solvent elimination interface for capillary LC-IR as shown in Figure 1.3.2. Recently this interface was applied in capillary liquid chromatography [1.44]. As described by Lendl et al., the piezoceramic element of the dispenser was driven by a DC power supply together with a computer controlled arbitrary waveform generator providing electronic pulses with defined amplitude, rise, width, and decay time (see Figure 1.3.3). To enable lateral location of the deposits on a CaF_2 window a computer controlled x , y -stage with controlled step sizes was implemented in the set-up. The flow-through micro-dispenser was capable to provide droplets of picoliter size. Dried

residues of chlorinated pesticides from river water samples were analyzed by mid-IR and Raman microscopy and limits of identification of 2 ng analyte on-column with a precision of approximately 10% RSD were achieved.

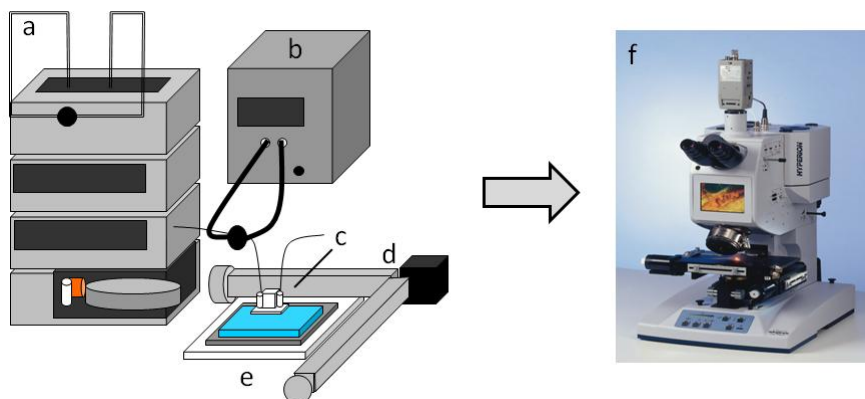


Figure 1.3.3. Fully automatic piezoactuated flow-through microdispenser as a solvent elimination interface for capillary LC-IR; a: capillary LC system with flow manager, C_{18} column (300 μm ID x 15 cm, 3 μm , 100 \AA) and autosampler, b: UV detector, c: piezoceramic element of the dispenser driven by a DC power supply and a computer controlled arbitrary waveform generator, d: computer controlled x, y-stage with controlled step size (5 μm , 90 mm x 40 mm), e: IR transparent window, f: mid-IR microscope with a measurement spot of 100 x 100 μm

Table 1.3.1. Applications of off-line LC-IR, GPC-FTIR and 2D-LCxGPC-FTIR spectrometry.

Nebulizer type	Analytical Column(s)	Mobile Phase System	Application	Ref.
Thermospray	250x4.6, C_{18}	MeOH:H ₂ O	linear alkylbenzene sulphonates	[1.45]
Thermospray	250x4.6, C_{18}	MeOH:H ₂ O	anionic surfactants	[1.46]
Thermospray	125x4.9, 5 μm , C_{18}	MeOH, ACN and H ₂ O	glycine & phenolic antioxidants	[1.47]
Thermospray & ultrasonic neb.	250x4.6, 10 μm , C_{18} ; 100x4.6, 5 μm , Hypersil ODX duet	ammonium acetate, ACN, H ₂ O and MeOH	Reactive dyes & carbamate pesticides	[1.48]
Pneumatic neb.	Homemade capillary column: 300x0.32, 300x0.45, 3.5 μm C_{18}	ACN	polymer additives	[1.49]
Thermospray	150x4.6, Hypersil SDX duet	ACN:H ₂ O (with acetic acid)	dye samples	[1.50]
Ultrasonic neb.	300x7.5, 10 μm , PLgel (3 columns)	THF	polystyrene & poly(methyl methacrylate)	[1.51]
custom built coaxial sprayer	150x1.0, C_{18}	10 mM acetic acid:ACN	terpenoids	[1.52]

Nebulizer type	Analytical Column(s)	Mobile Phase System	Application	Ref.
Ultrasonic neb. IRC Bourne Scientific	150x4.6, 5 μm , C ₁₈	ACN:toluene	C ₆₀ and C ₇₀ fullerenes	[1.53]
Ultrasonic neb. IRC Bourne Scientific	150x3, Zorbax C ₁₈	H ₂ O(0.1% v/v formic acid):ACN	catechins & methyl xanthenes	[1.54]
Lab Connections LC-Transform 500	300x7.5, 10 μm , PLgel (2 columns)	THF	polystyrene & polycarbonate	[1.55]
Lab Connections LC-Transform 500	300x7.6, 5 μm , 10 ³ Å, PLgel & 300x7.6, 5 μm , 10 ⁵ Å, PLgel	DCM	polymer blends & copolymers	[1.41]
Ultrasonic neb.	250x4.6, 5 μm , C ₁₈	ammonium acetate & MeOH	water soluble vitamins	[1.56]
Ultrasonic neb. IRC Bourne Scientific	100x4.6, C ₁₈ & 25x4.6, 5 μm , C ₁₈	H ₂ O:ACN	microbial components	[1.57]
LC-Transform 100	300x8, SDV	THF	crosslinked styrene-butadiene rubbers	[1.58]
LC-Transform 100	4 serial PLgel columns	THF	grafting of epoxidized natural rubber	[1.59]
Ultrasonic neb. Lab Connections LC-Transform 300	3 Styragel columns	1,2,4-Trichlorobenzene	ethylene-methyl methacrylate block polymers	[26]
LC-Transform interface LCT-1	30x4.6, 3 μm , silica gel	hexane, toluene and 2-butanone	random styrene-butyl acrylate copolymers	[1.60]
Lab Connections LC-Transform 500	1D: 150x3.2, 5 μm , Silica 2D: 150x6.0, 3 μm , HSPgel-RT	1D: chloroform:diethyl ether 2D: chloroform	degradation of poly(bisphenol A)carbonate	[1.61]
Not indicated	150x2,1, 3.5 μm , C8	H ₂ O, ACN & formic acid	degradation products of cefpodoxime proxetil	[1.62]
Ultrasonic neb. Lab Connections LC-Transform 300	250x4.6, 5 μm , silica gel	TCB & EGMBE	ethylene-propylene copolymers	[1.63]
Ultrasonic neb. Lab Connections LC-Transform 300	different column types	decalin & 1-decanol	ethylene-vinyl acetate copolymers	[1.64]
Ultrasonic neb. Lab Connections LC-Transform 300	5 Styragel columns	1,2,4-trichlorobenzene	PP-g-PS graft copolymers	[1.65]
DiscovIR-LC	500x10, linear divinyl benzene	THF	styrene-butadiene-styrene copolymer	[1.66]
Lab Connections LC-Transform 600	150x2.0, 3 μm , C ₁₈	ACN:0.1% triethylamine	degradation product in a pharmaceutical product	[1.67]
Ultrasonic neb. Lab Connections LC-Transform 300	different column types	decalin & cyclohexanone	ethylene-acrylate copolymers	[1.68]
Ultrasonic neb. Lab Connections LC-Transform 300	250x4.6, 10 μm , silica gel 250x8, 20 μm , PL Mixed A (4 columns)	1,2,4-trichlorobenzene, decalin & cyclohexanone	ethylene-vinyl acetate copolymers	[1.69]
Ultrasonic neb. Lab Connections LC-Transform 300	Set 1: 300x8, 10 μm , SDV Set 2: 300x8, 10 μm , Styragel	TCB	olefin copolymers	[1.70]

Notes: DCM: dichloromethane; THF: tetrahydrofurane; ACN: acetonitrile; TCB: tetrachlorobenzene; EtOH: ethanol; MeOH: methanol; EGMBE: ethylene glycol monobutylether; neb.: nebulizer.

On-line LC-IR

Alternatively, in the on-line approach a flow cell is used for continuous on-the-fly spectra acquisition of the eluting solution. The on-line coupling via a flow-cell interface is based either on transmission, reflection or attenuated total reflectance measurements. The useful detection window range is defined by the IR absorption characteristics of the cell window materials and by the absorbance of the components of the mobile phase. Major advantages of the on-line approach are its improved chromatographic resolution, the enabling of real time measurements, the possibility of using non-volatile buffers [1.4, 43], the instrumental simplicity, the user friendly operation and handling, its low cost and its suitability for quantitative applications. The on-line coupling also allows the measurement of infrared spectra of analytes without any orientation, crystallization or oxidative degradation which might occur when solvents are removed [1.71] and further hyphenation with additional detectors is possible.

In the last years a number of applications have been described focusing on on-line isocratic GPC and LC-IR using a flow cell interface, without introducing significant instrumental developments in this field. Under isocratic conditions, accurate background compensation can be achieved by subtracting a mobile phase spectrum measured either at the beginning of the run or directly before the elution of the analyte of interest. This straightforward approach has been successfully applied in a number of procedures in LC, GPC and 2D LCxGPC as indicated in Table 3.2. Comprehensive two-dimensional chromatography (LCxGPC)-FTIR was assessed by the functional-group analysis of a series of styrene-methylacrylate (SMA) copolymers with varying styrene content [1.72] and by the study of chemical changes in poly(bisphenol A)carbonate as a result of degradation [1.61]. However, it can be limited by the intense absorption of the LC solvents and additives and therefore slight drifts in the eluent composition might modify strongly the IR background, thus producing anomalous band shapes, negative signals and sloping baselines in the recovered analyte spectra [1.73].

In on-line coupling of LC the use of ATR-FTIR is an alternative detection approach that has been successfully employed. Louden et al. [1.74] applied a multiply-hyphenated detection system to the analysis of a mixture of nonsteroidal antiinflammatory drugs separated by reversed-phase LC. In this set-up the analytes were characterized by

diode array UV, ^1H nuclear magnetic resonance, FTIR spectroscopy and time-of-flight mass spectrometry. Hyphenation was achieved using an ATR stainless steel flow cell with a ZnSe crystal and a volume of 400 μL . This combination allowed an almost complete structural characterization. Louden et al. [1.75] applied the same set-up to the analysis of a partially purified plant extract in which 20-hydroxyecdysone and polygodine B were identified despite incomplete chromatographic resolution and the presence of coeluting interferences. In another work a similar set-up was used for the analysis of model pharmaceuticals using high temperature reversed-phase LC with a deuterium oxide mobile phase [1.76].

Edelmann et al. [1.77] employed a diamond ATR flow cell for on-line FTIR detection of organic acids, sugars and alcohols in red wines by LC. The chemical inertness of the employed diamond enabled the use of a strongly acidic mobile phase. Although the analyte peaks were not baseline resolved, the LC-IR data sets were analyzed using multivariate curve resolution–alternating least squares (MCR-ALS). Then a linear regression curve was calculated from peak areas measured from the MCR-resolved elution profiles.

The use of single reflection ATR infrared microspectroscopy was presented by Patterson et al. [1.78]. They placed a hemispherical germanium internal reflection element (IRE), which only permits a single internal reflection, at the end of a capillary LC column focusing an FTIR microscope on this spot and achieving injection mass detection limits in the low microgram range. Despite of the potential of this approach and in order to improve the analytical features, the authors also proposed a series of modifications such as: (i) reducing the diameter of the column to half the diffraction-limited diameter of the infrared beam at the IRE/solution interface; (ii) adapting the use of a single bounce ATR to the LC system; (iii) reducing the size of the IR detector and (iv) applying a selective film on the IRE.

Table 1.3.2. Applications of isocratic on-line liquid chromatography-Fourier transform infrared (LC-IR), size exclusion chromatography-Fourier transform infrared (PGC-FTIR) and two dimensional liquid chromatography x gel permeation chromatography-Fourier transform infrared (2D-LCxGPC-FTIR) spectrometry using a flow cell interface.

Chromatographic mode	Analytical Column(s)	Mobile Phase System	Application	Ref.
NP-LC	250x4.6, 5 µm, DuPont ZORBAX-sil	DCM:n-hexane, 35:65 v/v, THF:n-hexane, 2:98 v/v 2-propanol:n-hexane, 0.1:99.9 v/v ACN-saturated n-hexane, 2.0 v/v	β-cypermethrin diastereomers	[1.79]
RP-LC	250x3.0, 5 µm, C18	ACN:H ₂ O, 72:25	peroxide-based explosives	[1.71]
GPC	300x7.6, 5 µm, 10 ³ Å, PLgel and 300x7.6, 5 µm, 10 ⁵ Å, PLgel	DCM	polymer blends & copolymers	[1.41]
GPC	250x7.5, 5 µm, PLgel (2 serial columns) and 150x6.0, HPS-gel	Chloroform	homopolymers & polymer blends	[1.80]
GPC	300x7.5, 10 µm, PLgel (3 serial columns)	TCB	branched polyolefins	[1.81]
GPC	300x7.5, 3 µm, PS-Gel	CHCl ₃ , CHCl ₃ mixed with 1.1, 2 and 3 v/v % EtOH	PEG of different molar masses	[1.82]
2D-LCxGPC	1D: 150x3.9, 4 µm, Silica 2D: 150x6.0, HPS-gel-RT	1D: from 90-10% n-heptane:DCM to 93:7% DCM:MeOH 2D: chloroform	styrene methylacrylate copolymers	[1.72]
2D-LCxGPC	1D: 150x3.2, 5 µm, Silica 2D: 150x6.0, 3 µm, HSPgel-RT	1D: chloroform:diethylether, 98.5:1.5 v/v 2D: chloroform	degradation of poly(bisphenol A)carbonate	[1.61]

Notes: DCM:dichloromethane; THF: tetrahydrofuran; ACN: acetonitrile; TCB: tetrachlorobenzene; EtOH: ethanol; MeOH: methanol; NP: normal phase; RP: reversed phase

1.3.3 Potential and limitations of on-line LC-IR

In the past, on-line IR detection in LC has been hindered by a number of technical limitations that restricted its applicability to real life analytical problems, with its viability being frequently questioned. Therefore it is worth paying attention to the main drawbacks of the on-line approach: i) the limited sensitivity of IR detection and ii) the dominating absorption of the mobile phase components [1.4].

Concerning the lack of sensitivity, different efforts for its improvement have been made and recent advances in instrumentation enable the possibility of developing set-ups that could help to overcome the low sensitivity of IR detection. One limiting factor for IR detection in LC is the intensity of the radiation generated by the global sources used in FTIR spectrometers. Whereas it affects the sensitivity of both, normal and reversed phase LC analysis, it is especially troublesome in the reversed phase due to the intense IR absorption of water.

In recent years, the development of QC-laser technology has provided valuable tools for the current demands of on-line liquid flow systems as the signal to noise ratio can be increased. Since the initial development of a working QC-laser by Faist et al. [1.9] in 1994, there has been a big progress in the development of mid-infrared light sources. QC-lasers with high output power have become commercially available and applications in analytical procedures and devices [1.83] have been developed. Miniaturized, broadly tuneable EC-QC-lasers operating as high power mid-IR sources at room temperature are available with center wavelengths spanning the mid-IR spectrum from 2400 to 820 cm^{-1} and providing tuning of up to 250 cm^{-1} [1.15].

Although QC-lasers were initially used in analytical chemistry as powerful light sources for trace gas analysis, their potential utility for the analysis in the condensed phase was soon demonstrated by Lendl et al. [1.84]. In this initial work using a FP QC-laser in an aqueous flow analysis system, the authors showed that this arrangement could yield signal to noise ratios up to 50 times higher than those provided by FTIR instruments equipped with a global IR source and a MCT detector.

Köhled et al. [1.85] investigated the potential applicability of QC-lasers for on-line detection in CE and reported the first successful hyphenation of a FP QC-laser to CE in 2005. The use of a QC-laser with an emission maximum at 1080 cm^{-1} permitted specific

functional group detection and the use of a transmission flow cell with a pathlength of 60 μm .

A QC-laser emitting at 1067 cm^{-1} for specific detection in isocratic on-line LC-IR was reported for the first time by Edelman et al. [1.86] using a custom-made flow cell. The flow cell design included two diamond windows with adjustable spacing and two hollow waveguides to direct the IR radiation. Using an ion exchange resin column with Ca^{2+} as counter ion and a solution of 0.04% of formic acid as mobile phase, the detection of carbohydrates and organic acids present in wine samples was achieved. The use of the QC-laser permitted an increase of the optical pathlength from 25 to 125 μm , thus increasing the sensitivity of the IR detection.

In short, the increasing output levels, reduced system size, weight and power consumption of QC-laser mid-IR sources provide a clear path to scaling down dedicated on-line IR detection systems appropriate for LC that should enable new applications. Apart from the laser sources, room temperature MCT detectors with improved sensitivity [1.22], miniaturized flow cells with nL volumes and capillary-LC systems are among the most relevant developments of special significance that could be highlighted. Employing those new components for the IR detection in LC separations, the noise levels are expected to be reduced and flow cells with higher optical pathlengths could be used.

Another starting-point to improve sensitivity is to exploit the advantages of miniaturization in LC-IR. Radial dispersion causes the distribution of the sample after its injection over the entire cross-section of the chromatographic column. Reducing the internal diameter (ID) of the column, the dilution is lower resulting in an increased sensitivity of detection, because the concentration of the sample at the end of the column is inversely proportional to the square of the column diameter. According to this down-scaling factor, theoretically a maximum 235-fold increase in sensitivity can be achieved by replacing a 4.6 mm ID analytical column with a 300 μm ID capillary column. It has to be emphasized, that this gain in sensitivity can only be achieved in case the same amount of sample is injected onto both columns. In practice this is not possible as the maximum allowable injection volume decreases with the column ID. Hence, normally lower gains in concentration sensitivity are obtained because the

increase in the chromatographic peak concentration can be partially or fully compensated by the reduction of the injection volume [1.87].

The low flow rates typically used in capillary LC ($1\text{--}20\ \mu\text{L min}^{-1}$) require appropriate adaptations of the detection system. Concerning on-line IR measurements, the use of low-volume flow cells becomes necessary reducing post-column dead volumes to avoid peak broadening and thus a decreasing sensitivity. Adequate nL-volume flow cells for this purpose were already developed in 2002 by Köhler et al. [1.88] (see Figure 1.3.4) and used to hyphenate capillary electrophoresis with FTIR spectrometry.

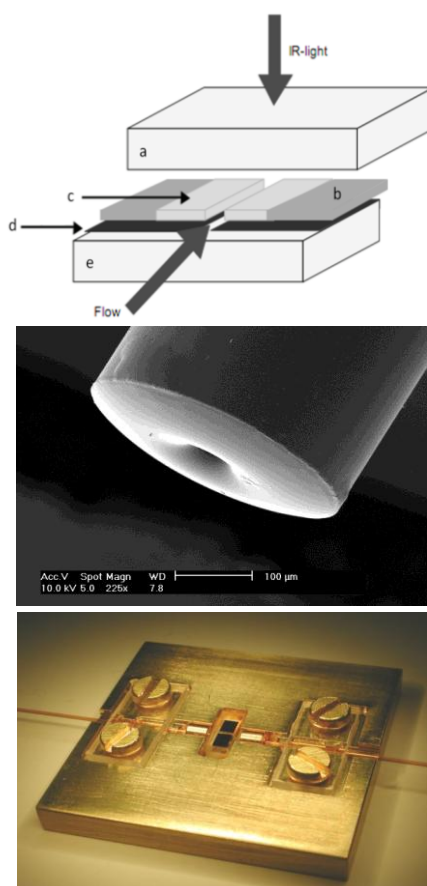


Figure 1.3.4. Top: nL flow cell for on-line coupling of LC-IR systems; a: CaF₂ window, b: epoxy adhesive, c: SU8 photoresist layer (optical pathlength) d: titanium layer (optical blind) e: CaF₂ window; middle: SEM micrograph showing the capillary with epoxy o-ring and bottom: assembled nL flow cell [1.88].

Under isocratic conditions the spectral contribution of the mobile phase components can be compensated by subtracting a reference spectrum measured either at the beginning of the run, or directly before the elution of the analyte of interest. Concerning the problems related to the strong absorbance of the mobile phase, the application of on-line LC-IR requires an accurate background subtraction which is not straightforward when the composition of the solvent is not constant during the run. Until some years ago it was generally agreed on that on-line mid-IR detection is not compatible with gradient techniques due to strong changes in shape and intensity of the absorption bands of the mobile phase components occurring during gradient separations, as shown in Figure 1.3.5. Intermolecular interactions between the mobile phase components during a gradient often produce shifts in the position of the background absorption bands. For example, in acetonitrile:water systems, as the acetonitrile concentration increases, the composition of the mixture progressively shifts from pure H₂O to (CH₃CN)_m·(H₂O)_n complexes to pure (CH₃CN) [1.89]. Different species with characteristic infrared absorptions have been identified including: (CH₃CN)·(H₂O)₅, (CH₃CN)₂·(H₂O)₄ and (CH₃CN)₂·(H₂O). Additionally, changes in the IR background absorption intensity can be up to several orders of magnitude more intense than those due to analyte elution (see Figure 1.3.5, bottom). Therefore, the IR spectra recorded during a LC run contain spectral contributions of the eluting sample components and a number of solvent complexes with changing concentrations during the gradient which is difficult to estimate.

Increasing the use of chemometric techniques allowing for an efficient compensation of the eluent absorption, would permit a significant extension of the usefulness of on-line LC-IR in many areas including industrial and biochemical analysis. Therefore, there is an ongoing interest in the development of chemometric methods for background correction in on-line LC-IR.

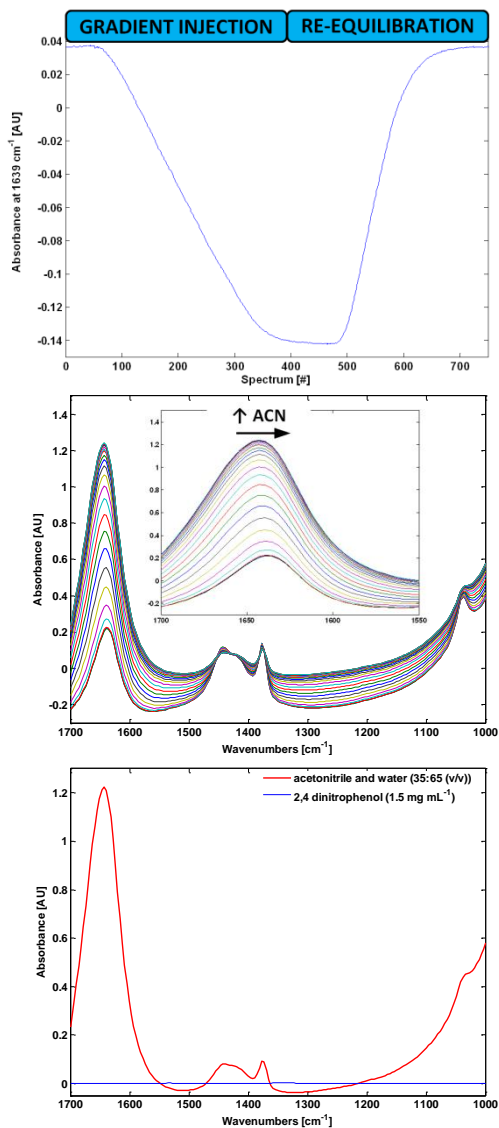


Figure 1.3.5. Top: Chromatogram recorded during a blanc run using an acetonitrile:water gradient from 35 to 85% acetonitrile, middle: spectra recorded during an acetonitrile:water gradient from 35 to 85% acetonitrile, the inset shows a close-up view of the region between 1700 and 1550 cm⁻¹ where the band shift to lower wavenumbers when augmenting the acetonitrile concentration can be clearly appreciated and bottom: spectrum of a mixture of acetonitrile and water at 35:65 v/v (red line) and spectrum of 2,4 dinitrophenol at a concentration of 1.5 mg mL⁻¹ (blue line) measured using an optical pathlength of 10 μm.

In 2004, Boelens et al. [1.73, 90] developed a new method to correct the background absorption, taking into account eluent spectral shape and intensity variations during analyte elution. In this two-step method first, the baseline spectra were modelled using a limited number of principal components and subsequently, an asymmetric least squares (asLS) regression method was applied using these principal components to correct the background contribution of the measured spectra during elution. Although the method is proposed for infrared detection, only LC-Raman and LC-DAD data have been analyzed so far.

The capabilities of some chemometric algorithms using iteratively applied multi-way methods such as parallel factor analysis (PARAFAC) and PARAFAC2 were evaluated by István et al. [1.91]. Background corrections carried out on simulated on-line LC-IR runs showed that although PARAFAC2 performs better than PARAFAC, it does not give correct decompositions. On the other hand, multivariate curve resolution with alternating least squares (MCR-ALS) did not provide accurate results. In this work, István et al. proposed the use of a new method named objective subtraction of solvent spectrum with iterative use of PARAFAC and PARAFAC2 (OSSS-IU-PARAFAC and OSSS-IU-PARAFAC2). The main assumptions and restrictions that define the conditions of applicability of this method are: i) the eluent composition should be constant during the experiments, limiting its applicability to isocratic conditions; ii) interactions between the eluent and the sample components should not modify the eluent spectrum; iii) partial coelution of analytes resulting in a modification of their spectra may be manifested as a new component in the mixture and iv) the elution profiles of any given component should remain constant between the different LC runs.

In summary, the available chemometric methods for the compensation of the background eluent contribution to the overall signal are not straightforward and/or are not applicable to gradient elution. Moreover, only very few examples of applications can be found in literature demonstrating the potentials and limitations of LC-IR systems in real-life analytical problems. Therefore there is a need for further development of chemometric methods to enable a user-friendly application of LC-IR in combination with different chromatographic modes and mobile phase systems stressing the broad range of possible applications.

1.4 Motivation

IR spectrometry used for detection in LC can provide useful information which is not amenable to other detectors. The coupling of LC to IR spectrometry is of great interest because high resolution provided by LC is combined with the non-destructive and molecular specific information of IR spectrometry. Although the on-line approach presents some important advantages over the off-line approach, its potential cannot yet be fully exploited due to the limited sensitivity of IR detection and difficulties in on-line measurements arising from the dominating absorption of most of the commonly used mobile phase components.

On account of this, to augment the feasibility of LC-IR on-line coupling, on the one hand side instrumental developments are needed to improve sensitivity. Employing new QC-laser light sources, room temperature MCT detectors with improved sensitivity, miniaturized flow cells with nL volumes and capillary-LC systems for the IR detection in LC separations, the noise levels are expected to be reduced permitting the use of flow cells with higher optical pathlengths, achieving improved LODs and facilitating the implementation of new applications. On the other hand side, further developments in the field of chemometric data treatment are needed for increasing sensitivity and selectivity (multivariate advantage) and as a result its applicability to real-world analytical problems (i.e. extension to gradient elutions), because up to now, chemometric methods for the compensation of the background contribution have been insufficiently demonstrated. In other words, efforts concerning the instrumental development of more sensitive LC-IR systems are only useful in combination with chemometric method developments for an increase in the applicability of the technique. It can be concluded that mathematical and technical advances give rise to exciting new possibilities for the use of vibrational detection systems in LC.

Based on this, the present thesis dealing with the development of the on-line coupling of LC-IR can be divided into three parts. The first part deals with innovations on the field of isocratic separations, revealing latest improvements of on-line LC-IR under isocratic conditions, such as the use of the rapid scan mode and novel chemometric approaches, to improve chromatographic resolution (Chapter 2). The second part concentrates on new chemometric methods for background compensation and their

application to gradient systems (Chapters 3 to 6). The objective of this part is to detect and remove undesired sources of variation in LC-IR hyphenated data systems including eluent absorption and detector drifts in an automated way which could be used 'on-the-fly' in dedicated systems and at the same time to enhance sensitivity and spectral and/or chromatographic resolution. Instrumental developments are discussed in the last part with the objective of exploiting recent advances in instrumental developments concerning IR sources and miniaturized devices to increase the sensitivity of the LC-IR coupling (Chapter 7). The developments will focus on the coupling of capillary-LC employing nL flow cells and the use of QC-lasers as IR sources. All developed strategies are demonstrated by means of different examples of applications to show the improvements and limitations of the chemometric and instrumental developments.

1.5 References for Chapter 1

- [1.1] K. Cammann, *Instrumentelle Analytische Chemie – Verfahren Anwendungen Qualitätssicherung*, Spektrum Akademischer Verlag GmbH, Heidelberg, Berlin, 2001.
- [1.2] P.R. Griffiths, *Handbook of Vibrational Spectroscopy*, John Wiley & Sons, New York, 2002.
- [1.3] M. Kölhed, *Novel on-line mid Infrared Detection Strategies in Capillary Electrophoretic Systems*, Department of Analytical Chemistry, Stockholm University, Stockholm, 2005.
- [1.4] P.R. Griffiths, J. de Haseth, *Fourier Infrared Transform Spectroscopy*, second ed., John Wiley & Sons, New York, 2007.
- [1.5] D. Lin-Vien, N.B. Colthup, W.G. Fateley, J.G. Grasselli, *The handbook of infrared and Raman characteristic frequencies of organic molecules*, Academic Press, Inc., 1991.
- [1.6] G. Socrates, *Infrared and Raman characteristic group frequencies: tables and charts*, John Wiley & Sons, Chichester, 2000.
- [1.7] B. Schrader, *Infrared and Raman Spectroscopy*, VCH: Weinheim, 1995.
- [1.8] R.F. Kazarinov, R.A. Suris, *Fizika i Tekhnika Poluprovodnikov*, 5 (1971) 797-800.
- [1.9] J. Faist, F. Capasso, D.L. Sivco, C. Sirtori, A.L. Hutchinson, A.Y. Cho, *Science*, 264 (1994) 553-556.
- [1.10] C. Mann, Q. Yang, F. Fuchs, W. Bronner, K. Kohler, J. Wagner, *TM-Technisches Messen*, 72 (2005) 356-365.
- [1.11] S. Schaden, *Application of Mid-Infrared Quantum Cascade Lasers for Quantitative Analysis in Aqueous Phase*, Institute of Chemical Technologies and Analytics, Vienna University of Technology, Vienna, 2006.
- [1.12] J. Kuligowski, *Entwicklung eines MIR-Sensors zur Bestimmung von Kohlenwasserstoffen in Wasser*, Fachhochschul-Diplomstudiengang Biotechnische Verfahren, Tulln, 2007.
- [1.13] J. Faist, C. Gmachl, F. Capasso, C. Sirtori, D.L. Sivco, J.N. Baillargeon, A.Y. Cho, *Applied Physics Letters*, 70 (1997) 2670-2672.
- [1.14] M. Brandstetter, A. Genner, K. Anic, B. Lendl, *Analyst*, 135 (2010) 3260–3265.
- [1.15] Daylight Solutions, <http://www.daylightsolutions.com/products/lasers/>.

- [1.16] A.A. Kosterev, Y.A. Bakirkin, F.K. Tittel, *Applied Physics B - Lasers and Optics*, 80 (2005) 133-138.
- [1.17] M. Lackner, C. Forsich, F. Winter, S. Anders, G. Strasser, *Optics Communications*, 216 (2003) 357-360.
- [1.18] W.H. Weber, J.T. Remillard, R.E. Chase, J.F. Richert, F. Capasso, C. Gmachl, A.L. Hutchinson, D.L. Sivco, J.N. Baillargeon, A.Y. Cho, *Applied Spectroscopy*, (2002) 706-714.
- [1.19] A.A. Kosterev, A.L. Malinovsky, F.K. Tittel, C. Gmachl, F. Capasso, D.L. Sivco, J.N. Baillargeon, A.L. Hutchinson, A.Y. Cho, *Applied Optics*, 40 (2001) 5522-5529.
- [1.20] M. Kölhed, M. Haberkorn, V. Pustogov, B. Mizaikoff, J. Frank, B. Karlberg, B. Lendl, *Vibrational Spectroscopy*, 29 (2002) 283-289.
- [1.21] S. Schaden, A. Dominguez-Vidal, B. Lendl, *Applied Spectroscopy*, 60 (2006) 568-571.
- [1.22] S.A. Vigo Systems, <http://www.vigo.com.pl/>.
- [1.23] Hamamatsu, Technical information: Characteristics and use of infrared detectors.
- [1.24] L.R. Snyder, J.J. Kirkland, J.W. Dolan, *Introduction to Modern Liquid Chromatography*, John Wiley & Sons, Inc., Hoboken, New Jersey, 2009.
- [1.25] U.D. Neue, *LC columns - Theory, Technology, and Practice*, Wiley-VCH, New York, 1997.
- [1.26] A.M. Striegel, W.W. Yau, J.J. Kirkland, D.D. Bly, *Modern Size-Exclusion Liquid Chromatography. Practice of Gel Permeation and Gel Filtration Chromatography.*, John Wiley & Sons, Inc., Hoboken, New Jersey, 2009.
- [1.27] P. Schoenmakers, *Annual Reviews of Analytical Chemistry*, 2 (2009) 333-357.
- [1.28] E.S. Grumbach, J.C. Arsenault, D.R. McCabe, *Beginners Guide to UPLC – Ultra Performance Liquid Chromatography*, Waters Corporation, Milford, 2009.
- [1.29] S. Eeltink, W.M.C. Decrop, G.P. Rozing, P.J. Schoenmakers, W.T. Kok, *Journal of Separation Science*, 27 (2004) 1431-1440.
- [1.30] J.J. Kirkland, *Analytical Chemistry*, 64 (1992) 1239-1245.
- [1.31] J.S. Baker, J.C. Vinci, A.D. Moore, L.A. Colon, *Journal of Separation Science*, 33 (2010) 2547-2557.
- [1.32] G. Quintas, J. Kuligowski, B. Lendl, *Analytical Chemistry*, 81 (2009) 3746-3753.

- [1.33] J. Moros, S. Garrigues, M. de la Guardia, *Trac-Trends in Analytical Chemistry*, 29 578-591.
- [1.34] S. Armenta, S. Garrigues, M. de la Guardia, *Trac-Trends in Analytical Chemistry*, 26 (2007) 775-787.
- [1.35] M. Galignani, M.D. Brunetto, *Talanta*, 64 (2004) 1127-1146.
- [1.36] A.J. Hobro, B. Lendl, in: S. Schlücker (Ed.) *Surface Enhanced Raman Spectroscopy – Analytical, Biophysical and Life Science Applications*, Wiley–VCH, 2010, pp. 155–169.
- [1.37] C. Fujimoto, K. Jinno, *Trac-Trends in Analytical Chemistry*, 8 (1989) 90-96.
- [1.38] G.W. Somsen, C. Gooijer, U.A.T. Brinkman, *Journal of Chromatography A*, 856 (1999) 213-242.
- [1.39] R. Schindler, B. Lendl, *Analytical Communications*, 36 (1999) 123-126.
- [1.40] M. Kölhed, B. Lendl, B. Karlberg, *Analyst*, 128 (2003) 2-6.
- [1.41] S.J. Kok, C.A. Wold, T. Hankemeier, P.J. Schoenmakers, *Journal of Chromatography A*, 1017 (2003) 83-96.
- [1.42] M. Haberkorn, J. Frank, M. Harasek, J. Nilsson, T. Laurell, B. Lendl, *Applied Spectroscopy*, 56 (2002) 902-908.
- [1.43] I. Surowiec, J.R. Baena, J. Frank, T. Laurell, J. Nilsson, M. Trojanowicz, B. Lendl, *Journal of Chromatography A*, 1080 (2005) 132-139.
- [1.44] S. Armenta, B. Lendl, *Analytical and Bioanalytical Chemistry*, 397 (2010) 297-308.
- [1.45] M.A. Mottaleb, *Mikrochimica Acta*, 132 (1999) 31-39.
- [1.46] M.A. Mottaleb, *Analytical Sciences*, 15 (1999) 1137-1140.
- [1.47] M.A. Mottaleb, *Analytical Sciences*, 15 (1999) 57-62.
- [1.48] J.C. Jones, D. Littlejohn, P.R. Griffiths, *Applied Spectroscopy*, 53 (1999) 792-799.
- [1.49] I. Bruheim, P. Molander, E. Lundanes, T. Greibrokk, E. Ommundsen, *Hrc-Journal of High Resolution Chromatography*, 23 (2000) 525-530.
- [1.50] M.A. Mottaleb, D. Littlejohn, *Analytical Sciences*, 17 (2001) 429-434.
- [1.51] K. Torabi, A. Karami, S.T. Balke, T.C. Schunk, *Journal of Chromatography A*, 910 (2001) 19-30.
- [1.52] J. Geiger, E.H. Korte, W. Schrader, *Journal of Chromatography A*, 922 (2001) 99-110.
- [1.53] J.M. Treubig, P.R. Brown, *Journal of Chromatography A*, 960 (2002) 135-142.

- [1.54] C.S. Robb, S.E. Geldart, J.A. Seelenbinder, P.R. Brown, *Journal of Liquid Chromatography & Related Technologies*, 25 (2002) 787-801.
- [1.55] S.J. Kok, N.C. Arentsen, P. Cools, T. Hankemeier, P.J. Schoenmakers, *Journal of Chromatography A*, 948 (2002) 257-265.
- [1.56] Y. Li, P.R. Brown, *Journal of Liquid Chromatography & Related Technologies*, 26 (2003) 1769-1786.
- [1.57] S.W. Huffman, K. Lukaszewicz, S. Geldart, S. Elliott, J.F. Sperry, C.W. Brown, *Analytical Chemistry*, 75 (2003) 4606-4611.
- [1.58] H. Pasch, A. Siewing, L.C. Heinz, *Macromolecular Materials and Engineering*, 288 (2003) 771-777.
- [1.59] A.J.P. Van Zyl, S.M. Graef, R.D. Sanderson, B. Klumperman, H. Pasch, *Journal of Applied Polymer Science*, 88 (2003) 2539-2549.
- [1.60] I.G. Romero, H. Pasch, *E-Polymers*, (2005).
- [1.61] L. Coulier, E. Kaal, T. Hankemeier, *Journal of Chromatography A*, 1130 (2006) 34-42.
- [1.62] N. Fukutsu, T. Kawasaki, K. Saito, H. Nakazawa, *Journal of Chromatography A*, 1129 (2006) 153-159.
- [1.63] A. Albrecht, L.C. Heinz, D. Lilge, H. Pasch, *Macromolecular Symposia*, 257 (2007) 46-55.
- [1.64] A. Albrecht, R. Brull, T. Macko, H. Pasch, *Macromolecules*, 40 (2007) 5545-5551.
- [1.65] T. Macko, U. Schulze, R. Brull, A. Albrecht, H. Pasch, T. Fonagy, L. Haussler, B. Ivan, *Macromolecular Chemistry and Physics*, 209 (2008) 404-409.
- [1.66] W. Carson, J. Dwyer, B. Boumajny, *International Journal of Polymer Analysis and Characterization*, 13 (2008) 463-470.
- [1.67] T. Murakami, H. Konno, N. Fukutsu, M. Onodera, T. Kawasaki, F. Kusu, *Journal of Pharmaceutical and Biomedical Analysis*, 47 (2008) 553-559.
- [1.68] A. Albrecht, R. Brull, T. Macko, P. Sinha, H. Pasch, *Macromolecular Chemistry and Physics*, 209 (2008) 1909-1919.
- [1.69] A. Albrecht, R. Brull, T. Macko, F. Malz, H. Pasch, *Macromolecular Chemistry and Physics*, 210 (2009) 1319-1330.
- [1.70] H. Pasch, A. Albrecht, R. Bruell, T. Macko, W. Hiller, *Macromolecular Symposia*, 282 (2009) 71-80.

- [1.71] R. Schulte-Ladbeck, A. Edelmann, G. Quintas, B. Lendl, U. Karst, *Analytical Chemistry*, 78 (2006) 8150-8155.
- [1.72] S.J. Kok, T. Hankemeier, P.J. Schoenmakers, *Journal of Chromatography A*, 1098 (2005) 104-110.
- [1.73] R.J. Dijkstra, H.F.M. Boelens, J.A. Westerhuis, F. Ariese, U.A.T. Brinkman, C. Gooijer, *Analytica Chimica Acta*, 519 (2004) 129-136.
- [1.74] D. Louden, A. Handley, S. Taylor, E. Lenz, S. Miller, I.D. Wilson, A. Sage, *Analytical Chemistry*, 72 (2000) 3922-3926.
- [1.75] D. Louden, A. Handley, S. Taylor, E. Lenz, S. Miller, I.D. Wilson, A. Sage, R. Lafont, *Journal of Chromatography A*, 910 (2001) 237-246.
- [1.76] D. Louden, A. Handley, S. Taylor, I. Sinclair, E. Lenz, K.D. Wilson, *Analyst*, 126 (2001) 1625-1629.
- [1.77] A. Edelmann, J. Diewok, J.R. Baena, B. Lendl, *Analytical and Bioanalytical Chemistry*, 376 (2003) 92-97.
- [1.78] B.M. Patterson, N.D. Danielson, A.J. Sommer, *Analytical Chemistry*, 75 (2003) 1418-1424.
- [1.79] K. Istvan, G. Keresztury, J. Fekete, *Journal of Liquid Chromatography & Related Technologies*, 28 (2005) 407-421.
- [1.80] H.F.M. Boelens, P.H.C. Eilers, T. Hankemeier, *Analytical Chemistry*, 77 (2005) 7998-8007.
- [1.81] K. Tribe, G. Saunders, R. Meissner, *Macromolecular Symposia*, 236 (2006) 228-234.
- [1.82] M. Malanin, K.J. Eichhorn, A. Lederer, P. Treppe, G. Adam, D. Fischer, D. Voigt, *Journal of Chromatography A*, 1216 (2009) 8939-8946.
- [1.83] QuantaRed Technologies, GmbH, <http://www.quantared.com/>.
- [1.84] B. Lendl, J. Frank, R. Schindler, A. Muller, M. Beck, J. Faist, *Analytical Chemistry*, 72 (2000) 1645-1648.
- [1.85] M. Kölhed, S. Schaden, B. Karlberg, B. Lendl, *Journal of Chromatography A*, 1083 (2005) 199-204.
- [1.86] A. Edelmann, C. Ruzicka, J. Frank, B. Lendl, W. Schrenk, E. Gornik, G. Strasser, *Journal of Chromatography A*, 934 (2001) 123-128.

- [1.87] M. Kranendijk, J.C.M. Waterval, G.W. Somsen, G.J. de Jong, *Journal of Separation Science*, 28 (2005) 1796-1802.
- [1.88] M. Kölhed, P. Hinsmann, P. Svasek, J. Frank, B. Karlberg, B. Lendl, *Analytical Chemistry*, 74 (2002) 3843-3848.
- [1.89] T. Takamuku, M. Tabata, A. Yamaguchi, J. Nishimoto, M. Kumamoto, H. Wakita, T. Yamaguchi, *Journal of Physical Chemistry B*, 102 (1998) 8880-8888.
- [1.90] H.F.M. Boelens, R.J. Dijkstra, P.H.C. Eilers, F. Fitzpatrick, J.A. Westerhuis, *Journal of Chromatography A*, 1057 (2004) 21-30.
- [1.91] K. Istvan, R. Rajko, G. Keresztury, *Journal of Chromatography A*, 1104 (2006) 154-163.

CHAPTER 2. IMPROVEMENTS IN ISOCRATIC ON-LINE GPC-IR AND ON-LINE LC-IR

In this chapter, innovations in the field of isocratic separations are discussed. The first part deals with the hyphenation of GPC to an FTIR spectrometer with an ATR flow cell interface. Up to now, this coupling has mainly been applied in combination with reversed phase separations [2.1-4] or using special columns for sugar analysis [2.5]. To show the applicability of the GPC-ATR set-up for food analysis, it was used for the analysis of lecithin and soybean oil. Whereas similar configurations have shown to be a useful tool for the analysis of polymers [2.6-9], it has never been used in food analysis. In addition, a simple approach for the selection of the optimum wavenumber for the extraction of the chromatograms with respect to selectivity maximization is presented. The second part also presents a new application of on-line GPC-FTIR for food analysis. Here, the polymerization grade of fried olive oil samples was investigated using a standard flow cell interface. To eliminate the contribution of interfering substances, a multivariate calibration approach called Science Based Calibration (SBC) was applied post-run to the data leading to improved accuracy levels.

The third part shows the determination of glycolic acid in cosmetic samples employing a standard flow cell for the on-line hyphenation of a RP-LC system to the FTIR spectrometer. An additional objective of this study was to test the usefulness of the rapid scan data acquisition mode to increase the sampling frequency of FTIR data acquisition.

The results of the aforementioned studies can be found in literature [2.10-12]. Moreover, the methods described in the first and second part have been employed to obtain reference values for the development of multivariate approaches for the direct

determination of lecithin in soybean oil [2.13] as well as the polymerization grade of vegetable oils [2.14-16], respectively.

2.1 On-line GPC-ATR-IR determination of lecithin and soybean oil in dietary supplements

2.1.1 Introduction

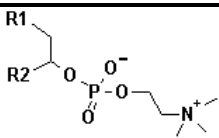
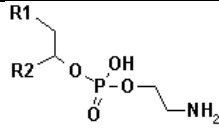
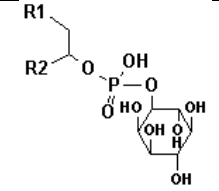
The coupling of GPC with ATR-FTIR presents important advantages due to the isocratic use of dichloromethane that permits to increase the working spectral range because of the low IR absorption of dichloromethane and the reduced optical path of ATR cells. The relative high sample amounts injected in GPC and the high concentration of analytes in many samples in the field of food analysis, reduce the importance of the limited sensitivity of ATR measurements. In the past, FTIR detection in GPC has been demonstrated to be very useful in polymer analysis [2.6-9], but to our knowledge, this hyphenated technique has never been used in food analysis.

Lecithin, ingested as a dietary supplement, has therapeutic use as dietetic support. In addition, it acts as a vehicle for essential fatty acids useful as growth factors, in the prevention of atherosclerosis and to protect against hypertension, thrombosis and ulcers [2.17]. Together with soybean oil, lecithin can be found at percentage concentration levels in a number of dietary products.

The major phospholipids in lecithin are phosphatidylcholine (PC), phosphatidylethanolamine (PE), and phosphatidylinositol (PI). It can be seen in Table 2.1.1 that the molecular structure of the major phospholipids is similar as they show several common features, such as the presence of two fatty acids and the phosphoric group. The AOAC Official Method 999.14 for lecithin determination in dietary supplements is based on the determination of choline by an enzymatic colorimetric method after an alkaline digestion of the sample [2.18]. The total amount of phospholipids can also be measured by acid digestion and subsequent phosphorus analysis by the Bartlett arseno-molybdate method. FTIR spectrometry has been extensively used to analyze phospholipid orientation in functionalized monolayers [2.19], conformation disorder in phospholipids bilayers [2.20] and to determine water penetration in lipid bilayer membranes [2.21]. Moreover, the group of Nzai and Proctor [2.22, 23] demonstrated that FTIR can be considered as a fast, simple and reliable analytical tool for the phospholipid analysis in soybean oil in contrast to the

conventional Bartlett method and thin layer chromatography imaging densitometric methodologies. More recently, a partial least squares regression model has been developed for the determination of phospholipids in rapeseed oils at various stages of a technological process [2.24]. Results reported in this study were satisfactory but, in order to remove spectral interferences from C–H and C–O–C stretching, bending and wagging of tryglicerides, a previous subtraction of standard solutions of refined bleached deodorized rapeseed oil was necessary and so, a previous knowledge of the sample composition was needed to obtain accurate results.

Table 2.1.1. Molecular structure of lecithin phospholipids.

Compound	Molecular structure ^a
L- α -Phosphatidylcholine	
3-sn-Phosphatidylethanolamine	
L- α -Phosphatidylinositol	

Note: Molecular structure^a: R1 and R2 stand for fatty acids (16:0, 18:0, 18:1, 18:2 or 20:4)

In references [2.22, 23] for FTIR determination of lecithin, a standard phospholipid calibration mixture of PE, PC and PI similar to the phospholipid composition of soybean oil was used for the calibration of the method using area measurements of spectral bands obtained in the transmission mode in the region between 1200 and 970 cm^{-1} . In spite of the good results, a number of drawbacks can be identified: (i) the sample preparation based on the heating of samples with water followed by washing with acetone and further purification on a silicic acid column is time consuming (more than 3 h) and difficult to automate involving the use of 450 mL of organic solvents per

sample, (ii) the presence of interferences due to an incomplete removal during the sample preparation might produce spectral interference leading to inaccurate results and (iii) the procedure involves a previous extraction of the phospholipids, eliminating the possibility to analyze the oily fraction for a deeper characterization of the sample.

In order to overcome the aforementioned drawbacks, the use of on-line hyphenated GPC and FTIR for the simultaneous determination of total phospholipids and soybean oil in dietary supplements is proposed. A significant increase in the selectivity of the measurements is achieved by the on-line use of a separation method (GPC) prior to the FTIR measurement, and also by the use of the first derivative (FD) spectra acquired during the analyte elution (GPC-ATR-(FD)-FTIR). Additionally, a simple method for the selection of the most appropriate wavenumber for the extraction of the analyte chromatograms is proposed.

2.1.2 Material and methods

Apparatus and Reagents

A Hewlett-Packard (Palo Alto, CA, USA) HP1050 high performance liquid chromatography system, equipped with two Waters (Barcelona, Spain) Envirogel GPC columns (19x150 mm, 19x300 mm), and a sample injection loop of 2 mL was employed for chromatographic separations. Dichloromethane was used as mobile phase at a flow rate of 5 mL min⁻¹ [2.25]. Two milliliters of sample extract or CH₂Cl₂ solutions of standards were injected into the chromatographic system.

For ATR spectra acquisition an in-compartment DuraSampIR II accessory (Smiths Detection Inc., Warrington, England) with a nine reflection diamond DuraDisk plate and a micro flow cell was installed on a Bruker (Bremen, Germany) IFS 66/v FTIR spectrometer equipped with a liquid nitrogen refrigerated MCT detector and a vacuum system. The scanner of the interferometer was operated at a HeNe laser modulation frequency of 100 kHz. Spectra were recorded in the region between 4000 and 750 cm⁻¹, with a spectra resolution of 8 cm⁻¹ and a zerofilling value of 2. Averaging 20 scans per spectrum, a spectra acquisition frequency of 15 spectra min⁻¹ was provided.

Granulated soybean lecithin standard (97%, w/w) was supplied by Guinama (Valencia, Spain). Seven formulated lecithin samples, three powdered ones and four kinds of pills,

and refined soybean oil were obtained from local markets. Dichloromethane was provided from Scharlau (Barcelona, Spain).

Sample preparation

Synthetic samples were prepared by weighing the required amounts of lecithin standard and soybean oil in dichloromethane. For sample preparation, one gram of sample was accurately weighed in a volumetric flask, diluted to 10 mL with dichloromethane and placed in an ultrasonic water bath for 5 min. The solution was centrifuged at 3000 rpm for 5 min and then filtered through a 0.22 μm PTFE membrane.

Software and data treatment

For instrumental and measurement control as well as for data acquisition, the OPUS software (version 4.1) from Bruker (Bremen, Germany) was employed. Spectra treatment and data manipulation were carried out using Matlab 7.0.1 from Mathworks Inc. (Natick, MA, USA).

The concentrations of lecithin and soybean oil were calculated from peak height values of the extracted chromatograms using the first derivative intensities at 1034 and 1138 cm^{-1} , respectively. These values were interpolated in external calibration lines established using six solutions of both analytes in concentration ranges from 0 to 100 and from 0 to 50 mg mL^{-1} for lecithin and soybean oil, respectively.

2.1.3 Results and discussion

FTIR spectra of analytes

Figure 2.1.1 shows typical ATR-FTIR spectra of standard solutions of soybean oil and lecithin in dichloromethane. The figure shows the high spectral overlapping between the considered compounds due to high molecular similarities between lecithin and triglycerides. In the lecithin IR spectra, the most intense bands are those corresponding to (i) the alkane bands corresponding to symmetric CH_2 , antisymmetric CH_2 , antisymmetric CH_3 stretching and CH_2 scissoring vibrational modes at 2854, 2928, 2956 and 1462 cm^{-1} , respectively; (ii) the carbonyl stretching vibration, located at 1736 cm^{-1} ; and (iii) the highly overlapped PO_2^- and P-O-C infrared active vibrations in the region

between 1200 and 970 cm^{-1} , centered around 1061 cm^{-1} . On the other hand, various bands can be identified in the soybean oil spectrum including the carbonyl C=O stretching band at 1740 cm^{-1} , the CH_2 and CH_3 scissoring vibrations at 1462 and 1376 cm^{-1} , as well as intense C–O stretching bands at 1165 and 1099 cm^{-1} . Absorption bands located at 2854, 2956 and 3009 cm^{-1} arise due to the symmetric CH_2 stretching and asymmetric CH_3 and CH_2 stretching vibrations, respectively.

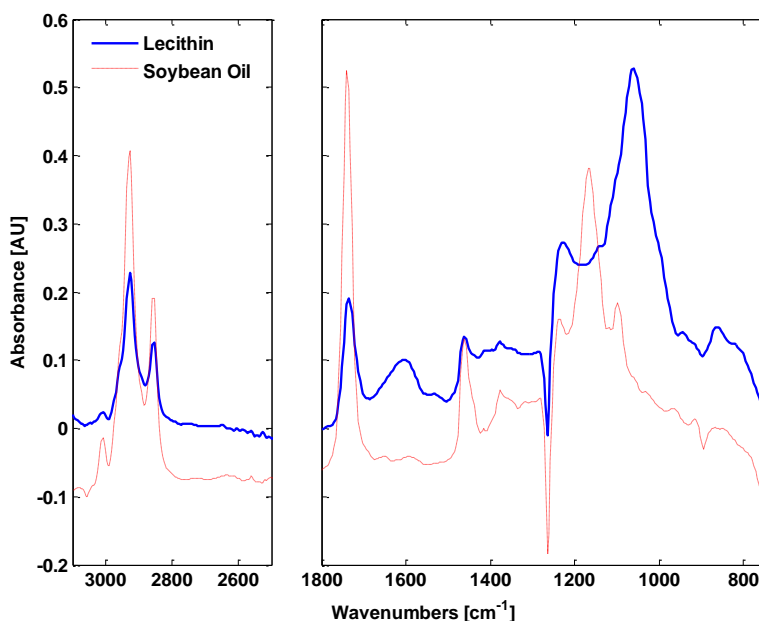


Figure 2.1.1. ATR-FTIR spectra of lecithin and soybean oil standard solutions in dichloromethane at a concentration of 50 mg mL^{-1} . Note: Spectra were shifted in the y direction to clearly show their characteristic bands.

Due to high spectral overlapping, the use of a multivariate approach would be necessary in order to develop a quantitative method for the determination of lecithin. In this case, the accuracy of the analytical results directly depends on the presence of spectral interferences not considered in the selected calibration set and thus, for each analyzed sample the suitability of the calibration set has to be verified to ensure the accuracy of the whole procedure. Therefore the hyphenation of a chromatographic

method with FTIR is justified as it reduces the range of possible interferents and thus presents the additional advantage of a wider range of applicability.

Use of first derivative spectra in on-line GPC-ATR-FTIR

Figure 2.1.2 shows a surface plot of spectra obtained as a function of time during the injection of a standard solution into the GPC system, containing lecithin and soybean oil at 50 mg mL^{-1} each. This plot leads to the conclusion that the employed columns do not provide baseline resolved peaks for phospholipids and soybean oil. On the other hand, as illustrated in Figure 2.1.1, the high spectral overlapping between the analytes avoids a complete resolution of the elution profiles of lecithin and soybean oil based only on the use of the zero order ATR-FTIR spectra.

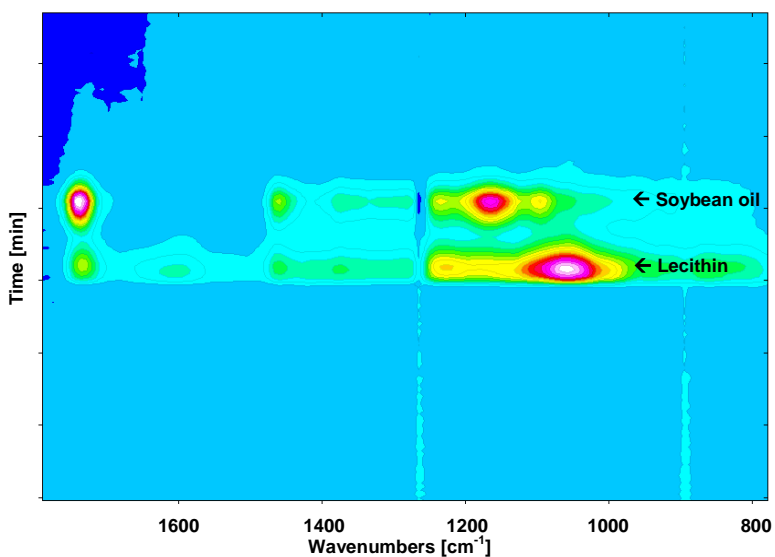


Figure 2.1.2. Surface plot obtained from the injection of a lecithin and soybean oil standard mixture.

The use of first derivative (FD) spectra is a well established technique to enhance spectral resolution and to eliminate background absorption or baseline shifts. The first derivative results in maxima where the original spectrum had maximum slopes and crosses zero where the original had a maximum. Therefore, additive constant

background effects are removed and selective spectral features are enhanced, but its use has the inconvenience of increasing the noise. The Savitzky–Golay algorithm was selected to perform the first derivative of the ATR-FTIR spectra. Employing this algorithm, data within a moving window was fitted by a polynomial of a given order to generate a differential of a chosen degree [2.26]. In other words, the algorithm fits a curve through a section of the spectrum and then calculates the slope of the tangent to this curve at the central point. To ensure that the derivative represents the local behavior of the spectrum, the number of data points defining the width of the moving window must be chosen correctly, also taking into account the spectral resolution. In this work, a 5 points moving window and a polynomial function of order 3 were selected.

Determination of lecithin and soybean oil contents

The use of on-line GPC-FTIR produces big amounts of data and, because of that, one of the most critical and time consuming steps is the selection of specific wavelengths for the quantitative determination of the analytes. The aim of this work was the development of a method for the determination of lecithin and soybean contents in samples, considering only a single wavenumber per analyte in order to simplify the process. To automate and speed up the wavenumber selection process, a fast and simple method was developed. The proposed wavenumber selection method is based on the calculation of a factor (F_i) which is a number in absorbance units that varies from 0 to a maximum value which depends on the height of the peak of the analyte and the overlapping with the interferent (see Equation 2.1.1), where $A_{i,analyte}$ and $A_{i,interferent}$ are the target and interferent chromatographic peak heights measured in the extracted chromatogram for each wavenumber (i) in the derivative spectra.

$$F_i = |A_{i,analyte} - A_{i,interferent}| \cdot \left| \frac{A_{i,analyte}}{A_{i,interferent}} \right| \quad (\text{Equation 2.1.1})$$

The calculation of the factor F_i over a defined spectral range allows to easily locate the wavenumber which minimizes the effect of the interfering compound on the chromatogram of the analyte and maximizes the intensity of the analyte signal. Figure 2.1.3 shows the first derivative spectra of lecithin and soybean oil standards in

dichloromethane, as well as the calculated F_i values in the spectral range between 4000 and 750 cm^{-1} .

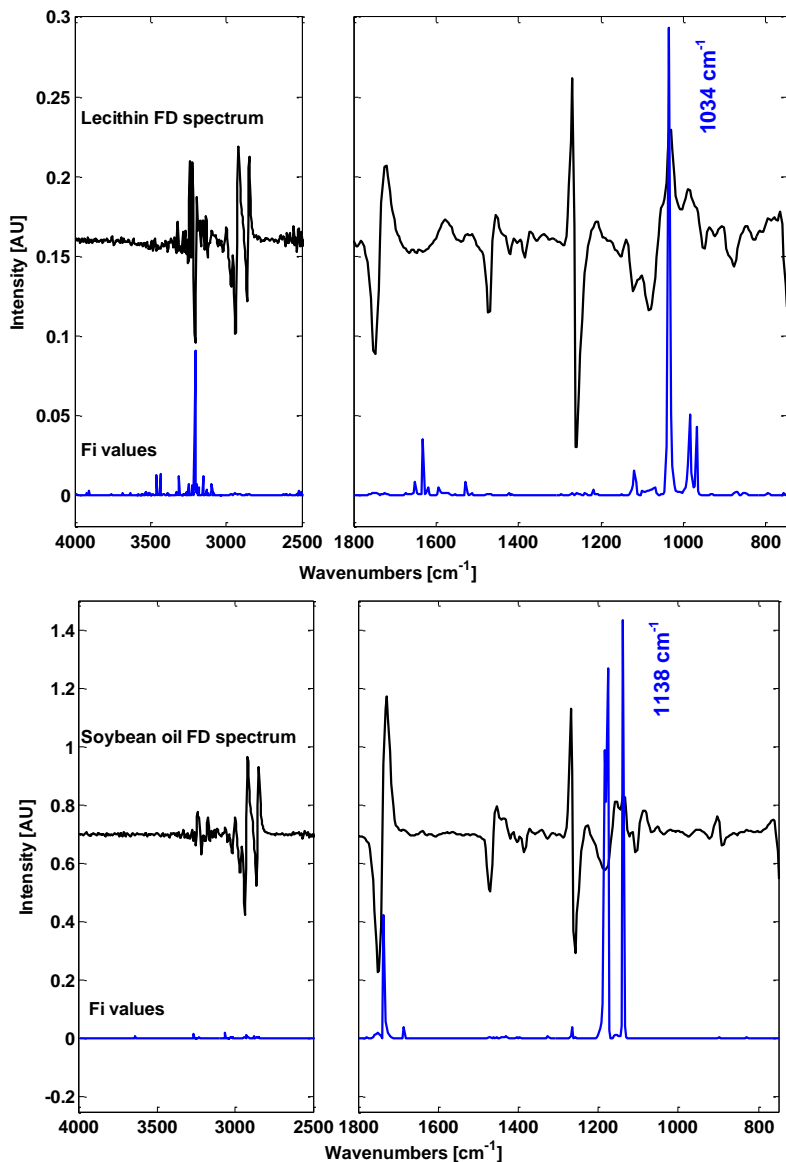


Figure 2.1.3. First-derivative FTIR spectra of lecithin and soybean oil standards in dichloromethane, and the corresponding F_i values calculated for each analyte, Note: concentrations as indicated in Figure 2.1.1.

From these plots it can be seen that several wavenumbers could be used for the extraction of lecithin and soybean oil chromatograms. In this case, the maximum F_i values were located at 1034 and 1138 cm^{-1} for lecithin and soybean oil, respectively and thus these values were used throughout this work for the extraction of the individual elution profiles.

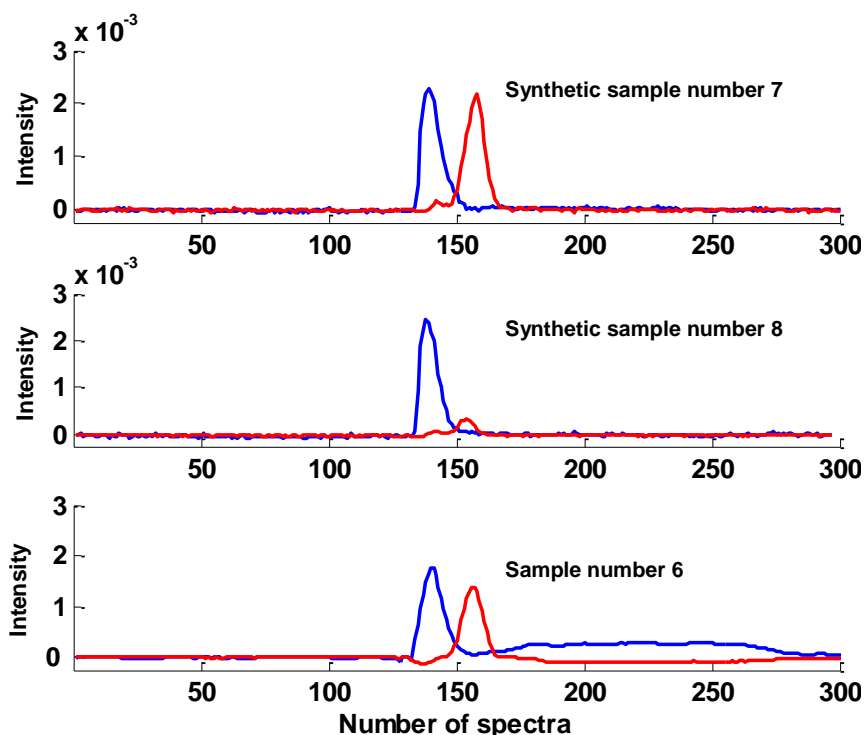


Figure 2.1.4. On-line GPC-ATR-(FD)-FTIR chromatograms of synthetic and commercial samples extracted using the selected conditions (1034 cm^{-1} for lecithin and 1138 cm^{-1} for soybean oil).

Figure 2.1.4 shows the extracted chromatograms from the injection of different samples and standard solutions under the selected conditions. The procedure was shown to be useful and easy to apply. The whole wavenumber selection process only took a few seconds, being the obtained results appropriate for an accurate quantification of both considered compounds. Chromatograms shown in Figure 2.1.4 evidence that the chromatographic overlapping of the considered compounds is not of

concern and the extracted chromatograms are selective for both analytes. Additionally, it provides excellent evidence of the usefulness of the hyphenation of GPC and ATR-FTIR eliminating the spectral contribution of sample constituents with significant absorption at the selected wavenumbers.

On the other hand, the F_i plots could be used to evidence the need of either a change in the chromatographic conditions or the use of a multivariate calibration method as applying optimum conditions (highest F_i values), a complete resolution of the elution profiles of the two considered analytes could not be achieved.

The main characteristics of the developed on-line GPC-ATR-(FD)-FTIR method are indicated in Table 2.1.2. The achieved sensitivity was sufficient to carry out the determination of lecithin and soybean oil in dietary supplements, with limits of detection (LOD) of 2 and 4 mg mL⁻¹ for lecithin and soybean oil, respectively. The repeatability of the procedure was evaluated as the relative standard deviation (RSD) of the measurements obtained from five independent injections of a standard solution containing 10 g L⁻¹ of each analyte, resulting in RSD values of 2.5 and 3.4% for lecithin and soybean oil, respectively.

Table 2.1.2. Analytical characteristics of the method developed for lecithin and soybean oil determination by on-line GPC-ATR-(FD)FTIR.

Analyte	Calibration curve $y = a + b C$ [mg mL ⁻¹]		R ²	LOD [mg mL ⁻¹]	RSD [%]	Linear range [mg mL ⁻¹]
	[a±sa]	[b±sb]				
Lecithin	$(0.6 \pm 1.0)10^{-4}$	$(1.06 \pm 0.02) \cdot 10^{-4}$	0.9992	2	2.5	2 – 100
Soybean Oil	$(-0.4 \pm 0.5)10^{-4}$	$(8.9 \pm 0.9) \cdot 10^{-5}$	0.9994	4	3.4	4 – 50

To verify the applicability and accuracy of the developed procedure, synthetic samples containing different lecithin:soybean oil ratios were analyzed. The concentration values were calculated and standard deviations were obtained by the proposed method. Actual values and the relative errors [%] are shown in Table 2.1.3. The regression lines between the actual (x) and found (y) concentrations were $y = (0.3 \pm 0.3) + (0.98 \pm 0.05)x$ for lecithin and $y = (0.5 \pm 0.4) + (0.99 \pm 0.01)x$ for soybean oil. From the intercept and slope confidence intervals, calculated as $(t_{n-2} \cdot s_a)$ and

($t_{n-2} \cdot s_b$) respectively, it can be concluded that the GPC-ATR-(FD)-FTIR does not need blank correction and is free from systematic errors. However, the accuracy levels resulting from the analysis of synthetic samples involve the absence of matrix interferences from other sample constituents. So, in order to ensure the accuracy of the method, it would be necessary to test the method for the analysis of different types of commercially available samples.

Table 2.1.3. On-line GPC-ATR-(FD)FTIR determination of lecithin and soybean oil in synthetic samples.

Synthetic sample	Concentration ([mg mL ⁻¹], n = 3)				Relative error [%]	
	Lecithin _{ACTUAL}	Soybean Oil _{ACTUAL}	Lecithin _{FOUND}	Soybean Oil _{FOUND}	Lecithin	Soybean Oil
1	50.8	24.8	50.4 ± 1.5	25.3 ± 0.5	-0.8	2.0
2	99.2	9.5	96.7 ± 0.3	10.3 ± 0.1	-2.5	9.0
3	66.5	21.5	65.6 ± 0.8	22.0 ± 0.5	-1.3	2.6
4	50.5	49.5	49.7 ± 1.0	49.6 ± 1.4	-1.6	-5.2
5	99.6	21.9	98.3 ± 0.8	23.4 ± 1.3	-1.3	7.0
6	24.5	50.0	24.8 ± 0.5	49.0 ± 0.1	1.0	-2.0
7	20.5	24.9	20.7 ± 0.8	24.5 ± 0.1	1.1	-1.6
8	24.6	4.8	23.8 ± 0.6	4.7 ± 0.1	-3.5	-1.4
9	0.0	25.1	< LOD ^a	24.9 ± 0.2	-	-0.8
10	67.9	0.0	67.4 ± 1.1	< LOD ^a	-0.7	-

Note: <LOD^a: below limit of detection

Sample analysis employing on-line GPC-ATR-FTIR

A set of seven commercially available dietary supplement samples was analyzed using the proposed methodology. As indicated in Table 2.1.4, the obtained results are in good agreement with those reported by the manufacturer. The concentrations found were statistically comparable for all analyzed samples for lecithin and soybean oil, according to the Student t-test (95% significance level, 2 degrees of freedom), obtaining calculated t values lower than 4.3 in all cases.

Table 2.1.4. On-line GPC-ATR-(FD)-FTIR determination of lecithin and soybean oil in commercial samples.

Sample	Presentation	Composition ([%] w/w, n = 3)				Difference [%]	
		Lecithin _{DECL}	Soybean Oil _{DECL}	Lecithin _{FOUND}	Soybean Oil _{FOUND}	Lecithin	Soybean Oil
1	Powder	97	-	96.8 ± 1.0	-	-0.2	-
2	Powder	97	-	97.6 ± 1.0	-	0.6	-
3	Powder	97	-	97.7 ± 0.9	-	0.7	-
4	Pills	67	5.3	68.8 ± 1.1	5.4 ± 0.1	2.7	1.0
5	Pills	69	5.5	64.6 ± 2.8	5.6 ± 0.1	-6.4	1.3
6	Pills	70	-	67.6 ± 1.9	11.3 ± 0.2	-3.4	-
7	Pills	18	-	18.3 ± 0.6	-	1.5	-

Note: DECL stands for declared.

It must be highlighted that in one of the samples (sample number 6) the presence of oil in the chromatogram could be clearly identified although this compound was not specified on the label. In order to confirm the presence of soybean oil in sample 6, spectra extracted from the chromatogram at 7.9 min were compared with previously measured reference spectra. In Figure 2.1.5 the spectrum extracted during the soybean oil elution in sample 6 and that of a soybean oil standard are compared. The correlation coefficient (r) between two spectra y_1 and y_2 is defined as the ratio of the covariance ($Cov(y_1, y_2)$) and the product of the two standard deviations σy_1 and σy_2 . According to this definition, a value of $r = 1$ indicates identical spectra. The aforementioned coefficient was calculated using the spectral intervals: 2992–2715 cm^{-1} , 1950–1430 cm^{-1} and 1245–800 cm^{-1} obtaining a value of 0.992. This value shows the high comparability of both spectra and the suitability of FTIR spectrometry to obtain useful qualitative information on the sample composition.

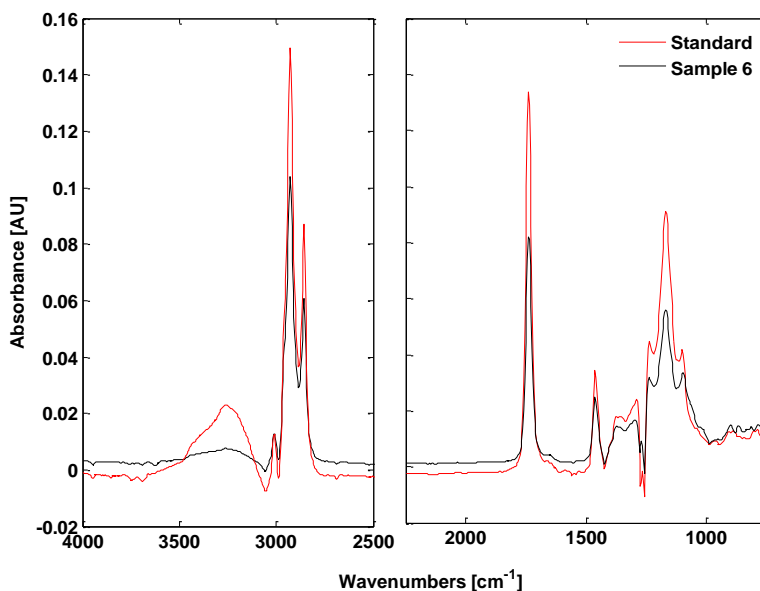


Figure 2.1.5. Comparison of a spectrum obtained from the elution of sample 6 at 7.9 min and a reference spectrum of soybean oil.

2.1.4 Conclusions

On-line GPC-ATR-(FD)-FTIR is a viable technique for the analysis of lecithin and soybean oil in dietary supplements. Both analytes can be selectively extracted in dichloromethane, separated by GPC in less than 12 min and identified and quantified by FTIR detection using the first derivative spectra. Obtained sensitivity and precision values demonstrated the ability of this detection technique to accurately identify and quantify both analytes without additional previous sample pretreatment and without the need of a complex clean-up of extracts or fraction collection after chromatography. Because of that, the developed method can be considered as an alternative to other detection techniques such as UV, RI or ELS detection in the GPC determination of lecithin and soybean oil. The simple procedure developed to carry out the wavenumber selection for the extraction of the characteristic elution profiles has proved to be a fast and accurate tool.

2.2 Monitoring of polymerized triglycerides in deep-frying olive oil by on-line GPC-IR spectrometry using the Science Based Calibration multivariate approach

2.2.1 Introduction

Olive oil is worldwide used for the preparation of a variety of food products. However, when heated, it is subjected to a series of degradation reactions. This degradation process varies according to different factors such as the type of food frying (composition, continuous or intermittent frying, quantity of fried food), fryer (capacity, surface, T, metals in contact with the oil), oil (nature, thermo-stability, amount of fresh oil) and others including the presence of protective gas, antioxidants or antifoams [2.27]. Frying olive oil, a wide variety of products can result from different chemical reactions of the unsaturated fatty acyl groups in the different triacylglycerides (TGs). According to their molecular weight and structure, the non-volatile compounds formed during a frying process can be classified in three groups: i) Polymer triacylglycerides (PTGs); dimers and oligomers are the major compounds in used frying fats and are also the major degradation compounds formed during frying [2.28]; ii) oxidized monomers; those are TGs with at least one of their fatty acyl groups oxidized and with a molecular weight close to the parent TGs and iii) TGs containing short-chain components and volatile compounds with molecular weights lower than those of parent TGs. All the aforementioned reactions (including oxidations, hydrolysis and polymerizations) take place in the unsaturated fatty acyl groups attached to the glyceridic backbone and, therefore, the stable final products are triglyceride monomers, dimers and oligomers containing modified and non-modified acyl groups. The simultaneous formation of positional and geometrical isomers gives rise to thousands of new compounds as a consequence of the frying process [2.28].

The determination of PTGs in used frying fats is nowadays employed extensively, being the accuracies of the total polar compounds and PTG determinations used as reference criteria for the evaluation of new analytical methods [2.27]. Besides, concentration levels of PTGs have been found to correlate with those of polar compounds [2.27, 29,

30]. The IUPAC Commission on Oils, Fats and Derivatives adopted GPC methods for the determination of PTGs [2.31] and polar compounds (including TGs, diacylglycerols PTGs and oxidized TGs) [2.32] in 1992 and 2000, respectively. Regarding detection in GPC systems used in oil analysis, evaporative light scattering (ELS) and refraction index (RI) detectors are widely employed. Quantitative results are obtained from the quotient between peak area of the PTGs peaks and total peak area of the chromatogram, expressed as % w/w of total oil. The use of the aforementioned detectors is supported by the lack of UV chromophor groups in the target analytes, the high levels of TGs in real samples, as well as by their relative low cost and easy operation. In spite of that, the information provided by these systems is rather limited. Thereby, the interest on the development of cost-effective detection systems providing molecular information about the eluting analytes in used oil analysis is justified.

As stated before, FTIR spectrometry is a well established detection technique that provides highly specific molecular information of a wide range of compounds [2.33]. Mid-FTIR spectrometry in combination with chemometrics has been widely used in the study of edible oil degradation processes through the direct measurement of sample spectra [2.34-37]. However, to our knowledge, there are no precedents on the on-line use of mid-FTIR detection in GPC for the monitoring of the degradation process of oils during the deep-frying process. Due to the relatively high sample amounts injected in GPC, the high concentration of the oil degradation products as wells as the isocratic use of a highly IR transparent mobile phase, FTIR detection seems feasible for this application.

In this study the quantification of the total PTG content in olive oils during deep-frying processes has been investigated using on-line GPC-FTIR. Special emphasis was placed on the evaluation of the applicability of a multivariate approach called Science Based Calibration (SBC) for increasing sensitivity and selectivity in GPC-FTIR. The SBC approach, developed by Marbach [2.38, 39], combines the main features of 'classical' and 'inverse' calibrations. The spectral signal of the target analyte is estimated in a physical way and the spectral noise in a statistical way. Although a detailed description of the procedure is out of the scope of this work, the basic steps involved in the prediction of the analyte concentration in unknown samples by SBC are indicated in the experimental section.

2.2.2 Material and methods

Apparatus and Reagents

A Hewlett-Packard (Palo Alto, CA, USA) HP1050 high performance liquid chromatography system, equipped with a polystyrene-divinylbenzene column (PLgel 100A, 3 μm , 300 x 7.5 mm) from Polymer Laboratories, Varian, Inc. (Church Stretton, Shropshire, UK) and a sample injection loop of 20 μL was employed for chromatographic separations. Dichloromethane was used as mobile phase at a flow rate of 750 $\mu\text{L min}^{-1}$.

For GPC-FTIR analysis, an IR transparent flow cell was assembled using a ZnSe and a CaF_2 window and an aluminium spacer with a channel of 3.5 mm and an optical pathlength of 150 μm . FTIR spectra acquisition was carried out using a Bruker (Bremen, Germany) IFS 66/v FTIR spectrometer equipped with a liquid nitrogen refrigerated MCT detector, a vacuum system and a dry air purged sample compartment. The scanner of the interferometer was operated at a HeNe laser modulation frequency of 100 kHz. Spectra were recorded in the range between 4000 and 950 cm^{-1} using a spectrum of the flow cell filled with the mobile phase and measured at the beginning of each GPC run as background. For each recorded spectrum, 25 scans were co-added. A resolution of 8 cm^{-1} and a zero-filling factor of 2 were applied.

For oil heating, a 1 L fryer with convective heating element, model Professional 1 (1000 W) from Taurus (Lérida, Spain) equipped with a stainless steel body and a non-stick tank with optimal heat transmission was used. Temperature applied for oil heating was measured and controlled using a thermocouple with an electrically controlled heater, model AKO (Barcelona, Spain).

Dichloromethane (99.8%, stabilized with 0.2% ethanol) was purchased from Scharlau (Barcelona, Spain). 1,2,3-tri(*cis*-9-octadecenoyl)glycerol and 1,2-di(*cis*-9-octadecenoyl)-*rac*-glycerol were purchased from Sigma (Buchs, Switzerland). *Cis*-9-octadecenoic acid was purchased from Fluka (Buchs, Switzerland). Fresh olive oil samples were directly purchased from the Spanish market.

Software and data treatment

For instrumental and measurement control as well as for data acquisition, the OPUS software (version 6.5) from Bruker was employed. Data manipulation was carried out with Matlab 7.0.1 from Mathworks Inc. (Natick, MA, USA) using in-house written functions. Spectral correlation (SC) between two spectra y_1 and y_2 was calculated as the ratio from the covariance ($Cov(y_1, y_2)$) and the product of their corresponding standard deviations $s(y_1)$ and $s(y_2)$.

Thermal treatment of oil samples

0.75 L olive oil was placed in the fryer and subjected to continuous heating at 180°C up to 30 h. To follow the oil degradation during the deep frying process, 1 mL sample aliquots were collected in glass vials at different intervals and were stored at -18°C in the dark to prevent further oxidation until analysis. The process was repeated twice using different olive oil samples (sample sets A and B). A total of 48 sample aliquots (23 in the first replicate and 25 in the second one) were analysed. An additional experiment (sample set C) was carried out adding 150 g French fries to the oil and heating it during 6 h. French fries were exchanged every 15 minutes. A total of 11 samples were collected at different intervals.

Sample preparation

300 mg of sample were accurately weighed in a volumetric flask and diluted to 10 mL with dichloromethane. Each solution was sonicated for 5 minutes in an ultrasonic water bath and then filtered through a 0.22 μm PTFE membrane prior to injection into the GPC-FTIR system.

Basics of the SBC for signal treatment

A detailed description of the SBC method can be found in references [2.38] and [2.39]. Briefly, each spectrum ($x^T(1 \times k)$) can be described as:

$$x^T = y \cdot g^T + x_n^T \quad (\text{Equation 2.2.1})$$

being y and $g^T(1 \times k)$ the concentration and the spectrum of the analyte, respectively. $x_n^T(1 \times k)$ corresponds to absorption in the measured spectrum due to instrumental noise and interfering compounds and k is the number of variables.

For a set of m spectra, $X (m \times k)$, the signal can be described by $\bar{y} \times g^T$ and $\sigma_y \times g^T$, where \bar{y} is the mean analyte concentration and σ_y is the standard deviation of y . The spectral noise is also described by a mean value, \bar{x}_n^T , and a covariance matrix, $\Sigma (k \times k)$. If the differences between the spectra included in $X (m \times k)$ are only due to variations in the concentrations of other sample constituents and to instrumental noise sources, then, after mean centering, the measured spectra represent only spectral 'noise' and $\bar{X} = \bar{X}_n$, where \bar{X} is the mean centered matrix $X (m \times k)$. According to this, the covariance of the spectral 'noise', $\Sigma (k \times k)$, is calculated as:

$$\Sigma \cong \frac{\bar{X}^T X}{m-1} \quad (\text{Equation 2.2.2})$$

A b_{opt} vector is calculated according to Equation 2.2.3:

$$b_{opt} = \frac{\sigma_y^2 \Sigma^- g}{1 + \sigma_y^2 g^T \Sigma^- g} \quad (\text{Equation 2.2.3})$$

where Σ^- corresponds to the inverse of Σ . If σ_y^2 tends to ∞ , this equation can be simplified to:

$$b_{opt(1)} = \frac{\Sigma^- g}{g^T \Sigma^- g} \quad (\text{Equation 2.2.4})$$

Finally, the vector $b_{opt(1)}$ is used in Equation 2.2.5 to predict the concentration of the analyte (y_{pred}) in each unknown sample spectrum (x_{pred}).

$$y_{pred} = \bar{y} + (x_{pred} - \bar{x})^T \cdot b_{opt(1)} \quad (\text{Equation 2.2.5})$$

being, \bar{y} the mean value of y and \bar{x} the mean of the measured 'noise' spectra $X (m \times k)$. In short, the predicted analyte concentration is based on the information content of a 'noise' matrix, $X (m \times k)$, and on an experimentally obtained analyte spectrum, g^T in an adequate spectral range.

2.2.3 Results and discussion

FTIR spectra of the mobile phase

Figure 2.2.1 (top) shows a single-channel signal of the GPC flow cell filled with mobile phase (i.e. dichloromethane) in the 4000 – 950 cm^{-1} mid-IR region. As dichloromethane presents absorption bands in this region, the transmission depends on the flow cell's pathlength. Thus, a compromise between detection sensitivity and the total width of the spectral range useful for the identification of the analytes must be made.

Considering that the concentrations of PTGs and TG in fried oil are in the percentage level, it was decided to use a pathlength of 150 μm .

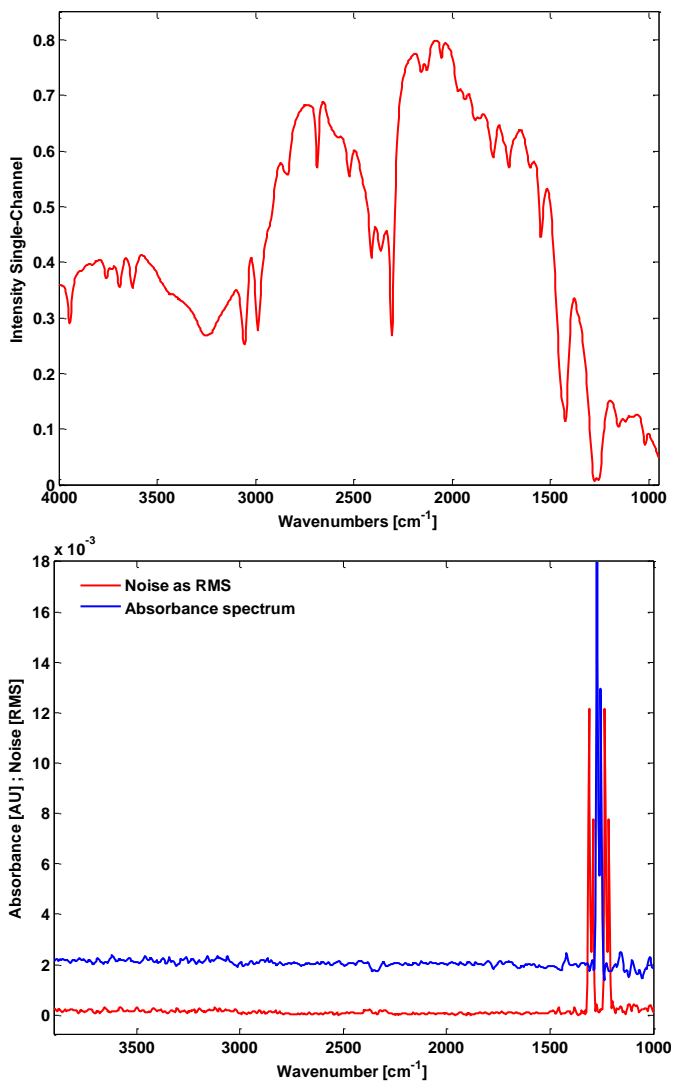


Figure 2.2.1. Top: single channel signal of the GPC flow cell filled with mobile phase (dichloromethane), bottom: absorbance spectrum (blue line) measured at the beginning of a GPC-FTIR chromatogram using a constant background of the flow cell filled with mobile phase and noise (red line) measured as root-mean-square through the spectrum. Note: The absorbance spectrum was shifted in the y direction; noise calculated from absorbance values of 20 variable (wavenumber) intervals in a moving-window mode.

In Figure 2.2.1 (bottom, blue line) an IR absorbance spectrum measured at the beginning of a GPC-FTIR run is presented. The noise (red line), calculated as the root mean square (RMS) of the absorbance values of 20 consecutive wavenumbers in a moving-window fashion over the 4000-950 cm^{-1} mid-IR range is also shown in Figure 2.2.1 (bottom). It can be seen, that the light throughput between 1300 and 1240 cm^{-1} was decreased to a great extent by the dichloromethane absorption increasing the noise in this region. However, the noise levels in the intervals 4000-1300 cm^{-1} and 1240-950 cm^{-1} were low with values of $1.01 \cdot 10^{-4}$ and $3.09 \cdot 10^{-4}$ AU, respectively.

Determination of PTG in oil samples

Figure 2.2.2 shows contour plots of on-line GPC-FTIR chromatograms obtained from the injection of the same olive oil sample before (Figure 2.2.2, top) and after (Figure 2.2.2, bottom) deep-frying at 180°C during 25 h. Whereas it was not possible to obtain a clear resolution between TG and PTGs formed during frying, the chromatographic pattern showed in both cases a peak at 10.1 min which was ascribed to monomeric TG. Peaks with retention times between 7.7 and 9.8 minutes were ascribed to TG dimers, trimers and higher oligomers as well as to a combination of breakdown products with TG [2.40]. A comparison of the retention times of the degraded oil GPC peaks with a standard solution containing tri-acylglyceride (1,2,3-tri(*cis*-9-octadecenoyl)glycerol), di-acylglyceride (1,2-di(*cis*-9-octadecenoyl)-*rac*-glycerol) and free fatty acid (*cis*-9-octadecenoic acid) standards with retention times of 10.1, 11.5 and 12.4 min, respectively, confirmed the previous classification of the eluting peaks (data not shown).

Figure 2.2.3 shows extracted spectra from the chromatogram of the degraded oil shown in Figure 2.2.2 (bottom) at 7.9, 8.7, 9.0 and 9.3 min and a reference TG spectrum extracted at 10.1 min from the injection of the same oil before the heating treatment shown in Figure 2.2.2 (top). Shown infrared spectral bands and their assignments [2.34, 35] are given in Table 2.2.1.

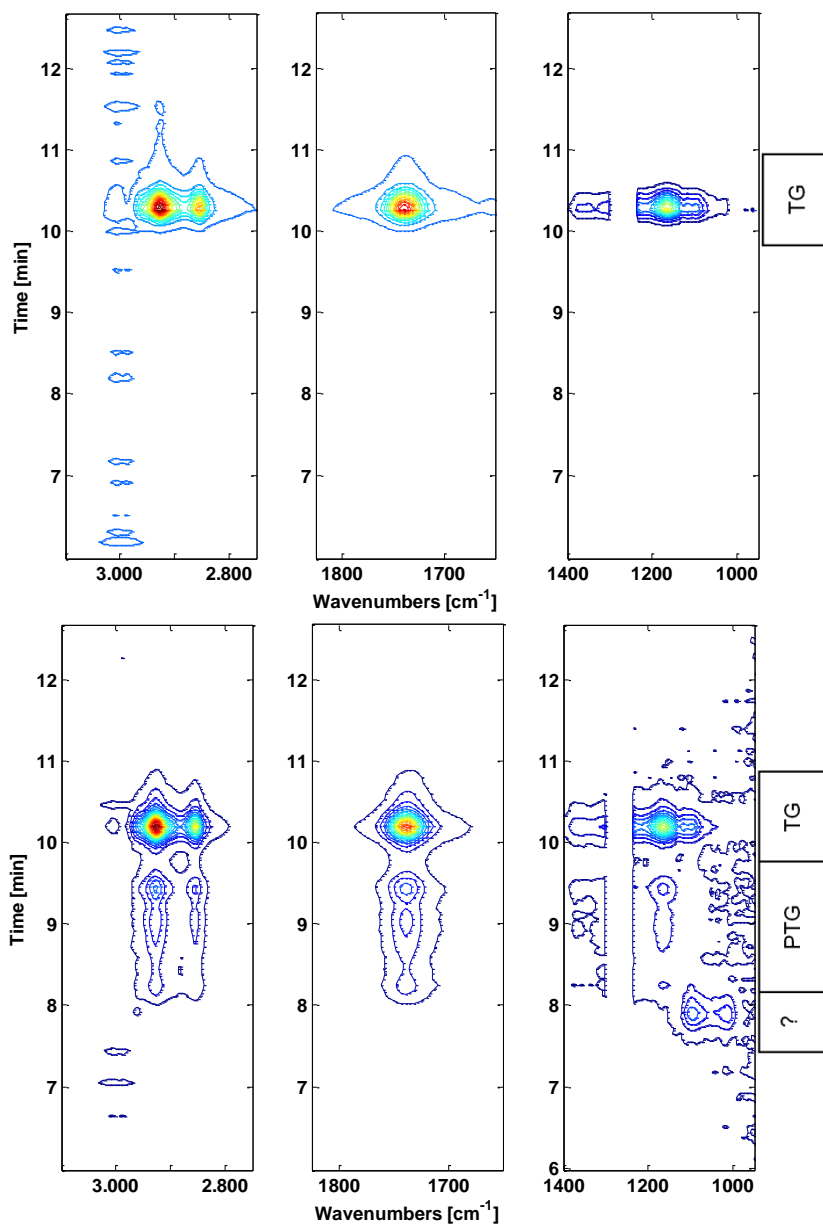


Figure 2.2.2. Contour plots of on-line GPC-FTIR chromatograms of an olive oil sample before (top) and after (bottom) a deep-frying process at 180°C during 25 h. Note: Signals between 1240 and 1290 cm⁻¹ were not included in the plot due to detector saturation.

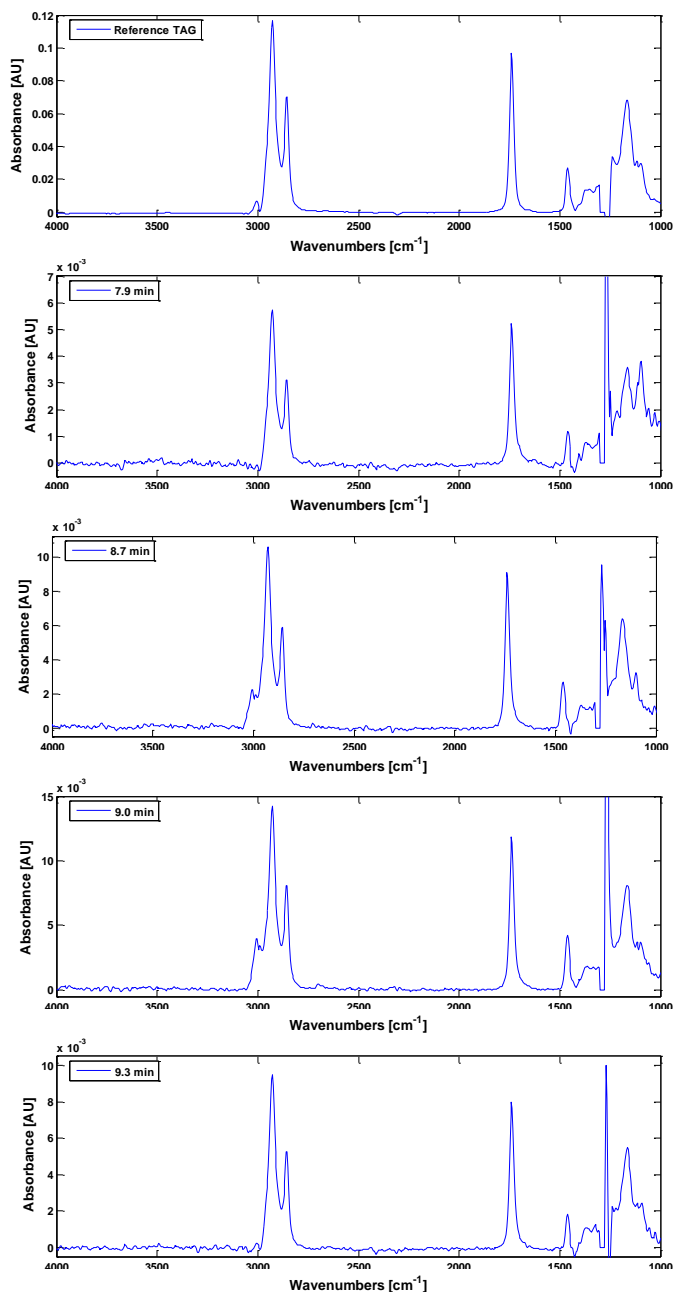


Figure 2.2.3. Reference TG spectrum obtained from the injection of the fresh olive oil sample A and spectra extracted from the injection of the same sample after 25 h of deep-frying at 180°C into the on-line GPC-FTIR system, at 7.9, 8.7, 9.0 and 9.3 min elution times.

Table 2.2.1. Infrared band assignments [2.35, 36].

Wavenumber [cm ⁻¹]	Functional group and mode of vibration
3025	=CH <i>trans</i> stretching
3006	=CH <i>cis</i> stretching
2953	CH (CH ₃) asymmetric stretch
2924	CH(-CH ₂ -) asymmetric stretch
2854	CH(-CH ₂ -) symmetric stretch
1746	-C=O ester stretching
1653	-C=C- <i>cis</i> stretching
1465	-CH ₂ scissoring
1377	HCH symmetric bending
1238	-C-O, -CH ₂ - stretching, bending
1161	-CH ₂ - wagging
1118	-C-O stretching

The very high spectral similarity between the different PTG peaks and the TG spectrum is reflected by the calculated spectral correlation (*SC*) values for sample A using the spectral regions indicated in Table 2.2.2: i) 4000 -1322 cm⁻¹ + 1214 - 950 cm⁻¹; ii) 1900 - 1322 cm⁻¹ + 1214 - 950 cm⁻¹ and iii) 1900 - 1600 cm⁻¹. These spectral regions have been selected to compare the effect of the most intense and characteristic vibrations of PTGs in the mid-IR region on the quality of the results. The first and second intervals exclude the 1322-1214 cm⁻¹ and 4000-1900 and 1322-1214 cm⁻¹ regions, respectively, because of their higher noise levels (see Figure 2.2.1, bottom). The third interval focuses on a narrow spectral region with a high signal to noise ratio to evaluate in a realistic way whether the proposed multivariate approach improves the sensitivity and to which extent. Spectral correlation values in the 0.99-0.9999 range were also found between the reference TG spectrum and spectra of PTGs extracted from the chromatograms of other degraded samples, fried in the absence or in presence of foodstuff (data not shown).

Table 2.2.2. Spectral correlations between the different peaks extracted from the injection of the olive oil sample A after heating for 25 h at 180°C, at 7.9, 8.7, 9.0, 9.3 and 10.1 min and a reference TG spectrum extracted from the injection of the same oil before heating.

Interval	4000 - 1322 cm ⁻¹ + 1214 - 950 cm ⁻¹					1900 - 1322 cm ⁻¹ and 1214 - 950 cm ⁻¹					1900 - 1600 cm ⁻¹							
	7.9 min	8.7 min	9.0 min	9.3 min	10.1 min	TG	7.9 min	8.7 min	9.0 min	9.3 min	10.1 min	TG	7.9 min	8.7 min	9.0 min	9.3 min	10.1 min	TG
7.9 min	1	0.1140	0.2830	0.2164	0.1524	0.1580	1	0.0791	0.2249	0.1571	0.0873	0.0898	1	0.7092	0.7078	0.7155	0.7176	0.7171
8.7 min		1	0.9873	0.9305	0.9699	0.9680		1	0.9458	0.9631	0.9739	0.9724		1	0.9988	0.9988	0.9979	0.9976
9.0 min			1	0.9873	0.9757	0.9775			1	0.9922	0.9794	0.9800			1	0.9994	0.9986	0.9982
9.3 min				1	0.9943	0.9949				1	0.9942	0.9945				1	0.9994	0.9990
10.1 min					1	0.9997					1	0.9999					1	0.9999
TG																		1

A peak at 7.9 min from an unidentified contamination source could also be observed showing a FTIR spectrum clearly different from that of TG ($SC_{(\text{interference, TG})} = 0.1582$ in the 4000-950 cm^{-1} interval). The presence of this peak can be troublesome because it strongly overlaps with the front of high-order PTGs.

For the extraction of 'triglyceride' chromatograms, the SBC approach was used as indicated in the previous section. The accuracy of the SBC-predicted values relies on an appropriate selection of i) the spectral range, ii) the g^T vector and iii) the X ($m \times k$) matrix. Considering the aforementioned aspects, three different spectral intervals were evaluated: i) 4000 - 1322 cm^{-1} + 1214 - 950 cm^{-1} ; ii) 1900 - 1322 cm^{-1} + 1214 - 950 cm^{-1} and iii) 1900 - 1600 cm^{-1} .

Regarding the reference spectrum, it has to be remarked that under the IR-acquisition conditions used in this work, results found by SBC to extract 'PTG specific' chromatograms using the spectrum of PTG extracted from the chromatogram of heated olive oil samples in the 7.7 – 9.8 min time window were not satisfactory at all, because in all cases the TG peak was also clearly detected due to the high correlation between PTG and TG spectra (results not shown). Therefore, the use of a reference TG spectrum extracted from the chromatogram of a fresh olive oil sample at 10.1 min (Reference TAG, Figure 2.2.3) was tested as g^T vector. Thus, the use of SBC to calculate specific chromatograms for a family of compounds with highly correlated spectrum (HCS) in the mid-IR region was evaluated.

Regarding the 'noise' matrix (X ($m \times k$)), two possibilities were considered: i) the use of the chromatogram of a fresh olive oil sample, and ii) the use of a dichloromethane blank GPC-FTIR chromatogram. Using the chromatogram of a fresh olive oil sample as 'noise' matrix, the calculated relative concentrations of TG-HCS compounds during the chromatographic run were strongly inaccurate. Although results depend on the spectral region used (see Figure 2.2.4, top), chromatographic peaks were either below the limit of detection or showed a very poor signal to noise ratio. Alternatively, results improved when the 'noise' matrix X ($m \times k$) = X_B was composed by the spectra measured during the injection of a dichloromethane blank (thus including only instrumental noise and changes in the background eluent IR absorption during a GPC run). In this case the equation used to calculate the relative concentrations of TG-HCS compounds during each injected sample chromatogram was equal to:

$$y_{pred} = \bar{y}_{\chi_A} + (x_{pred} - \bar{x}_B)^T \cdot \frac{\Sigma_{\bar{B}} g}{g^T \Sigma_{\bar{B}} g} \quad (\text{Equation 2.2.6})$$

being \bar{x}_B the average concentration of TG-HCS compounds in the "noise" spectra equal to 0. As an example, Figure 2.2.4 (middle) shows the SBC chromatograms for the GPC-FTIR injection depicted in Figure 2.2.2, calculated using each of the considered IR ranges. Besides, Figure 2.2.4 (bottom) shows the GPC-FTIR chromatograms obtained performing a 'direct' integration of the spectral area in the same selected intervals, corrected using a single-point baseline at 1900 cm^{-1} .

From results shown in this figure it became clear that heating led largely to the formation of high molecular weight cross-linked TG. Low molecular weight products formed during the heating could not be detected in this study in any of the analyzed sample data sets.

The interference peak at 7.9 min could not be detected in any of the SBC chromatograms, thus confirming that the SBC approach increased the selectivity of the extracted chromatograms indicating that there exist significant spectral differences between the employed g^T vector and the interferent spectrum. On the contrary, using the 'direct' integration of the spectral area, the eluting peak at 7.9 min was detected when using the 4000 - 1322 cm^{-1} + 1214 - 950 cm^{-1} and the 1900 - 1322 cm^{-1} + 1214 - 950 cm^{-1} regions. Only when the C=O region between 1900 and 1600 cm^{-1} was used, the interference was not detected in the chromatograms obtained using the 'direct' integration of the spectral area (Figure 2.2.4, bottom).

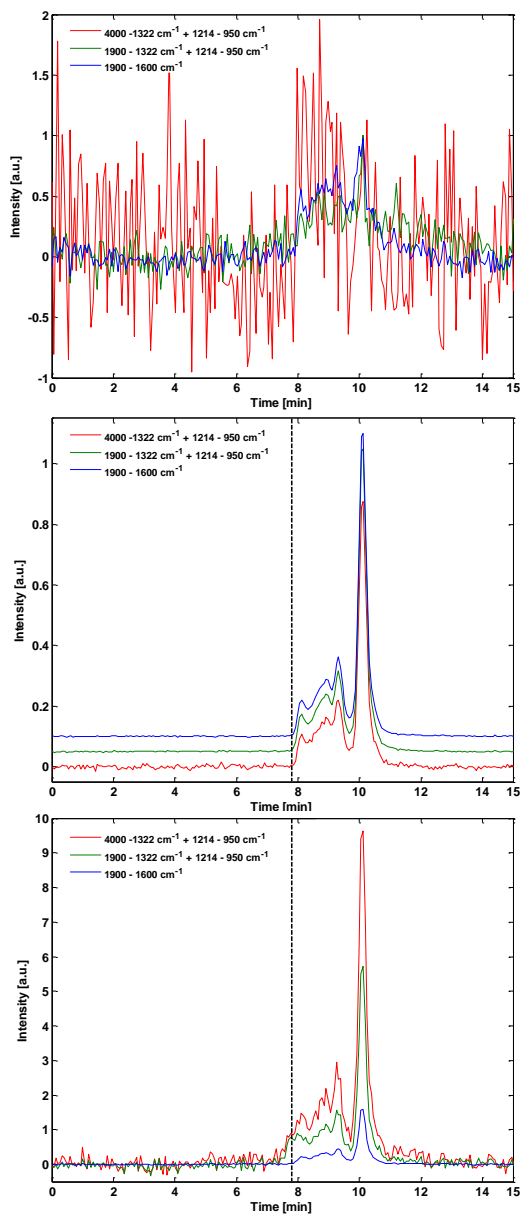


Figure 2.2.4. GPC-FTIR chromatograms extracted from the injection of olive oil sample A after 25 h of deep-frying at 180°C using SBC (top and middle) and direct integration of the spectral area using different spectral regions (bottom). Note: The different SBC conditions are specified in the text. The dashed line indicates the elution of the unknown interfering compound.

Evaluation of the analytical figures of merit of the GPC-FTIR method

In order to compare the sensitivity provided by SBC and the direct integration of the spectral area, a series of 8 fresh olive oil sample solutions in dichloromethane with concentrations of olive oil in the 0.2-29 mg mL⁻¹ range were injected into the GPC system. The main analytical features of both considered approaches are indicated in Table 2.2.3. From results found, it is clear that a significant improvement in the signal-to-noise-ratio could be achieved by the proposed multivariate approach for all three considered spectral ranges. The use of SBC provided lower limits of detection (LOD) and higher R² and repeatability values (evaluated as the relative standard deviation of 6 replicate injections of an olive oil standard with a concentration of 0.9 mg mL⁻¹) than the classical approach. The achieved sensitivity was proved to be enough to carry out the determination of PTGs during deep-frying studies even at the early stages of degradation, with limits of detection of the order of 0.6-0.8% w/w for an oil sample with a concentration of 30 mg mL⁻¹ if we consider that the LODs for TG and PTG are the same.

Monitoring of the total polymerized TG content

The monitoring of the total polymerized TG content during the frying process was carried out by the calculation of the PTG peak area divided by the total area of the chromatogram, and expressed as % w/w in the oil. Figure 2.2.5 shows the chromatograms calculated using SBC for the three sample data sets considered in this study, using the spectral region between 1900 and 1600 cm⁻¹ for calculation, as this region provided the lowest LODs (see Table 2.2.3). As it can be seen, the TG and PTG peaks are clearly identified in the three considered sets of heated samples.

Table 2.2.3. Main analytical features obtained using different spectral ranges and both considered approaches, SBC and direct measurement of the spectral area, found using different spectral ranges for the quantification of the TG peak in fresh olive oil solutions.

Spectral Interval [cm ⁻¹]	SBC ^a				Spectral Area ^b			
	4000 – 1322	1900 – 1322	1900 – 1600	1900 – 1600	4000 – 1322	1900 – 1322	1214 – 950	1214 – 950
(a±s _a)	0.007±0.003	0.007±0.002	0.008±0.003	0.008±0.003	0.05±0.06	0.04±0.03	0.014±0.005	0.014±0.005
(b±s _b)	0.01748±0.0002	0.01772±0.0002	0.01764±0.0002	0.01764±0.0002	0.156±0.004	0.101±0.002	0.0274±0.0003	0.0274±0.0003
R ²	0.9992	0.9995	0.9995	0.9995	0.9967	0.9982	0.9992	0.9992
RSD ^c [%] (n=6)	6.3	3.1	2.5	2.5	6.5	39.1	18.1	18.1
Noise ^d (RMS)	0.0047	0.0009	0.0008	0.0008	0.2136	0.1023	0.0632	0.0632
S/N ^e	10.0	49.7	53.7	53.7	1.1	1.8	7.4	7.4
LOD ^f [mg mL ⁻¹]	0.51	0.24	0.19	0.19	2.3	2.2	1.5	1.5
LOD ^{g,h} [% w/w]	1.7	0.79	0.65	0.65	7.6	7.3	5.0	5.0

SBC^a: SBC conditions as indicated in the text; Spectral Area^b: Spectral area corrected using a single-point baseline correction at 1900 cm⁻¹; RSD^c: Values obtained from six replicate measurements of a standard containing 0.9 mg mL⁻¹ olive oil (sample A); Noise^d: Noise measured as root mean square in the 0-9 min time interval in the chromatogram of a standard containing 0.9 mg mL⁻¹ olive oil (sample A); S/N^e: Signal to noise ratio from six replicate measurements of a standard containing 0.9 mg mL⁻¹ olive oil (sample A), calculated as $S/N = \bar{A}_{TG} \cdot \overline{Noise}_{RMS}$, where \bar{A}_{TG} is the mean TG peak area value and \overline{Noise}_{RMS} is the mean noise (as RMS) of olive oil (sample A), calculated as $S/N = \bar{A}_{TG} \cdot \overline{Noise}_{RMS}$; LOD^f: Limit of detection (LOD) of olive oil TG peak in dichloromethane calculated as $LOD = 3 \cdot s_b \cdot b^{-1}$, being s_b the standard deviation of six replicate measurements of a solution containing 0.5 mg mL⁻¹ olive oil (sample A) and b the slope of the calibration. LOD^g: % w/w concentrations of PTG and TG were calculated throughout this work as $100 \cdot A_{PTG} / (A_{PTG} + A_{TG})$ and $100 \cdot A_{TG} / (A_{PTG} + A_{TG})$, respectively, where A_{PTG} is the area of the PTG peak (retention time window from 7.7 to 9.8 min), and A_{TG} is the area of the TG peak at a retention time of 10.1 min.

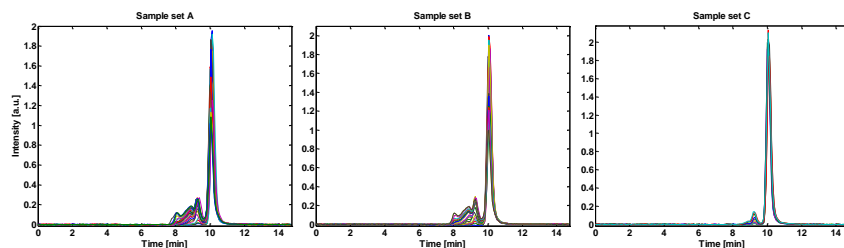


Figure 2.2.5. SBC chromatograms of different fried olive oil samples using the spectral region between 1900 and 1600 cm^{-1} for different oil sets (sample sets A, B, C) heated alone (sample sets A, B) or with potatoes (sample set C). Note: SBC conditions indicated in the text.

Figure 2.2.6 shows the evolution of the obtained total polymerized TG content as a function of the heating time for sample sets A, B and C using the chromatograms calculated with SBC for the three considered spectral intervals, as indicated in the figure, without any outlier removal. The values of PTG contents increase with increasing heating time. Differences in the polymerization rates between replicates which can be observed in this figure could be explained by uncontrolled experimental variables briefly described in the introduction which may affect the kinetics of polymerization.

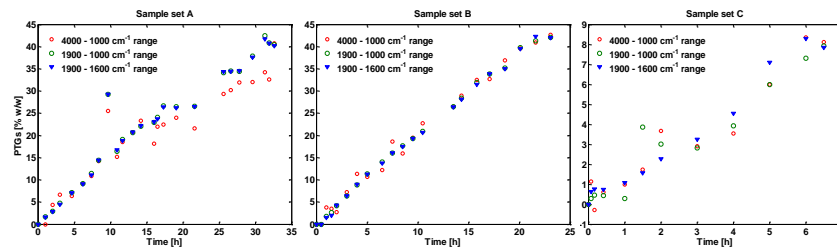


Figure 2.2.6. Evaluation of the calculated content of total PTG using different wavenumber intervals as a function of frying time for the three considered data sets indicated in Figure 2.2.5.

2.2.4 Conclusions

The extraction of GPC-FTIR chromatograms using a multivariate technique (SBC) might improve both, the sensitivity and selectivity of the technique as compared to the use of the 'classical' univariate approach consisting in measuring the change of the spectral area in a defined interval with time. Taking advantage of the high similarity between

mid-IR spectra of PTGs and that of TG, the proposed approach has been used for the monitoring of the polymerization process of olive oil during deep-frying experiments with a calculated LOD of 0.19 mg mL^{-1} corresponding to 0.65% w/w for an olive oil sample mass of 300 mg. Results included in this work have shown that the proposed GPC-FTIR approach does not need extensive sample clean-up or pre-concentration steps, thus it might be adapted for the analysis of PTGs in a broad range of situations. The developed method is simple and straightforward but, in order to ensure an adequate use, a previous study of the spectral similarities between the analytes that are pretended to be quantified and the interferences and mobile phase components is strongly recommended.

2.3 Determination of glycolic acid in cosmetics

2.3.1 Introduction

Lately, the use of α hydroxy acids (AHAs) in commercially available cosmetic formulations has noticeably increased. Glycolic acid is one of the most common AHAs that can be found in cosmetics. The concentration range, in which it can be found in market products, is quite broad ranging from 10% w/w in face creams to ~70% w/w in chemical peeling products for professional use. The determination of the concentration of AHAs in the above mentioned products is of special importance due to the direct relationship between the acid concentration and the potential to cause adverse reactions on the user [2.41]. AHAs containing products improve skin conditions and are therefore included in different formulations such as creams, make-up, hair, nail or bath products, colognes, and suntan preparations [2.42].

LC provides a rapid and simple strategy for the analysis of AHAs in complex matrices [2.43]. The most frequently employed LC methods include ion-exchange, ion-exclusion, ion-pair and reversed-phase chromatography. The choice of the LC method must be carried out according to the relative analyte concentration as well as the nature of the matrix in which the analytes are present. A number of methods have already been published using LC with UV detection for the quantification of glycolic acid in cosmetic samples [2.41, 43-46]. UV detection is used in LC for the determination of chromophor containing molecules due to its relative high sensitivity, the low cost and because of the fact that it can be used in both, isocratic and gradient elution mode, being also compatible with most of the solvents and additives. However, glycolic acid shows a weak UV absorbance due to the absence of chromophor groups in its structure. On the other hand, the C=O group as well as the CH₂ group of glycolic acid present intense bands in the mid-IR fingerprint region which are useful for its identification and quantification [2.47]. So, FTIR spectrometry offers a feasible alternative for the quantification of glycolic acid, without requiring the use of expensive detectors, like mass spectrometry, or the use of non-specific detectors with very low selectivity, such as RI or ELS detectors.

Whereas the use of FTIR detection in continuous flow systems is an established concept which in the present is used in many routine analytical procedures, it has been

scarcely employed in LC due to the limited sensitivity as compared to other common detectors like UV, fluorescence or mass spectrometry. The importance of this drawback can be minimized using narrow-bore LC columns with a small inner diameter of 2 mm. These columns provide optimal chromatographic resolution at reduced mobile phase flow rates, thus reducing the importance of the relative low time resolution of FTIR detection and improving the stability and overall performance of the flow cells used in on-line LC-IR [2.43]. Additionally, the solvent consumption is drastically reduced providing additional benefits for the environment and helping to reduce the analysis costs [2.48].

In this context, a method for the determination of glycolic acid in commercially available cosmetic samples, based on the use of hyphenated on-line FTIR detection in isocratic reversed phase LC, was developed and evaluated. To optimize FTIR data acquisition, the rapid scan mode was used resulting in a high spectral sampling frequency.

2.3.2 Material and methods

Apparatus and Reagents

A Dionex high performance liquid chromatography system, equipped with a 7725 Rheodyne manual injector (Cotati, CA, USA) and a 20 μL injection loop, was used for the chromatographic analysis. Separation was achieved using a C_{18} column (250 x 2.0 mm, 5 μm) under isocratic conditions with a mobile phase composed of acetonitrile:phosphate buffer (25 mM, pH 2.7), 3:97 v/v at a flow rate of 150 $\mu\text{L min}^{-1}$. For spectra acquisition, a Bruker IFS66 (Bruker, Bremen, Germany) FTIR spectrometer, equipped with a liquid nitrogen refrigerated mercury–cadmium–telluride (MCT) detector and a vacuum system, was employed. The scanner for the interferometer was operated at HeNe laser modulation frequency of 100 kHz and the spectral resolution was set to 8 cm^{-1} . Spectra were obtained averaging 25 scans. For the on-line LC-IR measurements, a flow cell with BaF_2 and ZnSe windows (5 x 24 mm), an optical pathlength of 14 μm and a volume of 1.7 μL was used.

A glycolic acid standard was purchased from Guinama (Valencia, Spain) with a purity of 99%. Acetonitrile (LC grade) and phosphoric acid were obtained from Scharlau

(Sentmenat, Spain). Water was purified with a Millipore system. Three cosmetic creams containing glycolic acid were purchased from local retail stores and pharmacies (Valencia, Spain). Sample A and B were cosmetic creams produced by Neostrata Laboratories with labeled glycolic acid concentrations of 15 and 8% w/w, respectively. Sample C was formulated by Eau Thermale Avène laboratories with a declared glycolic acid concentration of 6% w/w.

Standard and sample preparation

Six standard solutions with concentrations ranging from 0.174 to 1.96 mg mL⁻¹ were prepared in acetonitrile:25 mM phosphate buffer (pH 2.7) (3:97 v/v) and filtered through a 0.22 µm PTFE membrane. An accurate amount of cosmetic sample between 0.25 and 1 g was weighed in a 10 mL volumetric flask and diluted with an acetonitrile:25 mM phosphate buffer (pH 2.7) (3:97 v/v) mixture. An adequate sample amount was selected to fall within the concentration interval of the calibration line. Samples were sonicated during 20 minutes and filled up to volume after reaching room temperature. The obtained emulsions were centrifuged for 20 minutes at 3000 rpm and filtered through a 0.22 µm PTFE membrane before measurement. Extracted samples with glycolic acid concentrations higher than 1.96 mg mL⁻¹ were conveniently diluted. For recovery experiments, appropriate amounts of glycolic acid standard from 3.7 to 9.8 mg, were added to 400 mg of the three original cosmetic creams before sample treatment and analysis following the procedure indicated above. 20 µL of each standard solution and sample extract were injected into the chromatographic system.

Software and data treatment

For instrumental as well as measurement control and data acquisition, the OPUS software (version 4.1) from Bruker was employed. The measurement of the LC-IR chromatograms was performed in the rapid scan time-resolved acquisition mode, using the spectrum of the mobile phase measured before each LC injection as background. A waiting time of 50 ms between the acquisitions of consecutive interferograms was used to meet the requirements of the LC process velocity. Unlike the “chromatography” mode included in the OPUS software, in the rapid scan acquisition mode the obtained interferograms are averaged and stored in the RAM of the PCs

AQP. Subsequently, after completion of the data acquisition, they are transformed into IR absorbance spectra [2.49]. Under rapid scan measurement conditions it is possible to reduce the time gap between the measurements of consecutive spectra, thus increasing the spectral acquisition frequency from 15 spectra min^{-1} to 38 spectra min^{-1} using the experimental parameters described above.

The glycolic acid concentration of sample extracts was calculated from peak heights and peak areas of the extracted chromatograms interpolated in external calibration lines established using data from the injection of six standard solutions. The recovery percentages were established from the relative differences between the added concentrations and those found after analysis of the spiked samples.

2.3.3 Results and discussion

Spectra of glycolic acid and mobile phase used for sample extraction

Figure 2.3.1 (top) shows the single-channel spectrum of the LC flow cell filled with the mobile phase used for the extraction and chromatographic determination of glycolic acid. Measuring aqueous solutions in the mid-IR region is not straightforward since water shows intense absorption bands in this region, reducing the amount of transmitted, detectable light. The intense water bending absorption band at 1640 cm^{-1} is responsible for the reduced signal to noise ratio of, in this case, 3×10^{-4} AU (measured as root mean square) in the region between 1700 and 1600 cm^{-1} . However, Figure 2.3.1 shows that despite the high water content, the region between 1500 and 1100 cm^{-1} , which includes the most prominent analyte bands, provides adequate transmission resulting in a noise level of 7.2×10^{-5} AU. So, qualitative and quantitative analysis of glycolic acid can be carried out using the selected experimental conditions.

Figure 3.2.1 (bottom) shows the ATR spectrum of a 1 mg mL^{-1} glycolic acid standard in the aforementioned solvent using the same solvent as background. The most intense and characteristic bands correspond to the C=O group (1720 cm^{-1}), to the coupling of CH_2 and the CO groups (1242 cm^{-1}) and the CO vibration (1094 cm^{-1}) [2.47].

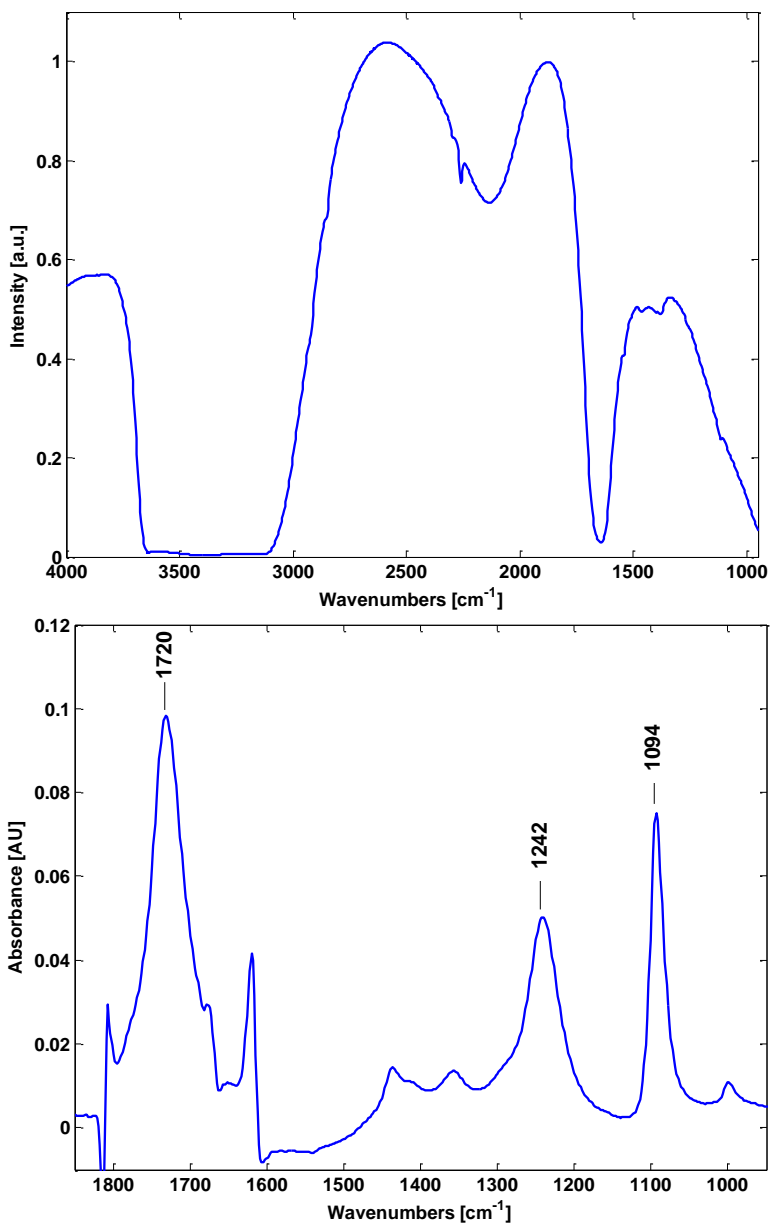


Figure 2.3.1. FTIR spectra of glycolic acid and the acetonitrile:phosphate buffer (25 mM, pH 2.7) (3:97 v/v) solution used for extraction and chromatographic determination; top: single-beam spectrum of the mobile phase; bottom: ATR spectrum of 1 mg mL⁻¹ glycolic acid standard.

On-line LC-IR characteristics

From the spectrum shown in Figure 2.3.1 (bottom) three main absorption bands useful for the determination of glycolic acid can be seen. The presence of the water absorption band at 1640 cm^{-1} strongly reduces the signal to noise ratio (S/N) in the extracted chromatograms calculated using the intense carbonyl band at 1720 cm^{-1} . The spectral region including the C=O band at 1094 cm^{-1} also shows a low S/N because of the reduced transparency of the flow cell windows. On the other hand, the characteristic coupling vibration of CH_2 and the C=O group of glycolic acid at 1242 cm^{-1} is located in a spectral region with a high transparency. Therefore, this latter band can be used to extract LC-IR chromatograms, as shown in Figure 2.3.2 where an extracted chromatogram of a face cream sample is depicted, confirming the nature of the eluting compound.

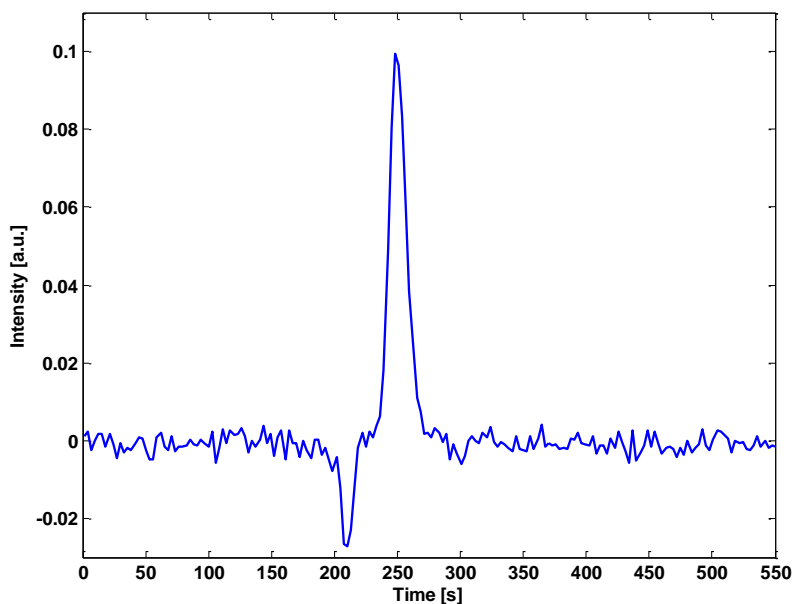


Figure 2.3.2. On-line LC-IR chromatogram obtained from the injection of the extract of a cosmetic sample with a declared glycolic acid concentration of 8% w/w.

The acquired FTIR spectra of all standard and sample solutions were integrated between 1288 and 1215 cm^{-1} with a linear baseline correction established between 1319 and 1150 cm^{-1} to extract the corresponding chromatograms. The obtained

chromatograms of standard solutions were used to establish external calibration lines via linear regression. Table 2.3.1 summarizes the main analytical features of the LC-IR calibrations based on the use of both, the chromatogram peak height and area values. The limit of detection (LOD) values and the limits of quantification (LOQ), were established from five repeated measurements of a standard solution with a concentration of 0.174 mg mL^{-1} of glycolic acid applying the equations $LOD = 3 \cdot \frac{s}{a}$ and $LOQ = 10 \cdot \frac{s}{a}$ being s the standard deviation and a the calibration slope. For precision (or more specific: system repeatability), expressed as the relative standard deviation (RSD) of the chromatographic signal of five repeated measurements of a standard solution with a concentration of 0.174 mg mL^{-1} of glycolic acid, appropriate values of 7.5% and 6% using peak height and area values, respectively, were achieved. From the features of the aforementioned calibrations it can be concluded that both, peak height and area measurements provided a good linearity in the evaluated concentration range. The achieved sensitivity was adequate for the analysis of glycolic acid in commercial cosmetic samples.

Table 2.3.1. Calibration features of on-line LC-IR determination of glycolic acid using peak height and peak area values.

Criterion	Calibration equation $y = (a \pm s_a) x + (b \pm s_b)$	R^2 ^a	LOD ^b	LOQ ^b	Linearity ^c	RSD ^d
peak height	$y = (6.30 \pm 0.08) \cdot 10^{-5} x + (1.4 \pm 0.8) \cdot 10^{-3}$	0.9994	47	156	0.16 – 1.96	7.5
peak area	$y = (3.440 \pm 0.008) \cdot 10^{-4} x + (0.0 \pm 0.8) \cdot 10^{-3}$	0.99998	34	115	0.12 – 1.96	6

Note: R^2 ^a: correlation coefficient, LOD^b and LOQ^b: limit of detection and limit of quantification in [mg L^{-1}]. These values were calculated from five repeated measurements of a standard solution with a concentration of 0.174 mg mL^{-1} of glycolic acid applying the equations $LOD = 3 \cdot \frac{s}{a}$ and $LOQ = 10 \cdot \frac{s}{a}$, being s the standard deviation and a the calibration slope, Linearity^c: measured in mg mL^{-1} , RSD^d: relative standard deviation in % calculated from five repeated measurements of a standard solution with a concentration of 0.174 mg mL^{-1} of glycolic acid.

Sample analysis employing on-line LC-IR

Three face cream samples A, B, and C, with different labeled concentrations of glycolic acid, were analyzed using the previously described on-line LC-IR procedure. The average concentrations and standard deviations obtained using peak height and peak area measurements as well as the labeled values are indicated in Table 2.3.2. Results found using the on-line LC-IR method are in good agreement with the labeled values.

Table 2.3.2. Results of the analysis of three cosmetic samples using on-line LC-IR.

Sample	Labeled content [% w/w]	Glycolic acid concentration found ^a [% w/w] ± s ^b (% RSD ^c)	
		Peak height	Peak area
Sample A	15	11.54 ± 0.16 (1.38)	14.97 ± 0.27 (1.8)
Sample B	8	7.44 ± 0.12 (1.6)	7.98 ± 0.17 (2.2)
Sample C	6	5.35 ± 0.31 (5.8)	5.99 ± 0.17 (2.8)

Note: Glycolic acid concentration found^a: average of three independent analyses; s^b: standard deviation; RSD^c: relative standard deviation in %.

The selectivity of the extracted chromatograms can be appreciated in Figure 2.3.2 and comes from both, the high resolution provided by the chromatographic separation and the selection of the IR absorption band used for the extraction of the chromatograms. Figure 2.3.3 shows two spectra extracted at 210 and 250 s from the injection of a cosmetic sample extract. The spectra correspond to an eluting interference compound and to glycolic acid, respectively. The spectrum of glycolic acid correlates very well with the reference spectrum measured in stopped flow mode (see Figure 2.3.1, bottom). On the other hand, the interference spectrum at 210 s can be used to confirm the presence of co-extracted compounds in the sample extracts.

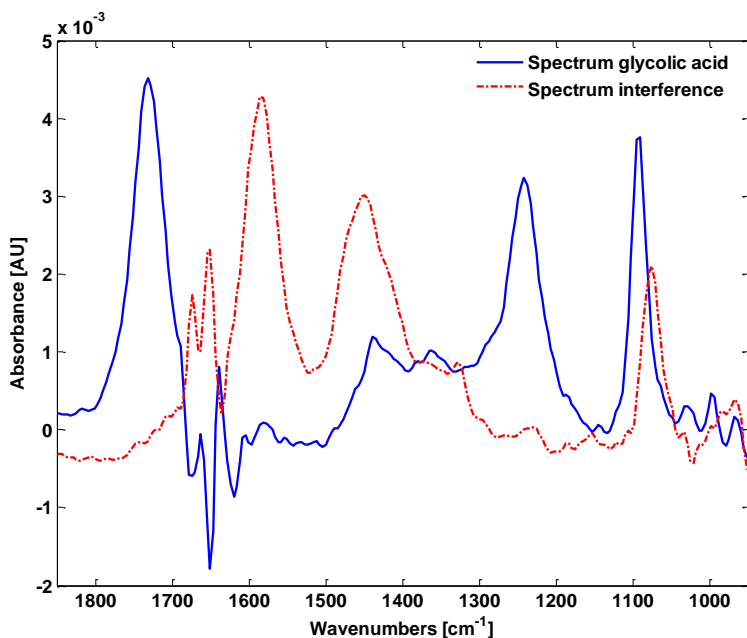


Figure 2.3.3. FTIR absorbance spectra extracted at two different defined elution times from the on-line LC-IR analysis of sample B.

The presence of the interfering compounds justifies the use of a chromatographic separation prior to IR detection rather than the use of IR based direct determination methods using chemometrics. To avoid that interfering co-extracted matrix components affect the accuracy of IR based direct determination methods, in this application basically three approaches can be identified: i) the use of a specific calibration model for each analyzed sample including spectra of the sample matrix in the model, ii) the improvement of the sample pretreatment process to perform a selective extraction of the analytes, for example by using solid phase extraction prior to the measurement, which would lead to a significant reduction of the overall sample throughput, or iii) the inclusion of possible interferences in the calibration set, which is only possible when a reduced set of well characterized samples is analyzed and the spectra of interfering substances are available. It can be concluded that none of the strategies indicated above can be recommended if the method will be directly applied to different kinds of unknown samples from different manufacturers. Therefore, although the direct determination is a faster alternative to the use of on-line LC-IR, the drawbacks for their use as a general method are evident.

To provide additional evidences of the accuracy of the on-line LC-IR method, samples were spiked with known amounts of glycolic acid between 3.7 and 9.8 mg and recovery percentages were determined from the extracted chromatograms of the spiked samples. Recovery values between 82.8 and 94.7% were achieved using peak height data. However, when the same chromatograms were analyzed using peak area measurements, recovery percentages ranged from 99.6 to 101.0%, always lying between 98 and 102%, which is a criterion often used in method validation, thus indicating once again the convenience of treating the chromatographic data in terms of peak area values.

2.3.4 Conclusions

A simple procedure was developed for the identification and quantification of glycolic acid in cosmetics. On-line LC-IR analysis of samples extracted with an acetonitrile:phosphate buffer (pH 2.7) provided quantitative recovery values of spiked samples and results which agree well with those reported by the manufacturers for market samples. The method also provides acceptable precision and sensitivity levels and allows the confirmation of the analyte nature in the eluted peak. Additionally, co-extracted compounds with similar spectral features found in the samples justified the use of LC-IR.

2.4 References for Chapter 2

- [2.1] D. Louden, A. Handley, S. Taylor, I. Sinclair, E. Lenz, K.D. Wilson, *Analyst*, 126 (2001) 1625-1629.
- [2.2] D. Louden, A. Handley, S. Taylor, E. Lenz, S. Miller, I.D. Wilson, A. Sage, *Analytical Chemistry*, 72 (2000) 3922-3926.
- [2.3] D. Louden, A. Handley, S. Taylor, E. Lenz, S. Miller, I.D. Wilson, A. Sage, R. Lafont, *Journal of Chromatography A*, 910 (2001) 237-246.
- [2.4] B.M. Patterson, N.D. Danielson, A.J. Sommer, *Analytical Chemistry*, 75 (2003) 1418-1424.
- [2.5] A. Edelmann, J. Diewok, J.R. Baena, B. Lendl, *Analytical and Bioanalytical Chemistry*, 376 (2003) 92-97.
- [2.6] H. Pasch, A. Siewing, L.C. Heinz, *Macromolecular Materials and Engineering*, 288 (2003) 771-777.
- [2.7] S.J. Kok, C.A. Wold, T. Hankemeier, P.J. Schoenmakers, *Journal of Chromatography A*, 1017 (2003) 83-96.
- [2.8] K.E. Esser, D. Braun, H. Pasch, *Angewandte Makromolekulare Chemie*, 271 (1999) 61-67.
- [2.9] J. Adrian, E. Esser, G. Hellmann, H. Pasch, *Polymer*, 41 (2000) 2439-2449.
- [2.10] J. Kuligowski, G. Quintas, F.A. Esteve-Turrillas, S. Garrigues, M. de la Guardia, *Journal of Chromatography A*, 1185 (2008) 71-77.
- [2.11] J. Kuligowski, G. Quintas, S. Garrigues, M. de la Guardia, *Chromatographia*, 71 (2010) 201-209.
- [2.12] J. Kuligowski, A. Breivogel, G. Quintas, S. Garrigues, M. de la Guardia, *Analytical and Bioanalytical Chemistry*, 392 (2008) 1383-1389.
- [2.13] J. Kuligowski, G. Quintas, S. Garrigues, M. de la Guardia, *Talanta*, 77 (2008) 229-234.
- [2.14] J. Kuligowski, G. Quintas, S. Garrigues, M. de la Guardia, *Analytical and Bioanalytical Chemistry*, 397 (2010) 861-869.
- [2.15] J. Kuligowski, D. Carrión, G. Quintas, S. Garrigues, M. de la Guardia, *Analytical and Bioanalytical Chemistry*, 399 (2011) 1305-1314.

- [2.16] J. Kuligowski, D. Carrión, G. Quintas, S. Garrigues, M. De la Guardia, *Food Chemistry*, sent for publication (2011).
- [2.17] L. Campanella, A.L. Magri, A. Sorbo, M. Tomassetti, *Journal of Pharmaceutical and Biomedical Analysis*, 29 (2002) 1135-1148.
- [2.18] J.I. Rader, C.M. Weaver, M.W. Trucksess, *Journal of Aoac International*, 87 (2004) 1297-1304.
- [2.19] R.V. Duevel, R.M. Corn, M.D. Liu, C.R. Leidner, *Journal of Physical Chemistry*, 96 (1992) 468-473.
- [2.20] R. Mendelsohn, M.A. Davies, J.W. Brauner, H.F. Schuster, R.A. Dluhy, *Biochemistry*, 28 (1989) 8934-8939.
- [2.21] H.L. Casal, *Journal of Physical Chemistry*, 93 (1989) 4328-4330.
- [2.22] J.M. Nzai, A. Proctor, *Journal of the American Oil Chemists Society*, 75 (1998) 1281-1289.
- [2.23] J.M. Nzai, A. Proctor, *Journal of the American Oil Chemists Society*, 76 (1999) 61-66.
- [2.24] A. Szydłowska-Czeraniak, *Food Chemistry*, 105 (2007) 1179-1187.
- [2.25] M. de la Guardia, *Journal of the Brazilian Chemical Society*, 10 (1999) 429-437.
- [2.26] P.A. Gorry, *Analytical Chemistry*, 62 (1990) 570-573.
- [2.27] C. Gertz, *European Journal of Lipid Science and Technology*, 102 (2000) 566-572.
- [2.28] M.C. Dobarganes, G. Márquez-Ruiz, in: M.D. Erickson (Ed.) *Deep frying: chemistry, nutrition, and practical applications*, AOCS Press, USA, 2006.
- [2.29] D. Firestone, in: M.D. Erickson (Ed.) *Deep frying: chemistry, nutrition and practical applications*, AOCS Press, USA, 2007.
- [2.30] S. Marmesat, E. Rodrigues, J. Velasco, C. Dobarganes, *International Journal of Food Science and Technology*, 42 (2007) 601-608.
- [2.31] *Standard Methods for the Analysis of Oils, Fats and Derivatives*, in: IUPAC Standard Method 2.508, International Union of Pure and Applied Chemistry, Blackwell, Oxford, 1992.
- [2.32] M.C. Dobarganes, J. Velasco, A. Dieffenbacher, *Pure and Applied Chemistry*, 72 (2000) 1563-1575.
- [2.33] P.R. Griffiths, J. de Haseth, *Fourier Infrared Transform Spectroscopy*, second ed., John Wiley & Sons, New York, 2007.

- [2.34] A.A. Christy, P.K. Egeberg, *Chemometrics and Intelligent Laboratory Systems*, 82 (2006) 130-136.
- [2.35] B. Muik, B. Lendl, A. Molina-Diaz, M. Valcarcel, M.J. Ayora-Canada, *Analytica Chimica Acta*, 593 (2007) 54-67.
- [2.36] R.M. Maggio, T.S. Kaufman, M. Del Carlo, L. Cerretani, A. Bendini, A. Cichelli, D. Compagnone, *Food Chemistry*, 114 (2009) 1549-1554.
- [2.37] J. Moros, M. Roth, S. Garrigues, M. de la Guardia, *Food Chemistry*, 114 (2009) 1529-1536.
- [2.38] R. Marbach, *Journal of Biomedical Optics*, 7 (2002) 130-147.
- [2.39] R. Marbach, *Journal of near Infrared Spectroscopy*, 13 (2005) 241-254.
- [2.40] J.D.J. van den Berg, N.D. Vermist, L. Carlyle, M. Holcapek, J.J. Boon, *Journal of Separation Science*, 27 (2004) 181-199.
- [2.41] S. Scalia, R. Callegari, S. Villani, *Journal of Chromatography A*, 795 (1998) 219-225.
- [2.42] E.A. Dutra, M. Santoro, G.A. Micke, M.F.M. Tavares, E.R.M. Kedor-Hackmann, *Journal of Pharmaceutical and Biomedical Analysis*, 40 (2006) 242-248.
- [2.43] I. Nicoletti, C. Corradini, E. Cogliandro, A. Cavazza, *International Journal of Cosmetic Science*, 21 (1999) 265-274.
- [2.44] M.L. Chang, C.M. Chang, *Journal of Pharmaceutical and Biomedical Analysis*, 33 (2003) 617-626.
- [2.45] W.S. Huang, C.C. Lin, M.C. Huang, K.C. Wen, *Journal of Food and Drug Analysis*, 10 (2002) 95-100.
- [2.46] L.H. Couch, P.C. Howard, *International Journal of Cosmetic Science*, 24 (2002) 89-95.
- [2.47] A. Salvador, M.C. Pena, M. de la Guardia, *Analyst*, 126 (2001) 1428-1431.
- [2.48] M. de la Guardia, J. Ruzicka, *Analyst*, 120 (1995) N17-N17.
- [2.49] B. Optics, OPUS manual, version 4.0, Bruker Optics, Ettlingen, Germany, 2002.

CHAPTER 3. BACKGROUND CORRECTION IN ON-LINE LC-IR USING REFERENCE SPECTRA MATRICES

In this chapter, chemometric methods for background compensation in LC-IR employing a reference spectra matrix are discussed. The general objective of background correction is to compensate undesired sources of variation due to the changing eluent absorption using gradient conditions in LC-IR hyphenated systems in an automated way and to enhance sensitivity and spectral and/or chromatographic resolution.

The basics of the on-line detection approach are well known: if there are p absorbing species in a sample, according to Lambert-Beer's law the recorded absorbance at each wavenumber is assumed to be the sum of contributions of all components. This can be extended to the whole spectrum and written in a matrix notation as:

$$D = CS^T + E \quad (\text{Equation 3.1})$$

where D ($z \times c$) is the original raw LC-IR data matrix with the overall spectral information of all absorbing species present in the system, C ($z \times k$) is the vector of the concentration profiles of the species, S^T ($k \times c$) is a matrix containing the pure spectra of the k components, E ($z \times c$) is the error-related matrix and k , c and z are the number of absorbing species, variables (wavenumbers) and spectra, respectively.

Under isocratic conditions, the eluent composition and hence its spectrum is known and theoretically constant. Therefore, direct subtraction of the solvent spectrum in the raw data matrix D allows reducing the complexity of the system, remaining the IR active eluting analytes as the only components in the background corrected data matrix. Of course, this approach has its practical limitations: for example, minor changes in the mobile phase composition delivered by the LC pump lead to strong

changes in intensity and shape of the eluent absorbance spectrum. Thus, a direct subtraction of a reference spectrum might lead to inaccurate background compensation obtaining noisy chromatograms and distorted spectra of the analytes. Under gradient conditions, background correction is not straightforward, as the eluent composition during the run changes, influencing band positions and shapes of the recorded mobile phase absorbance spectra.

Therefore, the development of procedures for an accurate background correction is of importance for a further extension of the use of on-line LC-IR using the flow-through approach. To overcome solvent interferences, a new strategy for spectral eluent subtraction in on-line LC-IR was reported [3.1]. This strategy simplifies the background correction problem, performing the correction under gradient conditions in a similar way as under isocratic and 'stopped-flow' conditions. In this approach based on the use of a reference spectra matrix (**RSM**), data obtained from the LC-IR run is viewed as a 'sample matrix' (**SM**) formed by a series of independent IR spectra of an unknown number of components (e.g. eluting analytes) in an eluent with an unknown composition. Additionally to the **SM**, a 'reference spectra matrix' that consists of a set of spectra of different mobile phase compositions within a certain range is acquired during a blank gradient run or during the re-equilibration of the chromatographic system, exploiting the instrumental capability of automatically measuring a **RSM**. An identification parameter (IP) that is characteristic of the mobile phase composition is calculated for each spectrum included in the **SM** and the **RSM**. Then, for each spectrum included in the **SM**, the spectrum with the closest IP value included in the **RSM** is selected as reference. In the following step background correction is accomplished by subtracting the selected **RSM** spectrum from the **SM** spectrum.

In the following, the RSM background correction procedure involving five steps, is described in detail. In step 1 the reference spectra matrix **RSM** ($r \times c$) and the sample matrix **SM** ($z \times c$) are measured, where r and z are the number of spectra included in the **RSM** and **SM**, respectively and c is the number of variables (wavenumbers) in the spectra of the **RSM** and **SM** data matrices. The acquisition of the **RSM** is carried out in practice by measuring spectra during a blank gradient in a defined composition range. Accordingly, the **SM** is constructed from a series of raw absorbance spectra measured during the LC run. The eluent composition range of the **SM** should be within the **RSM**

composition interval. As background, the empty sample compartment spectrum is used for both the **RSM** and the **SM** data sets.

Step 2 involves the calculation of an IP for each spectrum included the **SM** and the **RSM**. It has to be underlined that the value of the selected IP should be characteristic of the mobile phase composition throughout the evaluated eluent composition interval. Thereby, the usefulness of the IP depends on the ability of the selected statistic to discriminate subtle differences in similar spectra and so different IPs have been investigated.

First, the use of the absorbance ratio (AR) at two defined wavenumbers r_1 and r_2 was proposed. The AR of the spectrum s (AR_s) is calculated as described in Equation 3.2:

$$AR_s = \frac{y_{r_1}^s}{y_{r_2}^s} \quad (\text{Equation 3.2})$$

where $y_{r_1}^s$ and $y_{r_2}^s$ are the absorbance values at the wavenumbers r_1 and r_2 measured in the spectra $s = (1, \dots, z)$ for spectra included in the **SM** and $s = (1, \dots, r)$ for spectra in the **RSM**.

Another approach is based on the calculation of a multivariate Partial Least Squares (PLS) model using a defined region of the spectra included in the **RSM**, to relate each spectrum to the absorbance at a wavenumber r_1 . This is done in order to derive a single numeric value, characteristic for the actual, but unknown, composition of the solvent mixture of a given spectrum in the **RSM**. The PLS model established from the **RSM** is then applied to predict absorbance values at r_1 of the spectra included in the **SM**.

The third approach involves the comparison of characteristic absorption bands of the eluent during the chromatographic run of the **SM** with those of the **RSM** using a point-to-point matching method. Similarity or distance methods based on point-to-point matching are methods in which equal-length vectors describing two spectra are compared point by point, and a single statistic is obtained [3.2, 3]. The performance of the correlation coefficient on the mean centered absorbances (COR) was selected from a number of different similarity indices. The spectral similarity index COR between two spectra, $s_A(1 \times c)$ and $s_B(1 \times c)$, is calculated as described in Equation 3.3 from the mean centered vectors (Z_A and Z_B), where \bar{s}_n is the arithmetic mean absorbance in spectrum s_n ($n = A, B$):

$$COR = \frac{Z_A^T Z_B}{\|Z_A\| \cdot \|Z_B\|} \quad (\text{Equation 3.3})$$

where $Z_n = s_n - \bar{s}_n$.

In Step 3, using the AR and PLS approach, for each of the z spectra included in the **SM**, the most appropriate background spectrum $s_{y,s}$, $s = (1, \dots, z)$ is located in the **RSM** and selected for the further calculation of the background corrected spectrum. When employing COR, r similarity indices for the set of spectra included in the **RSM** ($r \times c$) with the sample spectrum s are calculated using the absorbance values in a defined spectral interval. Then, the **RSM** spectrum showing the highest similarity value is selected as the corresponding reference of spectrum $s_{y,s}$.

Step 4 is optional and has up to now only been used in combination with the AR approach. It consists of the calculation of a correction factor (KF) for each sample spectrum s . The objective of the KF is to correct minor changes in the spectral absorption intensity of the eluent during the chromatographic run. The factor KF_s is defined as the ratio of absorbance of the sample s at a defined wavenumber φ (y_φ^s) and the previously selected background spectrum $s_{y,s}$ at a defined wavenumber φ ($y_\varphi^{s_{y,s}}$) using the following expression:

$$KF_s = \frac{y_\varphi^s}{y_\varphi^{s_{y,s}}} \quad (\text{Equation 3.4})$$

Step 5 includes the subtraction of the eluent background spectrum from the sample spectrum using the following expression:

$$\text{Corrected}S_s = s - KF_s \cdot s_{y,s} \quad (\text{Equation 3.5})$$

where $\text{Corrected}S_s$ is the background corrected sample spectrum, s is the original sample spectrum, $s_{y,s}$ is the background spectrum included in the **RSM** and selected in Step 3 and KF_s is the calculated correction factor for the sample spectrum s . Note that $KF_s = 1$ if no correction factor is employed. The process is repeated for each **SM** spectrum until the whole LC chromatogram has been corrected.

This approach presents significant advantages over other chemometric techniques, such as MCR-ALS or PARAFAC: i) no previous estimation of the number of components present in the data matrix is needed; ii) the performance is not affected by a lack of trilinearity due to retention time drifts between runs, iii) no complex data pre-treatments are necessary (e.g. time-warping or the selection of initial estimates); iv)

the number of user-defined variables is substantially reduced, and v) it can be used for on-the-fly eluent absorption correction.

On the other hand, it presents a series of conditions of applicability: i) high instrument stability, ii) appropriate measurement of the **RSM** and **SM** and iii) the presence of a spectral region in the mobile phase spectra that is characteristic of its composition and free of interferences from other eluting compounds.

The main limitation of RSM-based methods is that the composition of each selected 'reference spectrum' must match the composition of the corresponding 'sample spectrum' to be background corrected as accurately as possible. Therefore, the number of spectra included in the **RSM**, as well as the distribution of compositions, has a direct impact on the accuracy of the background correction. In principle, the higher the **RSM**, the better the accuracy but as the data acquisition frequency is limited by the instrument this usually implies longer acquisition times and so, instrumental instabilities (e.g. detector drifts) affect the quality of the corrected spectra. Other practical considerations, such as the sample throughput or the gradient range, have to be considered when selecting the size of the **RSM**.

Furthermore it must be emphasized that slight drifts in the experimental conditions (e.g. T) might affect the spectrum of a defined mobile phase composition. From our experience with real (i.e. not simulated) data sets, we recommend to use **RSM** spectra measured during the re-equilibration of the LC-IR system after each gradient run. This straightforward approach can minimize some instrumental effects such as T changes, detector drifts or water vapor interferences, for example, which strongly affect the background correction.

Although chemometrics aims at providing useful tools for data processing, it seems that these methods are mainly used by chemometricians [3.4]. Therefore, to facilitate the application of the RSM-based background correction methods as well as for an easier and straightforward visualization and interpretation of the obtained results, the developed background correction algorithms were embedded in an in-house written Matlab Graphical User-friendly Interface (GUI-File). The GUI-File can be downloaded from http://www.iac.tuwien.ac.at/cavs/lc_ftir_toolbox.php.

Figures 3.1 and 3.2 show the main graphical window of the developed GUI-File. In this window the user has to select from the pop-up menus: a) the reference spectra matrix

(RSM), b) the spectra matrix to be background corrected (SM), c) the wavenumber vector d) the background correction method and e) the wavenumbers used for the calculation of the IP (r_1 , r_2 and φ , if necessary). Once the wavenumber vector has been selected, the axes located at the bottom (see Figure 3.1) become accessible for a visualization of the matrices. All used matrices have to be stored in the MATLAB® workspace. If the matrices were not stored in the workspace when the program function was launched, the workspace content must be updated by clicking the “Update WSP” push button. Additional tools for selecting IPs, importing and exporting spectra, performing isocratic background corrections as well as for carrying out common data pre- and post- processing such as baseline corrections, derivatization and normalization of spectra, among others, were also included in the GUI-File.



Figure 3.1. Initial graphic window of the developed Matlab Graphical User-friendly Interface.

As above stated, the selected IP affects the accuracy of the achieved background correction. Therefore, in this chapter the evaluation and comparison of different IPs is addressed. For this reason, several examples of applications employing acetonitrile:H₂O and methanol:H₂O mobile phase systems have been tested.

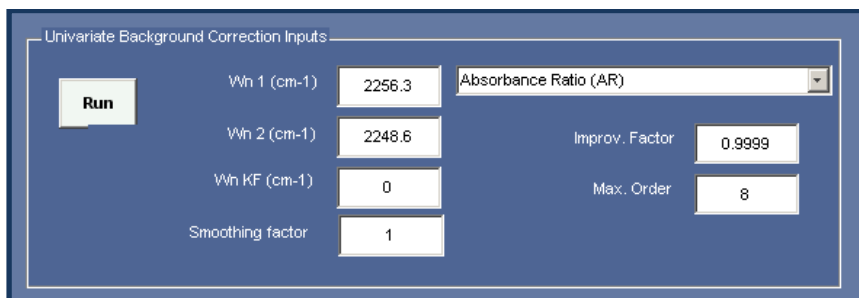


Figure 3.2. Matlab Graphical User-friendly Interface – detailed view of the panel for BGC-RSM inputs.

In the first section (3.1), the use of background correction in on-line gradient LC-IR is proposed to improve the accuracy of the determination of the critical chromatographic conditions of polyethylene glycol [3.5]. The previously developed RSM-based background correction approach, using an AR as IP (AR-BGC-RSM) was applied for the identification of the elution windows of polyethylene glycol. The application of the AR-BGC-RSM method was extended to methanol:water gradients with a methanol concentration ranging from 5 to 100% v/v. Additionally, a PLS model to accurately calculate the eluent composition during the gradient was developed.

In section 3.2, the previously developed AR-BGC-RSM strategy was employed for the quantitative determination of four selected carbohydrates (fructose, glucose, sucrose and maltose) in beverage samples [3.6]. To successfully resolve and quantify the analytes, linear gradient from 75 to 55% v/v acetonitrile in water were run. This method was employed in another study dealing with the direct determination of different sugars in depilatories to characterize the samples [3.7].

Section 3.3 describes the PLS-BGC-RSM method. This strategy was tested for background correction under isocratic as well as under gradient conditions running linear gradients covering acetonitrile concentrations between 40 and 100% v/v [3.8].

In section 3.4 the development of a background correction method based on the use of the correlation coefficient on mean centered absorbances (COR) as IP (p2p-BGC-RSM) is described [3.9, 10]. This approach was tested on chromatographic data acquired during the separation of four nitrophenols running acetonitrile (0.08% v/v TFA):water (0.08% v/v TFA) gradients with compositions ranging from 35 to 85% v/v acetonitrile.

3.1 Determination of critical eluent conditions for polyethylene glycols using univariate chemometric background correction

3.1.1 Introduction

Liquid chromatography is one of the most widely used techniques for the analysis and characterization of polymers. Liquid chromatography under critical conditions (LCCC) operates at the critical point of adsorption (CAP) at the transition from liquid adsorption to size exclusion chromatography. The CAP of a homopolymer is a specific combination of eluent composition, stationary phase and temperature. The identification of the CAP is a tedious, time-consuming and rather complicated process and, because of that, the development of methods and strategies to determine it is nowadays an active field of research in polymer analysis.

Bashir et al. [3.11] demonstrated that the composition at elution for high molecular molar mass polymers in chromatographic runs under gradient conditions is very close to the critical conditions. According to this, they proposed a general strategy to find the critical condition based on three steps: i) run a series of linear gradients with different slopes for a single high molar mass polymer and calculate the composition at elution; ii) perform isocratic runs to refine the calculated CAP at a composition a few percent higher than that established in the previous step; iii) plot the measured elution volumes in front of the different eluent compositions for the different molar masses assayed and establish the crossing point.

As it can be seen, the whole procedure is straightforward and permits an important simplification of the CAP finding process when compared to the trial and error procedures performed under isocratic conditions. To determine the eluent composition ($\%B_g$) throughout the run, the authors used the following expression:

$$\%B_g = (V_g - V_v - V_d) \frac{\Delta\%B_g}{F t_g} + \%B_0 \quad (\text{Equation 3.1.1})$$

being V_g the elution volume at peak maximum, V_v the column void volume, V_d the system dwell volume, $\%B_g$ the total change in composition, t_g the gradient time, F the flow rate and $\%B_0$ the initial composition.

The accuracy of the eluent composition during the elution of the polymer depends directly on the void volume calculation. The void volume was calculated injecting toluene using tetrahydrofuran as eluent. The dwell volume was calculated by subtracting the void volume from the onset of the increasing UV signal due to a linear gradient from pure methanol to methanol containing 0.3% acetone. The void volume is defined as “the total volume of the mobile phase in the column; the remainder of the column is taken up by packing material” [3.12]. There are different interpretations of this definition because in reversed phase LC there is no distinct boundary between mobile and stationary phases. Difficulties related to the measurement of this parameter have been reviewed by Rimmer et al. [3.12]. Therefore, it is expected that the development of a method for the simultaneous determination of both, the polymer elution profile and the eluent composition during the run would be very useful in further studies focusing on the determination of the critical conditions of polymers. In the majority of applications of liquid chromatography for polymer analysis, the prevalently used detectors are evaporative light scattering (ELSD), differential refractive index (dRID) and UV spectrometers. The use of these detectors has a number of well-known advantages but, the information that can be extracted from the chromatograms is rather limited and also presents additional drawbacks. For example, the use of ELSD produces a non-linear response; the sensitivity of the dRID is limited and the obtained information non-specific. UV is limited to polymers presenting chromogenic groups in their chemical structure [3.13]. Therefore the usefulness and applicability of the aforementioned chromatographic techniques can be significantly increased through the on-line hyphenation with detectors that provide an analyte fingerprint, such as the FTIR. Infrared spectroscopy has been widely used within the polymer industry during the last decades and can be considered as a well-established technique in this field. However, most of the reported LC-IR applications use solvent elimination interfaces before detection [3.14]. Only a reduced number of applications of isocratic on-line LC-IR dedicated to polymer analysis can be found in literature [3.14-16].

In this work, polyethylene glycol (PEG) of different molar masses, analyzed by on-line gradient LC-IR, has been chosen as a model example [3.11] to evaluate the performance of AR-BGC-RSM for the correction of the changing background signal in

different methanol:water gradients. The obtained polymer elution profiles were subsequently used to calculate the composition of the mobile phase directly from the infrared spectra using a partial least squares (PLS) procedure and to estimate the critical conditions.

3.1.2 Material and methods

Apparatus and Reagents

A Dionex (Sunnyvale, CA, USA) P680 high-performance liquid chromatographic system, equipped with a Kromasil 100 C₁₈ reversed phase column (250mm×2mm, 5 μm) from Eka Chemicals AB (Bohus, Sweden) and a sample injection loop of 20 μL, was employed for chromatographic separations. Linear methanol:water gradients were run from 5 to 100% v/v methanol (Merck, Darmstadt, Germany) in 7, 12, 15, 30, 60 and 90 min. PEG standards (MW 12000, 20000 and 40000) obtained from Fluka (Buchs, Switzerland) were used to estimate the critical compositions and to evaluate the performance of the background correction process.

For FTIR spectra acquisition a Bruker (Bremen, Germany) IFS 66/v FTIR spectrometer was employed. The instrument was equipped with a liquid nitrogen refrigerated MCT detector, a vacuum system and a dry air purged sample compartment. The scanner of the interferometer was operated at a HeNe laser modulation frequency of 100 kHz. Spectra were recorded in the range between 4000 and 750cm⁻¹, with a spectral resolution of 8 cm⁻¹ and a zerofilling value of 2. Throughout this study a flow cell with CaF₂ and ZnSe windows and a pathlength of 10 μm was employed. During gradient experiments, 25 scans per spectrum were averaged, providing a spectra acquisition frequency of 15 spectra min⁻¹. To improve the signal-to-noise ratio and to increase the acquisition frequency, isocratic experiments were carried out in the rapid scan time-resolved mode.

The calibration set for the PLS-FTIR determination of methanol percentage in the elution gradient included spectra of 22 standard solutions prepared using the LC pump and measured in the same conditions as employed for the gradient LC runs. The standard solutions covered a methanol range between 5 and 100% v/v in 5% increments and three additional solutions with concentrations of 77, 83 and 87% v/v

methanol. From each solution, a total of 25 spectra were recorded. PLS leave one out cross-validation was used for the calculation of RMSECV.

Software and algorithms

For instrumental and measurement control as well as for data acquisition, the OPUS software (version 4.1) from Bruker was employed. Background correction of data was run under Matlab 7.0 from Mathworks (Natick, USA, 2004) using an in-house written Matlab GUI file.

3.1.3 Results and discussion

FTIR spectra of PEG, methanol and water

Figure 3.1.1 (top) shows the spectrum of a PEG 40000 solution in the 4000-950 cm^{-1} range. A set of characteristic analyte bands can be seen in this interval, being the most intense bands located around 1100 cm^{-1} . Several group vibrations contribute to the shape of this band, including the C-O stretching vibration, the in-plane bending vibration of the C-O-H groups and the C-C stretching as well as the $-\text{CH}_2-$ deformation vibration, among others. According to a previous work [3.17], the shape of this band changes with the molecular weight of the polymer as well as with the water content of solutions. Additionally, in the spectral range from 1300 to 1400 cm^{-1} bands due to C-O-H in-plane deformations can be seen. These bands are almost identical for PEGs of different molecular weights.

Figure 3.1.1 (bottom) shows infrared spectra of methanol:water mixtures ranging from 5 to 100% v/v methanol. The interval between ~ 3000 and 1050 cm^{-1} encompasses four major methanol vibration bands located at 2947 cm^{-1} (CH_3 asymmetric stretching vibration), 2831 cm^{-1} (CH_3 symmetric stretching vibration), 2045 cm^{-1} (overtone and combination bands of intermolecular vibrations and OH stretching vibrations) and 1450 cm^{-1} (CH_3 deformation vibration). The strong absorption band due to the HOH bending mode of water molecules is located at ~ 1643 cm^{-1} . The OH stretching absorption of methanol and water molecules does not show a linear behavior with changing concentration because of saturation effects [3.18, 19].

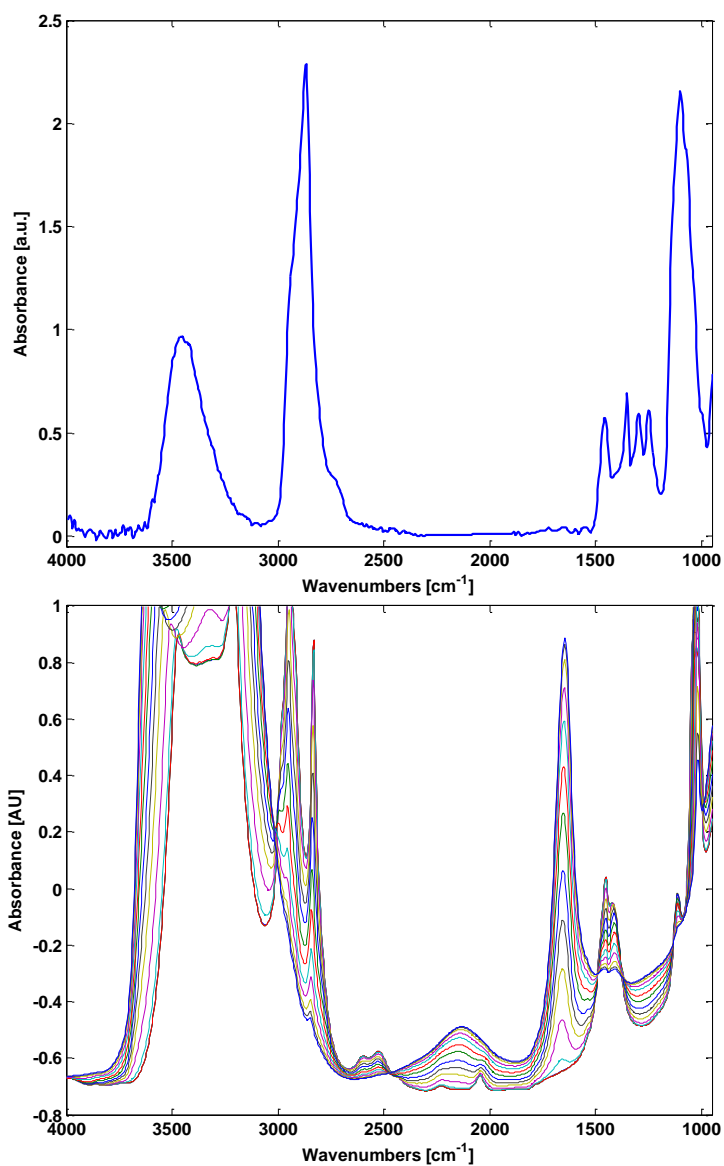


Figure 3.1.1. FTIR spectra of PEG 40000 and methanol:water solutions; (top) FTIR spectrum of a 4 mg mL⁻¹ PEG 40000 solution in methanol:water (5:95% v/v) measured against a blank of the same solvent and (bottom) spectra of different methanol:water solutions in the range from 5 to 100 % v/v obtained during the measurement of a blank injection using the spectrum of the empty sample compartment as a background.

From the methanol:water spectra shown in Figure 3.1.1 (bottom), it is clear that due to the changes in both, shape and intensity of mobile phase bands during the gradient, a constant background cannot be used to correct the spectra of the eluting analytes. Moreover, an additional feature that increases the difficulty of modeling the studied system is that the position of the HOH bending vibration and the HOH bending/hydrogen bond libration combination modes shift to higher frequencies at increasing methanol concentrations.

As mentioned above, the BGC-RSM method is based on the use of spectral features of the mobile phase to determine the reference spectrum to be subtracted using a previously recorded **RSM**. For an appropriate application of this method, the eluent spectra must have at least one characteristic absorption band free from interferences of the components of the injected sample. As it can be seen from Figure 3.1.1, the studied system fulfills this condition of applicability as most of the characteristic bands of the methanol:water system do not overlap with the PEG bands.

On-line monitoring of the mobile phase composition during the LC run employing PLS

The selection of the employed wavenumber interval is one of the most critical steps in the development of any PLS-based approach affecting both, the accuracy and the precision, of the calculated results. As the number of possible intervals increases with the width of the considered spectral range, two strategies were simultaneously considered to find the optimum: i) the use of the available chemical information on the system under study and ii) the use of chemometric tools to analyze the recorded data.

In order to improve the predictive capabilities of the model, spectral regions in which the eluent spectra overlap with PEG bands were excluded. On the other hand, the interval PLS (iPLS) algorithm developed by Noorgaard et al. [3.20] was used to facilitate variable selection. The iPLS procedure calculates local equidistant PLS models on subintervals of the spectrum using a previously defined range of latent variables.

Figure 3.1.2 (top) shows the iPLS plot obtained from the analysis of the methanol calibration set using different local models as well as the whole spectrum. From these data, the region between 2700 and 2400 cm^{-1} was selected for further analysis which provides the minimum root mean square error of cross validation (RMSECV). According

to that, the number of factors was selected using the minimum predicted error sum of squares (PRESS) as it can be seen in Figure 3.1.2 (bottom).

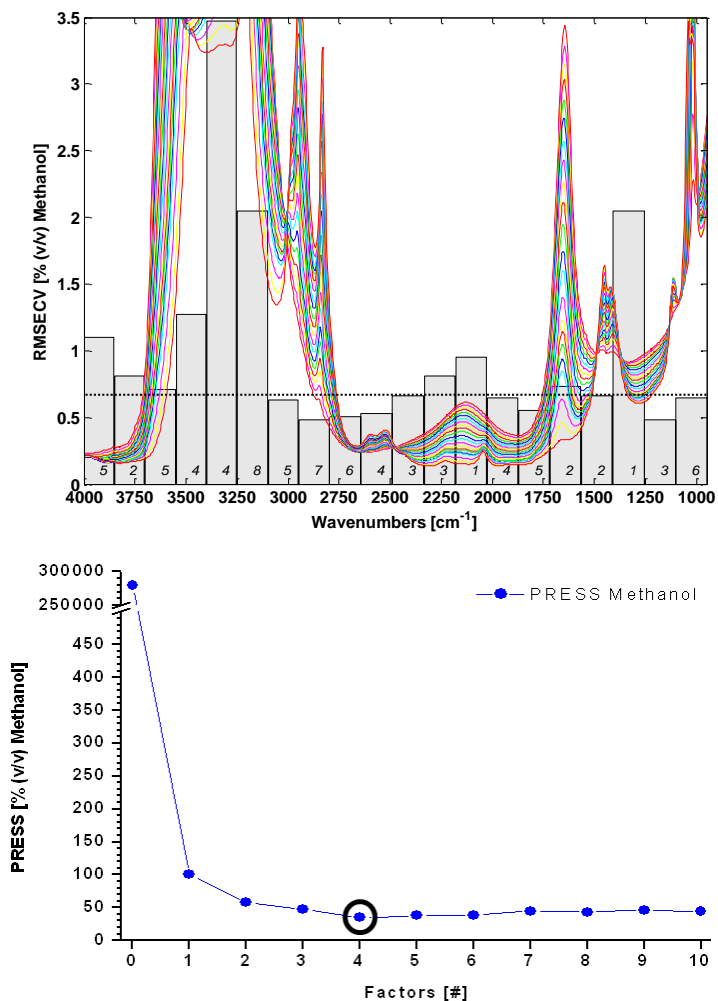


Figure 3.1.2. top: RMSECV for 20 iPLS models (italic numbers are the optimal number of factors in the considered interval) and full spectrum model using 3 factors (dotted line); bottom: plot of the PRESS as a function of the number of factors employed for PLS calculations using all variables.

The predictive capabilities of the developed PLS method were evaluated using three parameters: the correlation coefficient (r) and the root mean square error of

calibration (RSMEC) and cross validation (RMSCV). Results summarized in Table 3.1.1 clearly indicate that the calculated regression model is suitable for an accurate determination of the methanol content of the mobile phase during gradient elution providing excellent correlation coefficients for calibration and cross validation and root mean square errors lower than 0.3% v/v methanol.

Table 3.1.1. Summary of the most important parameters of the PLS calibration model for the determination of methanol during gradient elution.

Response	Methanol concentration
Spectral Region [cm ⁻¹]	2715 - 1870
Baseline correction [cm ⁻¹]	None
Smoothing	None
Factors	4
r_{CAL}^a	0.99997
RMSEC (% v/v Methanol) ^b	0.209
r_{CV}^c	0.99994
RMSECV (% v/v Methanol) ^d	0.296

Note: r_{CAL}^a : Correlation coefficient of the calibration; RMSEC (% v/v Methanol)^b: Root mean square error of calibration; r_{CV}^c : Correlation coefficient of the cross validation; RMSECV (% v/v Methanol)^d: Root mean square error of cross-validation.

Selection of parameters to perform the background correction

The selection of the wavenumbers $r1$ and $r2$ used to calculate the AR according to Equation 3.2 is the most important step to ensure an appropriate subtraction of the eluent spectrum using the AR-BGC-RSM method [3.1]. In order to find the optimum ratio (i.e. IP value), the accuracy of the background correction of a gradient blank injection was evaluated when all possible pairs of values ($\frac{r1}{r2}$) in a defined spectral range were tested. Results can be evaluated graphically as well as numerically.

For each tested pair of wavenumbers used for the calculation of the AR, a background corrected blank chromatogram was obtained. Therefore, results from the different background corrections can be viewed abstractly as a four dimensional space (with wavenumbers $r1$ and $r2$ used for each AR, the corrected absorbance at each wavenumber and the time axes). For an easier visualization and to reduce the space of

the results to be searched in the graphical evaluation process, it was reduced to a three dimensional surface by plotting the wavenumbers r_1 and r_2 used for the calculation of the AR and the noise (calculated as RMS) at a single wavenumber in the background corrected blank LC-IR chromatogram. Low noise values indicate an adequate background correction and so, from the obtained surface plots it is possible to identify the AR which provides the optimum result. The symmetric appearance of the plots is a result of the fact that the models calculated using the quotients of the absorbance at two wavenumbers and their reciprocals are equal. Moreover, the AR value of the points along the central diagonal is equal to 1 and so they cannot be used for the background correction. In short, only the upper or lower values of the diagonal of the aforementioned graphs are used.

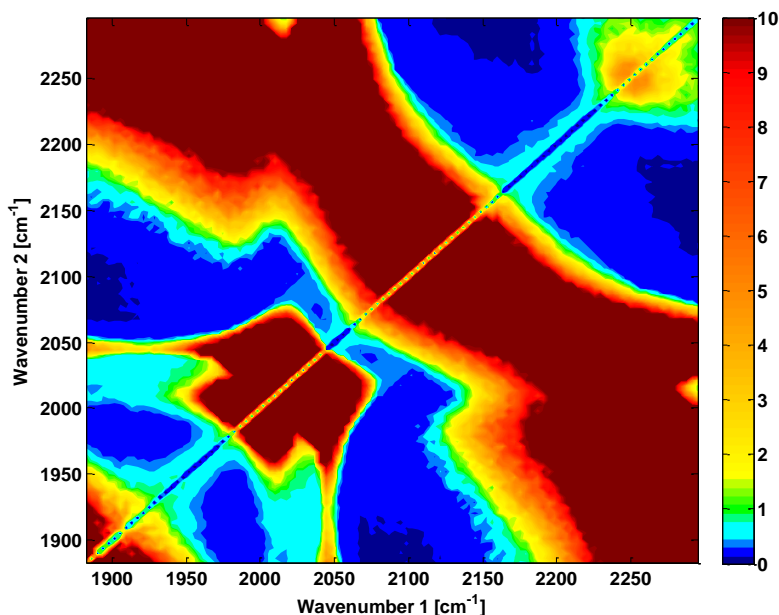


Figure 3.1.3. Response surface obtained during the AR selection for background correction in methanol:water solutions ranging from 5 to 100 methanol v/v using the noise at 1640 cm⁻¹ in the background corrected blank LC-IR chromatogram as response. Note: Noise values were measured in mAU.

As the spectral resolution or the width of the spectral range to be evaluated increases, the number of possible AR combinations grows, so it quickly becomes impractical to

calculate all the possible AR combinations in order to find the optimum. Therefore, the evaluated spectral range should be selected by taking into account chemical and/or spectroscopic information about the studied system. Here, in order to find the optimum AR, the accuracy of the background correction of a blank gradient injection when all possible pairs of wavenumbers r_1 and r_2 in the range between 2300 and 1880 cm^{-1} were used, was evaluated. 6050 corrected blank chromatograms were calculated when using a spectral resolution of 8 cm^{-1} and a zerofilling value of 2. The noise in the background corrected chromatograms extracted at 1640 cm^{-1} was used as selection criterion. Water presents a strong absorption band at 1640 cm^{-1} and thus subtraction errors are easy to identify because minor differences in the sample and reference spectra composition would produce high spectral differences in the corrected spectra.

Figure 3.1.3 shows noise values in the extracted chromatograms using a **RSM** composed by 1170 spectra covering methanol concentrations in the 5 - 100% v/v range and a blank gradient injection (**SM**), providing 274 spectra in the same eluent concentration range. It can be appreciated that the lowest noise values are achieved combining wavenumbers from the following regions: (i) 1950 to 2000 cm^{-1} with 1880 to 1970 cm^{-1} , (ii) 2050 to 2170 cm^{-1} with 1880 to 2050 cm^{-1} and (iii) 2200 to 2300 cm^{-1} with 2070 to 2200 cm^{-1} .

In order to find the optimum ratio, the accuracy of the background correction of a gradient blank injection was evaluated numerically. Table 3.1.2 summarizes 15 pairs of r_1 and r_2 wavenumbers which provided the highest background correction accuracy. Only minor differences among the 15 listed values were found. Noise values ranged between $1.9 \cdot 10^{-3}$ (AR = 2086.7 / 1893.9) and $2.0 \cdot 10^{-3}$ (AR = 2082.9 / 1882.3), comprising all the AR absorbance values in the interval between 2302 and 1882.3 cm^{-1} . Therefore, the one providing the lowest noise was selected for background correction of further injections.

Table 3.1.2. List of 15 absorbance ratios providing the lowest noise values in the extracted chromatograms at 1640 cm^{-1} .

Noise ^a [AU]	r1 [cm ⁻¹]	r2 [cm ⁻¹]
1.9021 10 ⁻³	2086.7	1893.9
1.9225 10 ⁻³	2109.9	1882.3
1.9351 10 ⁻³	2279.6	2160.0
1.9427 10 ⁻³	2109.9	1878.5
1.9700 10 ⁻³	2291.2	2129.2
1.9722 10 ⁻³	2283.5	2163.9
1.9767 10 ⁻³	2271.9	2156.2
1.9828 10 ⁻³	2298.9	2140.7
1.9845 10 ⁻³	2302.7	2156.2
1.9926 10 ⁻³	2287.3	2148.5
1.9940 10 ⁻³	2082.9	1893.9
1.9955 10 ⁻³	2275.7	2156.2
1.9961 10 ⁻³	2295.0	2125.3
2.0040 10 ⁻³	2271.9	2167.7
2.0081 10 ⁻³	2082.9	1882.3

Note: Noise^a: Noise measured as the root mean square of a chromatogram extracted from a background corrected blank gradient injection.

As an example, Figure 3.1.4 shows the uncorrected (top) and corrected (bottom) FTIR spectra corresponding to the blank LC injection used for the selection of the aforementioned background correction parameters and Figure 3.1.5 shows the extracted corrected and uncorrected chromatograms also corresponding to a blank injection measuring the absorbance at a band characteristic of methanol (1450 cm^{-1}). The use of a correction factor (KF), as mentioned in the five step summary (see Equation 3.4), was proposed in a previous work. However, the efficiency of its use depends strongly on the characteristics of the **RSM** and sample matrix analyzed (mainly their size and interval of eluent concentrations). In this work, the use of a KF did not improve the background correction (results not shown). Therefore, in order to simplify the process, $CorrectedS_s$ was calculated using a constant $KF_s = 1$.

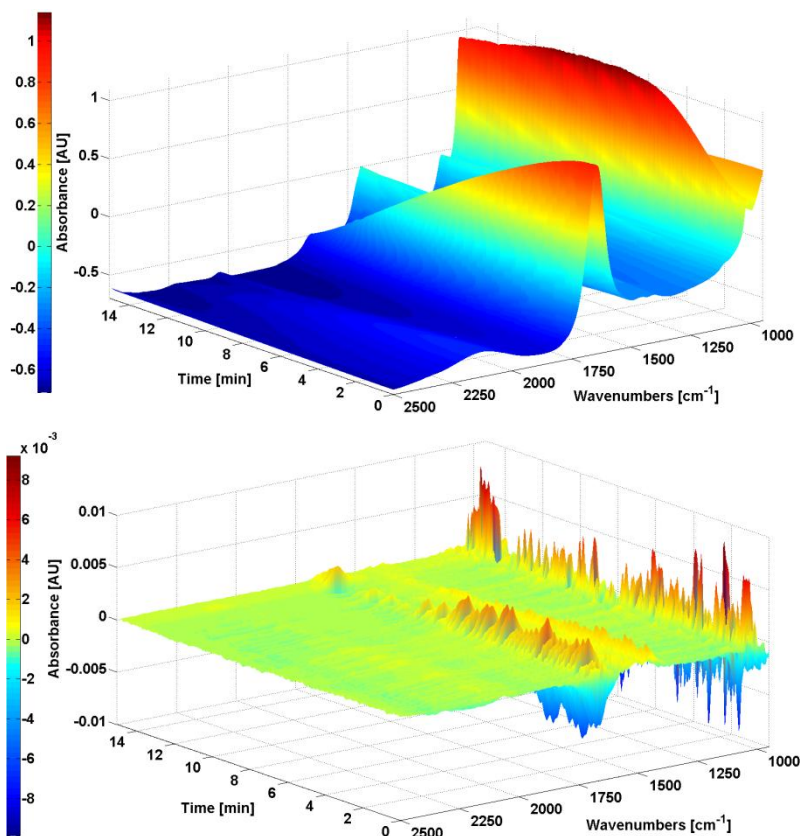


Figure 3.1.4. Uncorrected (top) and corrected (bottom) LC-IR spectra between 2500 and 950 cm^{-1} corresponding to a blank gradient LC-IR injection. Note: Spectra were measured on-line during a linear methanol:water gradient with mobile phase compositions ranging from 5:95 to 100:0 v/v methanol:water in 15 min.

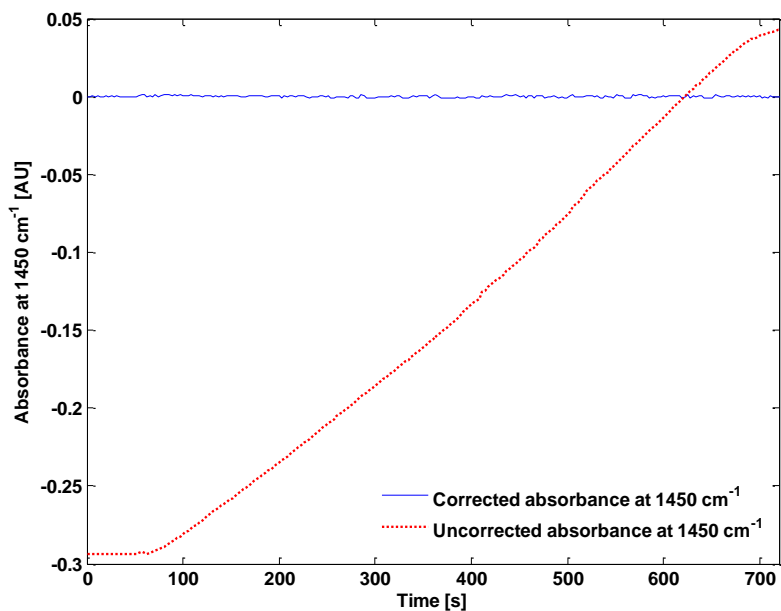


Figure 3.1.5. Background corrected and uncorrected chromatograms at 1450 cm⁻¹ from a blank injection.

On-line gradient LC-IR chromatograms of PEG 40000

A series of injections of PEG 40000 was carried out in linear methanol:water gradients. PEG chromatograms were obtained throughout this work by calculating changes in the absorbance at 1091.6 cm⁻¹ corrected using a single-point baseline at 1273 cm⁻¹. This region was selected to evaluate simultaneously the performance of the background correction and the analyte elution. Due to the strong absorption of methanol in this region, minor errors in the background correction could introduce spectral errors thus reducing the accuracy of the recovered polymer spectra, raising the limits of detection and reducing the repeatability of the chromatographic determinations.

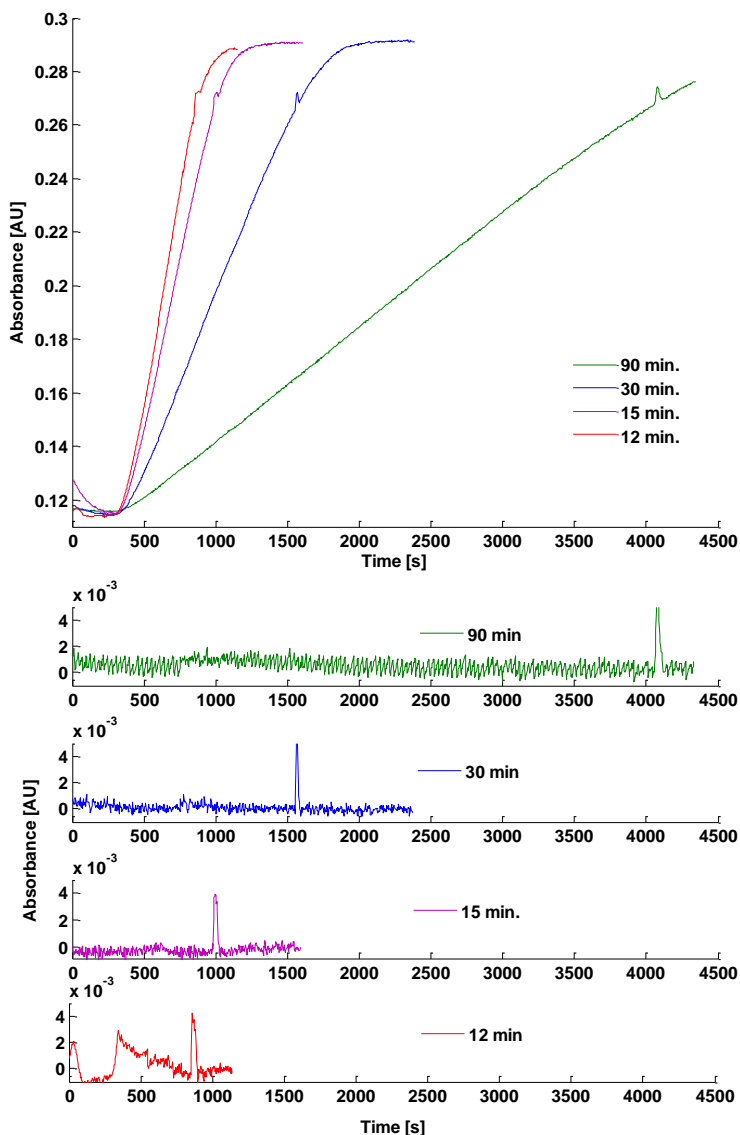


Figure 3.1.6. Extracted chromatograms obtained by measuring changes in the absorbance at 1091.6 cm^{-1} (corrected using a single-point baseline at 1273 cm^{-1}) from injections of PEG 40000 in different methanol:water gradients using uncorrected (top) and background corrected spectra (bottom). Note: Linear gradient composition: methanol:water from 5:95 to 100:0% v/v. Total gradient time from 12 to 90 min as indicated in the figure. PEG 40000 concentration: 2.5 mg mL^{-1} .

In some cases the location of the elution of the polymer during a gradient can be made directly from the raw chromatograms by measuring relative changes of the absorbance at defined wavenumbers at which the analyte presents absorption bands. In this case the elution peaks are detected as slight changes in the slope of the chromatogram. This approach is very simple and it might work under isocratic conditions but it becomes impractical at high gradient slopes (see Figure 3.1.6, top) because of two reasons: i) spectral changes related to the mobile phase modification during the gradient can be up to several orders of magnitude higher than those due to polymer elution and depend on the mobile phase and analyte absorption and ii) the relatively low time-resolution in on-line LC-IR increases the difficulty for an accurate location of minor changes in the slope of a chromatogram.

Figure 3.1.6 (bottom) shows the chromatograms extracted from the background corrected spectra using the previously selected parameters. The elution of the polymer can be easily located even when high gradient slopes were used and the recovered PEG spectra are well defined (see Figure 3.1.7).

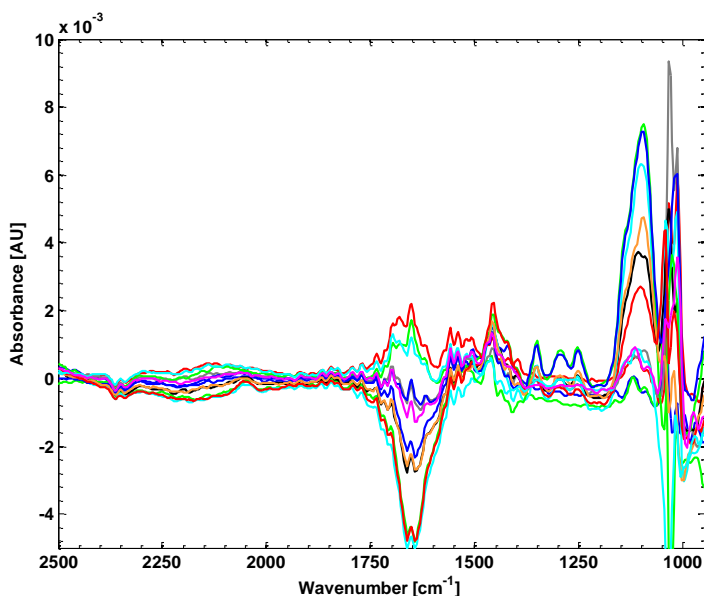


Figure 3.1.7. Background corrected spectra extracted from the injection of PEG 40000 into a linear methanol:water gradient from 5 to 100% v/v methanol (LC run time: 60 min), corresponding to the elution of the polymer.

Using the previously developed PLS method, the concentration of methanol during the elution of the polymer was calculated. Figure 3.1.8 shows that the eluent composition found during the polymer elution fits well with previously published results [3.11] and at increasing gradient slopes, the composition at elution is close to the critical concentration. The critical composition estimated from this plot (86.5% v/v methanol) indicates that both, the background correction process and the flow cell used, are appropriated for this type of determinations.

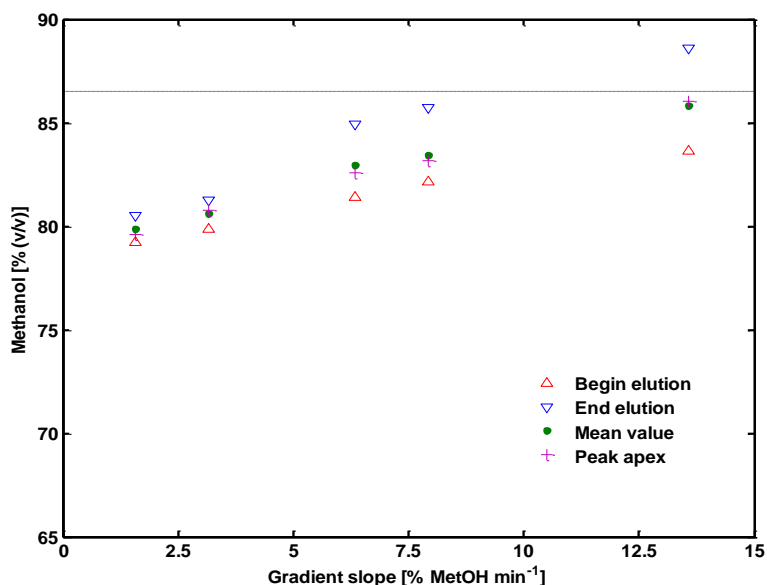


Figure 3.1.8. Mobile phase composition during the elution of a PEG 40000 standard as a function of the gradient slope; (---) CAP obtained in reference [3.11] for the considered system.

On-line isocratic LC-IR

The three chromatograms plotted in Figure 3.1.9 were obtained from the triplicate injection of three standards of PEG with different molar masses (12000, 20000 and 40000, from the top to the bottom), using a 86.5:13.5% v/v methanol:water mobile phase under isocratic conditions. This figure also shows PEG spectra extracted during elution. From the spectra measured during the elution of the different PEG polymers under isocratic conditions it can be appreciated that the absorbance of the eluent at the selected wavenumbers for the calculation of the AR is not significantly modified.

This also supports the previous selection of the AR values and can be used as an additional test in further AR selection processes.

Moreover, from data shown in Figure 3.1.9 it can be concluded that the background correction process works well also under isocratic conditions and the sensitivity of the on-line LC-IR procedure is good enough to observe the peaks of polymers in reversed phase LC.

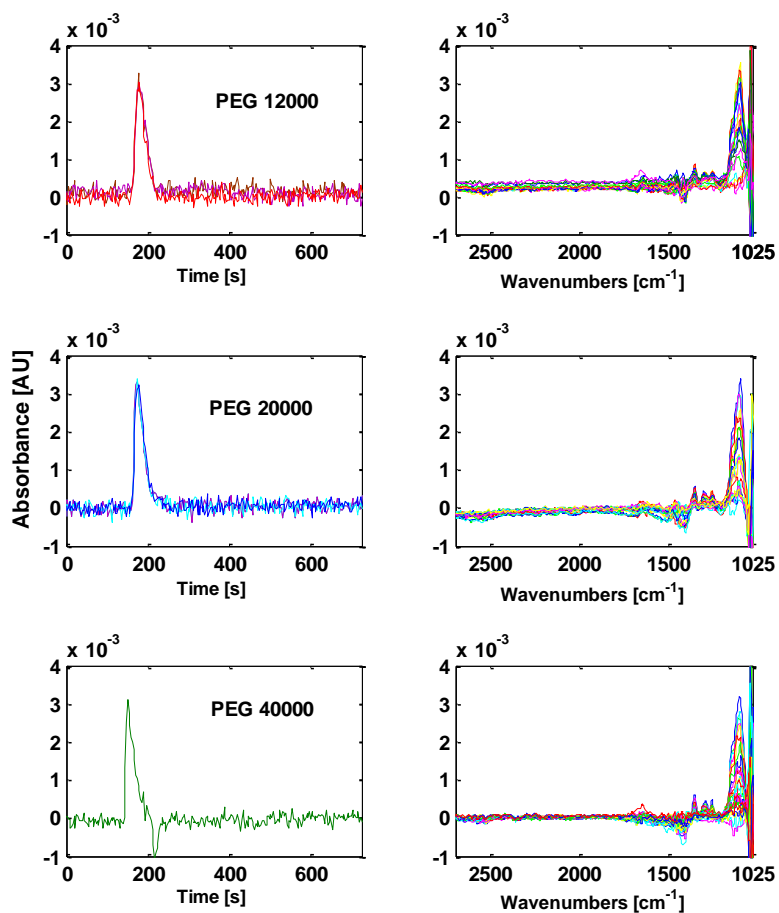


Figure 3.1.9. Isocratic LC-IR chromatograms and spectra of PEGs of different molar masses; (left) chromatograms obtained from the injection of 2.5 mg mL^{-1} standards of PEG 12000, 20000 and 40000 (from the top to the bottom), using an 86.5% v/v methanol mobile phase under isocratic conditions; (right) background corrected spectra obtained during the polymer elution.

3.1.4 Conclusions

On-line gradient LC-IR has proven to be a useful tool in polymer analysis when used in combination with the BGC-RSM background correction method. Results found for the estimation of the chromatographic critical conditions of PEG correspond to a methanol:water composition of 86.5:13.5% v/v and are in good agreement with previously published results.

It has been demonstrated that the combined use of on-line gradient LC-IR, the BGC-RSM background correction method and PLS, is an effective tool with great potential in polymer analysis that can be used in future works focusing on: i) the obtainment of detailed molecular specific information from polymer analysis in chromatographic systems and ii) the search for the critical conditions in non-studied systems.

3.2 Quantification of sugars in beverages using univariate chemometric background correction

3.2.1 Introduction

The term sugar is frequently used to describe monosaccharides as glucose and fructose and disaccharides as sucrose and maltose that are absorbed, digested and fully metabolized [3.21]. The current interest in the physiological role of carbohydrates, the technological developments in food processing and manufacturing and the different existing mandates of nutrition labeling (e.g. Food and Drug Administration [3.22]) have created a need for carbohydrate analysis at different production stages of foodstuff like alcoholic and non-alcoholic drinks, fruit juices, sweets or dairy products.

Liquid chromatography (LC) has often been employed for sugar analysis in different food matrices where the most commonly used detector is the refractive index detector (RID). However, it shows poor sensitivity, high instability with regard to fluctuations in the mobile phase composition and eluent temperature, low selectivity and incompatibility with mobile phase gradients [3.23, 24]. Evaporative light scattering detection (ELSD) is compatible with gradient elution and provides a significant increase in sensitivity as compared with RID, but it is also a low-selective detector. UV detection is not directly applicable for sugar analysis without a pre- or post-column derivatization of the analytes, due to the low UV absorbance of these compounds. The short wavelength required for their detection in UV without derivatization reduces the selectivity of the obtained chromatographic signal increasing the number of possible interferences, thus requiring extensive sample clean-up prior to the detection. Mass spectrometry (MS) is an expensive detection technique which provides high selectivity and sensitivity levels, but its field of application focuses on compounds at trace levels and not in the percentage range as it is the case of the main sugars present in foods.

Alternatively, IR spectrometry has proven to be a simple and rapid technique for the quantitative and qualitative determination of analytes at percentage levels. Using isocratic conditions, the capability of on-line LC-IR for the determination of sucrose, glucose and fructose in aqueous samples was demonstrated by Vonach et al. [3.25, 26]. Edelman et al. [3.27] reported the use of a quantum cascade laser as mid-IR source

for the direct determination of glucose and fructose in wine samples by on-line LC-IR. Later, Edelmann et al. [3.28] demonstrated the use of on-line LC-attenuated total reflectance (ATR) measurements for the analysis of organic acids, sugars and alcohols in red wine employing multivariate curve resolution-alternating least squares (MCR-ALS) for the quantitative analysis of overlapping compounds. Moreover, the on-line coupling of CE-IR for the separation and quantification of sucrose, glucose and fructose in fruit juices [3.29] has been demonstrated.

The use of micro-machined flow cells in on-line CE-FTIR enables non-destructive, real time detection of analytes. However from the instrumental point of view the complexity of the required set-up for the CE-FTIR coupling is much higher than that for LC-FTIR. On the other hand, the use of on-line gradient LC-FTIR is still challenging, because the use of a constant reference spectrum as employed under isocratic conditions is not suitable under gradient conditions [3.30].

In this study, FTIR is used as an on-line detector for LC separations under gradient conditions for the analysis of four model carbohydrates (fructose, glucose, sucrose and maltose) in beverages in order to: (i) test the suitability of the AR-BGC-RSM approach using the absorbance ratio (AR) as an identification parameter in the presence of increasing concentrations of sugars; (ii) enable a higher sample throughput than that obtained under isocratic conditions in an equivalent LC-FTIR system and (iii) evaluate the method for the analysis of commercially available beverage samples.

3.2.2 Material and methods

Apparatus and Reagents

A Dionex (Sunnyvale, CA, USA) P680 high performance liquid chromatographic system, equipped with a Kromasil 100 NH₂ column (250×2 mm, 5 μm) and a sample injection loop of 20 μL, was employed for chromatographic separations. Linear acetonitrile:water gradients were run from 75 to 55% acetonitrile (Merck, Darmstadt, Germany) in 15 min.

A flow cell with CaF₂ and ZnSe windows and a pathlength of 10 μm installed on a Bruker (Bremen, Germany) IFS 66/v FTIR spectrometer equipped with a liquid nitrogen refrigerated mercury-cadmium-telluride (MCT) detector, a vacuum system and a dry

air purged sample compartment was employed for FTIR spectra acquisition. The scanner for the interferometer was operated at a HeNe laser modulation frequency of 100 kHz. Spectra were recorded in the range between 4000 and 950 cm^{-1} using the spectrum of the empty sample compartment as background, with a resolution of 8 cm^{-1} and a zero filling factor of 2. Zero filling consists of adding zeros on both ends of the interferogram prior to Fourier transformation so that the spectral lines have a smoother shape. During on-line LC-FTIR gradient experiments, 25 scans per spectrum were averaged, providing a spectra acquisition frequency of 15 spectra min^{-1} .

d(-)-Fructose, d(+)-glucose, sucrose and maltose-1-hydrate of analytical grade were purchased from Scharlab (Barcelona, Spain). Beverage samples were directly obtained from the Spanish market.

Sample preparation

A volume of homogenized sample between 50 and 500 μL was introduced into a 5 mL volumetric flask. Then 3.5 mL of acetonitrile were added and the flask was filled up to volume with water. Before the injection into the chromatographic system, the solution was sonicated in an ultrasonic water bath for 5 min and filtered through a 0.22 μm PTFE membrane. Carbonated liquid samples were degassed in an ultrasonic water bath for 15 min prior to their dilution. In order to increase the applicability of the method reducing possible interferences, acetonitrile was selected for sample dilution and chromatographic separation because according to a previously published work [3.31] it precipitates proteins and starch present in sample matrices.

Software and algorithms

For instrumental and measurement control as well as for data acquisition, the OPUS software (version 4.1) from Bruker was employed. Background correction and data treatment were run under Matlab 7.0 from Mathworks (Natick, USA, 2004) using in-house written Matlab functions.

3.2.3 Results and discussion

FTIR spectra of sugars

Figure 3.2.1 shows spectra of solutions of fructose, glucose, sucrose and maltose dissolved in 70:30 v/v acetonitrile:water. All four studied compounds show characteristic absorption bands of carbohydrates in the spectral region between 1500 and 950 cm^{-1} . The bands at 1035, 1015 and 1260 cm^{-1} were assigned to the C–O stretch, C–C stretch and C–OH deformation modes, respectively [3.29, 32, 33]. So, it can be concluded that any of the aforementioned bands is suitable for the quantification of sugars in beverages. However, in order to do a correct quantification of sugars in LC–FTIR, the changes in the spectrum of the mobile phase during the elution of the analytes must be carefully checked to achieve an appropriate chemometric background correction.

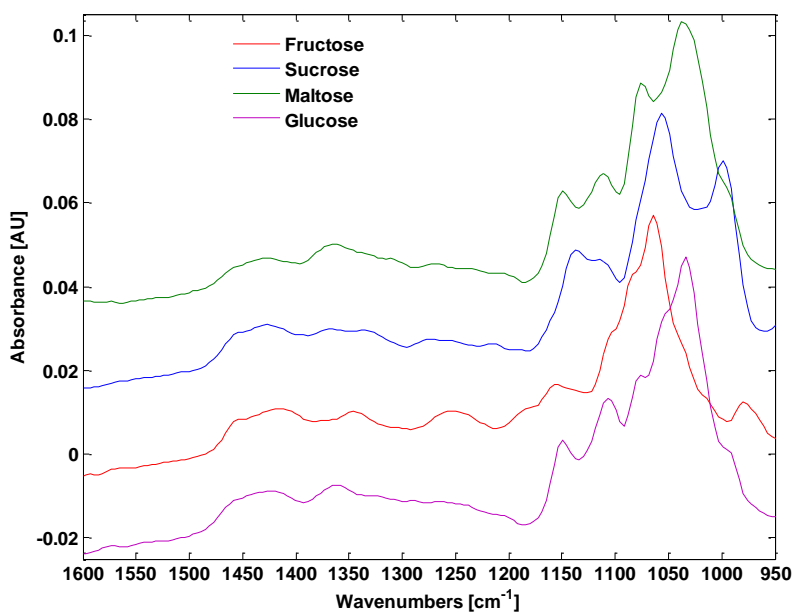


Figure 3.2.1. FTIR spectra of sugars in acetonitrile:water (70:30, v/v); fructose (6.1 mg mL^{-1}); glucose (6.0 mg mL^{-1}); sucrose (6.2 mg mL^{-1}) and maltose (6.0 mg mL^{-1}); spectra are shifted in the y direction for a better visibility.

Changes in the FTIR spectra of the mobile phase components during the elution of the analytes

For a proper use of the RSM-based background correction method, the mobile phase spectra should present at least one absorption band which can be used to identify the exact composition of the eluent during the chromatographic run. Special attention must be paid on the selection of the wavenumbers r_1 and r_2 employed for the calculation of the AR because spectral overlapping between the mobile phase and the eluting analytes at this wavenumbers leads to an inaccurate identification of the eluent spectra in the **RSM**, thus causing severe errors in both, spectra and elution profiles [3.1]. Additional difficulties can be created by modifications in position and bandwidth due to intermolecular interactions between analytes and the mobile phase components. Figure 3.2.2 (top) shows the spectrum of an acetonitrile:water (70:30, v/v) mixture between 4000 and 950 cm^{-1} . In the spectrum, four main water absorption bands can be identified at ~ 3400 (stretching band), 2115 (combination band), 1639 (deformation band) and near 1000 cm^{-1} (water libration bands), being in good agreement with reported data [3.29, 32, 33]. When using FTIR detection in aqueous systems, the intense absorption of water around $\sim 3400 \text{ cm}^{-1}$ leaves no detectable light, reducing the signal to noise ratio and obscuring the absorption of the analytes in this spectral region. Because of that, the region above 2400 cm^{-1} was not used throughout this work.

Two main acetonitrile bands were clearly distinguishable at 2252 and 2291 cm^{-1} , the first corresponding to the CN stretching mode, while the second one was assigned to a combination of both, CH_3 bending and C–C stretching modes [3.34].

It is well known that IR water bands can be modified by the presence of sugars, increasing considerably the difficulty of performing adequate IR background correction under gradient conditions. Recent studies of the interaction of water and carbohydrates by Max and Chapados [3.32, 33] have evidenced that the water deformation band (HOH bending vibration) at 1640 cm^{-1} increases its intensity and slightly shifts towards the blue region due to the formation of sugar hydrates, being displaced even several wavenumbers. Furthermore, spectra and abundances of the different hydrates of fructose, glucose or sucrose in aqueous solutions depend on their concentration [3.32, 33].

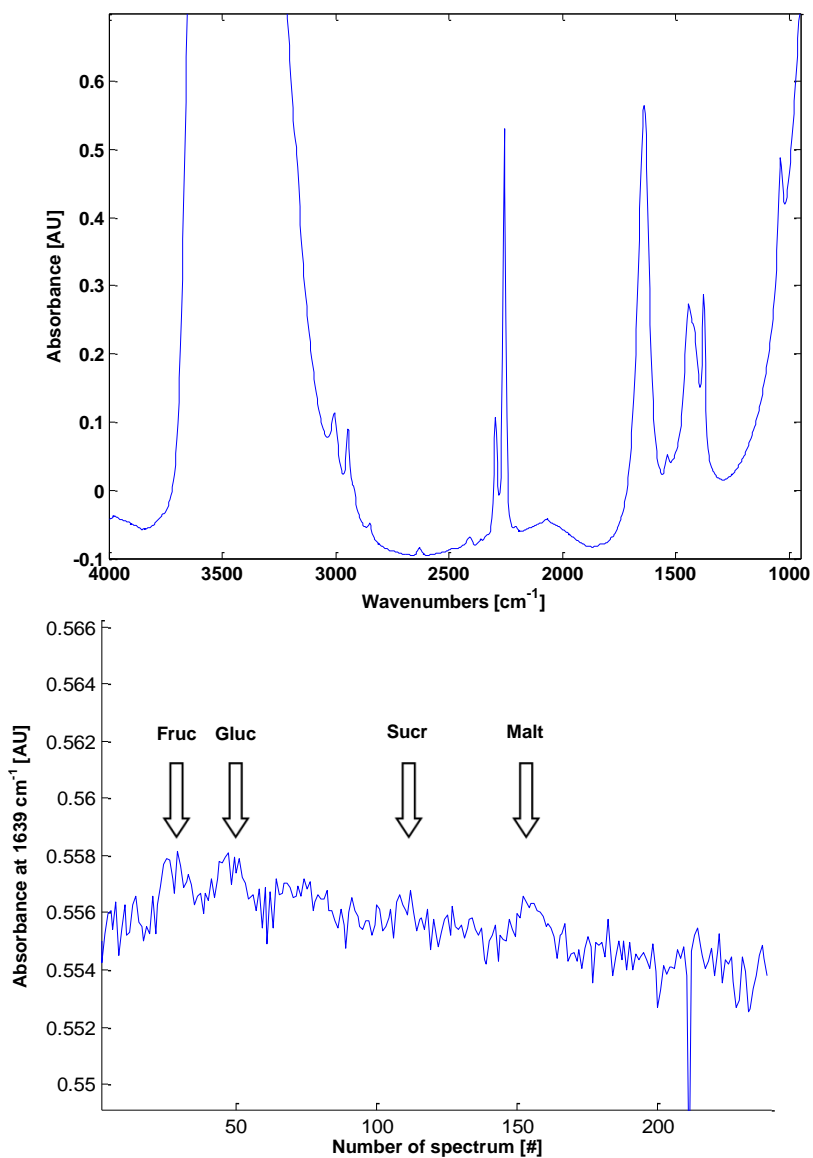


Figure 3.2.2. FTIR spectra of an acetonitrile:water (70:30, v/v) mixture (top) and variation of the absorbance at 1639 cm⁻¹ during the analysis of a sugar standard mixture (bottom); arrows indicate the sugar elution time windows.

To evaluate the effects of gradually increasing carbohydrate concentrations on the spectra of acetonitrile:water mixtures, 20 μL of 5 mg mL⁻¹ fructose, glucose, sucrose

and maltose mixtures were injected into an acetonitrile:water (70:30 v/v) flow system. It was found that, at the studied concentrations, using isocratic conditions and a spectral resolution of 8 cm^{-1} , the position of the maximum of the water deformation band at 1639 cm^{-1} remained constant during the elution of the studied carbohydrates. On the contrary, a slight increase in its intensity could be observed (see Figure 3.2.2, bottom). Therefore, in order to assure the accuracy of the background correction process during the elution of the four analytes, the use of the band at 1639 cm^{-1} is not recommended for the characterization of the mobile phase composition. In contrast, no effect on the peak shape of the CN bands in the $2300\text{--}2200\text{ cm}^{-1}$ spectral region was observed, therefore indicating that at this concentration level the spectrum of the eluent in this region is not affected by the presence of the analytes.

Selection of the BGC-RSM background correction parameters

One of the main features of the BGC-RSM method is its simplicity, limiting the user interaction during the background correction to the selection of the wavenumbers (r_1 and r_2) used for the calculation of the AR. The relative intensities of the CN stretching bands depend on the water concentration and this property can be used to correlate the band shape with the actual mobile phase composition. Accordingly, for an easy selection of these wavenumbers, all possible ARs within the CN stretching region (2180 and 2310 cm^{-1}) were assayed for an appropriate background selection from the spectra included in the **RSM** for the correction of a blank LC run. The employed output function was the noise (measured as RMS) in the extracted chromatograms at four characteristic eluent wavenumbers (2063 , 1640 , 1442 and 1065 cm^{-1}). Low chromatographic noise values indicated adequate background correction.

Results of the selection step are shown in Figure 3.2.3. The used **RSM** was composed by 986 spectra covering acetonitrile concentrations between 75 and 55% v/v acetonitrile and a blank gradient injection (**SM**) was formed by 317 spectra of mobile phase solutions in the same concentration range. From Figure 3.2.3 it can be concluded that the combinations of wavenumbers in the interval between 2255 and 2275 cm^{-1} with wavenumbers of the intervals from 1980 to 2230 cm^{-1} , 2240 to 2270 cm^{-1} and 2280 to 2300 cm^{-1} show the lowest noise at all evaluated wavenumbers. It is

remarkable, that in all cases the optimum values were obtained using the band at 2254 cm^{-1} , as expected from previously known spectral information.

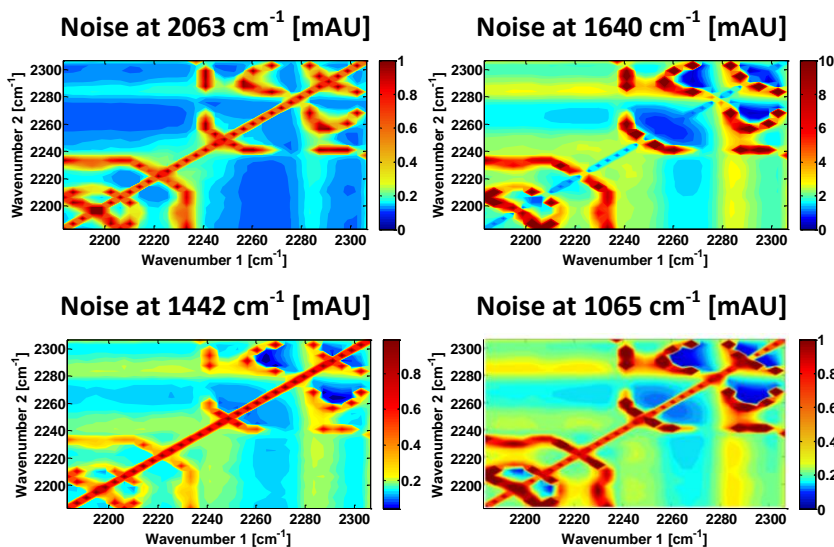


Figure 3.2.3. Response surfaces obtained during the AR selection for background correction in acetonitrile:water solutions ranging from 75 to 55% v/v acetonitrile using the noise at 2063, 1639, 1442 and 1065 cm^{-1} in the background corrected chromatogram as response. Note: Noise values in mAU.

Table 3.2.1 summarizes the five pairs of wavenumbers which provided the lowest noise in the extracted chromatograms at the four selected wavenumbers. The noise level in the extracted chromatograms at 2063, 1640 and 1442 cm^{-1} reached a minimum value using the absorbance at 2256.5 and 2252.6 cm^{-1} for the calculation of the AR, obtaining RMS values between $9 \cdot 10^{-5}$ and $2.9 \cdot 10^{-3}$ for 2063 and 1640 cm^{-1} , respectively. On the other hand, the minimum noise in the extracted chromatogram at 1065 cm^{-1} was achieved using the AR calculated from absorbance values at 2295 and 2249.5 cm^{-1} . The difference between the obtained noise values using this pair of wavenumbers and that obtained using the absorbance ratio between 2256.5 and 2252.6 cm^{-1} is only 2.1% and cannot be considered as relevant. Although there are minor differences between the obtained values, the obtained chromatographic noise values were excellent in any case. Based on foregoing data, the quotient between the

absorbance values at 2256.5 and 2252.6 cm^{-1} was selected for background correction of further measurements.

Table 3.2.1. Absorbance ratios (AR) that provided the lowest noise values in the extracted chromatograms.

Noise [AU]	r1 [cm^{-1}]	r2 [cm^{-1}]
Chromatogram extracted using absorbance values at 2063 cm^{-1}		
9.08 10^{-5}	2256.5	2252.6
1.09 10^{-4}	2260.3	2252.6
1.15 10^{-4}	2264.2	2248.7
1.23 10^{-4}	2260.3	2248.7
1.26 10^{-4}	2291.2	2268
Chromatogram extracted using absorbance values at 1640 cm^{-1}		
3.00 10^{-3}	2256.5	2252.6
3.78 10^{-3}	2291.2	2268
3.89 10^{-3}	2260.3	2252.6
3.98 10^{-3}	2264.2	2248.7
4.09 10^{-3}	2268	2244.9
Chromatogram extracted using absorbance values at 1442 cm^{-1}		
4.80 10^{-4}	2256.5	2252.6
5.33 10^{-4}	2260.3	2256.5
5.72 10^{-4}	2248.7	2268
5.82 10^{-4}	2264.2	2252.6
6.18 10^{-4}	2298.9	2291.2
Chromatogram extracted using absorbance values at 1065 cm^{-1}		
0.42 10^{-4}	2295	2244.9
4.20 10^{-4}	2291.2	2268
4.27 10^{-4}	2256.6	2252.6
4.47 10^{-4}	2298.9	2268
4.50 10^{-4}	2260.3	2248.7

Note: Noise measured as the root mean square of the extracted chromatogram at 2063, 1640, 1442 and 1065 cm^{-1} in the background corrected blank gradient injection.

As an example, Figure 3.2.4 shows the original data of a blank gradient injection (top) and the background corrected matrix (bottom) using the selected parameters. After background correction, the spectral noise is randomly distributed around zero and no absorption bands of the eluent as well as no time drift can be observed.

In spite of the excellent results obtained from the background correction of the blank gradient chromatogram, changes in the intensity of the CO₂ bands in the 2400 cm⁻¹ region might affect the performance of the background correction process. Hence, for an optimal performance of the method a strong and continuous purge of the sample compartment during spectra acquisition is recommended.

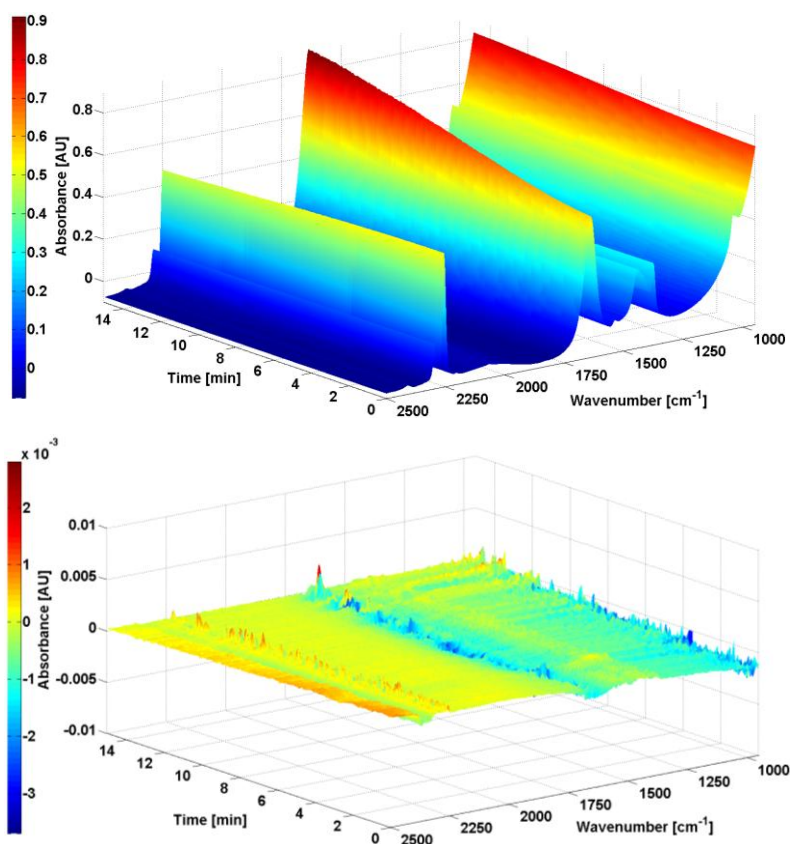


Figure 3.2.4. Uncorrected (top) and corrected (bottom) IR spectra in the 2500 to 950 cm⁻¹ region corresponding to a blank gradient LC-IR injection with a LC run time of 15 min and mobile phase compositions between 75 and 55% acetonitrile.

On-line LC–FTIR analysis of carbohydrates

Figure 3.2.5 shows original (top) and background corrected (bottom) spectra acquired during the elution of a standard carbohydrate solution of fructose, glucose, sucrose and maltose at a concentration of 2.5 mg mL^{-1} of each analyte. Visual inspection of the 3D graphs reveals that changes in the background signal due to the mobile phase gradient have been corrected to a great extent by the BGC-RSM subtraction procedure.

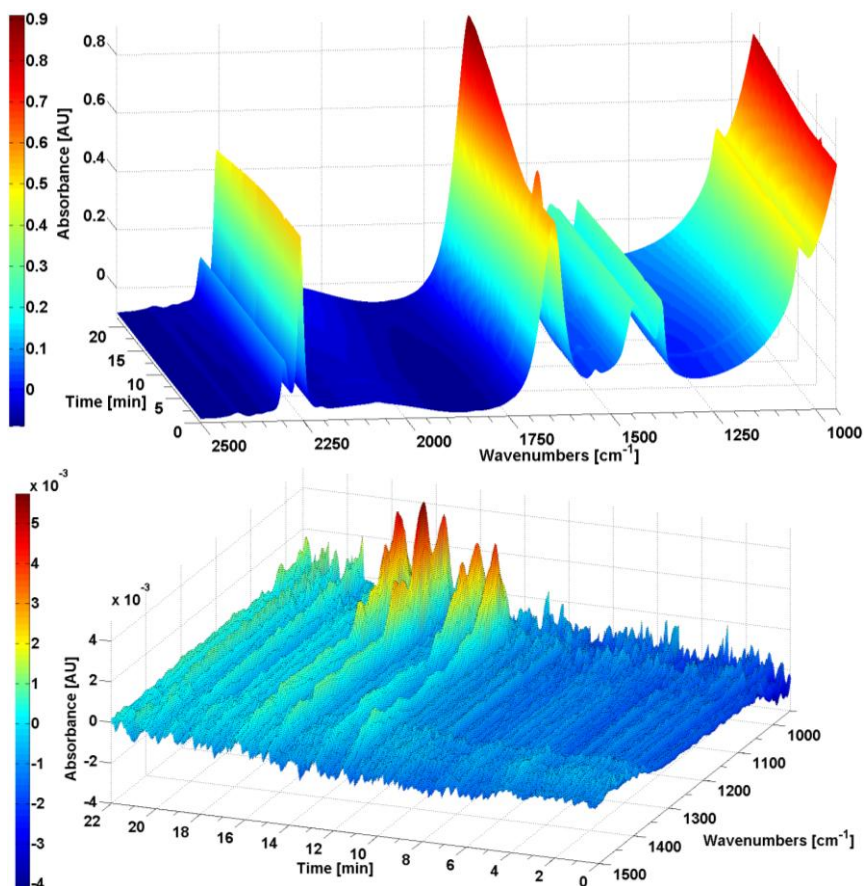


Figure 3.2.5. On-line gradient LC–FTIR spectra obtained from the injection of a sugar standard solution containing 2.5 mg mL^{-1} of fructose, glucose, sucrose and maltose; top: raw spectra between 2200 and 1000 cm^{-1} , bottom: spectra in the wavenumber range between 1500 and 1000 cm^{-1} corrected using the BGC-RSM method.

As an example, LC–FTIR chromatograms extracted from the injection of a standard solution containing 5.5 mg mL^{-1} of fructose, glucose, sucrose and maltose and from the injection of sample 1 are shown in Figure 3.2.6. The depicted chromatograms were obtained from the measurement of the area values of the spectra between 1108 and 1069 cm^{-1} , corrected using a baseline established at 1203 cm^{-1} . It can be seen, that the resolution is very good and the specific spectra of the analytes can clearly be distinguished (see Figure 3.2.7). The retention times, established from four injections of standard mixtures of the considered compounds were 11.8 ± 0.2 , 12.7 ± 0.2 , 15.0 ± 0.2 and 16.5 ± 0.2 min for fructose, glucose, sucrose and maltose, respectively.

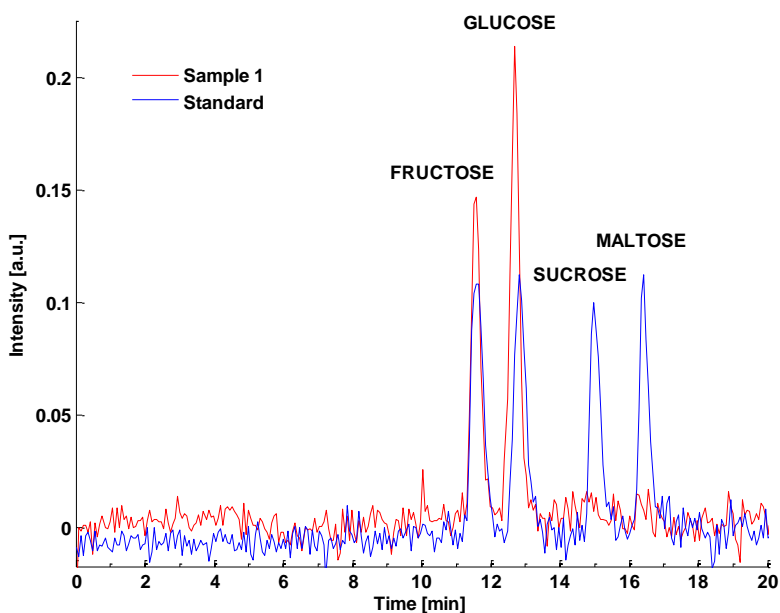


Figure 3.2.6. LC–FTIR chromatograms extracted from the injection of a standard solution containing 5.5 mg mL^{-1} of fructose, glucose, sucrose and maltose (red) and from the injection of sample 1 (blue); chromatograms were obtained from the measurement of the area between 1108 and 1069 cm^{-1} , corrected using a baseline established at 1203 cm^{-1} .

As it can be seen in the chromatograms of Figure 3.2.6, the lack of sloping baselines and the random distribution of the chromatographic noise support the suitability of the selected background correction conditions for obtaining the chromatograms of sugars during gradient elution.

To quantify the accuracy of the background correction, a numerical correlation was made through the determination of a “correlation coefficient (QC)”, where a QC = 100% indicates identical spectra. Using the spectral region between 1250 and 1060 cm^{-1} , the obtained QCs for the spectra shown in Figure 3.2.7 ranged between 96.25 and 98.73%. On the other hand, QCs were also calculated for corrected spectra obtained from sample injections and again excellent agreement between extracted and reference spectra was obtained (data not shown), which confirmed the identity of carbohydrates, thus increasing the reliability of the results.

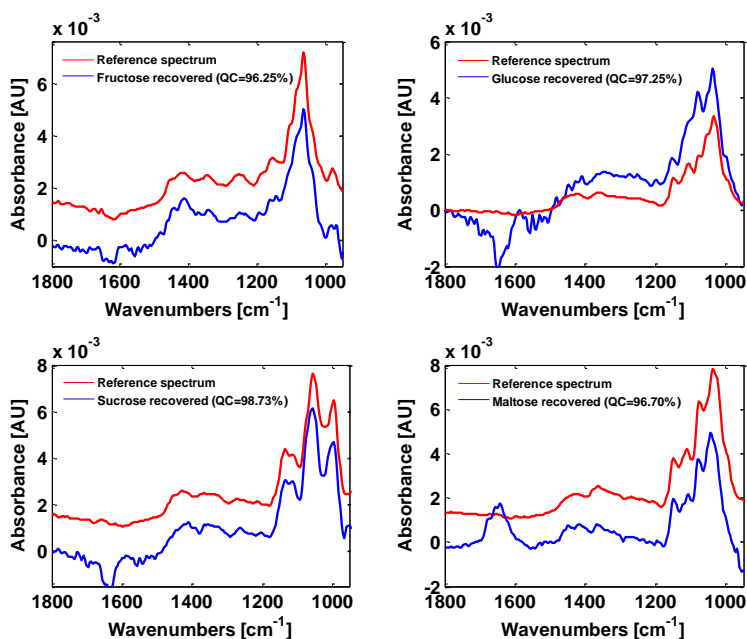


Figure 3.2.7. Recovered spectra of fructose, glucose, sucrose and maltose at their respective peak apex extracted from the sugar standard solution LC run shown in Figure 3.2.6 in comparison to reference spectra.

Calibration of analytes was made using the previously described experimental conditions. Fructose chromatograms were obtained from the measurement of the spectral area between 1108 and 1069 cm^{-1} , corrected using a baseline at 1203 cm^{-1} . Glucose, sucrose and maltose chromatograms were calculated from area measurements between 1177 and 1025 cm^{-1} , corrected using a baseline at 1177 cm^{-1} . Table 3.2.2 shows the obtained analytical parameters using peak height values from the extracted chromatograms. The linear regression coefficients obtained indicated a good adjustment of the data to each calibration curve. Limits of detection (LODs) in the 0.4 – 0.6 mg mL^{-1} range were estimated as the concentration at which the chromatographic signal to noise ratio was higher than 3. The precision of six independent injections of a standard calibration solution containing 3.0 mg mL^{-1} of each analyte provided relative standard deviations (RSDs) ranging between 3.3 and 4.1% for glucose and fructose, respectively. The obtained sensitivity and precision results together with the good correlation coefficients obtained for the recovered analyte spectra suggested that the developed method was appropriate for the quantitative determination and identification of sugars in beverages.

Determination of sugars in beverages

The applicability of the proposed method was evidenced by the analysis of a set of 7 commercially available samples purchased from the Spanish market. Table 3.2.3 lists the obtained sugar contents from duplicate analysis of diluted samples. Additionally, a recovery study was carried out in six of the analyzed samples. The employed spiked concentration ranges were: 0.97–2.54 g 100 mL^{-1} , 0.90–2.36 g 100 mL^{-1} , 0.97–3.133 g 100 mL^{-1} and 1.10–3.34 g 100 mL^{-1} for fructose, glucose, sucrose and maltose, respectively. Mean recovery values ranged between 105.1 and 92.5% (see Table 3.2.4).

Table 3.2.2. Analytical figures of merit of the on-line LC-FTIR determination of sugars.

Analyte	Calibration curve ^a [$y = a + bC$ [mg mL ⁻¹]] ($a \pm s_a$) (CI) ^e	R ²	Noise ^b	LOD ^c [mg mL ⁻¹]	Repeatability ^d [%]	Linear range [mg mL ⁻¹]
Fructose	(0.0008 ± 0.0006) (0.0014)	0.9995	0.4	0.4	4.1	LOD - 6.0
Glucose	(0.000 ± 0.006) (0.014)	0.9965	0.6	0.6	3.3	LOD - 5.2
Sucrose	(0.006 ± 0.006) (0.014)	0.9962	0.5	0.5	3.7	LOD - 4.9
Maltose	(0.013 ± 0.007) (0.016)	0.998	0.4	0.4	3.8	LOD - 5.2

Note: Calibration curve^a: obtained from 10 standard solutions, a and b are the intercept and the slope of the calibration lines; Noise^b: chromatographic noise measured as the root mean square (RMS) of the chromatographic signal extracted from a background correct blank gradient injection; LOD^c: limit of detection established as the concentration at which the signal to noise ratio is higher than 3; Repeatability^d: relative standard deviation for six independent measurements carried out at a concentration level of 3.0 mg mL⁻¹; (CI)^e: confidence interval calculated as $CI = s_a \cdot t_{p,n-2}$ ($p = 95\%$);

Table 3.2.3. On-line LC-FTIR determination of sugars in commercial samples.

Sample	Presentation	Found concentration [g 100 mL ⁻¹]				Total	Labeled content [g 100 mL ⁻¹]
		Fructose	Glucose	Sucrose	Maltose		
1	Soft drink	5.14	7.84	<LOD	<LOD	13.0	12.9
2	Soft drink	6.39	4.75	<LOD	<LOD	11.1	11.6
3 ^a	Soft drink	<LOD	<LOD	<LOD	<LOD	0.00	0.00
4	Soft drink	3.50	4.18	1.33	<LOD	9.0	8.9
5	Soft drink	0.16	0.87	6.26	<LOD	7.3	7.9
6	Energy drink	0.33	3.08	6.43	<LOD	9.8	10.7
7	Fruit juice	3.77	3.69	2.61	<LOD	10.1	12.4

Note: 3^a, Sample 3 was labeled as sugar free.

Table 3.2.4. Recovery study of fructose, glucose, sucrose and maltose in spiked commercial samples.

Sample	Presentation	g 100 mL ⁻¹ added				g 100 mL ⁻¹ found ^a (% Recovery)			
		Fructose	Glucose	Sucrose	Maltose	Fructose	Glucose	Sucrose	Maltose
1	Soft drink	2.54	1.90	2.98	1.84	7.69 ± 0.08 (100.4)	9.84 ± 0.09 (105.1)	2.92 ± 0.014 (98.1)	1.84 ± 0.05 (100.2)
2	Soft drink	2.06	2.36	3.33	3.34	8.36 ± 0.04 (95.6)	7.19 ± 0.09 (103.5)	3.34 ± 0.02 (100.2)	3.39 ± 0.09 (101.3)
4	Soft drink	1.00	0.93	0.97	1.19	4.48 ± 0.06 (98.0)	5.11 ± 0.04 (99.8)	2.39 ± 0.02 (104.0)	1.28 ± 0.05 (99.1)
5	Soft drink	0.97	0.90	1.30	1.10	1.13 ± 0.08 (100.0)	1.76 ± 0.09 (98.9)	7.54 ± 0.06 (98.7)	1.02 ± 0.08 (92.5)
6	Energy drink	1.43	0.97	1.07	1.17	1.78 ± 0.09 (101.4)	4.06 ± 0.04 (101.9)	7.45 ± 0.03 (95.8)	1.15 ± 0.07 (98.4)
7	Fruit juice	2.20	2.18	1.74	1.57	5.92 ± 0.02 (97.7)	5.90 ± 0.08 (101.4)	4.32 ± 0.08 (98.1)	1.65 ± 0.07 (104.9)

Note: g 100 mL⁻¹ found^a: recoveries from two independent replicates.

3.2.4 Conclusions

A simple on-line gradient LC method in combination with FTIR detection has been developed for the determination of four characteristic carbohydrates in beverages. Fructose, glucose, sucrose and maltose could be separated, identified and quantified in commercial samples with limits of detection between 0.4 and 0.6 mg mL⁻¹. The use of the univariate method for the selection of the background spectrum from a reference spectra matrix permitted an accurate chemometric eluent correction yielding distinguishable spectra of good quality for the studied analytes with correlation factors between 96.25 and 98.73% in comparison to reference spectra. The main advantages provided by the proposed on-line LC–FTIR approach include instrumental simplicity and low cost due to the possibility of using commercially available standard flow cells.

3.3 A Partial Least Squares procedure for background correction

3.3.1 Introduction

In order to overcome existing limitations of methods for background correcting IR spectra recorded during a chromatographic run, the aim of this work was the development of a PLS multivariate approach for the calculation of an IP (PLS-BGC-RSM) to be used for background correction for on-line LC-IR data recorded under both, isocratic and gradient conditions, combining high accuracy with minimal computational time and user interaction. The method was tested on real isocratic and gradient reversed phase on-line LC-IR injections of different analytes (caffeine, diuron, and atrazine) in acetonitrile:water binary mobile phases.

3.3.2 Material and methods

Apparatus and Reagents

The LC system consisted of a Waters (Waters, Milford, MA) 7100 quaternary pump with a six-port injection valve (Rehodyne, Bensheim, Germany) equipped with a 12.5 μL injection loop. Chromatographic separations were achieved using a C_{18} reversed-phase column (Nucleosil 100 RP C_{18} column, 150x2.1 mm, 3 μm , VDS Optilab, Berlin, Germany) and a flow rate of 150 $\mu\text{L min}^{-1}$. For isocratic analysis, a mobile phase composed of acetonitrile and water (1% v/v acetic acid) at 60:40 v/v was used. For gradient LC runs, an acetonitrile:water mobile phase was used running linear gradients from 60 to 100% acetonitrile.

A Bruker (Bruker Optics GmbH, Ettlingen, Germany) IFS 55 spectrometer equipped with a liquid nitrogen cooled mercury cadmium telluride (MCT) detector, a globar light source and a KBr beamsplitter was employed for spectral measurements. A flow cell with CaF_2 windows and an optical path length of 25 μm was employed. The spectra were collected co-adding 25 scans with a spectral resolution of 8 cm^{-1} at a mirror velocity of 180 kHz HeNe frequency and using an aperture of 8 mm for the IR beam. Prior to LC-IR data acquisition, a background spectrum of the empty sample compartment was acquired.

Diuron, atrazine, and caffeine standards were purchased from Fluka (Buchs, Switzerland). Water and acetonitrile (LC grade) supplied by Fluka and acetic acid supplied by Riedel de Haën (Seelze, Germany) were used for the separation procedure and for standard preparation. Analyte standards were prepared in 35:65 acetonitrile:water. All the solutions were filtered through a 0.22 μm nylon filter prior to injection.

Software and algorithms

Absorbance spectral data were obtained using the OPUS software (version 5.0) from Bruker (Bruker Optics, Ettlingen, Germany). The accuracy of the proposed method was assessed by comparing corrected spectra extracted from the peak apex with previously measured reference spectra of the analytes. The correlation coefficient (r) between two spectra y_1 and y_2 is defined as the ratio of the covariance ($Cov(y_1, y_2)$) and the product of the two standard deviations σ_{y_1} and σ_{y_2} . According to this definition, a value of $r = 1$ indicates identical spectra. All spectra were baseline corrected at 1890 cm^{-1} .

Chemometric data treatment was run under Matlab 7.7 (MathWorks, Natick, MA) using in-house-written Matlab functions. A partial least squares (PLS) model was established from the **RSM** data using the spectral interval between 2345 and 2145 cm^{-1} to relate the spectra to the absorbance at 1639 cm^{-1} . From the established model, a single numeric value was derived that is characteristic for the actual, but unknown, composition of the solvent mixture of a given spectrum contained in the **SM** and **RSM**.

3.3.3 Results and discussion

Selection of the spectral interval for the calculation of the Partial Least Squares (PLS) model

A selection of the variables used for the PLS model was carried out in order to achieve the best performance from detailed evaluation of the spectral features of the eluent in a defined concentration range. Figure 3.3.1 shows the infrared absorbance spectra of acetonitrile:water (1% v/v acetic acid) solutions with acetonitrile concentrations between 60 and 100% v/v between 2315 and 1050 cm^{-1} .

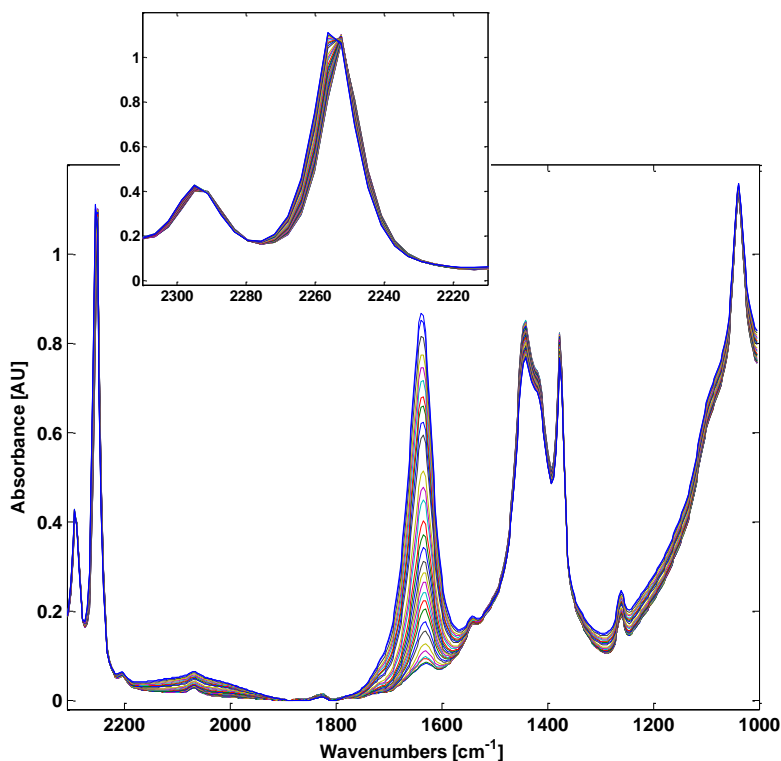


Figure 3.3.1. FTIR absorbance spectra in the spectral range between 2315 and 1050 cm^{-1} of a set of mobile phase solutions of water and acetonitrile with concentrations between 60 and 100% v/v acetonitrile measured with a resolution of 8 cm^{-1} ; inset: detailed view of spectra in the CN stretching region.

Characteristic absorption bands from the added acetic acid at 1712 and 1280 cm^{-1} due to C=O and C–O bonds of the COOH group, respectively, cannot be observed clearly due to their relatively low intensity. On the other hand, the intense water band at 1640 cm^{-1} and the broad combination band at 2115 cm^{-1} are clearly observed. Moreover, the libration band of water below 650 cm^{-1} produces a significant strong absorption that is visible near 1000 cm^{-1} . Acetonitrile presents three intense bands at 1442, 1416, and 1377 cm^{-1} due to the C–C–H deformation and the CH_3 rocking bands [3.35] located between 1130 and 950 cm^{-1} . Two sharp acetonitrile bands are also observed at 2252 and 2291 cm^{-1} . The first band originates from the CN stretching mode, while the second band is a combination of CH_3 bending and C–C stretching modes [3.34]. It has been shown previously that the shape of the CN stretching band changes with the

water content [3.34, 35]. In a previous work [3.34], this band was deconvoluted into two Lorentzians separated by 5 cm^{-1} (2254 and 2251 cm^{-1}). The first band was assigned to free acetonitrile molecules, and the latter band was attributed to hydrogen bonded acetonitrile molecules. When the water content was varied, the intensities of the two Lorentzian bands changed, but their wavenumber position did not change significantly. It is remarkable that there are different spectral ranges in which a prediction of the absorbance of one wavenumber that is characteristic of the eluent composition can be carried out. Here, the CN stretching region between 2345 and 2145 cm^{-1} and the absorbance at 1639 cm^{-1} as reference value were selected. Whereas for the establishment of a PLS model based on the recorded blank gradient LC-IR chromatogram (**RSM**), the spectral region from 2345 to 2145 cm^{-1} and the absorbance values at 1639 cm^{-1} are required, for the application of the PLS model to the recorded **SM** data set, only information in the region from 2345 to 2145 cm^{-1} is used. Due to the reduced number of analytes presenting absorption bands in this region, it may be concluded that the proposed method is of general applicability.

Figures of merit of the Partial Least Squares model

For the calibration set, 4440 spectra between 2400 and 950 cm^{-1} , obtained from the measurement of a linear gradient covering acetonitrile concentrations between 40 and 100% v/v, were used. The external validation set was composed of 234 spectra obtained during the measurement of a faster on-line LC-IR blank gradient in the same concentration range. The number of PLS factors was chosen according to the root mean square error of cross validation (RMSECV), selecting an additional factor when the RMSECV calculated using 'venetian blinds' CV improved by at least 2% and selecting as few factors as possible.

Figure 3.2.2 shows good correlation between the predicted values of absorbance at 1639 cm^{-1} and the actual values in the external validation set, using 6 factors for the calculation of the model. This figure also highlights the absence of systematic errors as the calculated intercept was found to be equal to 0 and the slope equal to 1, both being located inside the corresponding confidence ellipses for a 90% level of significance.

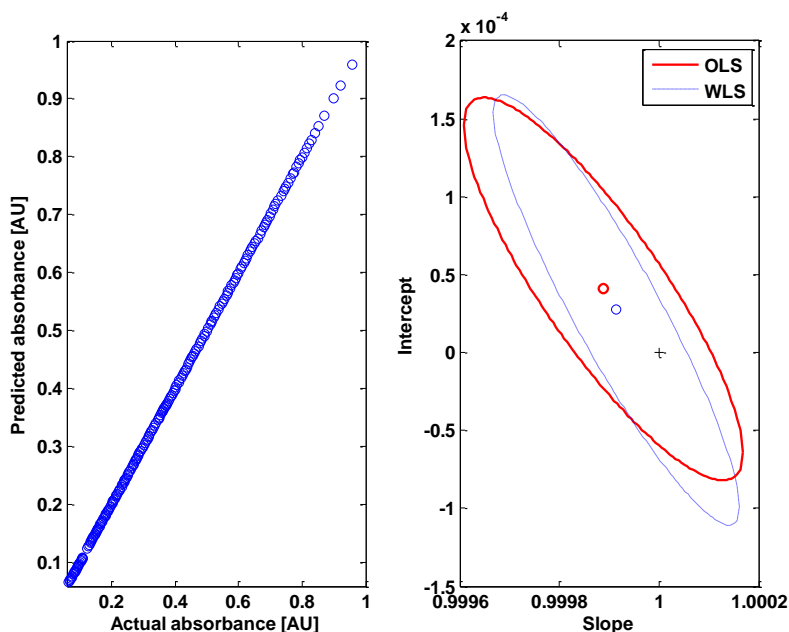


Figure 3.3.2. Regression between actual absorbance values and those predicted by the PLS model in the validation data set at 1639 cm^{-1} ; left: regression plot; right: elliptic joint confidence test for slope and intercept; Note: OLS stands for Ordinary Least Squares regression; WLS stands for Weighted Least Squares regression.

Furthermore, the regression and predictive capabilities of the PLS model are adequate as shown by the data summarized in Table 3.3.1, outlining the root mean square error of cross-validation (RMSECV), the correlation coefficient (r_{CAL}), the root mean square error of prediction (RMSEP), the mean difference and the standard deviation of mean differences between predicted versus actual absorbance values ($d_{(x-y)}$ and $s_{(x-y)}$, respectively), and the maximum percentage of error values to be expected for new predictions (QC) of the response parameter.

Table 3.3.1. Prediction capabilities and main parameters of the calculated PLS model for the prediction of the absorbance at 1639 cm^{-1} in unknown acetonitrile:water (1% v/v acetic acid) solutions.

Parameter	PLS model
Factors	6
Spectral region [cm^{-1}]	2345–2145
Baseline correction [cm^{-1}]	1890
Pre-processing	mean centering
Cross-validation	Venetian blinds
RMSECV [AU]	$4.0 \cdot 10^{-4}$
r_{CAL}	1.0000
RMSEP [AU]	$4.1 \cdot 10^{-4}$
$d_{(x-y)}$ [AU]	$1.2 \cdot 10^{-6}$
$s_{(x-y)}$ [AU]	$4.0 \cdot 10^{-4}$
QC [%]	0.3

Results from on-line LC-IR runs under isocratic conditions

The LC-IR measurement of a standard solution containing 3 mg mL^{-1} caffeine was carried out under isocratic conditions (acetonitrile:water (1% acetic acid), 60:40 v/v) to estimate whether the proposed subtraction procedure provided results comparable to those obtained using a constant reference background. The chromatographic noise values, measured as root mean square (RMS) in extracted chromatograms at three different solvent characteristic wavenumbers, were calculated. From the results shown in Table 3.3.2 it was concluded that the proposed approach provided signal-to-noise ratios statistically comparable to those found by the correction method based on the use of a constant background.

Table 3.3.2. Chromatographic noise values, measured as RMS at four wavenumbers where the solvent shows characteristic bands, found in a background corrected data set from a blank isocratic injection using a constant spectrum as reference and the proposed approach.

Background correction	RSM Noise ^a [AU]			
	1712 [cm ⁻¹]	1643 [cm ⁻¹]	1442 [cm ⁻¹]	1280 [cm ⁻¹]
Constant spectrum	2.9	9.3	4.5	2.3
PLS approach	3.1	7.6	4.7	2.3

Note: RSM Noise^a: Noise values multiplied by a factor of 10^{-4} .

The FTIR spectra extracted from the chromatogram during the elution of the analyte using both background correction approaches are shown in Figure 3.3.3. The similarity of the spectra in the region between 1700 and 1050 cm⁻¹ is reflected by a correlation coefficient of 0.99, showing that the obtained spectra using the proposed method are comparable to those obtained subtracting a constant background, do not show spectral artifacts and hence, can be used for both quantitative and qualitative analysis.

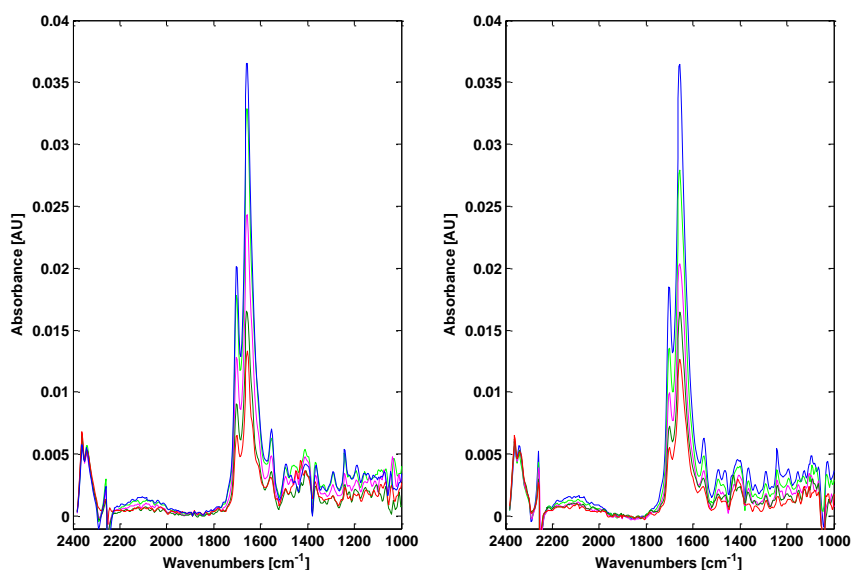


Figure 3.3.3. Spectra extracted during the elution of caffeine analyzed under isocratic conditions using the developed background correction approach (left) and a constant reference spectrum measured at the beginning of the run after equilibration of the chromatographic system (right).

Results from on-line LC-IR runs under gradient conditions

Figure 3.3.4 (top) shows original and corrected sets of spectra from a blank gradient injection as eluent composition changes from 40% to 100% v/v acetonitrile over a period of 15 minutes. For a better visualization of the performance of the background-correction method, Figures 3.3.4 (bottom) show the extracted chromatograms from the original and background corrected blank injection, at two wavenumbers (1639 and 1442 cm^{-1}) where the mobile phase components absorb strongly. Chromatographic noise values found in both chromatograms, as well as the absence of sloping baselines and the random distribution of the residuals, showed that the presented approach satisfactorily achieves chemometric correction of changing eluent spectra.

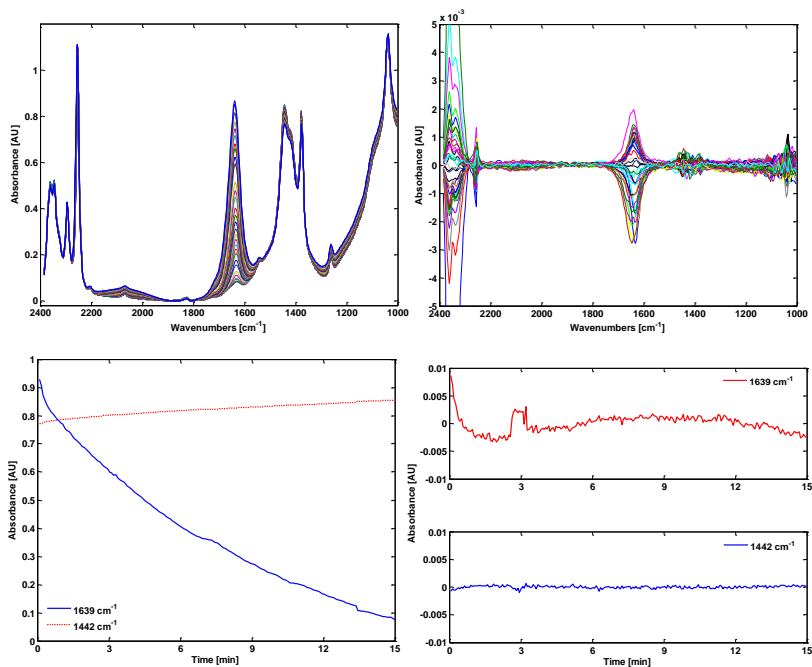


Figure 3.3.4. Top: on-line gradient LC-IR spectra obtained from a blank gradient injection before (left) and after (right) performing the background correction using the developed approach. Bottom: extracted chromatograms obtained from the measurement of the absorbance at 1639 and 1442 cm^{-1} before (left) and after (right) background correction.

Furthermore, a separation of two pesticides, diuron and atrazine, was carried out under the same gradient conditions. Figure 3.3.5 shows the extracted chromatogram at 1581 cm^{-1} and the spectra of both pesticides extracted from the peak apex, obtained after correcting the eluent contribution. The accuracy of the subtraction process was evaluated by comparing the extracted spectra of both pesticides from the peak apex with pesticide reference spectra previously measured, obtaining correlation factors of 0.94 and 0.93 for atrazine and diuron, respectively.

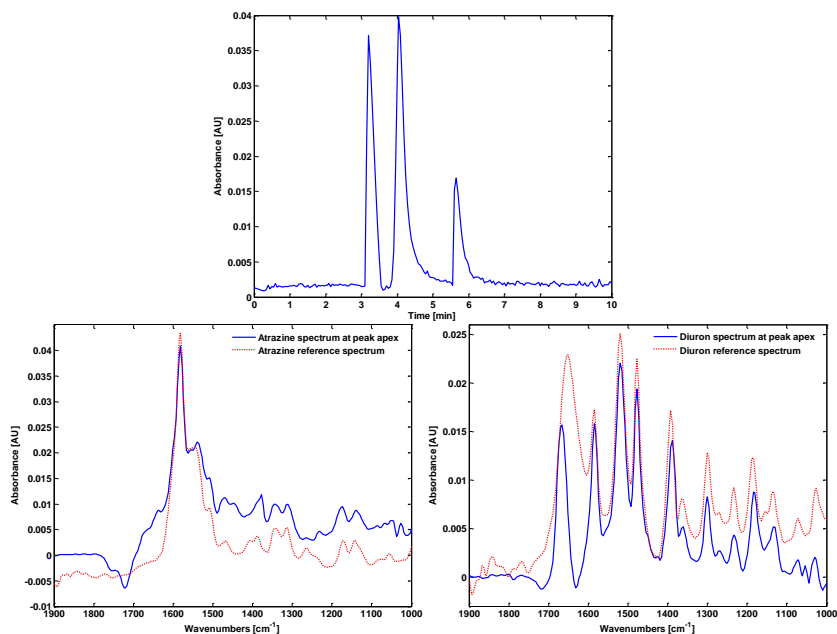


Figure 3.3.5. Top: background corrected on-line gradient LC-IR chromatogram obtained from the measurement of the absorbance at 1581 cm^{-1} , extracted from the injection of a mixture of atrazine and diuron standards into a linear acetonitrile:water (1% v/v acetic acid) gradient; bottom: background corrected spectra at the peak apex of both pesticides, atrazine (left) and diuron (right), in comparison to reference spectra.

3.3.4 Conclusions

This work shows the potential use of the proposed strategy, based on the use of a reference spectra matrix combined with a multivariate PLS regression, for background correction in continuous liquid flow systems. Its applicability for the measurement of the analyte spectra in isocratic and gradient LC has been tested, achieving highly promising results in both situations. The proposed approach presents better applicability than previously developed background correction approaches for isocratic LC-IR. Moreover, the user interaction is reduced, no prior standards are required and the need for previous knowledge of the analyte spectra is minimal.

3.4 Application of point-to-point matching algorithms for background correction

3.4.1 Introduction

In order facilitate the selection of the optimal conditions for background correction using a **RSM**, this work reports a new IP based on the direct comparison of characteristic absorption bands of the eluent during the chromatographic run with those of a reference data set in a point-to-point way (p2p-BGC-RSM). Following previous results, this work focuses on the development of a new background correction approach paying attention to features that facilitate its use reducing the number of user-defined variables. Different alternatives are presented and discussed on real LC-IR data sets obtained from the analysis of a solution of four nitrophenols as a model system using an acetonitrile (0.08% v/v TFA):water (0.08% v/v TFA) gradient with compositions ranging from 35 to 85% v/v acetonitrile.

3.4.2 Material and methods

Apparatus and Reagents

A Dionex (Sunnyvale, CA, USA) P680 high performance liquid chromatographic system, equipped with a C₁₈ column (150 x 2.0 mm, 5 µm) at 22°C was employed using a sample injection loop of 20 µL. Mobile phase gradients were run from 65:35 v/v water (0.08% v/v TFA):acetonitrile (0.08% v/v TFA) to 15:85 v/v water (0.08% v/v TFA):acetonitrile (0.08% v/v TFA) in 20 minutes (**SM** acquisition), re-equilibrating the system in 7 minutes (**RSM** acquisition).

An IR transparent flow cell was constructed using CaF₂ windows and an aluminium spacer with a channel of 2.5 mm width and a pathlength of 16.5 µm. For FTIR spectra acquisition a Bruker (Bremen, Germany) IFS 66/v FTIR spectrometer equipped with a liquid nitrogen refrigerated mercury–cadmium–telluride (MCT) detector, a vacuum system and a dry air purged sample compartment was used. The scanner for the interferometer was operated at a HeNe laser modulation frequency of 100 kHz. Spectra were recorded in the range between 4000 and 950 cm⁻¹ using the spectrum of

the empty sample compartment as background, with a resolution of 8 cm^{-1} and a zero-filling factor of 2. An aperture of 3 mm and a grating to attenuate the intensity of the irradiating light on the detector element were used to achieve optimum signal intensity. During gradient experiments, 25 scans per spectrum were averaged, providing a spectra acquisition frequency of $15\text{ spectra min}^{-1}$.

Reference spectra were acquired in stopped-flow mode filling the flow cell with standard solutions of each analyte using a 85:15 v/v water (0.08% v/v TFA):acetonitrile (0.08% v/v TFA) solution as reference background.

4-nitrophenol (4-NP), 2,4-dinitrophenol (2,4-dNP), 2-nitrophenol (2-NP) PESTANAL grade (Fluka, Buchs, Switzerland) and 3-methyl-4-nitrophenol (3m4-NP) (98%, Sigma-Aldrich, Switzerland) standard solutions were prepared by dissolving an appropriate amount of each component in a 85:15 v/v water (0.08% v/v TFA):acetonitrile (0.08% v/v TFA) solution. Solutions were filtered ($0.22\text{ }\mu\text{m}$) prior to injection. HPLC grade acetonitrile and trifluoroacetic acid (TFA) were obtained from Scharlau (Barcelona, Spain) and Sigma-Aldrich, respectively. De-ionized water was purified with a Millipore system.

Software and algorithms

For instrumental and measurement control as well as for data acquisition, the OPUS software (version 6.5) from Bruker was employed. Background correction was run under Matlab 7.7.0 from Mathworks (Natick, USA) using an in-house written Matlab function.

3.4.3 Results and discussion

Selection of the spectral interval used for the calculation of the similarity index

Figure 3.4.1 shows FTIR spectra measured during an on-line LC-IR gradient as described in the experimental section. The spectra show clearly the strong change in both, intensity and shape of the background absorption spectrum due to the acetonitrile and water bands in the $4000 - 950\text{ cm}^{-1}$ region. This can also be seen in the insert where the spectral region between 2318 and 2237 cm^{-1} is depicted. A detailed description of these bands can be found elsewhere [3.34]. The need for an accurate background

correction technique is evident if we consider that, on the one hand side, the absorption of the analytes rarely lies above 10×10^{-3} AU due to the reduced pathlength of the flow cell and because of the inherent low absorptivity of mid-IR bands. On the other hand side, changes in the eluent absorbance in the studied mobile phase composition interval ranged between 0.32 AU at 2252 cm^{-1} and -1.82 AU at 1658 cm^{-1} .

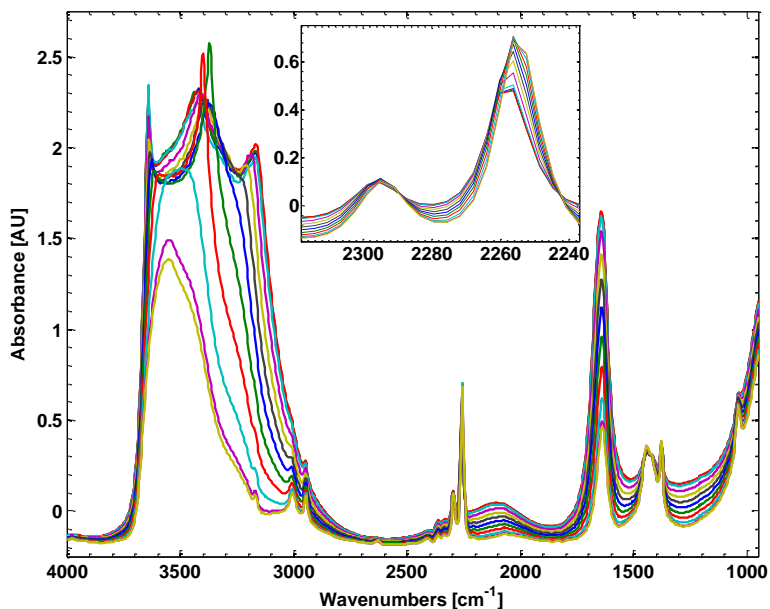


Figure 3.4.1. On-line FTIR spectra measured during a LC gradient with mobile phase compositions ranging from 35:65 v/v to 85:15 v/v acetonitrile (0.08% v/v TFA):water(0.08% v/v TFA).

The selection of an appropriate spectral interval is a critical step of any point-to-point comparison approach which can be time consuming. The number of selected variables should be kept as low as possible to reduce the effect of spectral interferences from the eluting compounds but it must include an adequate number of variables capable to discriminate minor differences between eluent spectra with very close compositions.

Taking into account the chemical and spectroscopic information about the studied mobile phase system, some regions of the absorbance spectrum can be excluded of further considerations. The very intense water absorbance band at about 3500 cm^{-1} leads to spectral saturation affecting a large part of the spectrum and therefore the

region above $\sim 2750\text{ cm}^{-1}$ cannot be used. Furthermore, in the analysis of nitrophenols, the region below 1800 cm^{-1} was not considered because of spectral overlapping of the mobile phase spectra with the spectra of the sample constituents.

In this work, an intuitive 'moving window' approach is proposed for the selection of an adequate spectral interval for background correction in the present mobile phase system and concentration interval. Briefly, in this approach, a spectral window starting at the variable t and ending at the spectral variable $(t + ws - 1)$, where ws is the window size, is selected. The spectral window is moved through a predetermined spectral range. At each position, the background eluent spectra are selected comparing the absorption spectra of the sample LC data set with those of the reference data set using the calculated spectral similarity index. Therefore, for each tested variable window, a background corrected chromatogram is obtained. Then, the noise level in the corrected chromatograms is calculated and plotted at wavenumbers where the eluent presents intense absorption bands, giving a quick and easy indication about the regions which provide accurate results. Visual inspection of this plot is used afterwards to select a combination of contiguous or non contiguous variables to define the optimal spectral window used for background correction.

In this work the chromatographic noise in the corrected chromatogram was measured as root mean square (RMS) at the wavenumbers 2295, 2256, 1640 and 1442 cm^{-1} , corresponding to characteristic acetonitrile and water vibrations. Results obtained for the considered similarity for an evaluated spectral interval between 2750 and 1800 cm^{-1} , using a window size of 21 variables and no correction factor, are shown in Figure 3.4.2. From this figure it can be seen that the best results for the studied similarity index COR were obtained when the selection was made according to the changes in the CN stretching band. From the information obtained by the 'moving window' approach applied to the present mobile phase system, the use of the spectral interval between 2318 and 2237 cm^{-1} centered at 2280 cm^{-1} was selected for the background correction of further LC-IR runs.

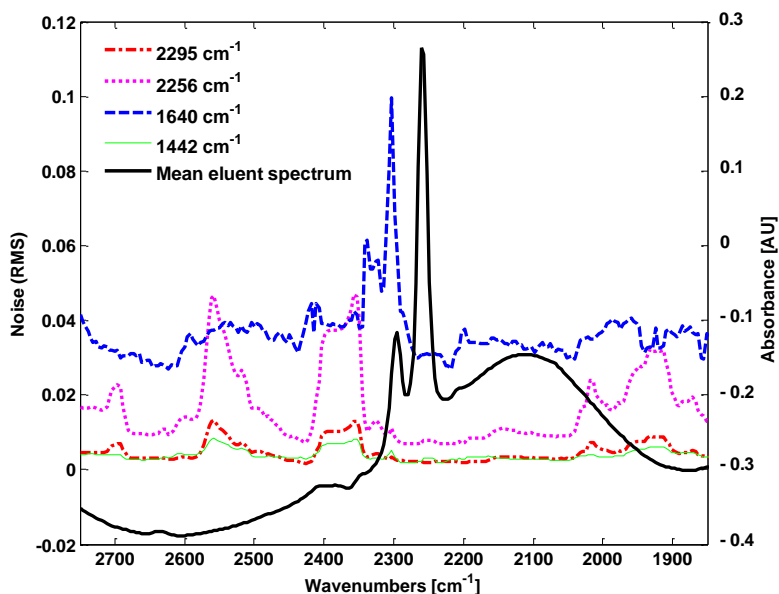


Figure 3.4.2. Chromatographic noise values in a background corrected chromatogram calculated at four mobile phase characteristic wavenumbers during the selection process of the spectral interval. Note: see text for details.

On-line LC-IR injection of nitrophenol standard solutions

On-line LC-IR chromatograms obtained from injections of standard solutions of four nitrophenols were background corrected using the point to point matching algorithm COR and the selected spectral region as described in the previous section. The data shown in Figure 3.4.3 was acquired during a gradient of water (0.08% v/v TFA):acetonitrile (0.08% v/v TFA) from 65:35 v/v to 15:85 v/v in 20 minutes. It can be seen that peaks are not baseline resolved using a rapid gradient of 20 minutes. However, as illustrated in this figure, the overlapping of chromatographic peaks does not affect the accuracy of the RSM-based background correction approach. Even when peak overlapping occurs, the background correction algorithm works well resulting in low noise values in the background corrected spectra over the whole mid-IR region where the spectra are not saturated. Peaks of the four analytes could be identified from the depicted chromatograms measured in 20 minutes at 10.4, 12.1 and 13.0 and 14.1 min corresponding to 4-NP, 3m4-NP, 2,4-dNP and 2-NP, respectively (see Table 3.4.1). The negative peak which can be observed at 10.4 min in the 2-NP

chromatogram in Figure 3.4.3 (bottom) is caused by the baseline correction used for the extraction of the trace.

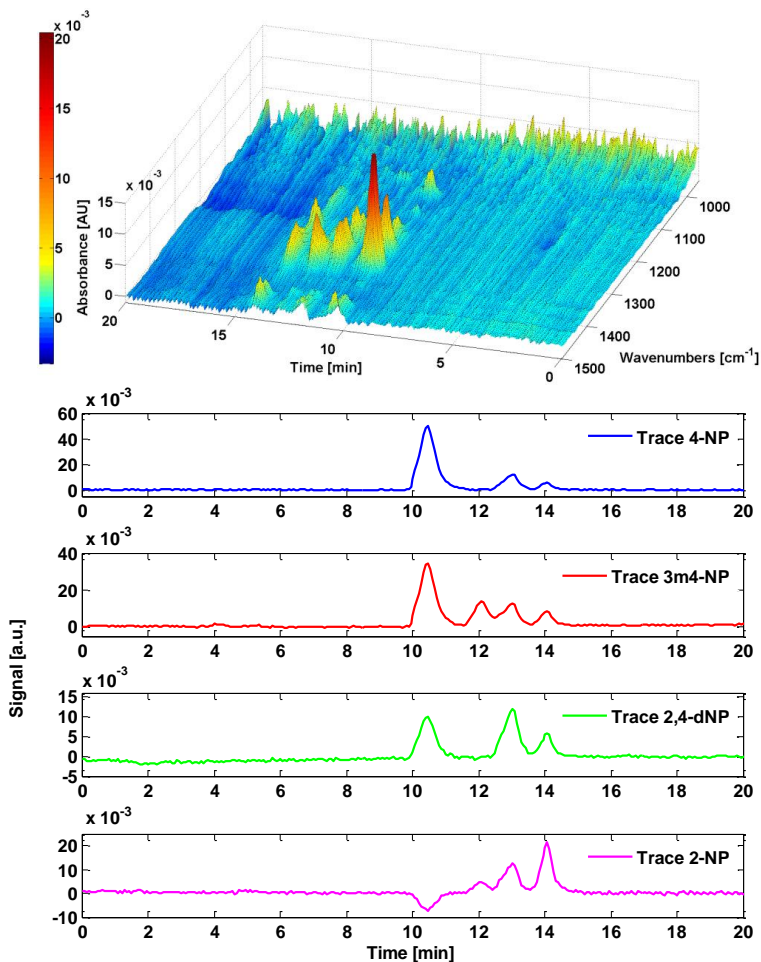


Figure 3.4.3. Top: Background corrected spectra measured upon injection of a nitrophenol standard mixture containing 3 mg mL^{-1} of 4-NP, 3.5 mg mL^{-1} of 3m4-NP, 6 mg mL^{-1} of 2,4-dNP and 5 mg mL^{-1} of 2-NP. Bottom: chromatograms extracted from background corrected data. Note: chromatograms were extracted as described in Table 3.4.1.

Table 3.4.1 summarizes the main analytical figures of merit considering the whole experimental process and the background correction method. Appropriate values for linearity were achieved resulting in R^2 between 0.97 and 0.9993, injecting a series of

five independent standard solutions with different concentrations of each analyte. The applied concentration ranges of the injected solutions as well as on column mass ranges are listed for all four analytes in Table 3.4.1.

In a previous work Quintás et al. [3.36] evaluated the on-line hyphenation of FTIR spectrometry and a capillary LC system with a mobile phase composed by acetonitrile (0.05% v/v TFA) and water (0.05% v/v TFA) within a composition range between 50 and 65% v/v acetonitrile, for the separation of the same set of analytes as used in this work. In the aforementioned study, accurate results were obtained employing a RSM-based background correction approach which used the difference in absorbance (relative absorbance – background correction – reference spectra matrix, RW-BGC-RSM) between 2256 and 2260 cm^{-1} and a correction factor established at 2260 cm^{-1} to improve the obtained results. To allow comparison of the aforementioned RW-BGC-RSM background correction method with the p2p-BGC-RSM approach, both procedures were applied to the same gradient measured between 35 and 85% v/v acetonitrile in 20 minutes injecting a standard solution. Whereas both approaches provided comparable results (data not shown), the selection of the conditions for the background correction in p2p-BGC-RSM was significantly simpler as compared to the RW-BGC-RSM procedure.

Table 3.4.1. Linear regression curves of 4-NP, 3m4-NP, 2,4-dNP and 2-NP using height values of the background corrected LC-IR chromatographic peaks.

Trace	Analytical signal (y) ^a		T _{RET} ^b [min]	y ^a =(k±s _y)xC[mg mL ⁻¹]+(d±s _d)	R ²	Conc. Range [mg mL ⁻¹]
	Absorbance	BLC ^c				
	(wavenumber [cm ⁻¹])	[cm ⁻¹]				
4-NP	A(1335)+A(1338)+A(1342)	A(1311)	10.4	(9.8±0.7)C + (-3±1)	0.97	0.4 – 5
3m4-NP	A(1335)+A(1338)	A(1215)	12.1	(2.2±0.1)C + (-0.3±0.3)	0.990	0.6 – 4
2,4-dNP	A(1346)+A(1350)	A(1512)	13.0	(1.24±0.01)C + (0±0.1)	0.9993	1 – 10
2NP	A(1324)+A(1327)+A(1531)+A(1535)	A(1500)	14.1	(2.8±0.1)C + (-0.3±0.2)	0.997	0.6 – 8

Note: Analytical signal (y)^a: The analytical signal (y) is the sum of single point baseline corrected absorbance values (A) at the wavenumbers indicated between brackets, T_{RET}^b: Retention time measured in minutes, BLC^c: Baseline correction.

Figure 3.4.4 shows recovered spectra from the peak maxima for all four analytes obtained from a standard injection after applying the p2p-BGC-RSM background correction method and the corresponding reference spectra previously obtained. For evaluation of the background correction accuracy, the correlation coefficient between each pair of spectra was calculated. The spectra extracted at the peak apex from the background corrected gradient chromatograms and their corresponding reference spectra showed spectral correlation values in the 1200 and 1550 cm^{-1} region equal to 91.7, 98.6, 97.8 and 98.4% for 4-NP, 3m4-NP, 2,4-dNP and 2-NP, respectively. These results evidenced that the selected conditions of measurement and the background correction were appropriate for the identification and quantification of the considered analytes.

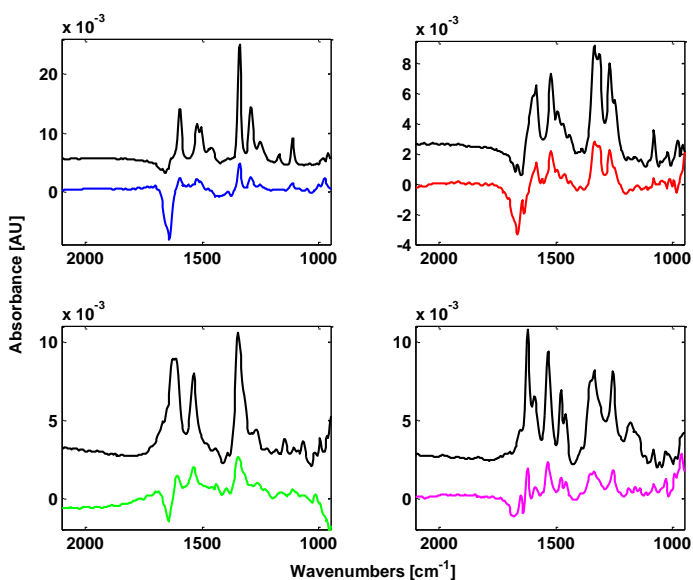


Figure 3.4.4. Background corrected spectra of the four nitrophenols at the peak apex extracted from the injection of a solution containing 1.25 mg mL^{-1} of 4-NP (top, left), 2 mg mL^{-1} of 3m4-NP (top, right), 2.25 mg mL^{-1} of 2,4-dNP (bottom, left) and 4.5 mg mL^{-1} of 2-NP (bottom, right). Reference spectra (black line) measured in stopped-flow are included for comparison.

3.4.4 Conclusions

The proposed background correction process has been employed in on-line LC-IR using acetonitrile (0.08% v/v TFA):water (0.08% v/v TFA) gradients between 35 and 85% acetonitrile for the determination of nitrophenols as model compounds, obtaining accurate results. Comparing the p2p-BGC-RSM method to a previously developed approach (RW-BGC-RSM), similar results were obtained with both procedures. However, the selection of the parameters for background correction was facilitated considerably as the user-interaction was reduced to the selection of the spectral interval and the window size used for the point-to-point spectral comparison. On the other hand, it could be shown that the background correction process is not influenced by the chromatographic resolution as it works not only with baseline resolved peaks but also with overlapping peaks.

In short, the main features of the proposed point-to-point selection criterion for RSM-based background correction approaches in on-line LC-IR are: i) the simplified and fast initial selection of the RSM-BGC parameters (window size, variable interval and correlation coefficient), and ii) the use of a single criterion for the selection of appropriate **RSM** reference spectra through a gradient with a wide range of mobile phase compositions.

3.5 References for Chapter 3

- [3.1] G. Quintas, B. Lendl, S. Garrigues, M. de la Guardia, *Journal of Chromatography A*, 1190 (2008) 102-109.
- [3.2] J.F. Li, D.B. Hibbert, S. Fuller, G. Vaughn, *Chemometrics and Intelligent Laboratory Systems*, 82 (2006) 50-58.
- [3.3] K. Varmuza, M. Karlovits, W. Demuth, *Analytica Chimica Acta*, 490 (2003) 313-324.
- [3.4] M. Daszykowski, B. Walczak, *Trac-Trends in Analytical Chemistry*, 25 (2006) 1081-1096.
- [3.5] J. Kuligowski, G. Quintas, S. Garrigues, M. de la Guardia, *Analytica Chimica Acta*, 624 (2008) 278-285.
- [3.6] J. Kuligowski, G. Quintas, S. Garrigues, M. de la Guardia, *Talanta*, 77 (2008) 779-785.
- [3.7] M. Cascant, J. Kuligowski, S. Garrigues, M. de la Guardia, sent for publication, (2011).
- [3.8] G. Quintas, J. Kuligowski, B. Lendl, *Applied Spectroscopy*, 63 (2009) 1363-1369.
- [3.9] J. Kuligowski, G. Quintas, S. Garrigues, M. de la Guardia, *Talanta*, 80 (2010) 1771-1776.
- [3.10] J. Kuligowski, G. Quintas, Chemometric background correction in gradient on-line liquid chromatography with infrared detection, *El Sevier, SciVerse, SciTopics*, 2010, http://www.scitopics.com/Chemometric_background_correction_in_gradient_on_line_liquid_chromatography_with_infrared_detection.html.
- [3.11] M.A. Bashir, A. Brull, W. Radke, *Polymer*, 46 (2005) 3223-3229.
- [3.12] C.A. Rimmer, C.R. Simmons, J.G. Dorsey, *Journal of Chromatography A*, 965 (2002) 219-232.
- [3.13] S.J. Kok, T. Hankemeier, P.J. Schoenmakers, *Journal of Chromatography A*, 1098 (2005) 104-110.
- [3.14] J. Adrian, E. Esser, G. Hellmann, H. Pasch, *Polymer*, 41 (2000) 2439-2449.
- [3.15] S.J. Kok, C.A. Wold, T. Hankemeier, P.J. Schoenmakers, *Journal of Chromatography A*, 1017 (2003) 83-96.
- [3.16] L. Coulier, E.R. Kaal, T. Hankemeier, *Polymer Degradation and Stability*, 91 (2006) 271-279.

- [3.17] M. Rozenberg, A. Loewenschuss, Y. Marcus, *Spectrochimica Acta Part a-Molecular and Biomolecular Spectroscopy*, 54 (1998) 1819-1826.
- [3.18] C.A. Holden, S.S. Hunnicutt, R. Sanchez-Ponce, J.M. Craig, S.C. Rutan, *Applied Spectroscopy*, 57 (2003) 483-490.
- [3.19] A.M. Zhao, E.R. Malinowski, *Analytical Chemistry*, 71 (1999) 602-608.
- [3.20] L. Norgaard, A. Saudland, J. Wagner, J.P. Nielsen, L. Munck, S.B. Engelsen, *Applied Spectroscopy*, 54 (2000) 413-419.
- [3.21] M.L. Wheeler, F.X. Pi-Sunyer, *Journal of the American Dietetic Association*, 108 (2008) S34-S39.
- [3.22] FDA Nutrition Labeling Manual, in, U. S. Food and Drug Administration, Center for Food Safety and Applied Nutrition, 1998.
- [3.23] A. Caceres, S. Cardenas, M. Gallego, A. Rodriguez, M. Valcarcel, *Chromatographia*, 52 (2000) 314-318.
- [3.24] W.L. Qian, Z. Khan, D.G. Watson, J. Fearnley, *Journal of Food Composition and Analysis*, 21 (2008) 78-83.
- [3.25] R. Vonach, B. Lendl, R. Kellner, *Analytical Chemistry*, 69 (1997) 4286-4290.
- [3.26] R. Vonach, B. Lendl, R. Kellner, *Journal of Chromatography A*, 824 (1998) 159-167.
- [3.27] A. Edelmann, C. Ruzicka, J. Frank, B. Lendl, W. Schrenk, E. Gornik, G. Strasser, *Journal of Chromatography A*, 934 (2001) 123-128.
- [3.28] A. Edelmann, J. Diewok, J.R. Baena, B. Lendl, *Analytical and Bioanalytical Chemistry*, 376 (2003) 92-97.
- [3.29] M. Kölhed, B. Karlberg, *Analyst*, 130 (2005) 772-778.
- [3.30] G.W. Somsen, C. Gooijer, U.A.T. Brinkman, *Journal of Chromatography A*, 856 (1999) 213-242.
- [3.31] J.T. Gotsick, R.F. Benson, *Journal of Liquid Chromatography*, 14 (1991) 1887-1901.
- [3.32] J.J. Max, C. Chapados, *Journal of Physical Chemistry A*, 111 (2007) 2679-2689.
- [3.33] J.J. Max, C. Chapados, *Journal of Physical Chemistry A*, 105 (2001) 10681-10688.
- [3.34] T. Takamuku, M. Tabata, A. Yamaguchi, J. Nishimoto, M. Kumamoto, H. Wakita, T. Yamaguchi, *Journal of Physical Chemistry B*, 102 (1998) 8880-8888.

[3.35] J.J. Max, C. Chapados, *Canadian Journal of Analytical Sciences and Spectroscopy*, 47 (2002) 72-90.

[3.36] G. Quintas, J. Kuligowski, B. Lendl, *Analytical Chemistry*, 81 (2009) 3746-3753.

CHAPTER 4. BACKGROUND CORRECTION IN ON-LINE LC-IR USING 'COLUMN-WISE' CHEMOMETRIC TECHNIQUES

In this Chapter, two fundamentally different background correction approaches are addressed employing column-wise techniques. In the first part, a method based on the use of a reference spectra matrix (**RSM**) and polynomial regressions is presented and applied for the analysis of carbohydrates in complex samples. Furthermore the method is compared to several BGC-RSM methods using different identification parameters (IPs) [4.1].

The second part describes a method for background correction based on cubic smoothing splines (CSS) working without the use of a **RSM** [4.2]. This method has been demonstrated using simulated data as well as for the analysis of polyethylene glycol (PEG) mixtures in three different alcoholic mobile phase systems: methanol:water, 2-propanol:water and ethanol:water. Moreover, results were compared to those achieved employing background correction based on the use of a reference spectra matrix with the absorbance ratio as an IP (AR-BGC-RSM).

4.1 Background correction based on polynomial regressions

4.1.1 Introduction

To overcome difficulties of the on-line coupling of LC-IR, especially under gradient conditions, promising approaches based on the use of a reference spectra matrix (**RSM**) have been discussed in the previous chapter. Real data obtained from acetonitrile:water and methanol:water LC gradients have been used for the evaluation different RSM-based methods (e.g. AR-BGC-RSM and PLS-BGC-RSM). The obtained results represent a significant step forward in analytical capabilities of the on-line hyphenation of FTIR spectrometry with separation techniques. However, methods based on the use of a **RSM** are not limited to the aforementioned approaches and offer alternative possibilities. The objective of this study was to set out to improve and expand the use of RSM-based background correction techniques by developing a new approach based on the use of polynomial fits named Polyfit-RSM.

4.1.2 Theoretical background

The Polyfit-RSM method is based on the use of a **RSM**. It is assumed that if during a chromatographic gradient the absorbance of the eluent at each wavenumber j (y_j) is dependent on its composition, then a polynomial regression curve of degree n_i , can be established between the absorbance values y_j and a series of reference values x which are equally dependent on the mobile phase composition. So, it should be possible to establish a model formed by as many polynomial functions as considered wavenumbers which can be subsequently used to predict and correct the eluent spectral contribution in each of the observed spectra during a gradient elution using their corresponding reference x values.

A binary LC gradient is a closed system in which the concentration of each mixture compound is obviously determined by the other one. It seems reasonable to expect a correlation between the mobile phase composition changes and the spectral features of the two components. According to this, it should be possible to correlate the eluent composition and thus its background absorption during the gradient with a defined

spectral feature related to the concentration of at least one of the mobile phase components. In this work, two alternative reference parameters (x) are evaluated; (i) the absorbance at a defined single wavenumber (SW-Polyfit-RSM) and (ii) the absorbance ratio at two wavenumbers (AR-Polyfit-RSM), being the selected parameters characteristics of the absolute or relative concentration of at least one of the components of the mobile phase, respectively.

Throughout this work, spectral data matrices are indicated as 'Matrix (rows, columns)' where the number of rows and columns correspond to the number of spectra and variables (wavenumbers) included in the data set, respectively. The use of spectral data included in a **RSM** (r, c) obtained by measuring the spectral changes occurring during the acquisition of a blank LC gradient, within a defined mobile phase composition interval, is proposed for the calculation of c polynomial functions $P(x)_j$ for each of the wavenumbers. The optimum degree (op_j) of the calculated polynomial fits might vary within a range for each considered wavenumber j . In the proposed approach, a maximum polynomial degree (N) is defined by the user before starting the calculation. Then, a series of N regressions are calculated for each wavenumber j and a subsequent selection of the optimum polynomial fit among them is carried out separately for each wavenumber.

The developed algorithm can be divided in five steps:

Step 1 involves the acquisition of the **RSM** (r, c) and the sample matrix **SM** (z, c).

In step 2 the polynomial regression are calculated and evaluated. This includes the calculation of $N \cdot c$ polynomial fits from the **RSM** (r, c), where N is the maximum polynomial degree to be evaluated and c is the number of variables (wavenumbers) included in the **RSM**. As a result, a series of n^{th} degree polynomials $n = (1, \dots, N)$ with the general form of

$$P(x)_j^n = y_j = p_1x^n + p_2x^{n-1} + \dots + p_nx + p_{n+1} \quad (\text{Equation 4.1.1})$$

are obtained, where p_1, p_2, \dots, p_{n+1} are the regression coefficients calculated from a set of r tabulated values of x (independent variable) which are the absorbance value at one or the absorbance ratio at two previously selected wavenumbers of each spectrum of the **RSM** versus y_j (dependent variable).

Step 3 involves the selection of the optimal polynomial degree for each wavenumber. The Polyfit-RSM generates huge amounts of data. For example, the $N \cdot c$ polynomial

fits calculated in the second step represent a total of 2604 models if only the spectral region between 2380 and 948 cm^{-1} (372 variables using a resolution of 8 cm^{-1} and a zerofilling factor of 2) and a maximum polynomial degree of 7 are selected. A visual examination of the fitted curves of the different polynomial degrees provides a simple evaluation of its goodness (e.g. detection of trends in the residuals calculated as the vertical distance from the data point to the fitted curve). However, working with a big amount of data it is troublesome and time-consuming. With respect to the visual approach, the use of calculated statistic indicators reduces the required time and the user interaction. Because of that, in this work the use of the degrees of freedom adjusted R -square statistic is proposed. This statistic uses the R square value and adjusts both, the numerator and the denominator by their respective degrees of freedom. The adjusted R -square of the polynomial regression $P(x)_j^n$ of degree n for the wavenumber j is defined as indicated in Equation 4.1.2:

$$(\text{adjusted } R - \text{square})_j^n = 1 - \frac{(r-1) \sum_{i=1}^n (y_{i,j} - \hat{y}_j)^2}{(r-m) \sum_{i=1}^n (y_{i,j} - \bar{y}_j)^2} \quad (\text{Equation 4.1.2})$$

where r is the number of spectra included in the **RSM**; m is the number of fitted coefficients estimated from the response values; $y_{i,j}$ is the response value i ($i = 1, \dots, r$) at wavenumber j ; \hat{y}_j is the predicted response value i ($i = 1, \dots, r$) at wavenumber j ; and \bar{y}_j is the mean of responses at wavenumber j . The usefulness of the aforementioned estimator for the automatic selection of the polynomial degree lies in the fact that, unlike the R -square, the adjusted R -square can decrease when the contribution to the explained deviation by increasing the polynomial order is lower than the effect on the degrees of freedom. From the analysis of each wavenumber j , N adjusted R -square values are calculated. An additional degree P was selected when the obtained adjusted R -square value improved by at least 0.1% when increasing the polynomial order by one.

Step 4 includes the calculation of the background spectra (*CalcBG*) using the previously calculated polynomial fits. From each spectrum included in the sample matrix **SM**, a set of z reference values (x_s) is determined by measuring the absorbance at a single wavenumber or an absorbance ratio, as indicated in step 2. Then, using the c polynomial regressions $P(x)_j^n$ calculated and selected in steps 2 and 3, the corresponding absorbance due to the eluent at j for each spectrum included in the **SM** (z, c) is calculated according to Equation 4.3.

$$y_{k,j} = p_{1,j}x_s^{op_j} + p_{2,j}x_s^{op_j-1} + \dots + p_{op_j,j}x_s + p_{op_j+1,j} \quad (\text{Equation 4.1.3})$$

where $y_{k,j}$ is the absorbance at wavenumber j in the sample spectrum number k for $k = (1, \dots, z)$ and $j = (1, \dots, c)$ and op_j is the optimal polynomial degree for wavenumber j selected in Step 3.

In step 5, the subtraction of the calculated eluent spectra is carried out. It involves the subtraction of the eluent spectral contribution to obtain the background corrected sample chromatogram (*CorrectedSM*(z, c)) using the expression:

$$\text{CorrectedSM}(z, c) = \text{SM}(z, c) - \text{CalcBG}(z, c) \quad (\text{Equation 4.1.4})$$

Requirements of the method

As described before, the method presents the following requirements:

- (i) A high instrumental stability is required. The analytical signal and thus the accuracy of results obtained by any of the proposed approaches based on the use of a reference spectra matrix for background correction in LC-FTIR are directly affected by changes in the instrumental response.
- (ii) The reference values (independent variable x) used for the calculation of the polynomial fits should be free from interferences of eluting compounds.
- (iii) The **RSM** and **SM** must have the same number of variables which means that they must be recorded with the same resolution and zero filling factor.
- (iv) The **SM** should only include spectra with eluent compositions within the mobile phase composition range used during **RSM** acquisition. A single point baseline correction at 1890 cm^{-1} of all the spectra was carried out to improve the accuracy of the background correction process.

4.1.3 Material and methods

Apparatus and Reagents

A Dionex (Sunnyvale, CA, USA) P680 high performance liquid chromatographic system, equipped with a Kromasil 100 NH_2 column (250×2 mm, 5 μm) from Scharlab S.L.

(Barcelona, Spain) was employed. A sample loop of 20 μL was used for the injection of soft drink samples. Carbohydrate analysis was carried out using linear acetonitrile:water gradients from 75% to 55% acetonitrile (Merck, Darmstadt, Germany) in 15 min.

For FTIR spectra acquisition a flow cell with CaF_2 and ZnSe windows and a pathlength of 10 μm was employed and installed on a Bruker (Bremen, Germany) IFS 66/v FTIR spectrometer equipped with a liquid nitrogen refrigerated mercury–cadmium–telluride (MCT) detector, a vacuum system and a dry air purged sample compartment. The scanner for the interferometer was operated at a HeNe laser modulation frequency of 100 kHz. Spectra were recorded in the range between 4000 and 950 cm^{-1} using the spectrum of the empty sample compartment as background, a resolution of 8 cm^{-1} and a zerofilling factor of 2. During gradient experiments, 25 scans per spectrum were averaged, providing a spectra acquisition frequency of 15 spectra min^{-1} .

A soft drink sample was directly obtained from the Spanish market.

Software and algorithms

For instrumental and measurement control as well as for data acquisition, the OPUS software (version 4.1) from Bruker was employed. The Matlab (The Mathworks, MA, USA) function *polyfit* was used to perform the polynomial fits. This function provides an n^{th} degree least squares polynomial curve fit to two vectors ($x(r, 1)$ and $y(r, 1)$), and returns a vector with the aforementioned $n + 1$ regression coefficients. For the PLS model calculation the iToolbox developed by Nørgaard and Leardi was employed. For Polyfit-RSM as well as PLS- and AR-BGC-RSM background correction, in-house written Matlab functions were employed. The 2Dcorrspec toolbox was used for 2D correlation spectroscopy.

4.1.4 Results and discussion

Eluent spectral changes during gradient

Figure 4.1.1 shows spectra measured during a blank gradient of acetonitrile:water from 75 to 55% v/v acetonitrile. Water absorption bands at 2115 cm^{-1} (combination band), 1639 cm^{-1} (deformation band) and a latter one starting near 1000 cm^{-1} (libration

band), can be identified. Two main acetonitrile bands are also distinguishable at 2252 and 2291 cm^{-1} , the first one corresponding to the CN stretching mode while the second one is assigned to a combination of both, CH_3 bending and C–C stretching modes [4.3]. A change in the intensity and shape of the HOH water deformation band at 1639 cm^{-1} can also be observed.

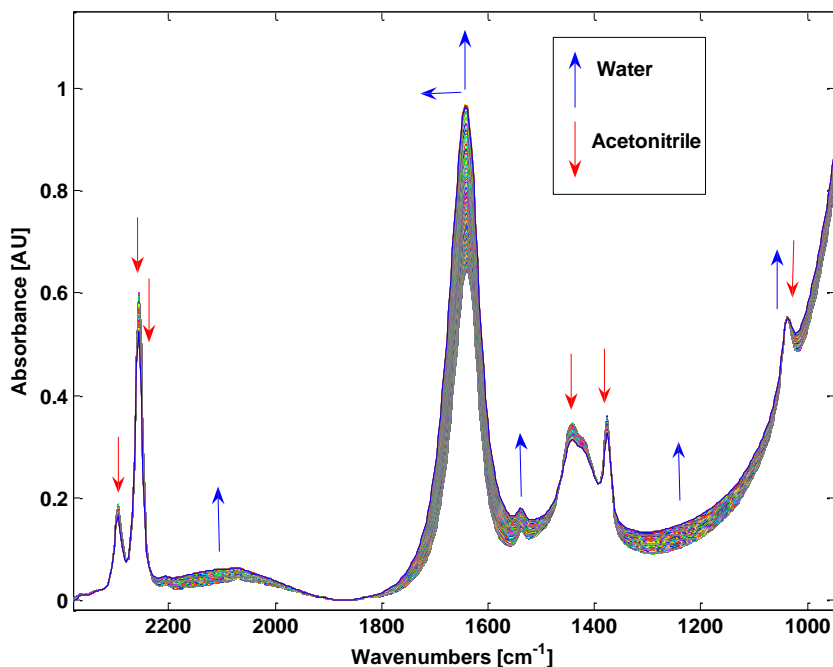


Figure 4.1.1. FTIR spectra obtained during the measurement of a linear acetonitrile:water gradient from 75 to 55% v/v acetonitrile in the spectral region between 2380 and 950 cm^{-1} ; arrows indicate the main changes, which can be observed in the spectra.

The proposed method is based on the assumption that changes in the absorbance spectra of the mobile phase components during the gradient are correlated and because of that, 2D correlation spectroscopy (2DCoS) has been employed as a valuable tool for determining the type of correlation between variables. Detailed descriptions of this technique can be found elsewhere [4.4]. The synchronous spectrum contains information about features that change in-phase representing the simultaneous changes of spectral intensities. The asynchronous spectrum represents sequential

changes of spectral intensities. The presence of a synchronous peak and the absence of an asynchronous peak indicate perfect in-phase correlation represented by a correlation coefficient of 1 or -1 . The presence of an asynchronous peak and the lack of a synchronous peak are caused by peaks that are completely out of phase showing a correlation coefficient of 0. The presence of peaks at the same wavelengths in the synchronous and in the asynchronous spectrum means that the absorbance values are not in perfect-phase opposition [4.4]. Synchronous and asynchronous 2DCoS maps obtained from the analysis of spectra measured during a blank gradient run in the region between 2325 and 950 cm^{-1} are shown in Figure 4.1.2.

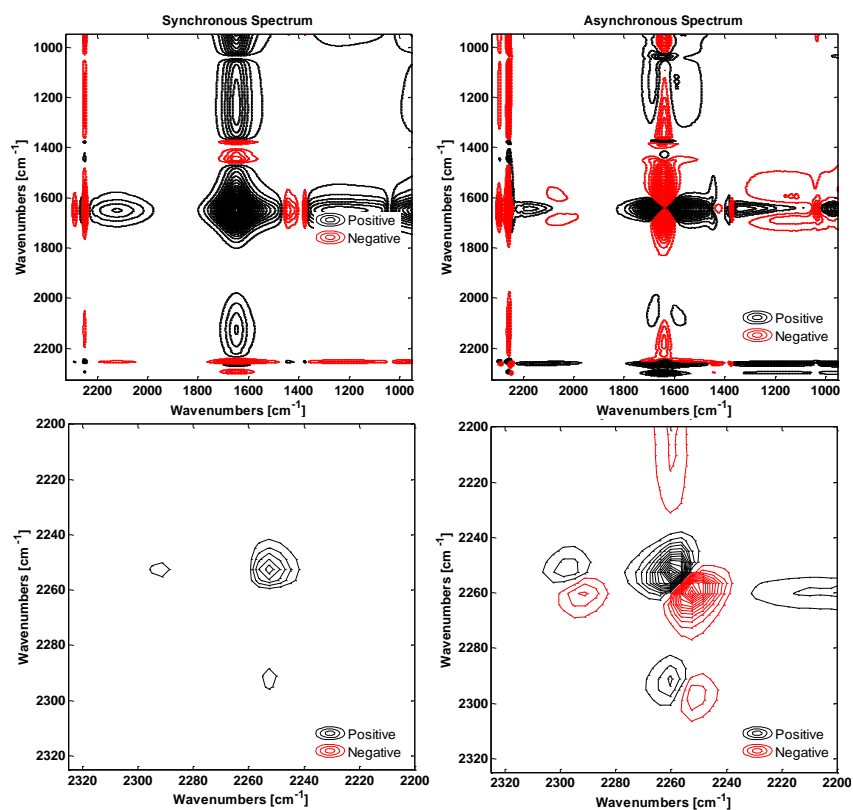


Figure 4.1.2. 2D synchronous (left) and asynchronous (right) correlation spectra for acetonitrile:water spectra acquired varying the acetonitrile concentration between 75 and 55% v/v; Note: top: synchronous and asynchronous 2D correlation spectra between 2325 and 950 cm^{-1} ; bottom: synchronous and asynchronous 2D correlation spectra between 2325 and 2200 cm^{-1} .

Autopeaks from the correlation of each resolution element with itself were found at ~ 2250 and 1640 cm^{-1} in the synchronous spectrum. Cross peaks were found in the synchronous map for the main representative acetonitrile and water absorption bands at ~ 2290 (-), 2250 (-), 2100 (+), 1640 (+), 1443 (-), 1377 (-) and 1200 (+) cm^{-1} . Positive cross peaks show up when the absorption bands at both wavenumbers change in the same direction whereas negative peaks represent a change in the opposite direction [4.5]. In this case cross peaks indicate the decrease of the acetonitrile bands parallel to the increase of the water bands during the LC gradient.

The asynchronous 2D correlation map shows numerous peaks indicating spectral changes of individual bands taking place at different eluent compositions. On the one hand, the acetonitrile and water content during the gradient are inversely proportional; on the other hand, the presence of other constituents has an effect on the CN stretching band. It is known that when acetonitrile is mixed with water the solution contains a heterogeneous microstructure that consists of CH_3CN or water clusters. 2DcoS under temperature perturbation has been used to study the microstructure of acetonitrile:water mixtures being found a new feature at 2256 cm^{-1} which has been related to an intermediate microstructure between clusters of acetonitrile molecules and hydrogen-bonded acetonitrile molecules associated with clusters of water molecules [4.6]. A close-up view of the spectral region from 2200 to 2325 cm^{-1} in the asynchronous spectrum (Figure 4.1.2., bottom) shows the presence of peaks at the same wavelengths as those of the synchronous spectrum meaning that the corresponding absorbance values are not in perfect-phase opposition. As expected from the asynchronous correlation map, the presence of different types of IR absorbing acetonitrile species occurring at different water concentrations can be observed. Therefore, if the absorbance due to the mobile phase at each wavenumber is fitted to a water or acetonitrile concentration-related parameter like the absorbance value or the absorbance ratio at defined wavenumbers, then the polynomial fits are expected to have different optimum polynomial degrees.

Development of a polyfit-background correction method

Two alternative parameters were evaluated as independent reference variables to establish a model for the calculation of the theoretical background: (i) the absorbance

at a selected wavenumber (SW-Polyfit-RSM) and (ii) the ratio of the absorbance at two wavenumbers (AR-Polyfit-RSM). For the evaluation of the proposed method, the following data matrices were used: $RSM_{Blank-1}$ (550×372), $RSM_{Blank-2}$ (493×372), $RSM_{Blank-3}$ (328×372), $RSM_{Blank-4}$ (246×372), $RSM_{Blank-5}$ (140×372) and **Blank** (317×372) are the reference and blank gradient data matrices; RSM_{Sample} (456×372) and **SoftDrink** (320×372) are the reference and on-line LC-FTIR sample data matrices, respectively.

SW-Polyfit-RSM. To ensure the goodness of the selection of the single wavenumber (SW) used as independent reference variable x , the evaluation of the obtained results using all wavenumbers within a defined spectral range as a reference variable for the correction of a blank gradient chromatogram is proposed. The evaluated spectral range should be selected by taking into account chemical and/or spectroscopic information about the studied system. For each tested reference wavenumber, a corrected blank chromatogram was obtained. Therefore, obtained results can be viewed abstractly as a four dimensional space with tested reference wavenumber, corrected absorbance, wavenumber and time axes. For an easier visualization and to reduce the results space to be searched, a three dimensional surface with tested reference wavenumber, wavenumber used for noise evaluation and chromatographic noise was depicted, in which the chromatographic noise at each wavenumber was calculated as the root mean square (RMS) of the residuals in the corrected blank gradient.

For an evaluated interval ranging between 2180 and 2310 cm^{-1} , the optimum reference value was selected at 2210 cm^{-1} (see Figure 4.1.3). Obtained noise levels (measured as RMS) throughout the whole spectral range were minimal, even in regions of strong water absorption bands like for example at 1640 cm^{-1} . Noise values found in the corrected spectra were always below 1.55×10^{-3} AU with a maximal noise at 1678 cm^{-1} as shown in Figure 4.1.4 (top), which is very close to the instrumental noise in on-line measurements of aqueous solutions. Using the absorbance at 2210 cm^{-1} as reference value x and $N = 7$, most of the selected polynomial degrees chosen for the calculation of the fits varied between 1 and 4, with very few wavenumbers fitted using polynomial degrees higher than 4 (see Figure 4.1.4, middle). The degrees of freedom adjusted R -square values were close to 1 for most of the studied variables (see Figure 4.1.4, bottom). However, they became poor at 1894 , 1867 , 1396 and 1369 cm^{-1} . The

reason for the low fitting goodness is the very low change in absorbance occurring during the gradient at these wavenumbers (<0.5–1 mAU) which increases the effect of the instrumental noise and makes it difficult to get precise fitting results.

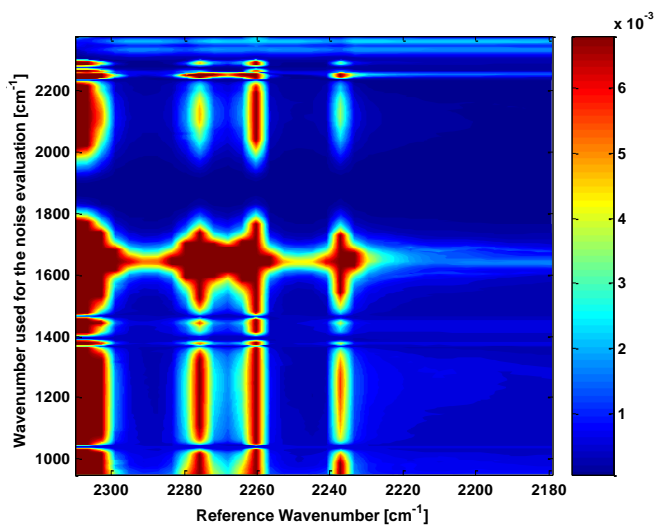


Figure 4.1.3. Evaluation of different wavenumbers used as reference value in SW-Polyfit-RSM.

AR-Polyfit-RSM. According to previous work [4.7], the use of the ratio of the absorbance values at 2256.5 and 2248.7 cm^{-1} was selected as independent variable in AR-Polyfit-RSM. Chromatographic noise levels found from the correction of a blank gradient chromatogram were similar in order of magnitude to those found using the SW approach (see Figure 4.1.4, top) and the same lack of fit at 1894, 1867, 1396 and 1369 cm^{-1} was observed (see Figure 4.1.4, bottom). Also the degree of the selected polynomials based on the AR was similar to the degree selected using the SW-based approach (see Figure 4.1.4, middle).

As an example, fits and residuals of the absorbance of a blank at 1640 cm^{-1} calculated before correction are shown in Figure 4.1.5 for both types of independent reference variables (SW and AR). Whereas the quality of the fit is improved substantially when the polynomial degree is increased from 1 to 2, no significant improvements were achieved using higher order polynomials (results not shown). Furthermore, the distribution of the residuals of the fits should be remarked. The lack of fit of linear

regressions is evidenced by the statistical indicators shown in Figure 4.1.5 and by the distribution of the residuals.

However, when the polynomial degree is incremented to 2, the residuals of the regression are randomly distributed around zero and the statistical parameters improved markedly. The use of polynomial degrees higher than 2 for the fitting at this wavenumber does not improve the quality of the fits, which supports the use of the degrees of freedom adjusted R -square to avoid overfitting of the data.

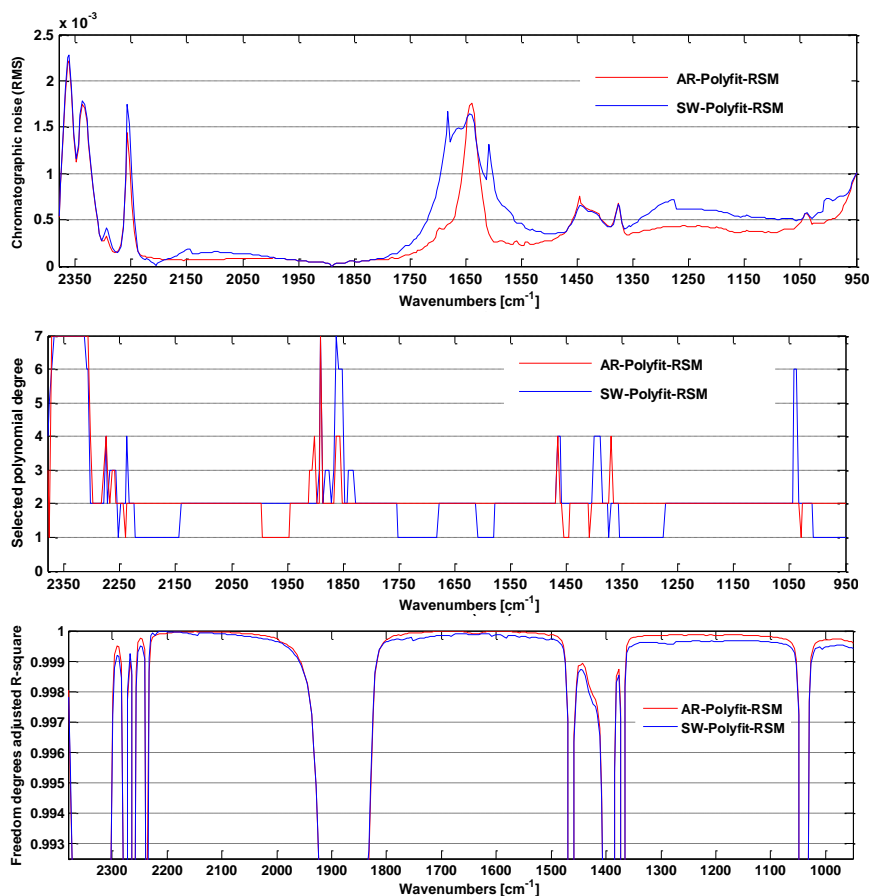


Figure 4.1.4. Top: levels of the chromatographic noise found from the corrected blank gradient chromatogram for AR-Polyfit-RSM and SW-Polyfit-RSM; middle: selected polynomial degree for AR-Polyfit-RSM and SW-Polyfit-RSM at different wavenumbers; bottom: comparison of the adjusted R -square values obtained from AR-Polyfit-RSM and SW-Polyfit-RSM; Note: noise at ~ 2350 cm⁻¹ was caused by CO₂ due to unstable conditions in the sample compartment during data acquisition.

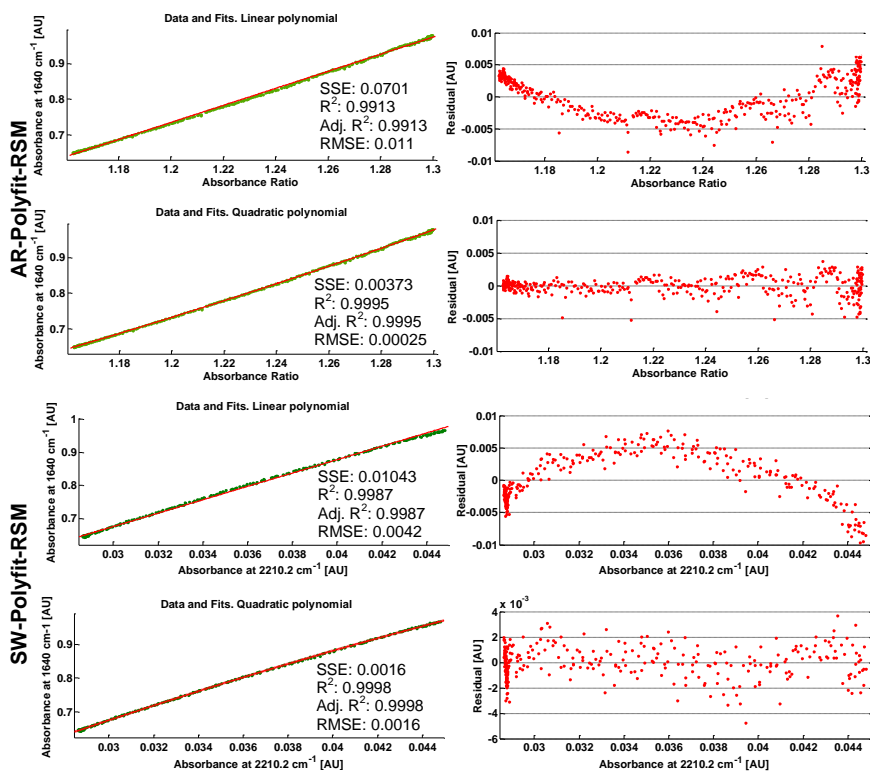


Figure 4.1.5. Fits and residuals for the absorbance at 1640cm^{-1} obtained by using AR-Polyfit-RSM and SW-Polyfit-RSM and polynomial degrees of 1 and 2; Note: SSE stands for sum of squares due to error; R^2 is the square of the multiple correlation coefficient; Adj. R^2 stands for the degrees of freedom adjusted R -square and RMSE is the root mean squared error.

Comparison between different RSM-based background correction approaches

The use of the Polyfit approach was compared to the PLS-BGC-RSM and AR-BGC-RSM methods described in Chapter 3. The settings for the PLS-BGC method were as follows: reference wavenumber: 1640 cm^{-1} , PLS spectral interval from $2345\text{ to }2145\text{ cm}^{-1}$, number of PLS-factors: 3. Settings for the AR-BGC method were as follows: AR = absorbance ($2256.5\text{ cm}^{-1}/2248.7\text{ cm}^{-1}$) and $KF = 1$. Results obtained from the background correction of a blank gradient showed that the chromatographic noise at characteristic wavenumbers appears to be significantly smaller by applying the Polyfit-RSM algorithm than that obtained by the previously developed procedures (see Table

4.1.1). Figure 4.1.6 shows background corrected spectra using different methods for the correction of a blank gradient data matrix.

Table 4.1.1. Noise values found measured as the root mean square (RMS) for chromatograms extracted at different wavenumbers from the background corrected blank gradient matrices obtained using four different approaches.

Background correction approach	RMS Noise ^a [AU] measured in the extracted chromatogram at [cm ⁻¹]								
	2295	2256	2071	1670	1643	1443	1377	1288	1038
PLS-RSM	1.21	4.00	0.29	4.67	4.68	1.63	1.73	1.78	2.16
AR-RSM	0.85	2.53	0.47	1.93	3.67	1.67	1.74	1.44	2.05
SW-Polyfit-RSM	0.41	1.75	0.14	1.45	1.64	0.66	0.65	0.69	0.57
AR-Polyfit-RSM	0.32	1.43	0.079	0.54	1.73	0.68	0.61	0.42	0.57

Note: Noise^a: values multiplied by 10⁻³; data obtained using the **RSM**_{Blank-1} (550 × 372) and **Blank** (317 × 372) matrices as **RSM** and **SM**, respectively.

To evaluate the effect of the reduction of the **RSM** size on the accuracy of the subtraction process, the chromatographic noise at 1640 cm⁻¹ was calculated from a blank gradient data set that was corrected by AR-RSM, PLS-RSM, AR-Polyfit-RSM and SW-Polyfit-RSM. In cases of AR-RSM and PLS-RSM results, the observed influence of the number of reference spectra was more evident than applying AR- and SW-Polyfit-RSM.

The noise values found using AR-Polyfit-RSM were 0.001755, 0.001758, 0.001757, 0.001775 and 0.001810 AU when using the **RSM**_{Blank-1}, **RSM**_{Blank-2}, **RSM**_{Blank-3}, **RSM**_{Blank-4} and **RSM**_{Blank-5} matrices for the correction of the **Blank** data matrix, respectively. The values obtained using the SW-Polyfit-RSM approach were 0.0016958, 0.0016801, 0.0016345, 0.0016427 and 0.0017158 AU when the **RSM**_{Blank-1}, **RSM**_{Blank-2}, **RSM**_{Blank-3}, **RSM**_{Blank-4} and **RSM**_{Blank-5} matrices were used for correcting the **Blank** data matrix, respectively. Although minor differences between the obtained noise levels can be observed, they cannot be considered relevant.

Using the AR-RSM approach results found were more influenced by the **RSM** size showing the following noise values: 0.002717, 0.002855, 0.002529, 0.002717 and

0.003153 employing the same matrices for the correction of the **Blank**. A similar trend was observed for PLS-RSM results, obtaining noise levels of 0.0021, 0.0024, 0.0025, 0.0029 and 0.0036, for the same **RSM** sizes as before. From these results it can be concluded that the Polyfit-RSM approach is more flexible than previous ones because the measurement of the **RSM** can be carried out during the re-equilibration of the system after each LC injection. Furthermore, the measurement of specific **RSMs** for each LC run allows a better compensation of slight instrumental changes as for example the water or CO₂ vapor concentration in the sample chamber.

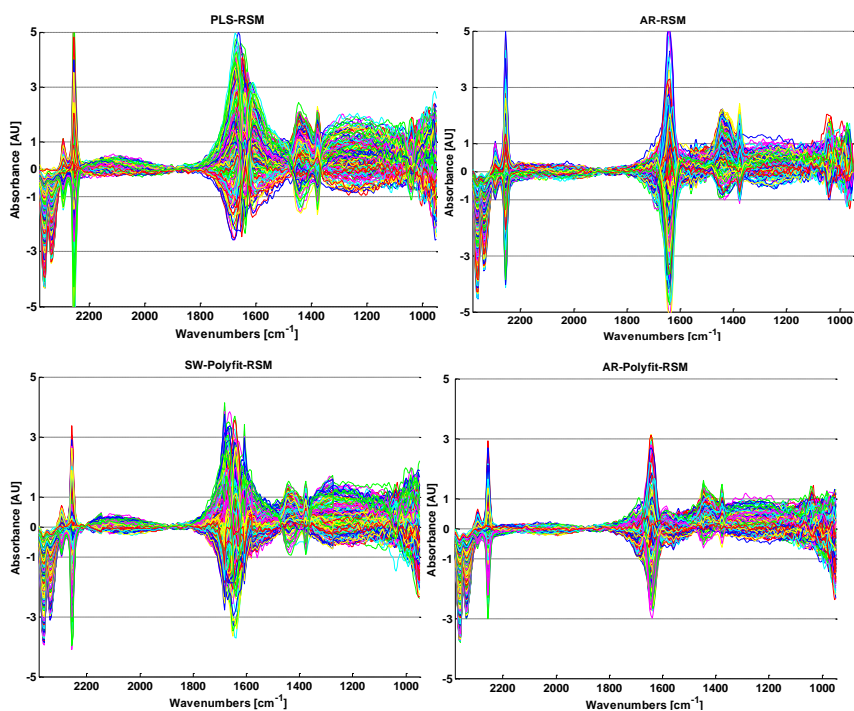


Figure 4.1.6. Spectra from a blank gradient LC-FTIR data set corrected using four different algorithms.

For further evaluation of the proposed approach, background correction of a real on-line gradient LC-IR chromatogram obtained from the injection of a diluted soft drink sample was carried out applying the four considered algorithms. Figure 4.1.7 shows extracted chromatograms of the background corrected LC-FTIR data matrices.

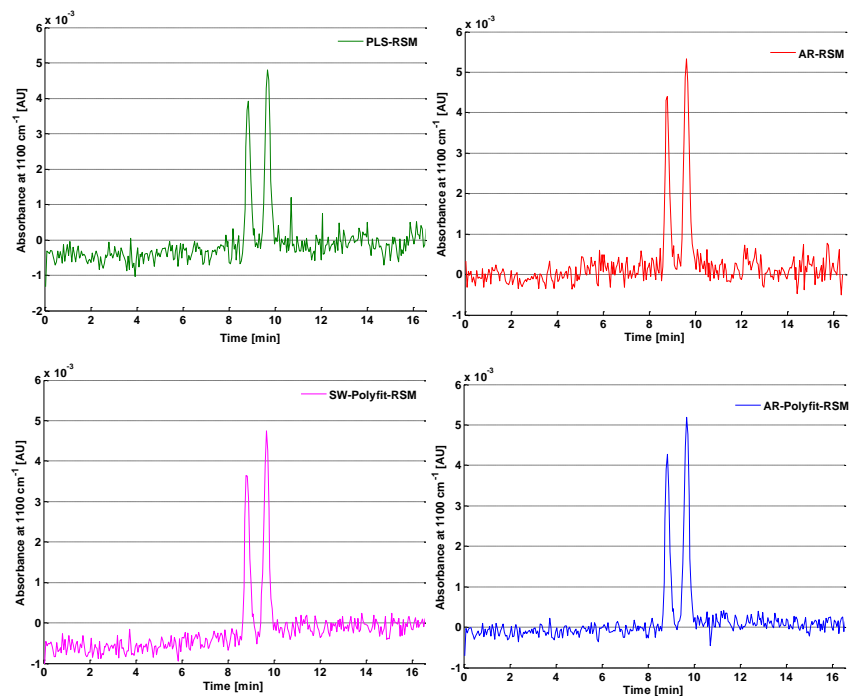


Figure 4.1.7. Chromatograms extracted from the injection of a diluted soft drink sample with 4 mg mL⁻¹ fructose and 6 mg mL⁻¹ glucose contents using four different background correction algorithms.

The carbohydrate peaks were identified with the help of standard solutions using their absorbance spectra and retention times. The first peak corresponds to glucose and the second one to fructose. The quality of the extracted chromatograms was better in case of polynomial based background correction than using previously developed algorithms. The quality of the recovered spectra using the polynomial approaches was also somewhat higher than compared to the other tested approaches as shown in Table 4.1.2. When SW-Polyfit and AR-Polyfit are compared, the results are of similar quality. However, best results were obtained by SW-Polyfit although from the quality parameters indicated in Table 4.1.2 it is difficult to state whether the differences are significant or not.

Table 4.1.2. Extracted correlation coefficients^a obtained using different spectral intervals for extracted spectra at the peak apex, obtained from the background corrected LC-IR injection of a diluted soft drink sample with 4 mg mL⁻¹ fructose and 6 mg mL⁻¹ glucose analyzed using an acetonitrile:water gradient and their corresponding reference spectra.

Background correction approach	Evaluated spectral region			
	1550 – 950 cm ⁻¹		1250 – 1060 cm ⁻¹	
	Fructose	Glucose	Fructose	Glucose
PLS-RSM	98.59	94.46	99.37	95.55
AR-RSM	98.08	94.48	99.57	95.56
SW-Polyfit-RSM	98.88	95.45	99.54	95.83
AR-Polyfit-RSM	98.19	94.99	99.58	95.66

Note: correlation coefficients^a between spectra x and y were calculated as $\frac{Cov(x,y)}{\sigma_x\sigma_y}$, being $Cov(x,y)$, σ_x and σ_y the covariance and their standard deviations, respectively; reference spectra of the analytes were obtained from the stopped flow measurement of 2 mg mL⁻¹ standard solutions in acetonitrile:water (70:30 v/v).

4.1.5 Conclusions

A new approach for the chemometric background correction in on-line hyphenated systems such as LC–FTIR under changing eluent conditions was developed. The proposed method called Polyfit-RSM has been tested on real reversed-phase on-line LC–FTIR data sets using a mobile phase composed by acetonitrile and water. Two parameters have been proposed as independent reference variables. Considering the two tested parameters, the use of SW appears to be the better choice, although results obtained from both introduced algorithms are very similar. The obtained results showed improved background correction as compared to previously developed methods also based on the use of a reference spectra matrix. Furthermore, the Polyfit-RSM approach reduces the influence of the size of the **RSM** on the accuracy of the background correction process, thus allowing the use of reduced size **RSMs**. This leads to a better compensation of slight instrumental changes, for example considering the water or CO₂ vapor concentration in the sample chamber, as compared to previously

available background correction procedures. It can be concluded that there is no single solution when the selection of the background correction parameters is pursued using only data from a blank gradient. Hence, it is advisable also to take into account specific characteristics of the system under study, e.g. IR spectral features of possible analytes present in the sample.

4.2 Cubic smoothing splines background correction

4.2.1 Introduction

To overcome difficulties arising from the on-line coupling of gradient LC-IR, recently a straightforward strategy to perform chemometric background elimination, called background correction based on the use of a reference spectra matrix (BGC-RSM) was developed [4.7]. This approach is based on the use of the spectral information of a set of spectra of different eluent compositions named 'reference spectra matrix' (**RSM**) and has been extensively discussed in Chapters 3 and 4.1. Basically, three constraints have to be fulfilled to apply BGC-RSM: i) the mobile phase spectra must have a spectral region characteristic of its composition and free from interferences from other eluting compounds, ii) an appropriate **RSM** has to be recorded and iii) high instrument stability is essential.

In the present study, a newly developed background correction method based on the use of cubic smoothing splines (CSS) was tested on on-line gradient LC-IR. The new method was compared to results obtained by the BGC-RSM approach. The usefulness of the proposed method was critically assessed using simulated and real reversed phase gradient LC-IR data using methanol, 2-propanol and ethanol as organic phase modifiers. The application of these alcohols as mobile phase components is challenging, because they show intense absorption bands in the mid-IR region which complicates background compensation. Additionally, the use of 2-propanol and ethanol as organic modifiers in liquid chromatography is of interest, because both alcohols are considered to have a low toxicity and therefore, when substituting acetonitrile or methanol as organic phase modifier, the method can be considered environmentally-friendly.

As a model example, the analysis of polyethylene glycols (PEGs) was employed. PEGs are widely employed as additives in cosmetic products [4.8] and pharmaceutical formulations [4.9] taking advantage of their low toxicity, their solubility and viscosity properties and the fact that they cause little or no ocular and dermal irritation [4.8]. In personal care products including creams, makeup, bath and hair care products, PEGs are often used at high percentage concentrations as solvents, humectants, binders,

emulsion stabilizers and viscosity-increasing agents. In pharmaceutical formulations, PEGs have been reported to affect oral absorption as well as renal elimination of different active drug components [4.9].

Emerging from the omnipresence of PEGs, adequate tools for qualification and quantification become necessary. Liquid chromatography (LC), gel permeation chromatography (GPC), thin-layer chromatography (TLC), supercritical fluid chromatography (SFC) and capillary zone electrophoresis (CZE) in combination with different detectors are commonly used for polymer analysis and characterization to obtain information about chemical properties as the average molecular mass and the composition of the polymer [4.10, 11]. Since PEGs lack of chromophors, detection can only be carried out in the low UV range or using refractive index (RI) detectors [4.12], entailing a rather unspecific detection or employing derivatization methods [4.11] increasing the time of analysis. Using evaporative light scattering detection (ELSD) there is no need for derivatization [4.13]. Furthermore, this detector is compatible with gradient elution and provides a significant increase in sensitivity as compared with RI detection, but it is also a low-selective detector and shows a non-linear response. Mass spectrometry (MS) detection is highly sensitive and also shows a very high specificity but its field of application focuses on trace level analysis. Besides, MS detectors are still expensive. In contrast, the on-line hyphenation with an infrared (IR) detector can be a useful alternative to standard detectors providing additional information on the analytes and avoiding time consuming sample preparation steps.

4.2.2 Theoretical background

The proposed approach applies univariate background correction to each variable (i.e. each wavenumber) individually. Spectra measured in the region before and after each peak cluster are used as knots to model the variation of the eluent absorption intensity with time using cubic smoothing splines functions, assuming that FTIR detection follows a linear, additive Lambert-Beer behaviour.

The proposed approach can be described in two steps: i) peak detection and ii) calculation of the background signal. The first step involves peak detection and the selection of a series of data points where no peaks are present to be subsequently used as knots for the calculation of the splines fit. In literature as well as in commercial

chromatographic software packages different approaches aiming at peak detection can be found [4.14, 15]. At least theoretically, many of these algorithms could be applied to identify analyte peaks in uncorrected LC-IR chromatograms. In spite of that, the strong change in the slope of the chromatograms hinders peak detection when the mobile phase composition changes rapidly, especially in spectral regions where the eluent absorbs strongly, or when the signal intensity due to the analyte absorption is small. The second step of the approach involves the background correction itself: firstly, using the selected knots a cubic smoothing spline is fitted to model eluent absorption. Then, background correction is accomplished by subtracting the interpolated eluent absorption to the raw LC-IR data.

The calculation of the cubic smoothing spline is carried out using the Matlab *csaps* function [4.16]. This function uses a smoothing parameter (p) which determines how closely the spline follows the given data (i.e. each considered chromatogram). The *csaps* function is very sensitive to the choice of p which consequently influences the accuracy of the background correction. Low values of p will lead to splines far away from the underlying trend (see Figure 4.2.1). As described in the reference [4.16], the sensitive range for p is around $\frac{1}{1+\varepsilon \cdot k}$, where $\varepsilon = \frac{h^3}{16}$, and h is the average difference between neighbouring sites. A close following of the data when $k = 0.01$ and some satisfactory smoothing when $k = 100$ is expected. This additional 'smoothing factor' k used for the calculation of p has to be carefully selected.

Figure 4.2.1 shows the effect of selecting different values of k between 0.01 and 100 on the background correction of a LC-IR injection of a PEG standard solution. Hence, throughout this work a constant value of 0.01 was used. Knot selection was performed manually. As a general criterion, every 15th point was selected as knot in baseline regions where no peaks were present. Additionally, a single data point between analyte peaks was also included as knot if peaks were completely resolved.

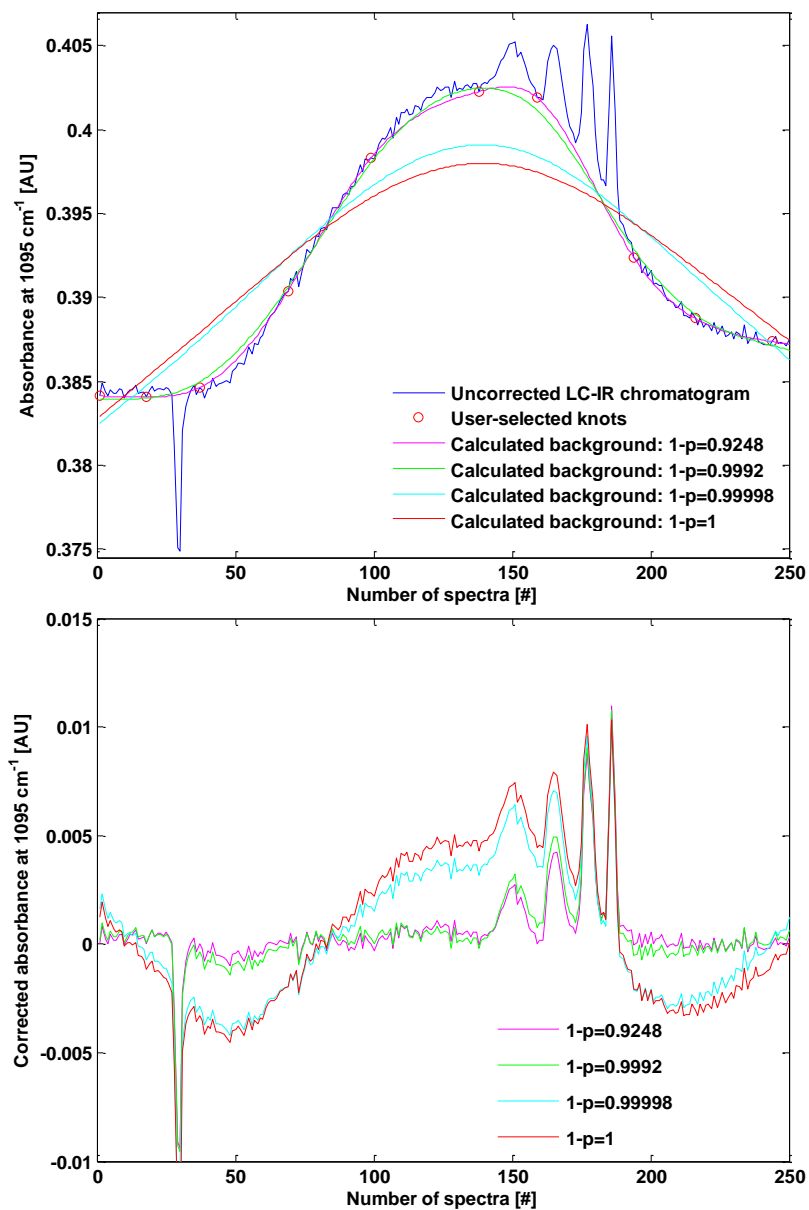


Figure 4.2.1. LC-IR chromatograms of a mixture of PEG 2000, PEG 4000, PEG 8000 and PEG 40000 obtained before (top) and after background correction (bottom) using different smoothing parameters (p) for the calculation of the background signal.

4.2.3 Material and methods

Simulated data

Four chromatographic data sets were simulated using real blank gradient elution data (D_{IR}) and a reference spectra set (S_{PEGs}) of PEG 2000, PEG 4000, PEG 8000 and PEG 40000 polyethylene glycol standards. PEG concentration profiles (C_{PEGs}) were generated using the *gspeak* function of the Peak Generation Matlab toolbox [4.17]. Then, the simulated chromatograms (D_{lc}) were calculated according to:

$$D_{lc} = C_{PEGs} S_{PEGs}^T + D_{IR} \quad (\text{Equation 4.2.1})$$

The peak heights of PEG 2000, PEG 4000, PEG 8000 and PEG 40000 simulated peaks were 0.0015, 0.004, 0.0035 and 0.005 with peak-sigma values of 1, 3, 1.5 and 1.5, respectively.

Four different situations were simulated: (i) all four peaks are baseline resolved choosing the peak position for the peak maximum at simulated retention times of 5.8, 6.8, 8.2 and 9.6 min for the four peaks, respectively; (ii) the first and the second peak are overlapping changing the retention time of the second peak to 6.5 min; (iii) the second and the third peak are overlapping changing the retention time of the second peak to 7.7 min and (iv) all four peaks are overlapping choosing retention times of 5.8, 6.5, 7.2 and 7.5 min, respectively.

Apparatus and Reagents

A Dionex P680 high performance liquid chromatographic system (Sunnyvale, CA, USA), equipped with a GENESIS C₄ column (150 x 2.1 mm, 4 μm, 300 Å) from Grace Davison Discovery (Deerfield, IL, USA) and a sample injection loop of 20 μL, was employed for chromatographic separations. Linear gradients were run with methanol:water, 2-propanol:water and ethanol:water mobile phases from 30 to 90, 10 to 25 and 10 to 40% v/v of organic solvent in 10, 15 and 10 min, respectively. Water was purified with a Milli-Q system from Millipore (Billerica, MA, USA). All solvents were of multisolvent grade and purchased from Scharlau Chemie S.A. (Barcelona, Spain).

A Bruker IFS 66/v FTIR spectrometer (Bremen, Germany) equipped with a liquid nitrogen refrigerated mercury–cadmium–telluride detector and a vacuum system was employed for spectra acquisition. The scanner of the interferometer was operated at a

HeNe laser modulation frequency of 100 kHz. Spectra were recorded in the range between 4000 and 950 cm^{-1} , with a spectral resolution of 8 cm^{-1} and a zerofilling value of 2. Co-adding 25 scans per spectrum, a spectra acquisition frequency of 15 spectra min^{-1} was provided. On-line hyphenation to the LC system was carried out using a flow cell with CaF_2 and ZnSe windows and a pathlength of 10 μm placed in the dry-air purged sample compartment of the spectrometer.

Standard mixtures of polyethylene glycol (PEG) were prepared by mixing pure standards of different molecular weights (2000, 4000, 8000 and 40000 g mol^{-1}) obtained from Fluka (Buchs, Switzerland) and dissolving them in different mobile phases. All solutions were filtered with a 0.22 μm nylon syringe filter prior to their injection into the chromatographic system. These standards were used to test and assess the chromatographic procedures and the background correction process.

Software and algorithms

For instrumental and measurement control as well as for data acquisition, the OPUS software (version 6.5) from Bruker was employed. Background correction of data was run under Matlab 7.7.0 (R2008b) from MathWorks (Natick, Massachusetts, USA) using the csaps Matlab function, in-house written functions and a Matlab GUI file. In-house written Matlab functions and GUI files used in this work are available on-line [4.18].

4.2.4 Results and discussion

Infrared spectra of mobile phase and PEG

Figure 4.2.2 shows infrared spectra of the three different mobile phase systems used in this work between 3000 and 950 cm^{-1} (left) and 1500 and 950 cm^{-1} (right). In the spectral interval between 2990 and 2835 cm^{-1} vibrational bands are caused by antisymmetric and symmetric CH_3 and CH_2 vibrations [4.19]. The band around 2100 cm^{-1} emerges due to overtones and combination bands of intermolecular vibrations and OH stretches [4.20]. In the region between 1470 and 1385 cm^{-1} several overlapping CH_3 and CH_2 deformation bands can be observed [4.19]. At $\sim 1643 \text{ cm}^{-1}$ the strong absorption band due to the HOH bending mode of water molecules is located. Because of saturation effects, the OH stretching absorption of alcohol and water molecules do not show a linear behavior with changing concentrations [4.20, 21]. Additionally, the

position of the HOH bending and HOH bending/hydrogen bond libration combination modes shift to higher frequencies with increasing alcohol concentrations. It is clear that due to the changes in shape and intensity of the mobile phase absorption bands during the gradient (see Figure 4.2.2), a constant background cannot be used to correct the spectra of the eluting analytes.

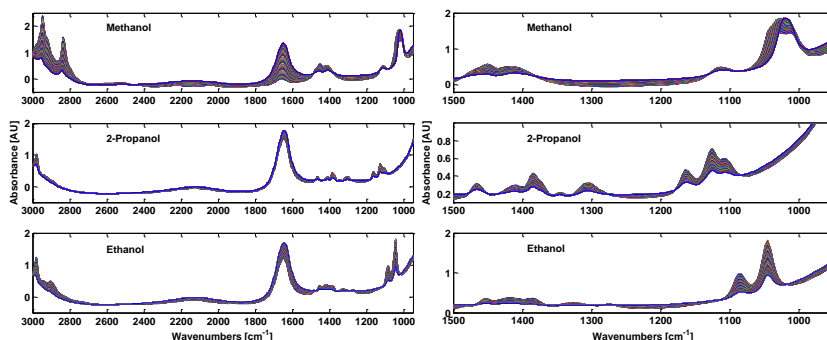


Figure 4.2.2. On-line FTIR spectra measured during LC gradient blank runs of methanol:water, 2-propanol:water and ethanol:water mixtures ranging from 30 to 90, 10 to 25 and 10 to 40% v/v organic solvent, respectively, between 3000 and 950 cm^{-1} (left) and between 1500 and 950 cm^{-1} (right).

Figure 4.2.3 shows spectra of PEG 4000 solutions in the 3000-950 cm^{-1} range. PEG 4000 was dissolved in mixtures of the three alcohols with water at the same concentrations as at the beginning of the applied gradients, respectively. A set of characteristic analyte bands arises in this interval, the most intense bands being located in the 1100 cm^{-1} region. The C-O stretching vibration, the in-plane bending vibration of the C-O-H groups and the C-C stretching as well as the deformational -CH₂- vibration contribute to the shape of this band, among others. The shape of this band changes with the molecular weight of the polymer as well as with the water content of solutions [4.22]. Due to structural similarities between the mobile phase components and the analyte, this band overlaps strongly with mobile phase absorption bands. Additionally, bands due to C-O-H in-plane deformations can be observed in the spectral range from 1300 to 1400 cm^{-1} . These bands are almost identical for PEGs of different molecular weights. In the spectral interval between 2924 and 2881 cm^{-1} vibrational bands due to antisymmetric and symmetric CH₃ and CH₂ vibrations can be observed [4.19].

Furthermore it can be seen that band shapes are affected by the solvent, being slightly different for PEGs dissolved in methanol, 2-propanol and ethanol aqueous solutions.

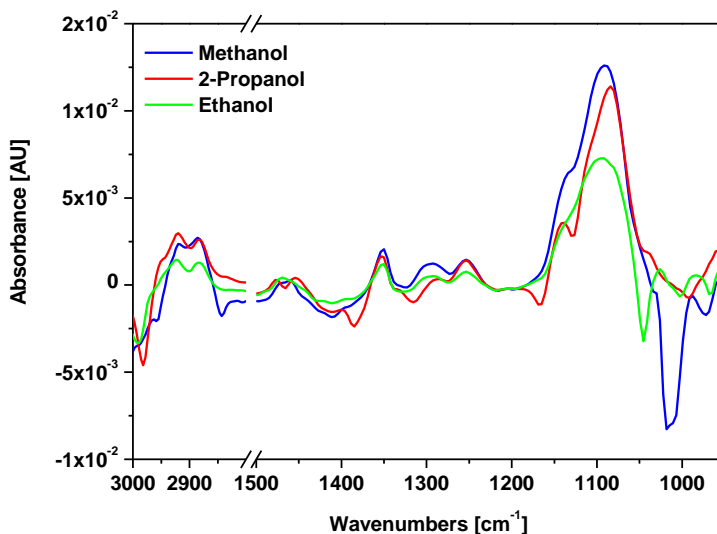


Figure 4.2.3. Spectra of PEG 4000 at 5 mg mL⁻¹ in methanol:water, 2-propanol:water and ethanol:water at 30, 10 and 10% v/v of organic solvent, respectively, acquired in a continuous flow experiment.

Simulated on-line LC-IR data

To evaluate the proposed background correction method, it was initially tested on simulated data calculated as described in the experimental section. Uncorrected chromatograms of the four simulated situations are depicted in Figure 4.2.4 (top). Whereas the elution of the analytes can be appreciated as a change of the slope in the chromatogram, the detection of small peaks might become difficult without appropriate background correction.

Peak detection and knot selection were performed manually. The selection of the knots is important as it influences the resulting chromatograms and consequently precision and accuracy as well as the quality of the recovered spectra required for qualitative and quantitative analysis. However, an additional advantage of the new background correction based on cubic smoothing splines over other methods is its potential for a high grade of automation during the whole process leading to a low

user-interaction. The use of an appropriate algorithm which reliably identifies the peaks and their beginning and ending will therefore directly reduce the time required for background correction of real LC-IR data and thus, it would facilitate the application of on-line LC-IR measurements in routine analysis.

As already stated before, the selection of the knots is a critical step of this approach. Figure 4.2.5 shows the influence of the selection of different knots on the recovered chromatograms. The worst results were obtained using every fifth spectrum for correction. The baseline shows a valley during analyte elution, being spectral shapes and chromatographic peak heights strongly modified because some of the data points (knots) used for the background calculation contain significant amounts of signal from the eluting analytes. As it can be seen in Figure 4.2.5, using every fifth spectrum in the interval from 0 to 5.7 min and from 7.9 to 12 min, the results can be improved. Selecting additional spectra at 5.9, 6.9 and 7.3 min different results were found. When analyte peaks overlap strongly, the correction gets worse including the spectrum of the valley between the two peaks in the knots vector. The selection process is also influenced by the chromatographic resolution of the peaks, as peak overlapping complicates the selection process of the knots.

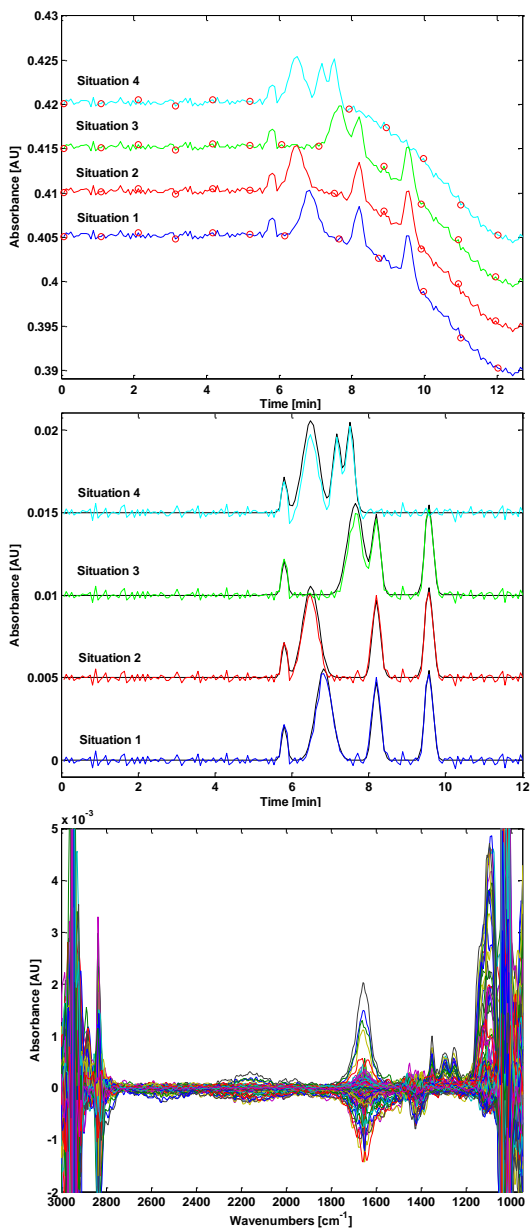


Figure 4.2.4. Simulated chromatographic separations of PEGs. Chromatograms extracted at 1095 cm^{-1} without background correction (top) and after applying the CSS correction method (middle), background corrected spectra of the simulated data set corresponding to situation 2 (bottom). Note: Red circles in the top panel indicate selected knots, black lines in the middle panel show corresponding simulated chromatograms before adding noise to simplify interpretation.

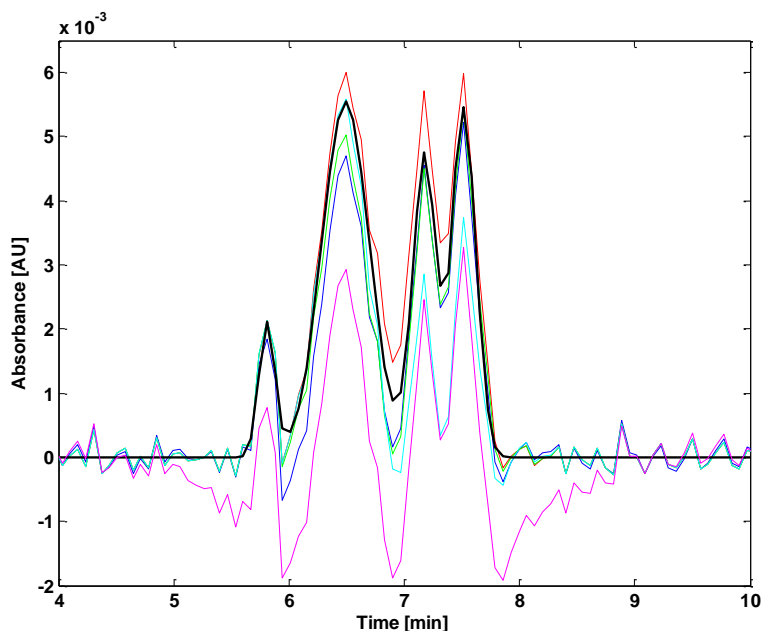


Figure 4.2.5. Chromatograms extracted at 1095 cm^{-1} using a single point baseline correction at 1400 cm^{-1} from situation 4 after applying the CSS method using different knots; pink line: using every fifth point as a knot (see correction step 1), dark blue line: using every fifth spectrum in the interval from 0 to 5.7 min and from 7.9 to 12 min, red line: same knots as blue line adding one spectrum at 5.9 min, green line: same knots as blue line adding two spectra at 5.9 and 6.9 min, light blue line: same knots as blue line adding three spectra at 5.9, 6.9 and 7.3 min, black line shows corresponding simulated chromatograms before noise addition to simplify interpretation.

Figure 4.2.4 (middle) shows background corrected chromatograms of all simulated situations and the corresponding simulated chromatograms without adding noise. In general it can be observed that even small peaks are now easy to identify in all chromatograms, the baseline shows randomly distributed noise and a lack of slope. From situation 1 it can be seen that the background correction method works well for baseline resolved peaks. All four peaks were recovered almost without affecting peak shape, height and area (data not shown). Situations 2 to 4 show that the background correction also works well in case of overlapping peaks if an appropriate knot selection is feasible. On the other hand, Figure 4.2.4 (bottom) shows the high quality of the background corrected spectra obtained from the simulated data set corresponding to situation 2. As it can be seen, spectra show a lack of sloping baseline drift. Apart from the saturated spectral regions above 2800 cm^{-1} and below 1060 cm^{-1} , the spectral noise

is reduced to a very low level of 3.4 mAU at 1643 cm^{-1} and 1.0 mAU in the region between 1470 and 1385 cm^{-1} were a strong water absorption band and intense absorption bands of the alcoholic mobile phase component interfere. In other spectral regions the peak to peak noise is even lower, like for example from 1360 to 1200 cm^{-1} , being 0.3 mAU.

Real on-line LC-IR data

Figure 4.2.6 shows spectra acquired during the injection of a standard mixture of four PEGs in a linear methanol:water gradient from 30 to 90% v/v methanol before (top) and after (bottom) background correction. The identification of the analytes is not possible without background correction due to the predominant absorbance of the mobile phase components and the strong changes in both, intensity and shape of the mobile phase bands. It is remarkable that after background correction the identification as well as the quantification of all four analytes is feasible.

To show the potential of on-line LC-IR applying background correction for quantitative applications, calibration lines have been established for all three mobile phase systems injecting 8 standard mixtures using methanol:water and 2-propanol:water and 10 for the calibration line of the ethanol:water mobile phase system. The analytical figures of merit of the three determinations are summarized in Table 4.2.1. Analyte specific chromatograms were extracted measuring the absorbance at 1095 , 1088 and 1103 cm^{-1} in methanol:water, 2-propanol:water and ethanol:water, respectively, applying a single point baseline correction at 1400 cm^{-1} . All calibration lines showed high linearity with coefficients of determination higher than 0.98. Limits of detection and limits of quantification, both measured in mg mL^{-1} , were established for the four analytes in the three mobile phase systems and varied respectively between 0.13 and 0.4 and between 0.4 and 1.4 in methanol:water, between 0.3 and 0.5 and between 0.9 and 1.8 in 2-propanol:water and between 0.3 and 0.8 and between 1.1 and 2.7 in ethanol:water. The repeatability was measured as the relative standard deviation (RSD [%]) and ranged between 1.4 and 6.6, 3.5 and 5.3 and 3.3 and 8.7% for methanol:water, 2-propanol:water and ethanol:water, respectively. Best results were obtained using the methanol:water mobile phase system. Results obtained for 2-propanol:water were similar to those of methanol:water. Noise was somewhat higher

using ethanol:water because of the higher background absorption of this mobile phase in the spectral range of the analyte signal. However, 2-propanol and ethanol are recommended due to their low toxicity, thus being more environmentally friendly solvents.

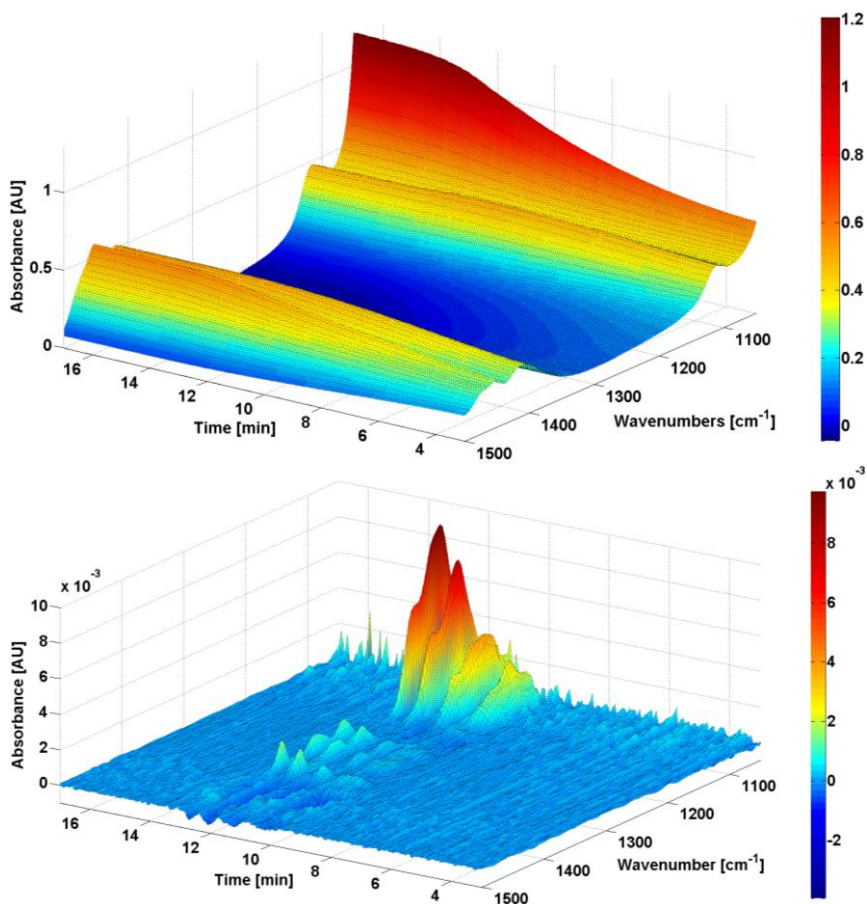


Figure 4.2.6. 3D plots of uncorrected spectra (top) and spectra obtained by applying the CSS method (bottom); Note: Spectra were acquired during injection of a standard mixture containing 5.1 mg mL⁻¹ of PEG 2000, 5.3 mg mL⁻¹ of PEG 4000, 5.6 mg mL⁻¹ of PEG 8000 and 5.1 mg mL⁻¹ of PEG 40000 between 1500 and 950 cm⁻¹ and 3 and 17 min.

Table 4.2.1. Figures of merit of the on-line LC-IR determination of PEGs using cubic smoothing splines background correction.

Mobile Phase	Analyte	Calibration Curve ^a	R ²	Noise ^b	LOD ^c	LOQ ^d	Rep ^e
		$y=(a+s_a)*x+(b+s_b)$ ($a \pm s_a$) ($b \pm s_b$)					
Meth:H ₂ O ^f	PEG 2000	(0.00038 ± 0.00002)	0.98	0.04	0.3	1.1	3.4
	PEG 4000	(0.00039 ± 0.00001)	0.99	0.05	0.4	1.3	4.8
	PEG 8000	(0.00040 ± 0.00002)	0.98	0.06	0.4	1.4	6.6
	PEG 40000	(0.00039 ± 0.00002)	0.98	0.02	0.13	0.4	1.4
2-Prop:H ₂ O ^g	PEG 2000	(0.00030 ± 0.00001)	0.989	0.05	0.5	1.8	5.3
	PEG 4000	(0.00040 ± 0.00002)	0.98	0.06	0.5	1.5	4.3
	PEG 8000	(0.00027 ± 0.00001)	0.986	0.02	0.3	0.9	3.7
	PEG 40000	(0.000242 ± 0.000005)	0.998	0.03	0.3	1.1	3.5
Eth:H ₂ O ^h	PEG 2000	(0.00031 ± 0.00002)	0.96	0.08	0.8	2.6	5.9
	PEG 4000	(0.00036 ± 0.00002)	0.98	0.10	0.8	2.7	5.1
	PEG 8000	(0.00033 ± 0.00001)	0.991	0.08	0.7	2.4	8.7
	PEG 40000	(0.000288 ± 0.000007)	0.994	0.03	0.3	1.1	3.3

Note: Calibration curve^a: obtained from standard mixtures, being a and b the slope and the intercept of the calibration lines; Noise^b: measured as the standard deviation of the peak areas of 5 independent injections of a standard mixture in AU; LOD^c: limit of detection [mg mL⁻¹] established for a signal to noise ratio of 3; LOQ^d: limit of quantification [mg mL⁻¹] established for a signal to noise ratio of 10; Rep^e: repeatability measured as relative standard deviation of 5 independent measurements in %; Meth:H₂O^f: analyte specific chromatograms were extracted measuring the absorbance at 1095 cm⁻¹ and applying a single point baseline correction at 1400 cm⁻¹ in methanol:water gradients; 2-Prop:H₂O^g: analyte specific chromatograms were extracted measuring the absorbance at 1088 cm⁻¹ and applying a single point baseline correction at 1400 cm⁻¹ in 2-propanol:water gradients; Eth:H₂O^h: analyte specific chromatograms were extracted measuring the absorbance at 1103 cm⁻¹ and applying a single point baseline correction at 1400 cm⁻¹ in ethanol:water gradients.

Figure 4.2.7 (left) shows chromatograms extracted after background correction of data obtained during the injection of a mixture of the four PEG standards at a concentration of 5 mg mL^{-1} in the three mobile phase systems, evidencing the adequate chromatographic resolution of the four peaks, the lack of a sloping baseline as well as the random distribution of the noise around the baseline. In accordance with the results obtained from the calibration data, it can be observed that the noise was slightly higher using ethanol:water than for the other mobile phase systems. Using methanol as organic modifier, better peak shapes were obtained than with 2-propanol or ethanol.

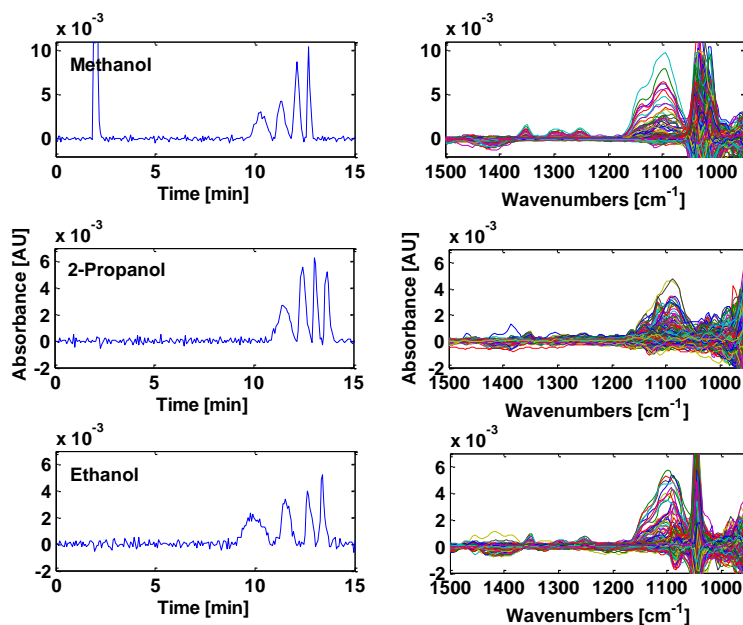


Figure 4.2.7. Left: Chromatographic separations of PEGs in different mobile phase systems; background corrected chromatograms extracted from the injection of a standard of 4 PEGs using methanol:water, 2-propanol:water and ethanol:water gradients ranging from 30 to 90, 10 to 25 and 10 to 40% v/v of organic solvent, respectively; right: corresponding background corrected spectra.

Figure 4.2.7 (right) shows the corrected spectra obtained during the whole chromatographic run. Due to the different chemical structure of the three alcoholic mobile phase components, spectral saturation and noise were affected. Using

methanol:water at a maximum methanol concentration spectra get completely obscured around 1030 cm^{-1} , using ethanol:water the strongest absorption is observed around 1045 cm^{-1} . Using 2-propanol:water, spectra get saturated below 950 cm^{-1} . Again, no sloping can be seen in any of the depicted spectra.

Table 4.2.2. Correlation between spectra extracted from background corrected chromatograms and reference FTIR spectra of PEGs.

Mobile Phase ^a	Analyte ^b	Correlation Coefficient ^c [%]			
		PEG 2000 Ref ^d	PEG 4000 Ref ^d	PEG 8000 Ref ^d	PEG 40000 Ref ^d
Methanol: H ₂ O	PEG 2000	96.7	97.1	97.0	98.7
	PEG 4000	99.1	99.1	99.1	98.4
	PEG 8000	97.6	98.0	97.9	99.7
	PEG 40000	97.4	97.7	97.6	99.9
2-Propanol: H ₂ O	PEG 2000	92.6	89.0	89.6	90.7
	PEG 4000	97.7	96.2	96.4	97.2
	PEG 8000	98.1	98.9	99.0	98.7
	PEG 40000	99.2	97.4	97.6	98.4
Ethanol:H ₂ O	PEG 2000	98.6	98.5	98.0	98.2
	PEG 4000	99.6	99.6	99.3	99.4
	PEG 8000	99.4	99.6	99.4	99.6
	PEG 40000	97.9	97.9	97.3	97.6

Note: Mobile Phase^a: Spectra were compared in the spectral interval from 1366 to 1070 cm^{-1} for the methanol:H₂O mobile phase system, and from 1366 to 1072 cm^{-1} for the 2-propanol:H₂O and the ethanol:H₂O mobile phase systems. Analyte^b: analyte spectra were extracted during analyte elution from background corrected chromatograms obtained during the injection of a standard mixture containing 5 mg mL^{-1} of each analyte. Correlation Coefficient^c: The correlation coefficient was calculated between two spectra y_1 and y_2 and is defined as the ratio from the covariance ($Cov(y_1, y_2)$) and the product of the two standard deviations σ_{y_1} and σ_{y_2} ; according to this definition, a value of percentage of correlation coefficient of 100 indicates identical spectra. Ref^d: reference spectra were obtained during Flow Injection Analysis (FIA) of standard solutions of each analyte at a concentration of 5 mg mL^{-1} and using the same mobile phase composition as at the beginning of the gradient in the corresponding mobile phase system.

To assess the ability to identify PEG spectra in the corrected data sets, the correlation coefficients between spectra extracted from background corrected chromatograms at the peak apex of each analyte, and reference spectra were calculated. The spectral intervals used for comparison varied for the three considered mobile phases. The range between 1366 and 1070 cm^{-1} was used for methanol:water and between 1366 and

1072 cm^{-1} for 2-propanol:water and ethanol:water. Results found are summarized in Table 4.2.2 and as can be seen, recovered PEG spectra allowed the identification of PEGs in all mobile phase systems showing correlation coefficients higher than 92%. Furthermore it can be observed that high spectral similarity avoids the differentiation of the four considered PEGs.

Comparison of the proposed method with the AR-BGC-RSM method

The new background correction approach was compared to the BGC-RSM approach, which has been successfully applied to methanol:water mobile phase systems [4.23] using an AR as IP. Figure 4.2.8 (left) shows three chromatograms extracted from the same data set obtained during the injection of a mixture of four PEGs at a concentration of 5 mg mL^{-1} . All chromatograms were extracted at 1095 cm^{-1} applying a single point baseline correction at 1400 cm^{-1} . The first one was extracted before applying any background correction. The second chromatogram was extracted after AR-BGC-RSM background correction improving the identification of the PEG peaks. The best results were obtained using the cubic smoothing splines background correction method which provided a baseline without slope and minimum noise levels.

Despite the results shown in Figure 4.2.8, it has to be remarked that the quality of the background correction obtained using the BGC-RSM approach also depends strongly on the size of the **RSM** (in this case it only contained 189 spectra), on the range of mobile phase compositions and on the stability of the instrument, which in this case showed a remarkable slope drift with time (data not shown). Figure 4.2.8 (right) shows the corresponding spectra of the same data set obtained during the whole chromatographic run. PEG spectra can be identified after applying both background correction methods and, once again, the best results were obtained using the cubic smoothing splines method.

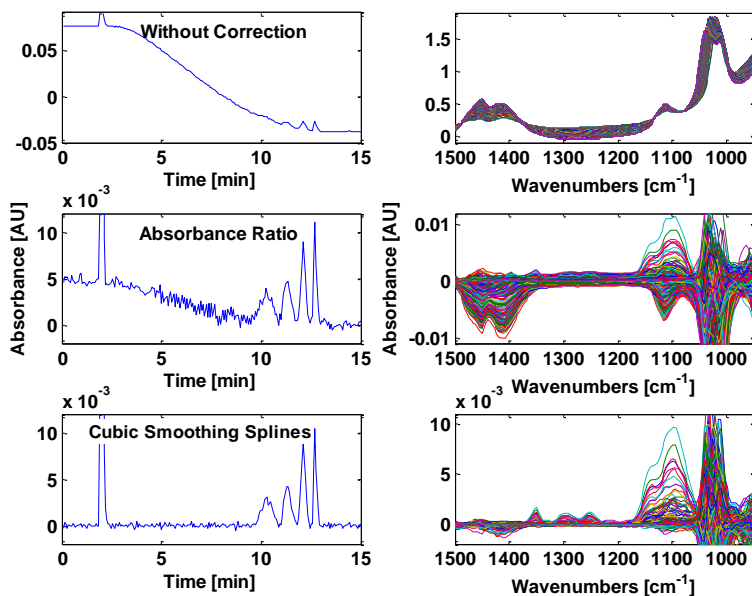


Figure 4.2.8. Chromatographic separations of PEGs using a methanol:water gradient and different background correction methods; chromatograms extracted from data acquired during the injection of a standard mixture containing 5 mg mL^{-1} of each of the 4 PEG standards in a methanol:water gradient ranging from 30 to 90% v/v methanol without background correction and after applying AR-BGC-RSM and CSS correction, respectively (left) and spectra corresponding to the chromatograms shown on the left acquired during the whole chromatographic run (right).

Table 4.2.3 summarizes the chromatographic noise values found at wavenumbers were the eluents show typical absorption bands before and after background correction. Applying both background correction methods, noise values could be reduced drastically. Comparing BGC-RSM and the cubic smoothing splines method, the latter one reduces the noise between 44 and 13 times at the 4 considered wavenumbers, therefore clearly improving the achievable limit of detection.

Table 4.2.3. Chromatographic noise values found for PEGs separated in methanol:water using different background correction strategies.

Correction method	Noise ₁₆₄₀ ^a	Noise ₁₄₅₀ ^a	Noise ₁₄₁₂ ^a	Noise ₁₁₁₅ ^a
Without Correction	652	182	184	147
AR-BGC-RSM	12	4	5	3
CSS-BGC	0.33	0.10	0.13	0.27

Note: Noise^a: noise values were measured as root mean square (RMS) in the time window where no analytes elute (between 2.7 and 9.2 min); all noise values are given in mAU.

For the application of the CSS background correction method no reference spectra matrix is needed. Furthermore, using the BGC-RSM approaches, high instrument stability is required, which is also not the case applying CSS. On the contrary, knot selection can be troublesome in the presence of a high number of overlapping peaks. The selection of an appropriate background correction method depends strongly on the instrumental conditions and must be decided case-by-case.

4.2.5 Conclusions

The CSS background correction method was tested and evaluated by means of simulated as well as real data sets. Applying the new background correction method to simulated data sets it could be shown that it works well for baseline resolved peaks. Background corrected spectra showed high quality and could be used to identify the analytes. Results lead to the conclusion that this background correction might be suitable for many practical applications. Furthermore, this method shows high potential to achieve a high grade of automatization in the background correction process as peak detection can not only be realized manually but also automatically. However, the critical step in the background correction process is the selection of the knots. Real data sets were obtained during the separation of PEGs of different molecular weights on a LC reversed phase column employing aqueous mobile phase systems with three different alcoholic organic modifiers (methanol, 2-propanol and ethanol). Obtained results provided chromatograms and recovered background corrected spectra suitable for identification and quantification of all four considered

analytes. Figures of merit of the method were adequate for quantitative analysis of PEGs showing high linearity (R^2 of above 0.98) and appropriate LODs and LOQs.

Results obtained by the AR-BGC-RSM approach are strongly dependent on quality and size of a previously obtained **RSM**. Using the proposed CSS approach, there is no need to record a **RSM** and therefore problems caused by poor instrument stability are avoided. Furthermore, the new method minimizes user-interaction as no variable selection prior to background correction is required. This makes the whole process more feasible and requires less user-experience.

4.3 References for Chapter 4

- [4.1] J. Kuligowski, G. Quintas, S. Garrigues, M. de la Guardia, *Journal of Chromatography A*, 1216 (2009) 3122-3130.
- [4.2] J. Kuligowski, D. Carrion, G. Quintas, S. Garrigues, M. de la Guardia, *Journal of Chromatography A*, 1217 (2010) 6733-6741.
- [4.3] T. Takamuku, M. Tabata, A. Yamaguchi, J. Nishimoto, M. Kumamoto, H. Wakita, T. Yamaguchi, *Journal of Physical Chemistry B*, 102 (1998) 8880-8888.
- [4.4] P.D. Harrington, A. Urbas, P.J. Tandler, *Chemometrics and Intelligent Laboratory Systems*, 50 (2000) 149-174.
- [4.5] M. Lopez-Pastor, M.J. Ayora-Canada, M. Valcarcel, B. Lendl, *Journal of Physical Chemistry B*, 110 (2006) 10896-10902.
- [4.6] E.M. Tee, A. Awichi, W. Zhao, *Journal of Physical Chemistry A*, 106 (2002) 6714-6719.
- [4.7] G. Quintas, B. Lendl, S. Garrigues, M. de la Guardia, *Journal of Chromatography A*, 1190 (2008) 102-109.
- [4.8] C. Fruijtjer-Polloth, *Toxicology*, 214 (2005) 1-38.
- [4.9] T.R. Buggins, P.A. Dickinson, G. Taylor, *Advanced Drug Delivery Reviews*, 59 (2007) 1482-1503.
- [4.10] K. Rissler, *Encyclopedia of Separation Science*, 2007, pp. 3889.
- [4.11] D. Brinz, U. Holzgrabe, *Electrophoresis*, 29 (2008) 3605-3611.
- [4.12] N. Li, D. Ziegemeier, L. Bass, W. Wang, *Journal of Pharmaceutical and Biomedical Analysis*, 48 (2008) 1332-1338.
- [4.13] V. Zabaleta, M.A. Campanero, J.M. Irache, *Journal of Pharmaceutical and Biomedical Analysis*, 44 (2007) 1072-1078.
- [4.14] B.M. Wise, N.B. Gallagher, R. Bro, J.M. Shaver, W. Windig, R.S. Koch, *PLS_Toolbox 4.0 for use with Matlab™*, Eigenvector Research Inc., Wenatchee, 2006.
- [4.15] J.Q. Zhang, E. Gonzalez, T. Hestilow, W. Haskins, Y.F. Huang, *Current Genomics*, 10 (2009) 388-401.
- [4.16] The MathWorks Inc., <http://www.mathworks.com/products/splines/demos.html?file=/products/demos/shipping/splines/csapsdem.html>, Natick, USA.

- [4.17] Biosystem Data Analysis Group, <http://www.bdagroup.nl/>, University of Amsterdam, Swammerdam Institute for Life Sciences, Amsterdam, The Netherlands.
- [4.18] Working Group on Process Analysis and Vibrational Spectroscopy (CAVS), <http://www.iac.tuwien.ac.at/cavs/>, Vienna University of Technology, Institute of Chemical Technologies and Analytics, Vienna, Austria.
- [4.19] D. Lin-Vien, N.B. Colthup, W.G. Fateley, J.G. Grasselli, *The handbook of infrared and Raman characteristic frequencies of organic molecules*, Academic Press, Inc., 1991
- [4.20] C.A. Holden, S.S. Hunnicutt, R. Sanchez-Ponce, J.M. Craig, S.C. Rutan, *Applied Spectroscopy*, 57 (2003) 483-490.
- [4.21] A.M. Zhao, E.R. Malinowski, *Analytical Chemistry*, 71 (1999) 602-608.
- [4.22] M. Rozenberg, A. Loewenschuss, Y. Marcus, *Spectrochimica Acta Part a-Molecular and Biomolecular Spectroscopy*, 54 (1998) 1819-1826.
- [4.23] J. Kuligowski, G. Quintas, S. Garrigues, M. de la Guardia, *Analytica Chimica Acta*, 624 (2008) 278-285.

CHAPTER 5. BACKGROUND CORRECTION IN ON-LINE LC-IR BASED ON FACTOR ANALYSIS, MULTIVARIATE CURVE RESOLUTION AND REFERENCE SPECTRA MATRICES

5.1 Introduction

Hyphenated LC instruments are capable of providing two-dimensional bilinear data and thus, factor analysis (FA) based methods have been employed to explore the underlying sources of variation in this type of data. Among these techniques, principal component analysis (PCA) [5.1], evolving factor analysis (EFA) [5.2, 3] and simple-to-use interactive self modeling analysis (SIMPLISMA) [5.4] have been widely used for the selection of pure spectra and elution profiles, for the determination of the number of eluting components with linearly independent spectra and/or eluting profiles (i.e. the *chemical rank*, which can be estimated by the pseudo rank, or by the mathematical rank in absence of noise) and for the resolution of overlapping or coeluting peaks. Besides, methods such as parallel factor analysis (PARAFAC [5.5], PARAFAC2 [5.6, 7]) or MCR-ALS [5.8-13] have been used to resolve the pure concentration profiles and pure instrumental responses in a variety of analytical situations. An important feature of all these methods is their second order-advantage, which allows for the quantification of the target analytes in the presence of unknown interferences when several chromatographic runs are analyzed together.

In 2003, Edelmann et al. [5.14] employed MCR-ALS for the quantitative analysis of co-eluting analytes in wine samples using isocratic LC-Fourier transform infrared

spectrometry (LC-IR). In this work, prior to MCR-ALS, background correction was achieved by subtracting the average baseline spectrum recorded directly before co-elution of the analytes and calculating first-derivative spectra in order to remove baseline drifts. Ruckebusch et al. [5.15] used MCR-ALS for resolving gel permeation chromatography-FTIR (GPC-FTIR) data collected on butadiene rubber and styrene butadiene rubber blends in order to access in-depth knowledge of polymers along the molecular weight distribution. In 2004 Boelens et al. [5.16, 17] developed a very efficient method to correct for the eluent background spectrum (EBS) in LC coupled to spectroscopic techniques (e.g. Raman, UV-Vis). In the EBS method, data acquired during the LC run is split into two parts. One part is a matrix where only the eluent is present (i.e. the background spectral subspace or B-subspace), and the other part is formed by spectra in which eluent and analyte(s) are both present (i.e. the elution spectra). First, all variation in the eluent spectra at baseline level is modeled in the background spectral subspace (i.e. B-subspace) built by PCA using a number of principal components selected according to the empirical IND algorithm [5.18]. Secondly, the PCA loading vectors are used for eluent background correction of the elution spectra. Therefore, in this approach it is assumed that the elution spectra are a linear combination of analyte and background spectra, the latter being described by the previously calculated loading vectors. These are fitted under the elution spectra by an asymmetric least-squares (asLS) method [5.19]. This algorithm assumes that the analyte spectrum consists of positive values only and negative residuals of the least-squares fit are penalized while performing the regression in an iterative way. The main limitation of the EBS method, as described by Dijkstra et al. [5.17], is that the elution time window of the analytes has to be known in advance thus limiting the applicability of the approach. For instance, if the identification of the elution window of the analytes is performed using an additional detection system like, for example UV, the presence of non-UV absorbing analytes might lead to an underestimation of the number of PCs required to describe the background absorption of the 'analyte' subspace. Besides, as the data set has to be split prior to background correction, it cannot be carried out on-the-fly.

In 2006, the use of PARAFAC and PARAFAC2 for chemometric eluent elimination was evaluated by István et al. [5.20]. From results found on simulated on-line LC-IR runs, the authors concluded that PARAFAC2 performs better than PARAFAC, but, like MCR-ALS, it did not give correct decompositions. The use of a new method named objective subtraction of solvent spectrum with iterative use of PARAFAC and PARAFAC2 (OSSS-IU-PARAFAC and OSSS-IU-PARAFAC2, respectively) improved results. In spite of that, the restrictions imposed by this approach (e.g. constant eluent composition or constant elution profiles of any given component among different LC runs) drastically reduced its practical applicability.

In summary, there is an on-going interest in compensating changes in baseline contributions of on-line LC data sets as they have large influence on the results. According to this, the resolution process of LC-IR data could be improved if solvent contribution, drift and detector changes are removed in advance [5.10]. Although different approaches have already been developed to overcome the challenges of on-line (gradient) LC-IR, there is still a need to develop user-friendly strategies with fewer conditions of applicability. Accordingly, the goal of the present study was to develop new approaches for background correction using the information content of the **RSM** and hence facilitate the use of MCR-ALS in the analysis of hyphenated LC-IR data [5.21]. Summarizing, two problems are studied: i) the development and application of background elimination methods, and ii) the use of MCR-ALS in on-line gradient LC-IR to resolve co-elution problems after background elimination. This Chapter also discusses several practical issues encountered in background correction in on-line LC-IR systems with the help of real gradient LC-IR data sets.

5.2 Theoretical background

Background correction

Data obtained from hyphenated LC systems can be seen as the sum of background, noise and analyte contributions [5.22]. Background and analyte contributions can be considered as bilinear contributions of spectra and concentration profiles. This implies that background absorption can be modeled as a combination of the contributions of a

series of 'pure' mobile phase components with their characteristic spectra and with their contribution to the overall absorption calculated according to their concentration or elution profile during the chromatographic run.

Accordingly, the methods described in this work are based on the calculation of both, the spectra and concentration profiles of the IR-absorbing components of the mobile phase during the chromatogram. These methods can be summarized in four steps: i) Splitting of the LC-IR data matrix in two new matrices, **SM** ($n \times j$) and **RSM** ($m \times j$), corresponding to the spectra acquired during the sample elution (n) and during the re-equilibration after the LC run (m), respectively, at j wavenumbers. Therefore, whereas the **RSM** matrix contains information only related to the spectral changes due to the mobile phase gradient, the **SM** also includes spectral variations due to the elution of the IR absorbing analytes. ii) Determining the number of chemical components due to the mobile phase gradient (k_{opt}) in the **RSM** employing Factor Analysis methods. iii) Calculation of the concentration profiles of the k_{opt} background components in the **SM** matrix, and iv) calculation and subtraction of the background contribution in the **SM** matrix. Following this scheme, two methods are described in this work.

Method 1: SIMPLISMA-BGC-RSM

In this method, the spectra of a user-defined number of 'pure' components (k_{opt}) are calculated from the **RSM** data matrix using SIMPLISMA. A critical step is the determination of the chemical rank (i.e. k_{opt}), as the over or under-estimation of that value will impair eluent subtraction accuracy. The use of the $\log(\text{eigenvalues})$ obtained from a singular value decomposition (SVD) analysis [5.9] of the **RSM** matrix is proposed. The chemical rank has a good correlation with the number of significant singular values of the data matrix, providing that the spectra of the absorbing components are linearly independent of each other [5.23]. After determination of the chemical rank, the spectra of the k_{opt} 'pure' components (i.e. $\mathbf{S}_k(j \times k_{opt})$) are calculated from the **RSM** data matrix using SIMPLISMA.

Each spectrum r ($1 \times j$) included in the **SM** ($n \times j$) can be expressed by the following equation:

$$r = \mathbf{C}_k \mathbf{S}'_k + \mathbf{Z} \quad (\text{Equation 5.1})$$

where $\mathbf{C}_k(1 \times k_{opt})$ corresponds to the concentrations of the k_{opt} background components with pure spectra \mathbf{S}_k and $\mathbf{Z}(1 \times j)$ to the absorbance due to the eluting analytes.

As the background absorption is much more intense than that due to the analytes, for each spectrum \mathbf{r} to be background corrected the corresponding \mathbf{C}_k values can be directly estimated by classical least squares (CLS) using Equation 5.2.

$$\mathbf{C}_k = (\mathbf{S}_k^T \mathbf{S}_k)^{-1} \mathbf{S}_k^T \mathbf{r}^T \quad (\text{Equation 5.2})$$

Afterwards, the background-corrected chromatogram (\mathbf{Z}) is obtained by subtracting the estimated spectral background.

Using the logarithm of the *eigenvalues* for chemical rank selection is simple but it might fail in some cases, like in the presence of significant components at low concentrations [5.24]. So, in addition, the optimization of the background correction accuracy of the **RSM** matrix as a function of k_{opt} is proposed. Using venetian blinds cross validation with one data split, the **RSM** ($m \times j$) is split into two blocks: **A** and **B**. Then, the SIMPLISMA background correction approach described before is performed iteratively on **B** employing the spectra of k components ($k = (1, \dots, k_{max})$) extracted using the **A** sub-dataset as **RSM**. For each considered k value, the background correction accuracy is measured as the mean absolute values of the corrected matrix **B**. The same process is performed using **B** as 'reference matrix' for the background correction of **A**. Finally, the mean of the correction accuracy values for each k value is calculated. From results obtained, the k_{opt} is selected as a function of the mean correction error which has to drop down to a threshold value defined by the user based on previous experience (e.g. noise values obtained under isocratic conditions using the same LC-IR set up).

Method 2: PCA-BGC-RSM

First, background absorption during gradient elution is gathered in the k_{opt} loading vectors $\mathbf{P}(j \times k_{opt})$ calculated by PCA of the spectral subspace formed by the **RSM** dataset. Then, new observations (i.e. spectra in **SM**) are projected onto the hyperspace defined by the PCA loading vectors to obtain their scores ($\mathbf{T}(n \times k_{opt})$). Next, the background estimate of the **SM** matrix is calculated as \mathbf{TP}' . Afterwards, the

background-corrected chromatogram is calculated by subtracting the estimated spectral background from the raw data.

The calculation of the Q statistic as the sum of squares of the residual values of new samples (i.e. **SM**) provides a measure of the variation of new data outside of the PCs included in the model calculated from the **RSM** data. Therefore, the presence of analytes in the **SM** spectra produces a change in the covariance structure of the model, increases the Q values obtained and allows for an easy identification of the elution windows of the analytes. This information can also be used, for example, to include 'background' **SM** spectra for a post-run background correction. The use of **RSM** data is not limited to the background correction methods described in this work. For example, the use of a **RSM** matrix as B-subspace in the EBS method [5.16, 17] appears to be a promising way to facilitate the use of this method as well.

Multivariate curve resolution – Alternating least squares (MCR-ALS)

MCR-ALS is a widely used multivariate self-modeling curve resolution [5.9]. When analyzing multivariate hyphenated chromatographic data, every chromatographic run can be expressed as:

$$\mathbf{D} = \mathbf{C} \mathbf{S}' + \mathbf{E} \quad (\text{Equation 5.3})$$

where rows of matrix $\mathbf{D}(n \times j)$ are the n spectra recorded and columns are the elution profiles at the j measured channels (i.e. wavenumbers in this work); $\mathbf{C}(n \times k)$ is the matrix of the elution profiles of the k compounds resolved, $\mathbf{S}'(k \times j)$ is the matrix of their corresponding resolved spectra and $\mathbf{E}(n \times j)$ corresponds to unexplained data variance.

To solve the bilinear model given before, an Alternating Least Squares (ALS) algorithm is used [5.10]. The iterative ALS algorithm calculates at each iteration estimates of \mathbf{C} and \mathbf{S}' pure matrices optimizing the fit to the original data matrix \mathbf{D} and minimizing the remaining unexplained variance \mathbf{E} . The optimization is performed for a number of components and employs initial estimates of either \mathbf{C} or \mathbf{S}' obtained using either Evolving Factor Analysis (EFA) or SIMPLISMA, among other possible methods. The optimization is finished when the restitution of the original data matrix \mathbf{D} is satisfactory and a convergence criterion is met [5.8, 24]. ALS results can be improved when

constraints are applied during the optimization with the goal of obtaining calculated spectra and concentration profiles with physically sound shapes [5.8, 9] like non-negative spectra and concentration profiles and unimodal elution profiles.

MCR-ALS analysis of background corrected data had two objectives: (i) resolve co-eluting compounds to obtain their elution and spectral profiles and (ii) improve background correction.

5.3 Material and methods

Apparatus and Reagents

Data set 1 consists of 773 FTIR spectra collected during the gradient LC injection of a diluted soft drink sample [5.25]. A Dionex (Sunnyvale, CA, USA) P680 high performance liquid chromatographic system, equipped with a Kromasil 100 NH₂ column (250 x 2 mm, 5 μm) from Scharlab S.L. (Barcelona, Spain) was employed and linear CH₃CN:H₂O gradients were run from 75 to 55% v/v CH₃CN. Data set 2 consists of 731 FTIR spectra collected during the gradient LC injection of a nitrophenol standard mixture [5.26] containing 4-nitrophenol (4-NP), 2,4-dinitrophenol (2,4-dNP), 2-nitrophenol (2-NP) and 3-methyl-4-nitrophenol (3m4-NP) in a 85:15 v/v H₂O (0.08% v/v TFA):CH₃CN (0.08% v/v TFA) solution. The standard mixtures were analyzed using the same LC system as described above, employing a C₁₈ column (150 x 2 mm, 5 μm) and running mobile phase gradients from 65:35 v/v H₂O (0.08% v/v TFA): CH₃CN (0.08% v/v TFA) to 15:85 v/v H₂O (0.08% v/v TFA): CH₃CN (0.08% v/v TFA). **RSMs** for both examples were recorded during system equilibration after gradient injection.

On-line hyphenation was carried out employing an IR transparent flow cell, constructed using CaF₂ and ZnSe windows and an aluminium spacer with a pathlength of 16.5 μm, installed on a Bruker (Bremen, Germany) IFS 66/v FTIR spectrometer equipped with a liquid nitrogen refrigerated mercury–cadmium–telluride detector, a vacuum system and a dry air purged sample compartment. The scanner of the interferometer was operated at a HeNe laser modulation frequency of 100 kHz. For data set 1 and 2 spectra were recorded in the range between 2379.9 and 948.9 cm⁻¹ and between 2457 and 948.9 cm⁻¹, using the spectrum of the empty sample compartment as background.

Spectra were acquired using a resolution of 8 cm^{-1} , a zerofilling factor of 2 and co-adding 25 scans per spectrum, which provided a spectra acquisition frequency of $15 \text{ spectra min}^{-1}$.

Software and algorithms

Bold-face capital letters represent matrices, bold-face lowercase characters represent vectors, and italic, lower case letters represent scalars. On-line LC-IR data was collected in spectral data matrices X ($n \times j$) where each row contains a spectrum n measured at j wavenumbers.

For data acquisition as well as instrumental and measurement control, the OPUS software (version 6.5) from Bruker was employed. Data analysis was run under Matlab 7.7.0 from Mathworks (Natick, USA, 2004) using in-house written MATLAB functions and the PLS Toolbox 6.0 from Eigenvector Research Inc. (Wenatchee, WA, USA). Multivariate Curve Resolution was carried out using the MATLAB MCR-ALS toolbox [5.27] available at <http://www.mcrals.info/>.

Prior to background correction, negative absorbance values were removed in each spectrum by subtraction of its minimum value. The quality of the background corrected and MCR-ALS recovered spectral profiles was evaluated using the criterion of similarity ($0 \leq r \leq 1$) [5.28], which entails a comparison of a reference spectrum with the spectrum to be evaluated according to the following equation:

$$R = \frac{r_i^T s_i}{\|r_i\| \|s_i\|} \quad (\text{Equation 5.4})$$

where r_i and s_i are the reference and recovered spectra of the compound i .

5.4 Results and discussion

Spectral changes

LC-IR spectra included in data set 1 acquired during an acetonitrile:water LC gradient injection are depicted in Figure 5.1. In reversed phase LC, the eluent absorbs intensely in the mid-IR region obscuring the absorption of the analytes [5.29]. In this type of measurements the intensities of the eluting analytes are usually $<10 \text{ mAU}$, whereas the mobile phase signal reaches intensities up to 1000 mAU . Strong changes in intensity

and shape of the background signal can clearly be observed in the region from 2400 to 950 cm^{-1} , were most of the investigated analytes show their characteristic bands, which evidences the need for an accurate method for the compensation of the IR background eluent contribution. A detailed view of the H_2O bending vibration in the region around 1640 cm^{-1} is provided to stress the occurring band shifts during the gradient which complicate accurate background compensation. A detailed description of the IR bands in $\text{CH}_3\text{CN}:\text{H}_2\text{O}$ systems can be found elsewhere [5.30].

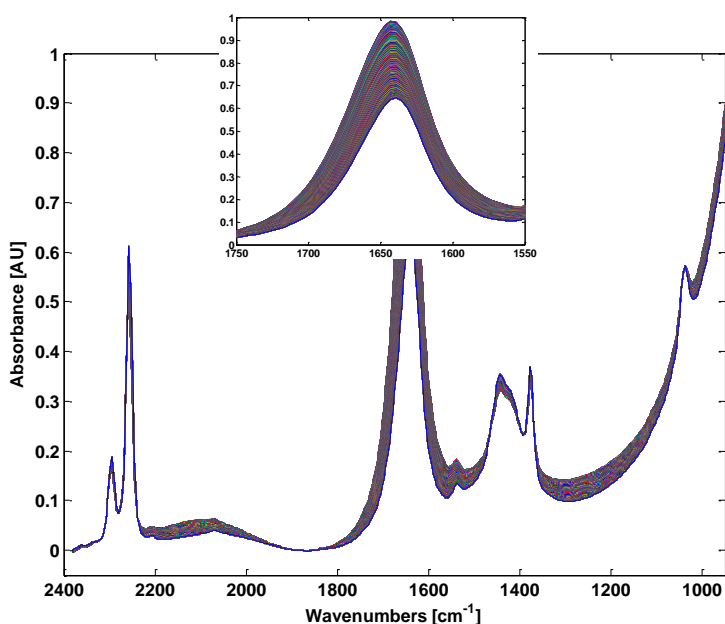


Figure 5.1. Spectra between 2400 and 950 cm^{-1} obtained during the re-equilibration of an LC-IR system after a CH_3CN (0.08% v/v TFA): H_2O (0.08% v/v TFA) gradient run from 35 to 85% v/v CH_3CN . The close-up view shows an amplification of the region between 1550 and 1750 cm^{-1} for a better visualization of the water band shift as a function of the elution gradient.

Data set 1: Carbohydrate analysis

Background correction

Figure 5.2 displays results obtained using the SIMPLISMA background correction approach. Figure 5.2a shows the plot of the $\log(\text{eigenvalues})$ in descending order obtained from the SVD analysis of the **RSM** (456×372) matrix. This figure suggests

the use of five components for background correction. The selection of this k_{opt} was supported by results depicted in Figure 5.2b. In this figure, as previously described, the effect of increasing k_{opt} on the background accuracy is evaluated using the **RSM** data and venetian blinds cross validation (CV) with one data split. A possible advantage of this second plot is that the spectral noise values depicted do have a meaning in the spectroscopic sense, since they are in the same units as the absorbance measurements and they can be compared directly with known estimates of noise level. In this case, for 5 components the mean noise level was $2 \cdot 10^{-5}$, which agrees with our independent estimations of noise level ($1.85 \cdot 10^{-5}$). This comparison facilitates the accurate selection of the adequate number of components. The combined use of both plots is an effective way to simplify the k_{opt} selection process.

Figure 5.2c shows the corresponding spectra of the pure components obtained using SIMPLISMA (i.e., \mathbf{S}_k). Band shapes and relative intensities of the extracted spectra are similar and describe the changes in intensity and shape observed during the $\text{CH}_3\text{CN}:\text{H}_2\text{O}$ gradient shown in Figure 5.1. Using these initial solvent spectra estimates, their corresponding elution profiles during the sample gradient (i.e. \mathbf{C}_k) were calculated by ordinary classical least squares (CLS). Subsequently, the whole solvent background contribution obtained by calculating the product of $\mathbf{C}_k \mathbf{S}_k^T$ was subtracted from **SM** matrix, obtaining data shown in Figure 5.2d. The correlation coefficients between reference analyte spectra and those extracted at the peak apex after background correction from 1396 to 1022 cm^{-1} were 0.95 and 0.88, for fructose and glucose, respectively. As an example, Figure 5.2e shows a chromatogram extracted at 1072 cm^{-1} where two peaks corresponding to fructose and glucose can clearly be identified. The baseline is characterized by the absence of slope and randomly distributed noise around zero absorbance.

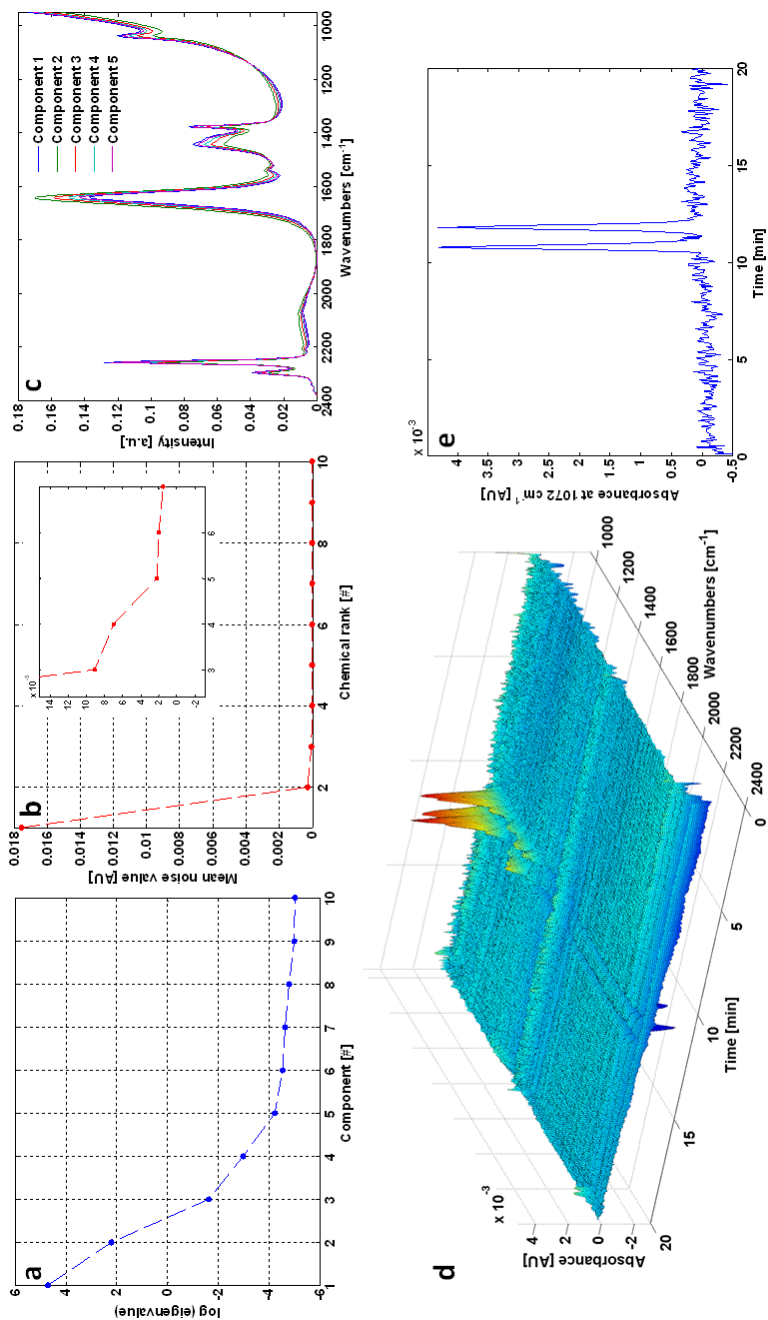


Figure 5.2. Results of the background correction of the Data set 1 following the SIMPLISMA approach.

Results of the PCA background correction approach using five principal components are shown in Figure 5.3. Figure 5.3 (top) shows the loadings calculated using the spectra included in the **RSM** (i.e. calibration block). Again, the spectral features of loadings agree well with the observed spectral changes during the LC gradient (see Figure 5.1). Then, using the score values obtained from the projection of the **SM** (317×372) spectra onto the space defined by the five PCA loading vectors, the background absorption is calculated as TP' , where **P** (372×5) is the k_{opt} loadings matrix and **T** (317×5) is the scores matrix of the **SM**.

Obtained background corrected spectra acquired during the injection of a sample containing fructose and glucose are shown in Figure 5.3 (middle). The correlation coefficients between reference spectra and those extracted at the peak apex after background correction in the 1396 to 1022 cm^{-1} range were 0.95 and 0.87 for fructose and glucose, respectively, using the PCA approach, being similar to those found using SIMPLISMA. From the plot of the calculated Q-residual values of the spectra included in both, the **RSM** and the **SM** matrix, the elution of the analytes can be easily identified (see Figure 5.3, bottom).

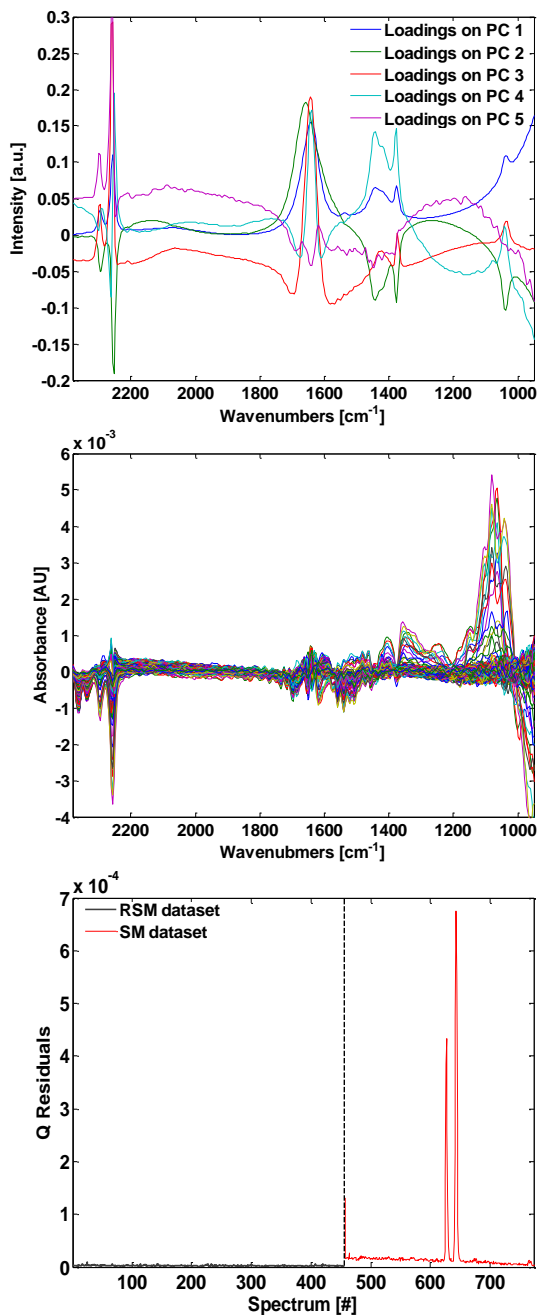


Figure 5.3. Results of the background correction of data set 1 following the PCA approach.

MCR-ALS

As previously shown, in this case both background correction methods provided similar results using five components. Results obtained using the SIMPLISMA approach have been chosen to show the performance of MCR-ALS analysis on background corrected data.

During MCR-ALS optimization, the model is fitted with a pre-defined number of components, k_{opt} , using initial estimates of either the C or the S^T matrix. Initially, $\log(\text{eigenvalues})$ obtained from a SVD analysis (see Figure 5.4, top, left) and EFA analysis (results not shown) of the background corrected SM matrix indicated the possible presence of four components. The initial estimates of spectra of these four components were obtained using SIMPLISMA. Using these spectra, the corresponding concentration profiles of the four components in the corrected SM matrix were calculated by CLS (see Figure 5.4, top, right). Whereas the concentration profiles calculated for components 1 and 3 had usual LC shapes, this was not the case for components 2 and 4, which only seem to contain background changes still present in the data set after its previous correction.

MCR-ALS was performed using the following ALS constraints applied to components 1 and 3: non-negativity of the concentration profiles and unimodality. Besides, a convergence criterion of 0.02 and spectra normalization to equal area were employed. Unimodality forces the concentration profiles to have a single peak apex. Its application has no sense for the resolution of residual solvent and instrumental drift contributions [5.31]. Under these conditions, convergence was achieved after 8 iterations, providing a percentage of explained variance of 90.2%. The time-dependent concentration profiles obtained from MCR-ALS resolution are shown in Figure 5.4 (bottom, left).

Concentration profiles of components 2 and 4 are noisy and showed anti-correlated trends related to residual solvent and background changes as well as to possible detector drifts. This was confirmed by spectral profiles shown in Figure 5.4 (bottom, right) in which spectral features due to CO_2 and H_2O vapor were only present in spectra of components 2 and 4. Correlation coefficients between optimum MCR-ALS spectral profiles and reference spectra were 0.94 and 0.89 for fructose and glucose, respectively, in the 1396 and 1022 cm^{-1} range.

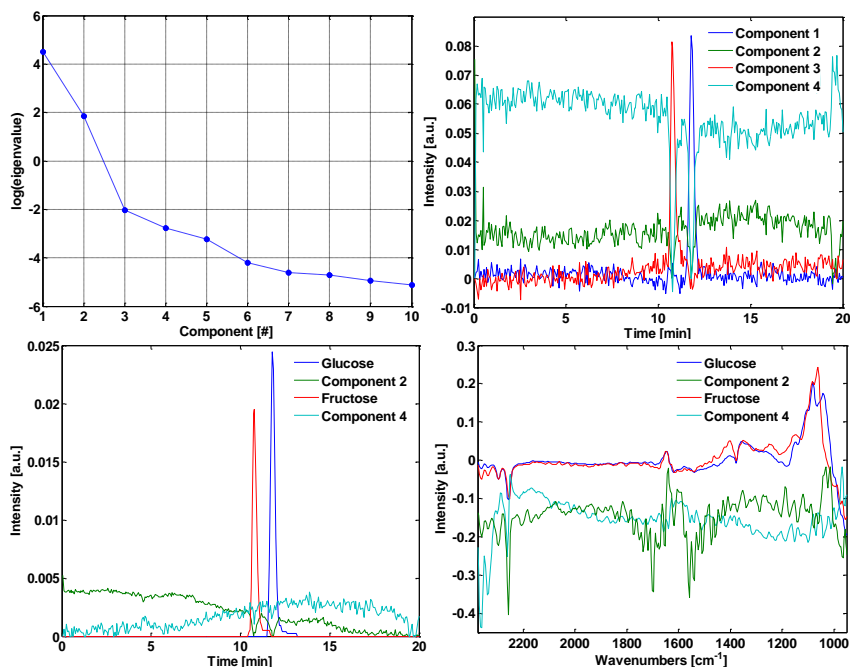


Figure 5.4. MCR-ALS analysis of Data set 1 after background correction: top: selection of the chemical rank using SVD (left) and SIMPLISMA initial estimates of the concentration profiles (right), bottom: calculated MCR-ALS concentration traces (left) and calculated MCR-ALS spectra (right).

Peak integration was easier and more reproducible due to the remarkable improvement of the signal-to-noise ratio of the elution profiles of components 1 and 3, as compared to those found in a typical extracted chromatogram at a selected wavenumber (see Figure 5.5).

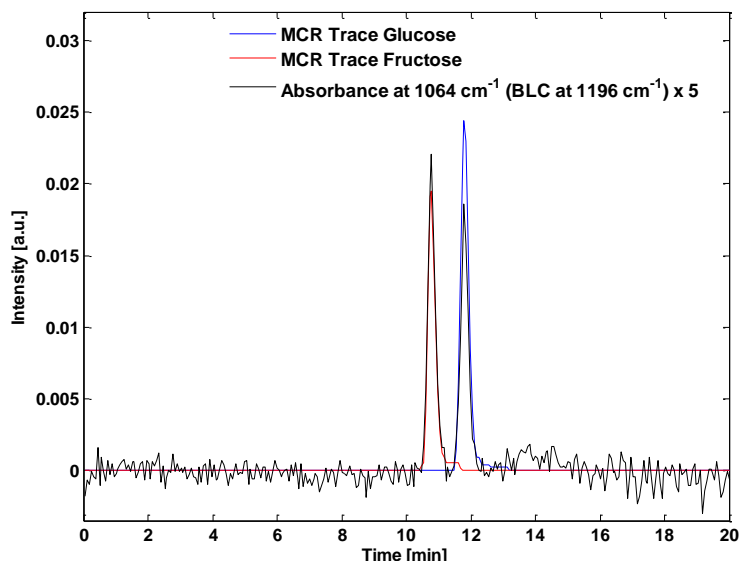


Figure 5.5. Resolved MCR-ALS concentration profiles of fructose and glucose together with an extracted background corrected chromatogram at 1064 cm^{-1} using a baseline correction at 1196 cm^{-1} .

Data set 2: Nitrophenol analysis

Background correction

In this second example, a standard mixture of four nitrophenols was analyzed by LC using a $\text{CH}_3\text{CN}:\text{H}_2\text{O}$ solvent gradient. In Figures 5.6a and b the $\log(\text{eigenvector})$ values and the noise levels found as a function of the chemical rank are represented. From results shown, a k_{opt} value of 6 was selected for background correction. Corresponding spectra of the six components obtained by SIMPLISMA are represented in Figure 5.6c. Again, the extracted spectra are in agreement with spectral changes observed as a consequence of the LC gradient.

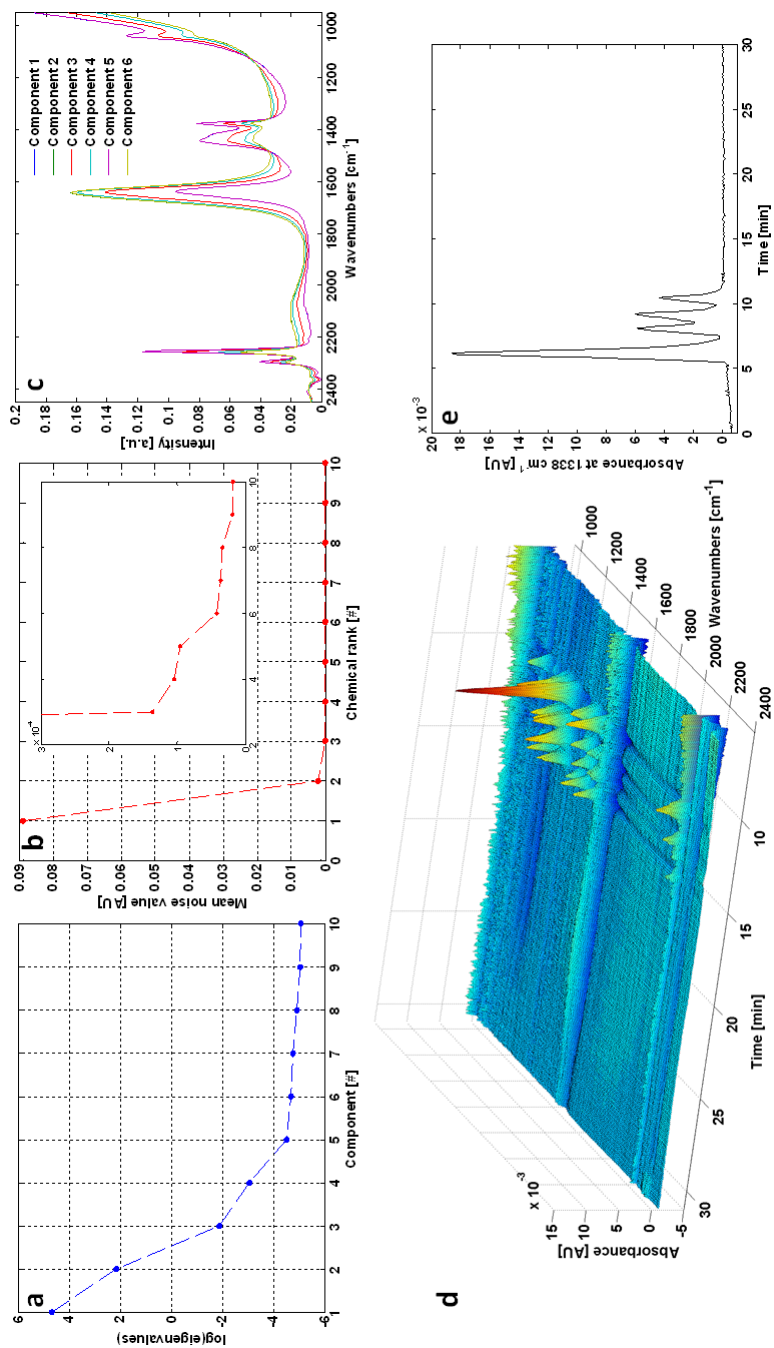


Figure 5.6. Results of the background correction of Data set 2 following the SIMPLISMA approach.

The resulting background corrected data set is depicted in Figure 5.6d. A good compensation of the mobile phase contribution to the overall signal can be observed. After background correction a non-sloping baseline was obtained and the four analytes were clearly identified. The chromatographic overlapping between components 2 and 3 is shown in Figure 5.6e where a chromatogram extracted at 1338 cm^{-1} using a single point baseline correction at 1404 cm^{-1} is depicted.

Remarkable low noise values were achieved throughout the whole spectrum. For example, the noise (measured as peak-to-peak) at 1800 cm^{-1} was below 0.2 mAU. Even at 1640 cm^{-1} , where water shows very intense absorbance, the observed noise was below 3 mAU. Correlation coefficients between the spectra at the peak apex after background correction using the SIMPLISMA approach and the reference spectra were 0.96, 0.93, 0.95 and 0.90 for 4-NP, 2-NP, 3m4-NP and 2,4-dN, respectively, in the spectral region from 1000 to 1700 cm^{-1} .

Results of the PCA background correction approach using 6 principal components to describe the **RSM** (352×392) data variance are summarized in Figure 5.7. Figure 5.7 (top) shows the calculated PCA loadings (**P**) and in Figure 5.7 (middle) the background corrected data matrix **SM** (379×392) is represented. Correlation coefficients between the spectra at the peak apex after background correction and the reference spectra were in this case 0.96, 0.92, 0.93 and 0.88 for 4-NP, 2-NP, 3m4-NP and 2,4-dN, respectively, using the same spectral range as before. In spite of the good background correction accuracy, a series of negative bands are present in the background corrected data. These spectral artifacts could not be eliminated by using a different number of principal components to model the eluent subspace (data not shown). Again, the elution of the analytes could be accurately determined from the Q-residuals plot shown in Figure 5.7 (bottom).

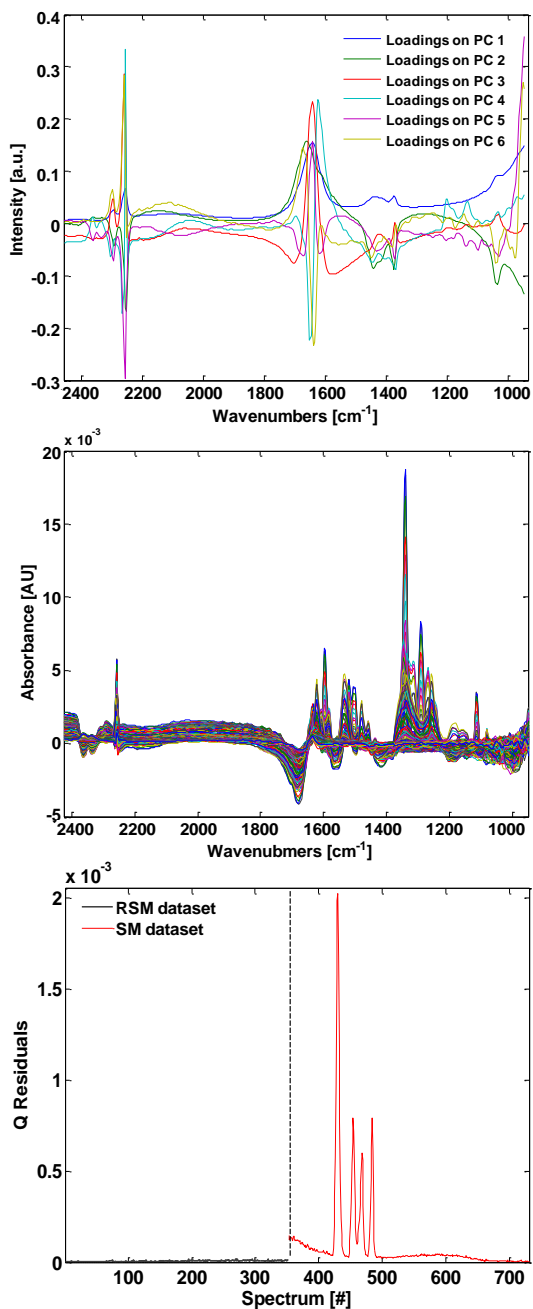


Figure 5.7. Results of the background correction of Data set 2 following the PCA approach.

MCR-ALS

MCR-ALS was applied to the background corrected data using the PCA approach. Here, a total number of six components was selected from the $\log(\text{eigenvalues})$ plot obtained from SVD analysis of the background corrected **SM** matrix (see Figure 5.8 top, left). Figure 5.8 (top, right) shows the concentration profiles of the components obtained using SIMPLISMA and CLS which were subsequently used as initial estimates for the ALS resolution. A visual observation of the initial estimates helps to conclude that components 1, 2, 4 and 5 correspond to the four analytes 4-NP, 2-NP, 3m4-NP and 2,4-dN, respectively, and components 3 and 6 contained remaining spectral variation due to eluent gradient changes as well as changes in the instrumental conditions (e.g. detector drifts).

Non-negativity and unimodality constraints (applied to components 1, 3, 4 and 5) were imposed to ALS optimization. Spectra normalization to equal area and a convergence criterion of 0.02 were also employed. Convergence was achieved after 8 iterations, with a lack of fit of 21% and a percentage of explained variance of 92%. Outcomes of the MCR-ALS optimization are shown in Figure 5.8 (bottom, left). Elution peaks of 4-NP, 2-NP, 3m4-NP and 2,4-dN can be clearly seen in the MCR-ALS elution profiles. Again, correlation coefficients between reference and MCR-ALS recovered spectra in the 1700 and 1000 cm^{-1} range were calculated to evaluate the spectral recoveries. Values found for 4-NP, 2-NP, 3m4-NP and 2,4-dN after ALS resolution of the **SM** corrected using the PCA approach were 0.97, 0.92, 0.95 and 0.90, respectively.

Using the SIMPLISMA corrected **SM** data matrix, ALS spectral recovery values obtained for 4-NP, 2-NP, 3m4-NP and 2,4-dN after 3 iterations were 0.96, 0.93, 0.92 and 0.86, respectively, in the 1700 and 1000 cm^{-1} range. Correlation values before and after MCR-ALS were also in this case comparable. As an example, the spectrum extracted from the peak apex of 4-NP of the background corrected data, its reference spectrum measured under stopped-flow conditions and the MCR-ALS calculated spectrum are depicted in Figure 5.8 (bottom, right). Whereas after MCR-ALS analysis of background corrected data only minor changes in the spectral recovery values were found, ALS resolved concentration profiles showed, as previously, improved signal-to-noise ratios

in comparison to those obtained from extracted chromatograms at selected wavenumbers.

It must be remarked that, like in the previous example, the use of further options of MCR-ALS (e.g. matrix augmentation, equality constraints for concentration and/or spectra) was out of the scope of the present work. For quantitative and qualitative analysis, the use of multiple matrices of different mixtures at different concentration levels would likely improve the presented results. An evaluation of the use of these options and constraints for LC-IR data is still in progress and will be reported.

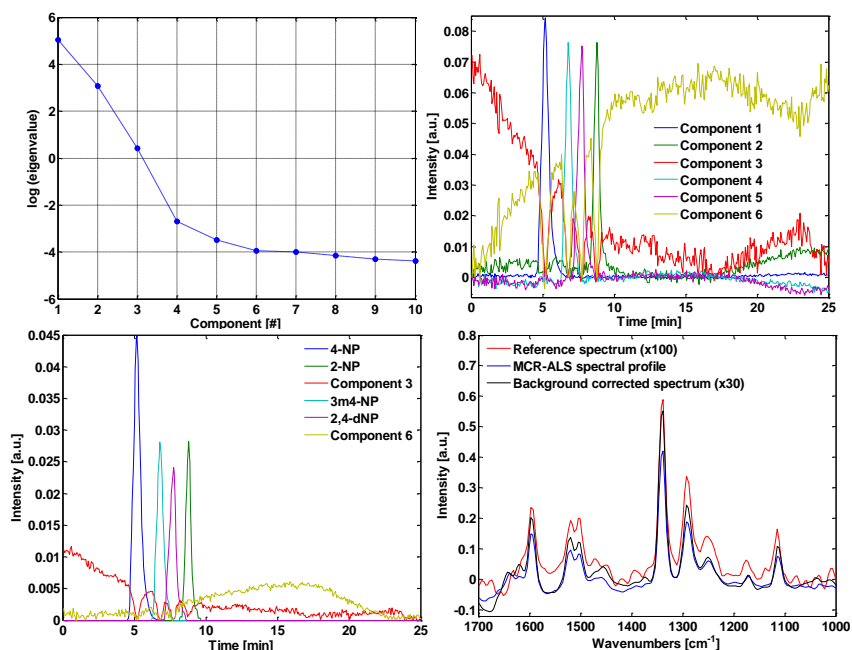


Figure 5.8. MCR-ALS analysis of Data set 2 after background correction; top: selection of the chemical rank using SVD (left) and SIMPLISMA initial estimates of the concentration profiles (right) and bottom: calculated MCR-ALS concentration traces for the 6 components (left) and reference spectrum, calculated MCR-ALS spectral profile and spectrum extracted at the peak apex after background correction of 4-NP (right).

5.5 Conclusions

The contribution of background absorption to overall LC-IR signals could be compensated using two straightforward approaches based on PCA and SIMPLISMA and on the use of the spectral information obtained during the equilibration of the LC system.

When applying MCR-ALS directly to on-line gradient LC-IR data for the resolution of the spectra and concentration profiles of eluting analytes, good results are difficult to obtain due to the high background contribution. On the contrary, when MCR-ALS was applied to background-corrected data, chemical rank selection and both, peak and spectral resolution could be achieved. Besides, remaining signal variation due to background absorption and detector drift could also be compensated. Results found in on-line gradient LC-IR analysis of carbohydrates and nitrophenols as model examples illustrate well the potential of the assessed approach.

5.6 References for Chapter 5

- [5.1] S. Wold, K. Esbensen, P. Geladi, *Chemometrics and Intelligent Laboratory Systems*, 2 (1987) 37-52.
- [5.2] M. Maeder, *Analytical Chemistry*, 59 (1987) 527-530.
- [5.3] H.R. Keller, D.L. Massart, *Analytica Chimica Acta*, 263 (1992) 21-28.
- [5.4] W. Windig, J. Guilment, *Analytical Chemistry*, 63 (1991) 1425-1432.
- [5.5] R.A. Harshman, M.E. Lundy, *Computational Statistics & Data Analysis*, 18 (1994) 39-72.
- [5.6] H.A.L. Kiers, J.M.F. Ten Berge, R. Bro, *Journal of Chemometrics*, 13 (1999) 275-294.
- [5.7] R. Bro, C.A. Andersson, H.A.L. Kiers, *Journal of Chemometrics*, 13 (1999) 295-309.
- [5.8] R. Tauler, *Chemometrics and Intelligent Laboratory Systems*, 30 (1995) 133-146.
- [5.9] A. de Juan, R. Tauler, *Journal of Chromatography A*, 1158 (2007) 184-195.
- [5.10] E. Pere-Trepat, A. Hildebrandt, D. Barcelo, S. Lacorte, R. Tauler, *Chemometrics and Intelligent Laboratory Systems*, 74 (2004) 293-303.
- [5.11] E. Pere-Trepat, S. Lacorte, R. Tauler, *Analytica Chimica Acta*, 595 (2007) 228-237.
- [5.12] E. Pere-Trepat, R. Tauler, *Journal of Chromatography A*, 1131 (2006) 85-96.
- [5.13] S. Mas, G. Fonrodona, R. Tauler, J. Barbosa, *Talanta*, 71 (2007) 1455-1463.
- [5.14] A. Edelmann, J. Diewok, J.R. Baena, B. Lendl, *Analytical and Bioanalytical Chemistry*, 376 (2003) 92-97.
- [5.15] C. Ruckebusch, F. Vilmin, N. Coste, J.P. Huvenne, *Applied Spectroscopy*, 62 (2008) 791-797.
- [5.16] H.F.M. Boelens, R.J. Dijkstra, P.H.C. Eilers, F. Fitzpatrick, J.A. Westerhuis, *Journal of Chromatography A*, 1057 (2004) 21-30.
- [5.17] R.J. Dijkstra, H.F.M. Boelens, J.A. Westerhuis, F. Ariese, U.A.T. Brinkman, C. Gooijer, *Analytica Chimica Acta*, 519 (2004) 129-136.
- [5.18] E.R. Malinowski, *Analytical Chemistry*, 49 (1977) 612-617.
- [5.19] P.H.C. Eilers, *Kwant. Meth.*, (1988).
- [5.20] K. Istvan, R. Rajko, G. Keresztury, *Journal of Chromatography A*, 1104 (2006) 154-163.

- [5.21] J. Kuligowski, G. Quintas, R. Tauler, B. Lendl, M. De la Guardia, *Analytical Chemistry*, DOI: 10.1021/ac2004407 (2011).
- [5.22] D. Bylund, R. Danielsson, K.E. Markides, *Journal of Chromatography A*, 915 (2001) 43-52.
- [5.23] C.J. Xu, Y.Z. Liang, Y. Li, Y.P. Du, *Analyst*, 128 (2003) 75-81.
- [5.24] M. Meloun, J. Capek, P. Miksik, R.G. Brereton, *Analytica Chimica Acta*, 423 (2000) 51-68.
- [5.25] J. Kuligowski, G. Quintas, S. Garrigues, M. de la Guardia, *Talanta*, 77 (2008) 779-785.
- [5.26] J. Kuligowski, G. Quintas, S. Garrigues, M. de la Guardia, *Talanta*, 80 (2010) 1771-1776.
- [5.27] J. Jaumot, R. Gargallo, A. de Juan, R. Tauler, *Chemometrics and Intelligent Laboratory Systems*, 76 (2005) 101-110.
- [5.28] V. Gómez, M. Miró, M.P. Callao, V. Cerdà, *Analytical Chemistry*, 79 (2007) 7767-7774.
- [5.29] M. Kölhed, B. Lendl, B. Karlberg, *Analyst*, 128 (2003) 2-6.
- [5.30] T. Takamuku, M. Tabata, A. Yamaguchi, J. Nishimoto, M. Kumamoto, H. Wakita, T. Yamaguchi, *Journal of Physical Chemistry B*, 102 (1998) 8880-8888.
- [5.31] E. Pere-Trepas, S. Lacorte, R. Tauler, *Journal of Chromatography A*, 1096 (2005) 111-122.

CHAPTER 6. CHEMOMETRIC EXTRACTION OF 'ANALYTE-SPECIFIC' CHROMATOGRAMS IN ON-LINE LC-IR

6.1 Introduction

Chemometrics has been applied to chromatography for a variety of purposes such as signal enhancement (de-noising), warping (synchronization of the time axis of different chromatograms) and many other tasks [6.1]. Concerning on-line LC-IR, there has been a steady effort to develop and/or apply existing univariate and multivariate chemometric approaches to improve background correction accuracy. Among others, recently a new strategy for background correction based on the use of a reference spectra matrix (**RSM**) has been developed as described in Chapters 3 and 4. Although the usefulness and ease of application of this approach have been demonstrated, it presents a series of requirements and conditions of applicability: i) a very good instrument stability is needed; ii) an appropriate measurement of the **RSM** has to be carried out; and iii) the mobile phase spectra should present a spectral region characteristic of its composition free from interferences from the eluting compounds. While the first two conditions depend on the quality of the instrument and the users expertise, the latter might reduce the applicability of the technique, especially if a relatively narrow mid-IR spectral range is used for the measurement, e.g. if instead of a FTIR spectrometer equipped with a Global mid-IR source, high power tuneable laser sources [6.2] capable of providing continuous tuning of up to 250 cm^{-1} are employed to improve the sensitivity of the detection. Therefore, the development of alternative chemometric strategies for on-line IR detection is crucial for an extension of both, the applicability of

this type of spectrometry as well as for a further improvement of its sensitivity in LC systems.

Ralf Marbach at the VTT Optical Instrument Center (Oulu, Finland) [6.3-5] has developed a method for multivariate calibration named 'Science Based Calibration' (SBC) that combines the main features of 'classical' and 'inverse' calibrations. By estimating the spectral signal in a physical way and the spectral noise in a statistical way, the SBC method combines the prediction accuracy of the 'inverse' approach with the low cost and easy interpretability of the 'classical' models. Results obtained by SBC are based on user-estimates of both, the analyte signal (e.g. spectrum) and spectral 'noise', Σ . Previous works have shown that under many circumstances the SBC method can provide significant advantages over other widely used multivariate techniques such as Partial Least Squares (PLS). Using SBC, the cost and time of multivariate calibration can be drastically reduced while at the same time the quality of results is increased as a highly specific response is provided.

For a detailed description of the method see references [6.3] and [6.5] as well as Chapter 2.2 "Monitoring of polymerized triglycerides in deep-frying olive oil by on-line GPC-IR spectrometry using the Science Based Calibration multivariate approach". In short, using SBC, the concentration of the analyte (y_{pred}) in each unknown sample spectrum (x_{pred}) is predicted using the vector $b_{opt(1)}$ as described in Equation 6.1:

$$y_{pred} = \bar{y} + (x_{pred} - \bar{x})^T \cdot b_{opt(1)} \quad (\text{Equation 6.1})$$

being, \bar{y} the mean value of the analyte concentration and \bar{x} the mean of the measured 'noise' spectra X ($m \times k$).

As it can be seen, the prediction of the analyte concentration by SBC is based on the information content of a user defined 'noise' matrix and an analyte spectrum g^T ($1 \times k$). This feature is well aligned with the current characteristics of many on-line LC-IR detection systems: i) the spectra of the target analytes can often be obtained experimentally and ii) if the IR spectrum of the mobile phase is continuously recorded during a blank gradient LC run, then the resulting data matrix can be considered as a 'noise' matrix as it includes both, interfering spectra corresponding to the changes in the background absorption due to the composition gradient and instrumental noise.

Accordingly, the use of SBC in on-line systems with changing eluent composition (e.g. gradient elution) for the calculation of time-dependent concentrations of the target

analytes was evaluated as a straightforward way to extract 'analyte-specific' chromatograms. The proposed strategy aims to overcome existing limitations and requirements of RSM-based strategies for background correction in on-line LC-IR for both, quantitative and qualitative purposes.

To test the suitability of SBC in on-line LC-IR, a series of real on-line LC-IR separations of four nitrophenols (2-nitrophenol, 3-methyl-4-nitrophenol, 2,4-dinitrophenol and 4-nitrophenol) with highly correlated mid-IR spectra, was carried out under gradient conditions. Experimental conditions were chosen to achieve a significant overlapping of the chromatographic peaks of 3-methyl-4-nitrophenol, 2,4-dinitrophenol and 4-nitrophenol. Focusing on the determination of 2,4-dinitrophenol, the use of SBC was evaluated in two situations which differed in the amount of previous knowledge available about other sample constituents with strongly overlapping spectra.

6.2 Material and methods

Apparatus and Reagents

A Dionex (Sunnyvale, CA, USA) P680 high performance liquid chromatography system, equipped with a C₁₈ column (150x2.0 mm, 5 μm) maintained at 22°C was employed using a sample injection loop of 20 μL. Mobile phase gradients were run from 35:65 to 85:15 v/v acetonitrile:water in 20 minutes.

An IR transparent flow cell was constructed using CaF₂ windows and an aluminium spacer with a channel width of 3.5 mm and an optical pathlength of 16.5 μm. For FTIR spectra acquisition a Bruker (Bremen, Germany) IFS 66/v FTIR spectrometer equipped with a liquid nitrogen refrigerated MCT detector, a vacuum system and a dry air purged sample compartment was used. The scanner of the interferometer was operated at a HeNe laser modulation frequency of 100 kHz. Spectra were recorded in the range between 1700 and 1000 cm⁻¹, with a resolution of 8 cm⁻¹ and a zerofilling factor of 2 and using the spectrum of the empty sample compartment as background. A grating to attenuate the intensity of the irradiating light on the detector element was also used. During gradient experiments, 25 scans per spectrum were averaged, providing a spectra acquisition frequency of 15 spectra min⁻¹. Reference spectra of the analytes dissolved in 25:75 v/v acetonitrile:water were acquired in stopped-flow mode, after

filling the flow cell with standard solutions, using a spectrum of the solvent solution as background.

4-nitrophenol (4-NP), 2,4-dinitrophenol (2,4-dNP), 2-nitrophenol (2-NP) (PESTANAL, Fluka, Buchs, Switzerland) and 3-methyl-4-nitrophenol (3m4-NP) (98%, Sigma-Aldrich, Switzerland) standard solutions were prepared by dissolving an appropriate amount of each component in a 25:75 v/v acetonitrile:water solution. Compositions of the standard solutions used throughout this study are indicated in Table 6.1. Solutions were filtered (0.22 μm) prior to injection. HPLC grade acetonitrile was obtained from Scharlau (Barcelona, Spain). De-ionized water was purified with a Millipore system.

Table 6.1. Compositions of the solutions used throughout this study.

Standard	4-NP	3m4-NP	2,4-dNP	2-NP
1	5.08	8.93	9.68	7.75
2	0.00	4.46	4.84	0.00
3	0.51	3.57	3.87	0.78
4	1.27	2.23	1.84	1.94
5	1.27	4.46	1.21	0.97
6	0.36	0.64	0.69	0.55
7 ('sample blank')	1.69	2.98	0.00	2.58

Note: Concentrations in mg mL^{-1} .

Software and algorithms

For instrumental and measurement control as well as for data acquisition, the OPUS software (version 6.5) from Bruker was employed. Data treatment was run under Matlab 7.7.0 from Mathworks (Natick, USA). Matrix inversion, Σ^{-} , was performed using the *pinv* Matlab function which returns the Moore-Penrose pseudoinverse of Σ [6.6].

6.3 Results and discussion

FTIR spectra of mobile phase and analytes

Figure 6.1 (top) shows reference spectra of the four considered nitrophenols (4-NP, 3m4-NP, 2,4-dNP and 2-NP) in the region between 1700 and 1000 cm^{-1} . The most intense bands, located in the regions 1650-1450 cm^{-1} and 1375-1200 cm^{-1} , are assigned to the asymmetric and symmetric NO_2 stretching vibrations, respectively. Besides, C-N stretching frequencies of aromatic nitro-compounds arising in the region 1177-865 cm^{-1} due to the coupling between this vibrational mode and other ring vibrations [6.7] can be observed. In spite of the high structural and spectral similarity of the analytes, their IR spectra present significant characteristic differences which allow their identification.

Figure 6.1 (bottom) shows FTIR spectra in the spectral region between 1700 and 1000 cm^{-1} measured during the LC injection under gradient conditions of a standard solution containing 4-NP (1.27 mg mL^{-1}), 3m4-NP (4.46 mg mL^{-1}), 2,4-dNP (1.21 mg mL^{-1}) and 2-NP (0.97 mg mL^{-1}) using the spectrum of the empty sample compartment as a background. The water deformation band at 1639 cm^{-1} and the libration band below 650 cm^{-1} which produces a significant strong absorption near 1000 cm^{-1} can be identified. Besides, acetonitrile presents three intense bands at 1442, 1416 and 1377 cm^{-1} due to the C-C-H deformation vibration and between 1130 and 950 cm^{-1} caused by the CH_3 rocking absorption [6.8]. Compared to those of the mobile phase, the analyte absorption bands show a relatively low intensity and cannot be discerned in the acetonitrile:water system.

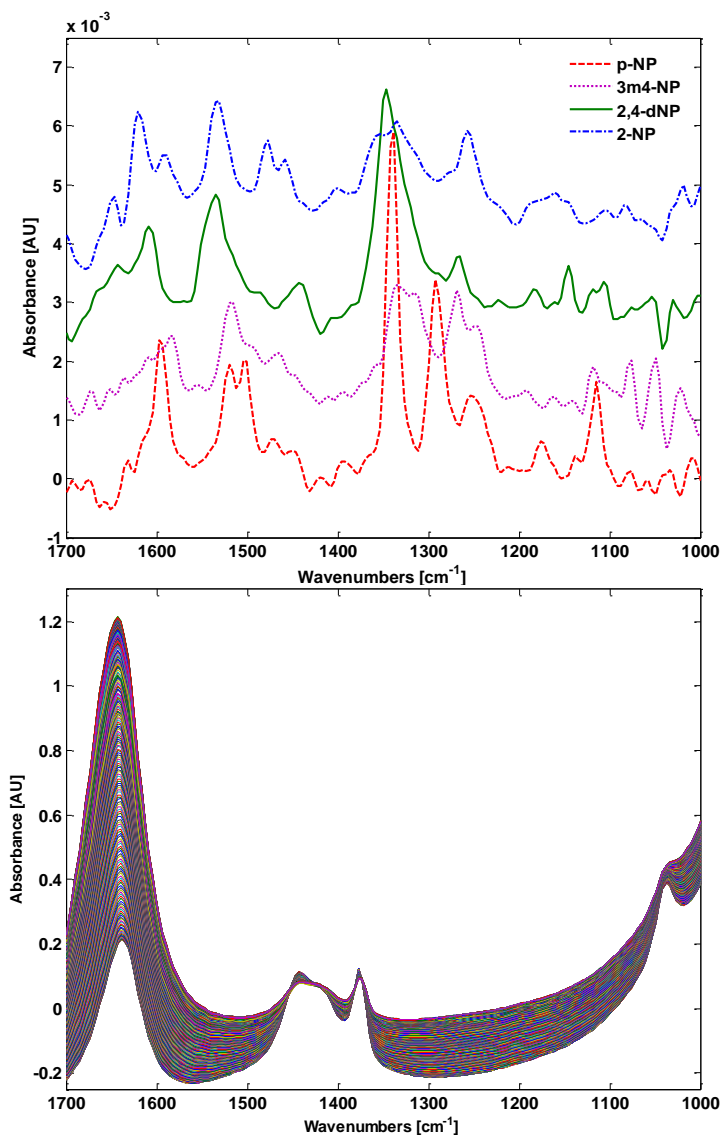


Figure 6.1. Top: FTIR spectra of the analytes dissolved in 25:75 v/v acetonitrile:water in the 1700–1000 cm^{-1} spectral range, using a spectrum of the solvent solution as background (spectra were shifted for a better visualization); bottom: representative set of FTIR spectra in the wavenumber region between 1700 and 1000 cm^{-1} measured during the LC injection of a standard solution containing 4-NP (1.27 mg mL^{-1}), 3m4-NP (4.46 mg mL^{-1}), 2,4-dNP (1.21 mg mL^{-1}) and 2-NP (0.97 mg mL^{-1}) under gradient conditions; spectra were recorded against a background of the empty sample compartment.

Use of SBC in on-line LC-IR

As aforementioned, the aim of this work was the evaluation of the multivariate SBC approach for the extraction of 'analyte-specific' IR chromatograms even when a high spectral and chromatographic overlapping between the analyte of interest and the mobile phase and other co-eluting sample constituents is present. On the one hand side, as it can be seen in Figure 6.1 (top), the characteristic absorption bands of 2,4-dNP overlap with those of 3m4-NP and 2-NP. Hence, it is not possible to select a spectral region free from interferences from the aforementioned compounds for the determination of 2,4-dNP. On the other hand side, the elution order of the selected analytes in the present reversed phase system is 4-NP, 3m4-NP, 2,4-dNP and 2-NP. Hence, the use of a 4-components model system in which 2,4-dNP was considered as the 'target analyte' and 4-NP, 3m4-NP and 2-NP as the 'sample matrix' constituents, was proposed. LC gradient conditions were chosen to i) cover a wide range of mobile phase compositions, and ii) achieve a low chromatographic resolution between the target analyte and other 'sample matrix' analytes.

Specificity of the signal. Using a reference spectrum of 2,4-dNP as a response vector, two different situations were analyzed differing in the amount of previously available information about the sample composition. In the first situation (situation A), the extraction of the 2,4-dNP chromatogram was carried out without any previous knowledge of the spectral features of other interferences present in the sample matrix. Thus, the vector $b_{opt(1)}$ was calculated using a set of spectra measured during the re-equilibration of the LC system after gradient injection as 'noise' matrix. In the second situation (situation B) the 'noise' matrix was composed by spectra recorded during the LC-IR analysis of one single 'sample blank' under gradient conditions. In this case, the 'sample blank' was a standard solution containing the three interfering analytes: 4-NP (1.69 mg mL^{-1}), 3m4-NP (2.98 mg mL^{-1}) and 2-NP (2.58 mg mL^{-1}). Therefore in this situation, the noise matrix can be considered a more representative population of 'noise' spectra as it includes instrumental noise effects, the variation in the background absorption of the eluent and spectra of interfering compounds.

Figures of merit. In a recent review [6.1] about the use (and abuse) of chemometrics in chromatography, Daszykowski et al. concluded that although the goal of chemometrics is to provide useful tools for data processing, it seems that these methods are mainly

used by chemometricians. An approach which has been previously used in different works [6.9-12], that likely will facilitate the application of the proposed multivariate method in analytical laboratories, is to perform standard univariate regressions using a 'surrogate' signal variable obtained from the multivariate method (SBC) directly related to the concentration of the target analyte. This transformation of a multivariate model to a univariate model provides an easier calculation of the figures of merit, such as the limit of detection (LOD) and thus, it is recommended to obtain a clearer and straightforward interpretation of the results.

In the original SBC approach [6.5], the response vector of the analyte of interest in absorbance units (AU) was scaled to obtain a g vector estimate in AU concentration⁻¹ dividing the analyte spectrum by its concentration. In this work, the SBC calculated concentrations were referred to a g vector estimate of unknown concentration. Chromatograms were obtained by plotting the predicted relative 2,4-dNP concentrations throughout the LC runs against time. Then, the peak height values of the concentration chromatograms were used as 'surrogate' signals.

Situation A. As described above, the spectral noise data matrix, \mathbf{X}_A (149x183), was composed by 149 spectra between 1700 and 1000 cm^{-1} (183 variables) measured during the re-equilibration of the system after each LC gradient injection. The equation used to calculate the relative concentrations of 2,4-dNP during each injected 'sample' chromatogram was equal to:

$$y_{pred} = \bar{y}_{X_A} + (x_{pred} - \bar{x}_A)^T \cdot \frac{\Sigma_A^{-1} g}{g^T \Sigma_A^{-1} g} \quad (\text{Equation 6.2})$$

being \bar{y}_{X_A} the average analyte concentration of the 'noise' spectra equal to 0.

The plot of the calculated relative 2,4-dNP concentrations during a chromatogram as a function of time can be viewed as an 'analyte-specific' chromatogram. Obviously, the specificity of the response or, in other words, the accuracy of the determination of the analyte concentration by the SBC model depends on the $b_{opt(1)}$ vector, i.e. on the quality of the estimation of the covariance matrix of the spectral noise, assuming that the 2,4-dNP spectrum was free from experimental error.

Figure 6.2 shows the calculated chromatograms of 2,4-dNP from the injection of standard solutions 1-6 with compositions indicated in Table 6.1. Elution peaks of 4-NP,

3m4-NP, 2,4-dNP and 2-NP could be identified at 10.53, 12.13, 13.07 and 14.13 min, respectively.

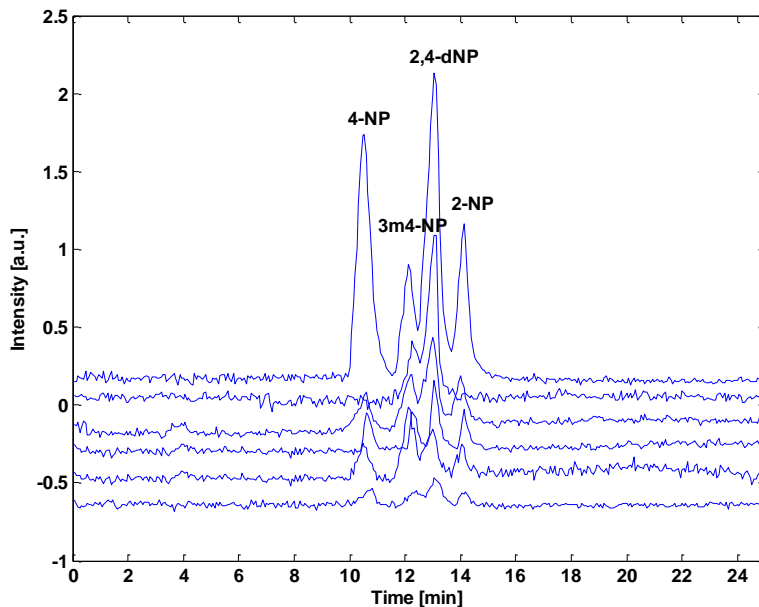


Figure 6.2. Chromatograms of 2,4-dNP obtained using the spectra measured during the re-equilibration of the LC system after a gradient injection for the calculation of the covariance matrix of the spectral noise (situation A); chromatograms were shifted to improve visibility.

As it can be seen in Figure 6.2, the presence of un-modeled interferents and the high correlation between the spectrum of the 'target' analyte and the response spectra of the other eluting analytes affect strongly the specificity (or accuracy) of the response. In spite of that, the regression between height values of the 2,4-dNP peak and concentration values provided an equation of: $y = (0.03 \pm 0.03) + (0.200 \pm 0.008)$ [2,4-dNP] (mg mL^{-1}), with $R^2=0.992$. It is remarkable that the very intense contribution of the changing eluent composition to the absorption was compensated and the chromatographic baseline showed no slope, being the residuals apparently randomly distributed around zero.

Situation B. Here, the spectral noise data matrix, X_B (375×183), was formed by 375 spectra between 1700 and 1000 cm^{-1} (183 variables) recorded during the injection of the 'sample blank' solution (see Table 6.1) into the LC-IR system under gradient

conditions. The equation used to calculate the relative concentration of 2,4-dNP in the 'sample' chromatograms was equal to:

$$y_{pred} = \bar{y}_{X_B} + (x_{pred} - \bar{x}_B)^T \cdot \frac{\Sigma_B g}{g^T \Sigma_B g} \quad (\text{Equation 6.3})$$

being \bar{y}_{X_B} the average analyte concentration of 'noise' spectra, also in this case, equal to 0.

Extracted chromatograms from injections of nitrophenol solutions 1-6 described in Table 6.1 are presented in Figure 6.3. The specificity of the response showed in the depicted chromatograms allows the identification and quantification of the 'target' analyte even when mixtures of related compounds are analyzed.

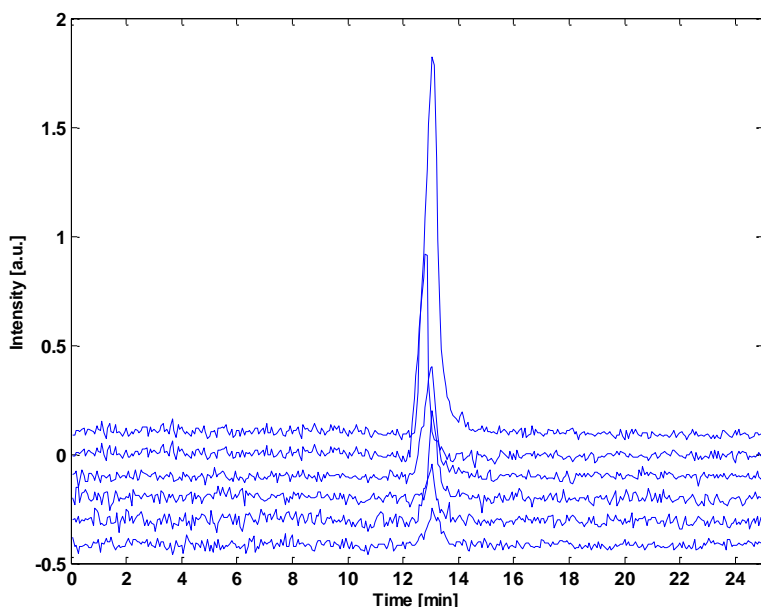


Figure 6.3. Extracted chromatograms of 2,4-dNP using spectra measured during the injection of a 'sample blank' for the calculation of the covariance matrix of the spectral noise (situation B); chromatograms were shifted to improve visibility.

An important advantage of the proposed approach over other multivariate techniques such as PLS is that to a great extent the specificity of the response is achieved using a single 'sample blank' injection as 'noise' matrix. This is of importance because in many situations, although a 'sample blank' is available, its composition is unknown. Hence,

the measurement of an appropriate calibration set with interferences covering a range of known concentrations is not possible.

A linear regression between 2,4-dNP concentrations and peak height values from the chromatograms obtained from the injections of the set of solutions indicated in Table 6.1 was calculated, providing an equation of $y = (0.02 \pm 0.01) + (0.178 \pm 0.003)$ [2,4-dNP] (mg mL^{-1}), with $R^2=0.9990$.

The possibility of using a 'sample blank' for the estimation of the covariance matrix of the spectral noise significantly improved the obtained results (see Figure 6.4). In this case, the calculated signal can be considered an 'analyte-specific' chromatogram which overcomes the strong changes in the background absorption and provides accurate results in the presence of strongly overlapped peaks with very similar spectra.

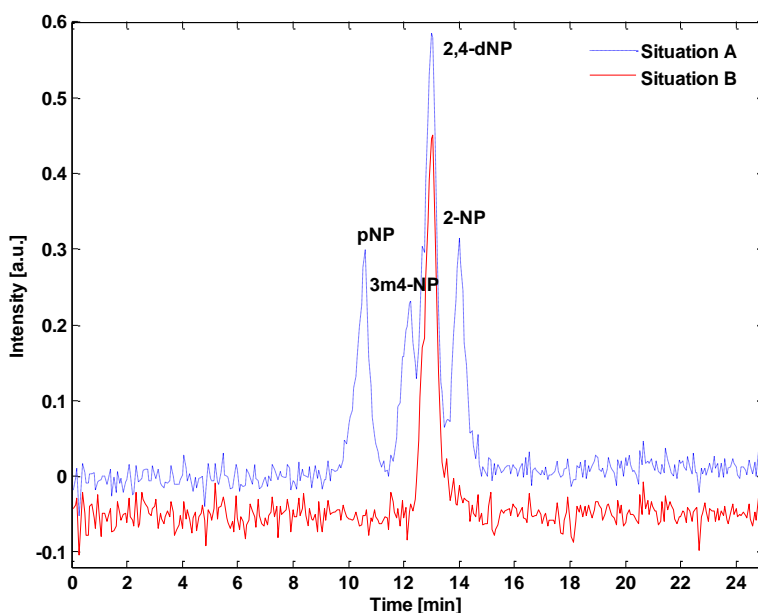


Figure 6.4. Comparison of 2,4-dNP chromatograms extracted using spectra measured during the re-equilibration of the LC system after gradient injection (situation A) and spectra measured during the injection of a 'blank sample' (situation B), for the calculation of the covariance matrix of the spectral noise; the offset used in 'situation B' is equal to -0.05 ; 2,4-dNP was used at a concentration of 1.84 mg mL^{-1} (standard solution number 4).

Sensitivity. The optimum error of prediction of the SBC method is defined as [6.5]:

$$SEP_{OPT} = \sqrt{\frac{1}{g^T \Sigma^{-1} g}} \quad (\text{Equation 6.4})$$

The SEP_{OPT} is the multivariate LOD of signal g in noise Σ , which is the sensitivity limit of the spectroscopic method. Unfortunately, LC sensitivity is affected by radial dispersion in the column after injection and in tubing connections as well as by the dead volume of the flow cell. Taking this into account, the calculated multivariate LOD might be over-optimistic. Therefore in this work, the LOD was estimated as the concentration of 2,4-dNP providing a peak height higher than three times the noise in the SBC chromatograms, obtaining a value of 0.21 mg mL^{-1} which fits well with the obtained results (see Figure 6.3).

In some situations, the identification of the elution of an analyte during a gradient run is possible considering the relative change in the slope of the chromatogram extracted from the raw signal (without background correction) at defined wavenumbers at which the analyte presents absorption bands. Figure 6.5 shows chromatograms extracted from the injection of a solution containing 4-NP (0.36 mg mL^{-1}), 3m4-NP (0.64 mg mL^{-1}), 2,4-dNP (0.69 mg mL^{-1}) and 2-NP (0.55 mg mL^{-1}) by measuring the changes in the absorbance of the raw spectra at 1535 cm^{-1} corrected using a baseline at 1377 cm^{-1} (top), and extracted chromatograms using the SBC procedure (bottom). From data depicted in this figure it can be concluded that the proposed procedure improves both, selectivity and sensitivity of the IR detection.

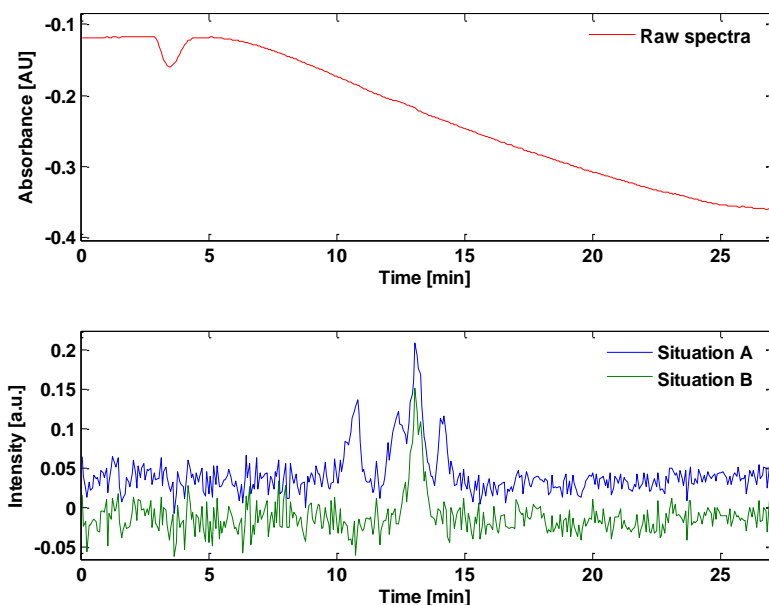


Figure 6.5. Chromatograms extracted from the injection of a solution containing of 4-NP (0.36 mg mL^{-1}), 3m4-NP (0.64 mg mL^{-1}), 2,4-dNP (0.69 mg mL^{-1}) and 2-NP (0.55 mg mL^{-1}) by measuring the changes in the absorbance of the raw spectra at 1535 cm^{-1} corrected using a baseline at 1377 cm^{-1} (top), and extracted chromatograms using the proposed multivariate procedure (bottom).

Note: Chromatogram 'Situation A' was shifted by 0.05 a.u. for a better visibility.

6.4 Conclusions

Results presented confirm that the 'Science Based Calibration' method is particularly well suited for recovering an 'analyte-specific' signal from on-line LC-IR chromatograms. Whereas its usefulness has been confirmed even when the analyte was injected in the presence of unknown interfering compounds, the benefits of the proposed approach could only be fully exploited when the number of un-modeled interfering compounds was reduced or eliminated before the calculation of the covariance matrix of the spectral 'noise', which was subsequently used for the calculation of the regression vector $b_{opt(1)}$.

The use of SBC presents major practical advantages over other multivariate methods (e.g. PLS), for its use in real world LC-IR applications. For example, the calculation of a PLS model for the determination of the concentration of the 'target' analyte during a gradient LC-IR separation would require the previous measurement of appropriate calibration and validation sets. Therefore, a deep knowledge of the sample constituents would be needed. Besides, the changing background eluent absorption would dramatically increase the number of standards required, being the calibration very time-consuming or even not possible in many cases. Whereas this work presents the advantages of SBC in a LC-IR system, additional work is in progress to evaluate its use with other multivariate detection techniques such as diode array detection (DAD) [6.13], fluorescence detection (FLD) or mass spectrometry (MS).

6.5 References for Chapter 6

- [6.1] M. Daszykowski, B. Walczak, *Trac-Trends in Analytical Chemistry*, 25 (2006) 1081-1096.
- [6.2] Daylight Solutions, <http://www.daylightsolutions.com/>.
- [6.3] R. Marbach, *Journal of Biomedical Optics*, 7 (2002) 130-147.
- [6.4] R. Marbach, U.S. Patent 6,629,041 B1, 2003.
- [6.5] R. Marbach, *Journal of near Infrared Spectroscopy*, 13 (2005) 241-254.
- [6.6] The Mathworks Inc., Matlab R2008b, version 7.0.0.
- [6.7] D. Lin-Vien, N.B. Colthup, W.G. Fateley, J.G. Grasselli, *The handbook of infrared and Raman characteristic frequencies of organic molecules*, Academic Press, Inc, 1991.
- [6.8] T. Takamuku, M. Tabata, A. Yamaguchi, J. Nishimoto, M. Kumamoto, H. Wakita, T. Yamaguchi, *Journal of Physical Chemistry B*, 102 (1998) 8880-8888.
- [6.9] A.C. Olivieri, N.K.M. Faber, J. Ferre, R. Boque, J.H. Kalivas, H. Mark, *Pure and Applied Chemistry*, 78 (2006) 633-661.
- [6.10] J. Saurina, C. Leal, R. Compano, M. Granados, M.D. Prat, R. Tauler, *Analytica Chimica Acta*, 432 (2001) 241-251.
- [6.11] M.C. Ortiz, L.A. Sarabia, A. Herrero, M.S. Sanchez, M.B. Sanz, M.E. Rueda, D. Gimenez, M.E. Melendez, *Chemometrics and Intelligent Laboratory Systems*, 69 (2003) 21-33.
- [6.12] A. Edelman, J. Diewok, J.R. Baena, B. Lendl, *Analytical and Bioanalytical Chemistry*, 376 (2003) 92-97.
- [6.13] J. Kuligowski, M.M. Galera, M.D.G. García, M.J. Culzoni, H.C. Goicoechea, S. Garrigues, G. Quintás, M. de la Guardia, *Talanta*, 83 (2011) 1158-1165.

CHAPTER 7. INSTRUMENTAL DEVELOPMENTS IN ON-LINE LC-IR

When on-line coupled LC-IR measurements are carried out, mainly two challenges could be identified throughout this thesis: i) as the mobile phases employed in LC absorb strongly in the mid-infrared, their accurate compensation is crucial to obtain characteristic analyte spectra and ii) FTIR detection in LC is characterized by a significantly lower sensitivity as compared to other more commonly used detectors such as UV-Vis spectrometry or mass spectrometry (MS). Whereas the first point was addressed in the foregoing chapters, this chapter is focused on recent advances in instrumentation used for liquid chromatography with on-line infrared detection, describing approaches of the implementation of miniaturized separation systems and flow cells [7.1] as well as potent laser light sources [7.2]. These improvements require reassessing the potential of the on-line approach in LC-IR.

7.1 On-Line Fourier transform infrared spectrometric detection in gradient capillary LC using nanoliter-flow cells

7.1.1 Introduction

Previous studies in isocratic on-line LC-IR provided detection limits in the low mg mL^{-1} range using attenuated total internal reflectance infrared microspectroscopy [7.3, 4], or a conventional internal reflection element mounted in a flow cell [7.5] as well as standard IR flow cells [7.6-10]. Whereas these reports show the usefulness of on-line IR detection for the analysis of sugars, organic acids and peroxides (explosives), an increase in sensitivity is needed to broaden the problem solving capabilities of this hyphenation.

When assessing the instrumental constraints of on-line LC-IR, several reasons can be identified being responsible for the apparent low sensitivity of on-line FTIR detection as compared to UV-Vis spectrometric detection in LC using 4.6 mm columns. The fact that absorptions of molecules in the infrared are generally significantly smaller than in the UV-Vis range sets a physical limitation. Furthermore, the maximum optical path of a flow cell used for on-line detection in the IR range is determined by the absorption of the mobile phase, being in the range of a few micrometers when using standard FTIR spectrometers for the measurement of aqueous solutions. This is contrary to the UV-Vis range where the used solvents are generally transparent. This consideration defines also the typical volume of an IR flow cell to be used. Considering an optical path of 25 μm as reported by Vonach et al., a flow cell volume of 10 μL could be estimated. This is significantly smaller than the volume of a peak eluting from a 4.6 mm separation column, which in the paper of Vonach was in the order of 250-400 μL at a flow rate of 500 $\mu\text{L min}^{-1}$. Considering only the differences in the optical path, a factor of 400 in terms of sensitivity is lost when compared to a 1 cm flow cell which is the standard in UV-Vis detection. In the case of infrared detection, the time required to record and store an infrared spectrum also needs to be taken into account when recording a transient signal such as a chromatographic peak. Vonach et al. achieved a recording rate of 19 spectra per minute, which corresponded to a volume of 26.3 μL per

spectrum. In this case, the cell volume and the time required to record a single spectrum were appropriate to follow the elution of a chromatographic peak without facing dilution of the peak maximum due to instrumental constraints. The achieved average limit of detection (LOD) calculated from the sugars and organic acids analyzed, and estimated as the threefold standard deviation of the method s_{x0} , which was calculated according to ISO 8466-1, was 0.2 mg mL^{-1} . The corresponding absolute LOD was therefore $4 \mu\text{g}$ as $20 \mu\text{L}$ of sample had to be injected.

After sample injection in liquid chromatography, radial dispersion causes the sample to distribute over the entire cross-section of the column. The dispersion in the column can be expressed by the standard deviation volume of the eluted peak (σ_v):

$$\sigma_v = \frac{\varepsilon \pi r^2 (1+k')}{n^{0.5}} \quad (\text{Equation 7.1.1})$$

where k' is the capacity factor; r , l , and n are the radius, length, and efficiency of the column, respectively; and ε is the fraction of the mobile phase in the column that is available to the solute. When the internal diameter (ID) of the column diminishes, the dilution is lowered resulting in an increased sensitivity of detection being that the concentration of the sample at the end of the column is inversely proportional to the square of the column diameter. Hence, according to the down-scaling factor f described in Equation 7.1.2, a maximum 235-fold increase in sensitivity can theoretically be achieved by replacing a 4.6 mm ID analytical column with a 300 μm ID capillary column [7.11]:

$$f = \frac{ID_{\text{standard column}}^2}{ID_{\text{capillary column}}^2} \quad (\text{Equation 7.1.2})$$

It should be realized that this impressive gain in sensitivity is only achieved in case the same amount of sample can be injected onto the different columns. However, this is not always possible as the maximum allowable injection volume decreases with the column ID. Therefore, lower gains in concentration sensitivity are normally obtained because the increase in the chromatographic peak concentration by reduction of the column ID can be partially or fully compensated by the reduction in the injection volume [7.12]. In the second edition of their book on Fourier Transform Infrared Spectrometry, published in 2007, Griffiths and de Haseth [7.13] estimated a limit of detection (LOD) of the order of $250 \mu\text{g}$ on-column for a typical reversed phase LC-IR separation carried out using a 4.6 mm ID column and a flow-through cell with $10 \mu\text{m}$

pathlength, 3 mm diameter and a volume of 70 nL. According to their estimation, LODs of the order of 1 μg on-column can be expected using capillary columns with an ID of the order of 300 μm .

Concerning on-line IR measurements in capillary LC, the lower flow rates (1-20 $\mu\text{L min}^{-1}$) used in capillary LC demand the use of low-volume flow cells because post-column dead volumes become critical as they can cause serious peak broadening and thus decrease sensitivity. Flow cells with nL-volumes were developed already in 2002 by Köhler et al. [7.14] and used to hyphenate capillary electrophoresis with FTIR spectrometry. These micromachined flow cells had path lengths ranging from 8 to 50 μm with corresponding volumes of 2.4 to 15 nL, respectively. Aqueous solutions comprising mixtures of adenosine, guanosine, and adenosine monophosphate were employed to test the system performance. The limits of detection for all the analytes were in the low g L^{-1} range.

This chapter reports, for the first time, on-line FTIR detection in capillary liquid chromatography employing gradient elution. Micromachined flow cells were used and chemometric background correction was applied to extract the analyte spectra from the recorded chromatographic data set. The quality of the obtained analyte spectra was assessed by comparing the recovered spectra with reference spectra recorded in solution. A further purpose was the evaluation of the advantages gained from miniaturization in terms of sensitivity of on-line LC-IR. For this purpose four nitrophenols (4-nitrophenol (4-NP), 2,4-dinitrophenol (2,4-dNP), 2-nitrophenol and 3-methyl-4-nitrophenol (3m4-NP)), listed as priority pollutants by the US Environmental Protection Agency (EPA), were selected as model compounds to be separated, quantified and identified by on-line reversed phase gradient LC-IR using an acetonitrile:water mobile phase.

7.1.2 Material and methods

Apparatus and Reagents

The LC system consisted of a Dionex (Sunnyvale, CA, USA) UltiMate[®] 3000 capillary LC system equipped an Acclaim PepMap C₁₈ (300 μm ID x 150 mm, 3 μm , 100 Å) capillary column. Separations were carried out at 25°C using a flow rate of 3 $\mu\text{L min}^{-1}$ and an

injection volume of 1 μL . Linear gradients were run from 50:50 to 35:65 v/v water (0.05% TFA):acetonitrile in 15 minutes. Standards with concentrations indicated in Table 7.1.1 were prepared, resulting in 65-890 ng on-column injections.

Infrared measurements were performed on a Bruker Equinox 55 (Bruker Optics, Ettlingen, Germany) FTIR spectrometer equipped with a liquid nitrogen cooled mercury cadmium telluride (MCT) detector. To accurately focus the IR beam on the micromachined flow cell, an in-house built beam condenser was used which was attached to the spectrometer and placed inside a dry air purged Perspex housing. The parallel beam was taken out of the spectrometer and focused on the flow cell using an off axis paraboloid mirror with a focal length of 69 mm. The flow cell consisted of 1 mm thick CaF_2 windows. It was produced starting from CaF_2 windows with a diameter of 2.54 cm by using micromachining technology. On one window an epoxy-based photoresist SU-8 (Microchem Corp., Newton, MA) polymer was applied whose thickness determined the optical path. Then, using a photomask and UV light, the channel structure was formed. The top CaF_2 window was then used to close the structure. On one of the CaF_2 windows, a 200 nm thick Ti layer was deposited by evaporation and patterned by a conventional liftoff technique. The Ti layer acted as an optical aperture strongly reducing IR radiation to pass the polymer which defines the flow channels. From the closed structure several micromachined flow cells could be obtained by cutting pieces of an area of 2 x 4 mm. The channel of the flow cells used in this work was 2 mm long with a cross section of 150 μm in width and an optical path of 25 μm . The volume of the flow cell was 7.5 nL. A detailed description and schematic views of both, the manifold and the construction of the flow cell can be found in previous works [7.14, 15].

Special care was taken to reduce peak broadening due to the connection of the LC system with the micromachined nL flow cell. The column outlet was connected to a 10 cm length untreated fused-silica capillary (ID 50 μm , OD 375 μm , Polymicro Technologies, Phoenix, AZ) using a zero dead volume connection (Dionex) which transferred the column eluate to the flow cell. Figure 7.1.1 shows a photograph of the system, where an additional UV detector was incorporated.

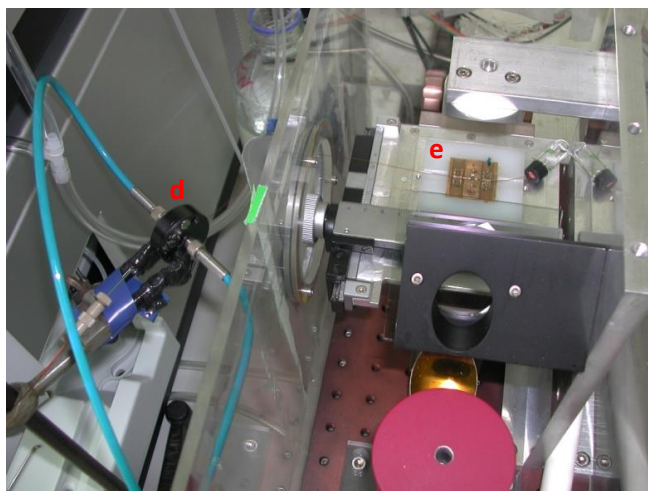
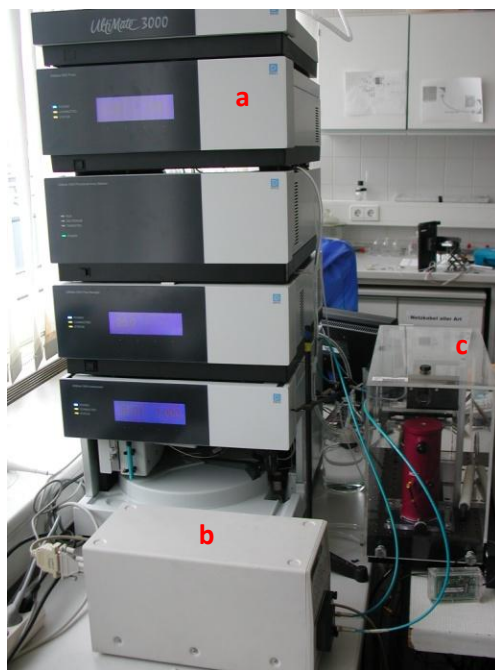


Figure 7.1.1. Top: UltiMate[®] 3000 capillary LC system from Dionex (a) with on-line UV (b) and IR detection (c), the in-house built beam condenser placed inside a dry air purged Perspex housing was employed to accurately focus the IR beam on the micromachined flow cell; bottom: close-up view of the connection of the LC capillary to the UV flow cell (d) and the micromachined IR flow cell (e).

The scanner of the spectrometer was operated at a HeNe laser modulation frequency of 180 kHz. Twenty five scans were co-added for each spectrum using a spectral resolution of 8 cm^{-1} and a zero filling factor of 2, providing a scanning frequency of 25 scans s^{-1} , a spectra acquisition frequency of 29 spectra min^{-1} and 4 cm^{-1} spectral data spacing. Each spectrum thus corresponded to a volume of approximately 100 nL. Reference FTIR spectra of the four analytes were obtained from the measurement of nitrophenol standard solutions under stopped-flow conditions.

4-nitrophenol (4-NP), 2,4-dinitrophenol (2,4-dNP), 2-nitrophenol (2-NP) (PESTANAL, Fluka, Buchs, Switzerland) and 3-methyl-4-nitrophenol (3m4-NP) (98%, Sigma-Aldrich, Switzerland) standard solutions were prepared by dissolving an appropriate amount of each compound in a 95:5 water (0.05% TFA):acetonitrile solution. Solutions were filtered ($0.22 \mu\text{m}$) prior to injection.

Software and algorithms

Background correction and data treatment were run under Matlab 7.0 from Mathworks (Natick, USA, 2004) using in-house written Matlab functions. A modification of a recently developed approach named univariate background correction based on the use of a reference spectra matrix (BGC-RSM), described in chapter 3, was used for background correction. In this work, the relative absorbance value (RW) defined as the difference in absorbance at two selected wavenumbers $r_1 = 2256 \text{ cm}^{-1}$ and $r_2 = 2260 \text{ cm}^{-1}$ was calculated as identification parameter (IP) being characteristic for the mobile phase composition:

$$RW_s = (y_{r_1}^s - y_{r_2}^s) \quad (\text{Equation 7.1.3})$$

where $y_{r_1}^s$ and $y_{r_2}^s$ are the absorbance values at the wavenumbers r_1 and r_2 [cm^{-1}] measured in the spectra $s = (1, \dots, z)$ for spectra included in the **SM** and $s = (1, \dots, r)$ for spectra included in the **RSM**. The two selected wavenumbers correspond to the stretching vibration of the $\text{C}\equiv\text{N}$ bond in acetonitrile which is shifted to lower frequencies due to hydrogen bonding with water. Therefore, by focussing on this area of the spectrum, the actual existing mobile phase composition can be determined.

7.1.3 Results and discussion

FTIR spectra of the mobile phase-flow cell system

Figure 7.1.2 shows representative FTIR spectra in the region between 4000 and 900 cm^{-1} of different eluent compositions between 50:50 and 35:65 v/v water (0.05% TFA):acetonitrile. The spectra show clearly distinguishable characteristic water and acetonitrile bands as described elsewhere [7.16]. Additionally, a set of SU-8 polymer absorption bands can be seen in the region 1540-1100 cm^{-1} . Negative bands between 2420 and 2240 cm^{-1} arise due to changes in the CO_2 (g) concentration during the measurements. Changes in intensity and shape of the absorption bands of the mobile phase components evidence the need for using an appropriate background correction.

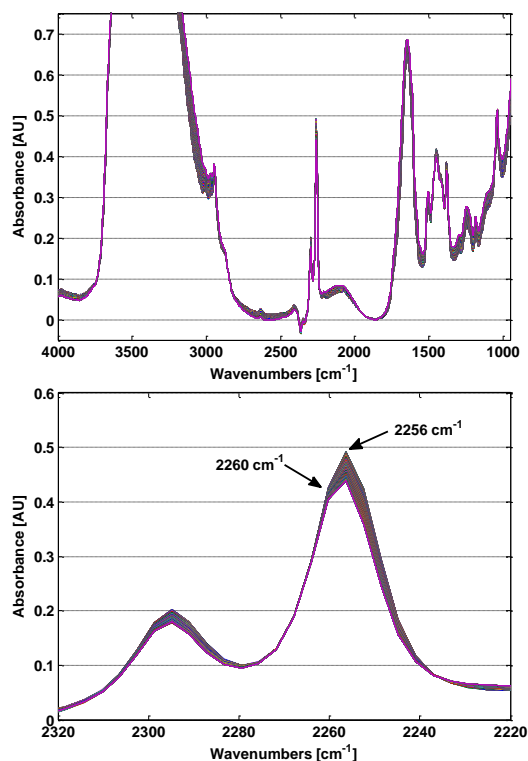


Figure 7.1.2. FTIR spectra of water (0.05% TFA):acetonitrile mixtures measured during a low-speed re-equilibration of the LC system after a gradient injection in the 4000 – 950 cm^{-1} (top) and in the 2320 – 2220 cm^{-1} region (bottom); mobile phase compositions ranged between 35:50 and 50:65 v/v water (0.05% TFA):acetonitrile.

The selection of the identification parameter for the selection of a background spectrum within the **RSM** is one of the most important steps of the BGC-RSM procedure. Figure 7.1.3 shows the change in the RW value during the injection of 1 μL of a standard solution containing 200 $\text{ng } \mu\text{L}^{-1}$ of 4-NP, 2,4-dNP, 2-NP and 3m4-NP (0-21 min), as well as during the re-equilibration of the LC system (21-52 min). Negative values between 4 and 5.5 min are caused by the elution of the sample solvent. This figure proves that the selected RW is characteristic of the mobile phase composition in the considered mixing ratios and that it is not influenced by the elution of the analytes. Hence it can be used to identify and select appropriate eluent spectra within the **RSM** for the correction of the eluent absorption.

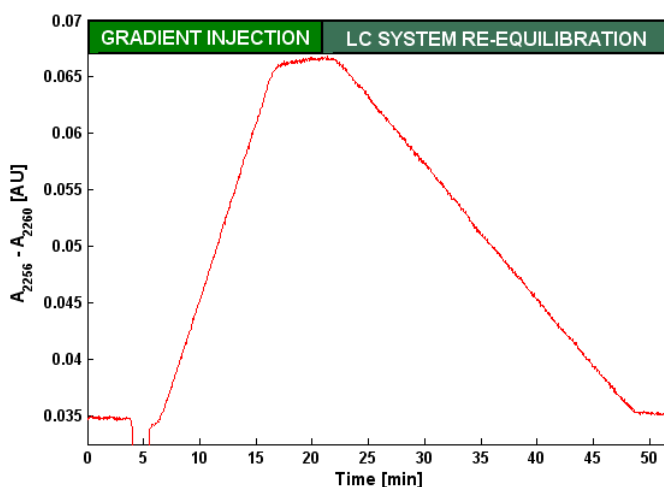


Figure 7.1.3. Change in the differential absorption at 2256 and 2260 cm^{-1} during a gradient LC run followed by a slow re-equilibration of the system.

On-line gradient capillary LC-IR

Background corrected spectra acquired upon injection of 1 μL of a standard mixture containing the four selected compounds 4-NP (270 $\text{ng } \mu\text{L}^{-1}$), 3m4-NP (230 $\text{ng } \mu\text{L}^{-1}$), 2,4-dNP (230 $\text{ng } \mu\text{L}^{-1}$) and 2-NP (230 $\text{ng } \mu\text{L}^{-1}$) are presented in Figure 7.1.4. As shown, the sample solvent elution peak starting at 4 min and the elution window of the analytes between 8 and 11 min can be easily identified.

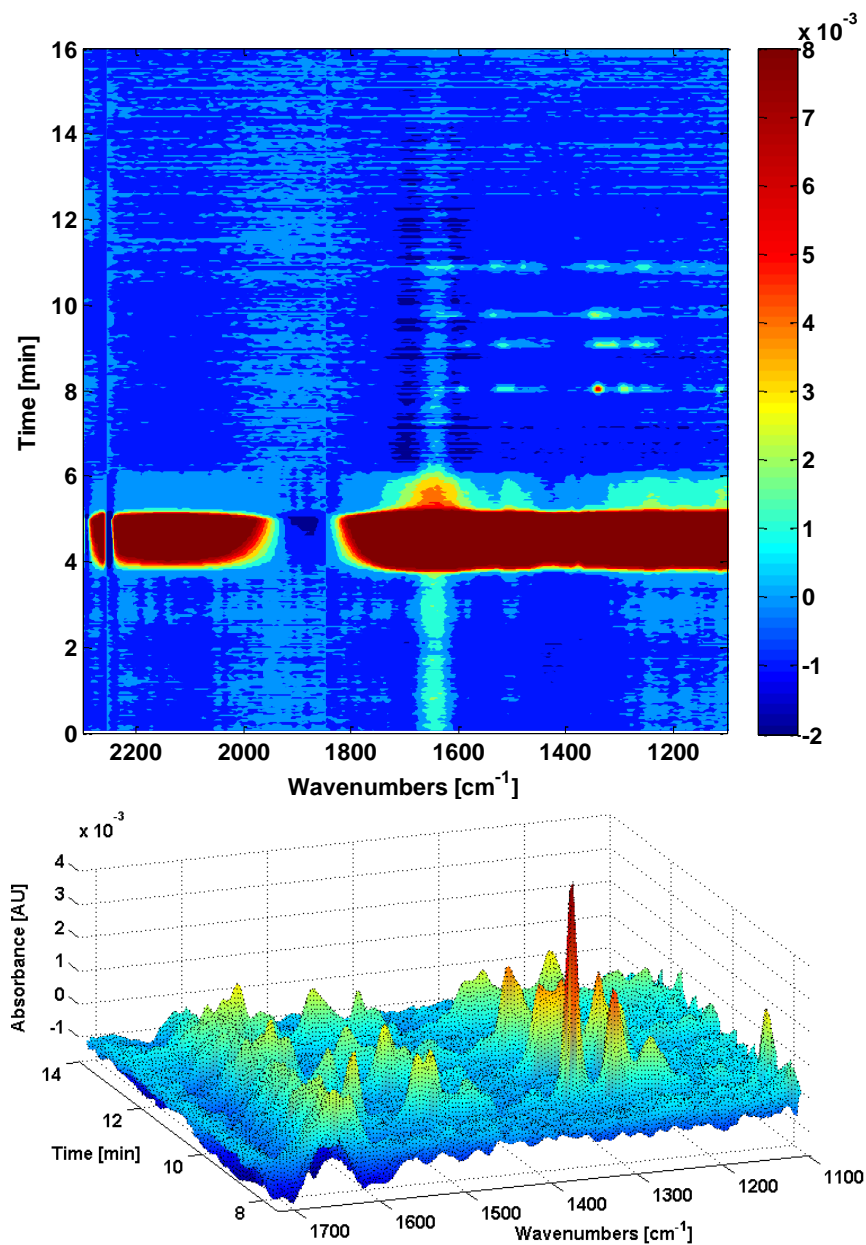


Figure 7.1.4. Top: surface plot of background corrected spectra acquired during injection of 1 μL of a standard mixture containing the four selected compounds 4-NP ($270 \text{ ng } \mu\text{L}^{-1}$), 3m4-NP ($230 \text{ ng } \mu\text{L}^{-1}$), 2,4-dNP ($230 \text{ ng } \mu\text{L}^{-1}$) and 2-NP ($230 \text{ ng } \mu\text{L}^{-1}$); bottom: three dimensional close-up view of the time window in which the analytes elute.

Figure 7.1.5 depicts FTIR chromatograms extracted from data shown in Figure 7.1.4. As illustrated in this figure, all the analytes could be baseline resolved under the chromatographic gradient conditions with retention times of 8.03, 9.07, 9.78 and 10.76 min for 4-NP, 3m4-NP, 2,4-dNP and 2-NP, respectively.

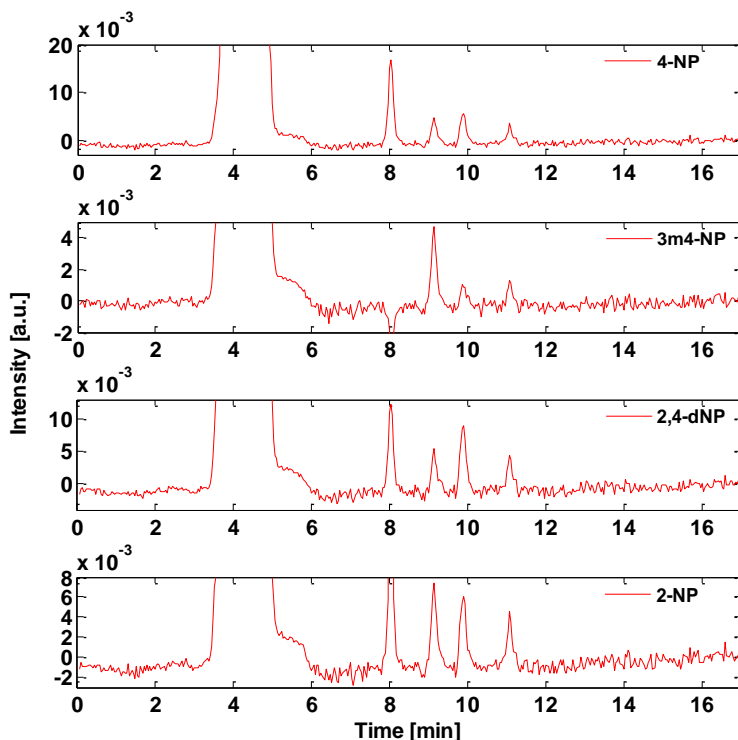


Figure 7.1.5. Extracted chromatograms from the injection of 1 μL of a single standard solution containing 270 $\text{ng } \mu\text{L}^{-1}$ of 4-NP and 230 $\text{ng } \mu\text{L}^{-1}$ of 3m4-NP, 2,4-dNP and 2-NP.

The presence of characteristic bands of the analytes (see Figure 7.1.6) allowed the selection of different integration conditions for the extraction of their respective FTIR chromatograms as indicated in Table 7.1.1, thus maximizing selectivity and sensitivity of the chromatographic signal. Table 7.1.1 also summarizes the main analytical features of the proposed hyphenation for the determination of the considered analytes.

Table 7.1.1. Calibration features of the on-line LC-IR determination of 4-NP, 3m4-NP, 2,4-dNP and 2-NP using height values of the calculated chromatographic peaks.

Analyte	Analytical signal ^a (y)	BLC ^c (cm ⁻¹)	Equation	R ²	Conc. range [ng μL ⁻¹]	LOD ^b [ng]	LOI ^e [ng]	RSD ^d [%]
4-NP	A(1334)+A(1338)+A(1342)	A(1315)	$y^2=(a\pm s_a)+ (b\pm s_b)C[\text{ng } \mu\text{L}^{-1}]$ (0.3±0.3)10 ⁻³ + (0.0643±0.0009)10 ⁻³ C	0.9992	65-695	35	65	4.6
3m4-NP	A(1269)+A(1311)	A(1292)	(0.1±0.1)10 ⁻³ + (0.0109±0.0003)10 ⁻³ C	0.997	150-890	50	150	6.8
2,4-dNP	A(1342)+A(1346)+A(1350)+A(1354)	A(1365)	(0.3±0.4)10 ⁻³ + (0.0296±0.0010)10 ⁻³ C	0.995	85-350	80	125	5.7
2NP	A(1331)+A(1335)+A(1338)	A(2075)	(-0.1±0.3)10 ⁻³ + (0.0174±0.0008)10 ⁻³ C	0.995	175-695	94	175	6.2

Note: Analytical signal^a: the analytical signal (y) is the sum of single point baseline corrected absorbance values (A) at the wavenumbers indicated between brackets; LOD^b: limit of detection in ng calculated for an injection volume of 1 μL as the threefold standard deviation of the method (*s*_{x0}) according to ISO 8466-1; LOI^e: limit of identification estimated as the lowest concentration providing: i) a recognizable spectrum of the analyte and ii) a signal-to-noise ratio of the chromatographic signal higher than 3; RSD^d: relative standard deviation in % calculated from five repeated measurements of standard solutions with a concentration equal to the LOD of each analyte; BLC^c: single point baseline correction.

Studies of linearity showed appropriate R^2 values, ranging from 0.995 to 0.9992, obtained for the four analytes by injecting two series of 5 standards at different concentration ranges for each analyte. Limits of detection (LODs) were calculated as the threefold standard deviation of the method s_{x0} , which was calculated according to ISO 8466-1. Limits of identification (LOI) were estimated as the lowest concentrations providing: i) recognizable spectra of the analytes in the region between 1700 and 1050 cm^{-1} and ii) a signal-to-noise ratio of the chromatographic signal higher than 3. Multiplication of the relative LODs and LOIs by the injection volume results in absolute LODs and LOIs expressed as ng analyte on-column. By using these criteria, the calculated LODs were 35, 50, 80 and 94 ng on-column for 4-NP, 3m4NP, 2,4-dNP and 2-NP, respectively. Estimated values of LOIs ranged between 65 and 175 for 4-NP and 2-NP, respectively. The relative standard deviations (RSD, $n=5$) of the peak height values found from the repeated injection of a standard with a concentration of 175 $\text{ng } \mu\text{L}^{-1}$ of each analyte were 4.6, 6.8, 5.7 and 6.2% for 4-NP, 3m4-NP, 2,4-dNP and 2-NP, respectively.

Although it is difficult to establish a direct comparison of sensitivities obtained using different LC-IR systems and analytes, the obtained LODs represent a significant improvement in the sensitivity compared to previous results reported in literature using on-line LC-IR. For example, Schulte-Ladbeck et al. [7.10] reported limits of detection for triacetoneperoxide (TATP) and hexamethylenetriperoxide diamine (HMTD) of 4440 and 2080 ng on-column using a LiChroSpher C_{18} column (250 x 3 mm, 5 μm) and an isocratic mobile phase of acetonitrile: H_2O 75:25 v/v for the separation and a CaF_2 flow cell with 25 μm pathlength for FTIR detection. More recently, Kuligowski et al. [7.17] reported a limit of detection for glycolic acid by isocratic on-line LC-IR in rapid scan acquisition mode of 680 ng on-column using a C_{18} column (250 x 2 mm, 5 μm) and an isocratic mobile phase of acetonitrile:phosphate buffer (25 mM, pH 2.7), 3:97 v/v for the separation and a CaF_2 flow cell with 14 μm pathlength and a volume of 1.7 μL for FTIR detection. In short, limits of detection are dependent on the analyte but are typically in the range of 50 $\text{ng } \mu\text{L}^{-1}$ by using micromachined nL-IR flow cells in capillary LC, and in the low $\mu\text{g } \mu\text{L}^{-1}$ range or higher using standard flow cells.

A major interest of FTIR detection in LC, compared to UV detection, is the possibility of both, detection and identification of the eluted analytes. FTIR spectra of the four nitrophenols were extracted from the background corrected FTIR chromatograms at selected retention times corresponding to their peak apex and were compared with reference spectra previously measured (see Figure 7.1.6). As shown, spectra extracted at the peak apex from the background corrected gradient chromatograms correlated well with the reference spectra. The calculated correlation coefficients at different concentrations indicated in the figure show that the selected conditions of measurement and background correction are appropriate for the identification and quantification of the analytes in the studied concentration ranges.

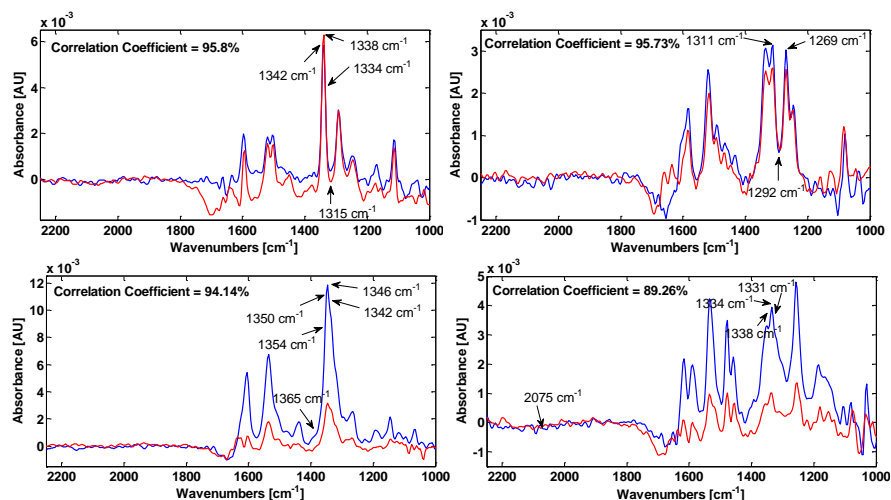


Figure 7.1.6. Background corrected spectra of the analytes at their corresponding peak apex obtained from the injection of 1 μL of a standard solution containing 270 $\text{ng } \mu\text{L}^{-1}$ of 4-NP (top, left) and 230 $\text{ng } \mu\text{L}^{-1}$ of 3m4-NP (top, right), 2,4-dNP (bottom, left) and 2-NP (bottom, right). Reference spectra (blue lines) are included in the figure for comparison; the correlation coefficient between two spectra y_1 and y_2 is defined as the ratio from the covariance ($\text{Cov}(y_1, y_2)$) and the product of the two standard deviations σ_{y_1} and σ_{y_2} ; according to this definition, a value of percentage of correlation coefficient of 100 indicates identical spectra.

7.1.4 Conclusions

The present study shows the capabilities of on-line FTIR detection in gradient capillary LC using micromachined nL-flow cells. Four model compounds could be separated and identified using an CH₃CN:H₂O gradient with limits of detection in the concentration range of 35-94 ng μL⁻¹. Considering the injection volume of 1 μL, this corresponds to 35-94 ng on-column representing an increase in mass sensitivity by a factor of approximately 30 as compared to LC systems employing a 4.6 mm column. Despite using a gradient technique, high quality analyte spectra could be extracted from the recorded data by using an advanced approach for background correction. This was evidenced by the achieved correlation coefficients ranging from 89 to 96% when injecting 230-270 ng of analytes, using the spectral region from 1700 to 1050 cm⁻¹. Due to the simplicity of the experimental approach it may be expected that this new type of on-line hyphenation in LC-IR may find its use also in routine laboratories as opposed to off-line detection.

7.2 High performance liquid chromatography with on-line dual Quantum Cascade Laser detection

7.2.1 Introduction

The coupling of high performance liquid chromatography (HPLC) to infrared spectroscopy is an ongoing research field [7.1]. The most important drawback of the LC-IR coupling is its low sensitivity caused by low optical path lengths which have to be used due to the strong background absorption of most common mobile phases including water. A possible approach to overcome this problem is to use more powerful light sources, like they are for example quantum cascade lasers (QC-lasers) [7.18, 19]. QC-lasers consist of several hundred layers of different semiconductor materials. The light generation mechanism is based on inter sub-band transitions of LO phonons within the semiconductors conduction band. As their emission wavelength depends on the thickness of the semiconductor layers, and not on the semiconductor material itself, lasers emitting at different wavelengths can be produced independently from the availability of semiconductor materials. Furthermore QC-lasers are small and therefore suitable for their application in portable sensor systems.

Whereas QC-laser detection has been applied for gas phase measurements in many cases [7.20-25], applications for liquid phase measurements were documented for the first time in 2000 by Lendl et al. [7.26] using a QC-laser for the detection of Flow Injection Analysis (FIA) peaks of phosphate. Further applications in aqueous systems using one QC-laser were developed for the detection of carbohydrates [7.8], adenine and xanthosine [7.27] and carbon dioxide [7.28, 29]. Detection systems consisting of two QC-lasers for the recording of FIA-peaks were applied for the on-line monitoring of sulfite oxidation [7.30] and for the simultaneous detection of glucose and sodium acetate [7.31], both in aqueous solutions.

On the other hand, FTIR spectroscopy is frequently used for the analysis of different organic components in wine [7.32]. In 1998, Schindler et al. developed a method for direct analysis of sugars, alcohols and organic acids in wine samples using a fully automated sequential injection system with FTIR detection in combination with multivariate evaluation of the spectroscopic data [7.33]. A commercially available

analytical tool, the WineScan from FOSS Analytical A/S (Denmark) [7.34] is also based on the acquisition of mid-IR spectral information with subsequent quantification applying multivariate methods such as PCA and PLS. Vonach et al. [7.7] analyzed different organic components in wine using on-line coupling of LC-IR and Edelmann et al. [7.8] quantified glucose and fructose in red wine samples using one QC-laser.

In this study, the simultaneous use of two QC-lasers is proposed as an effective way to increase the sensitivity and selectivity of on-line infrared detection in LC systems. The use of a dual QC-laser system leads to more selective and robust measurement systems as more structural information on the investigated system is obtained. To show the usefulness of the proposed detection system it was applied for the analysis of eight different components of wine and grape juice samples.

7.2.2 Material and methods

A photograph of the set-up including the QC-lasers and the optical components is shown in Figure 7.2.1. The entire experimental set-up also including temperature control, signal generation and data acquisition systems is schematically illustrated in Figure 7.2.2.

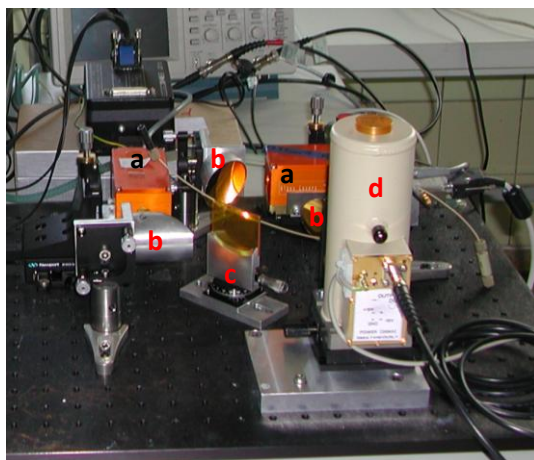


Figure 7.2.1. Experimental set-up including two QC-lasers (a), three gold mirrors (b), a ZnSe beamsplitter (c) and a MCT detector (d).

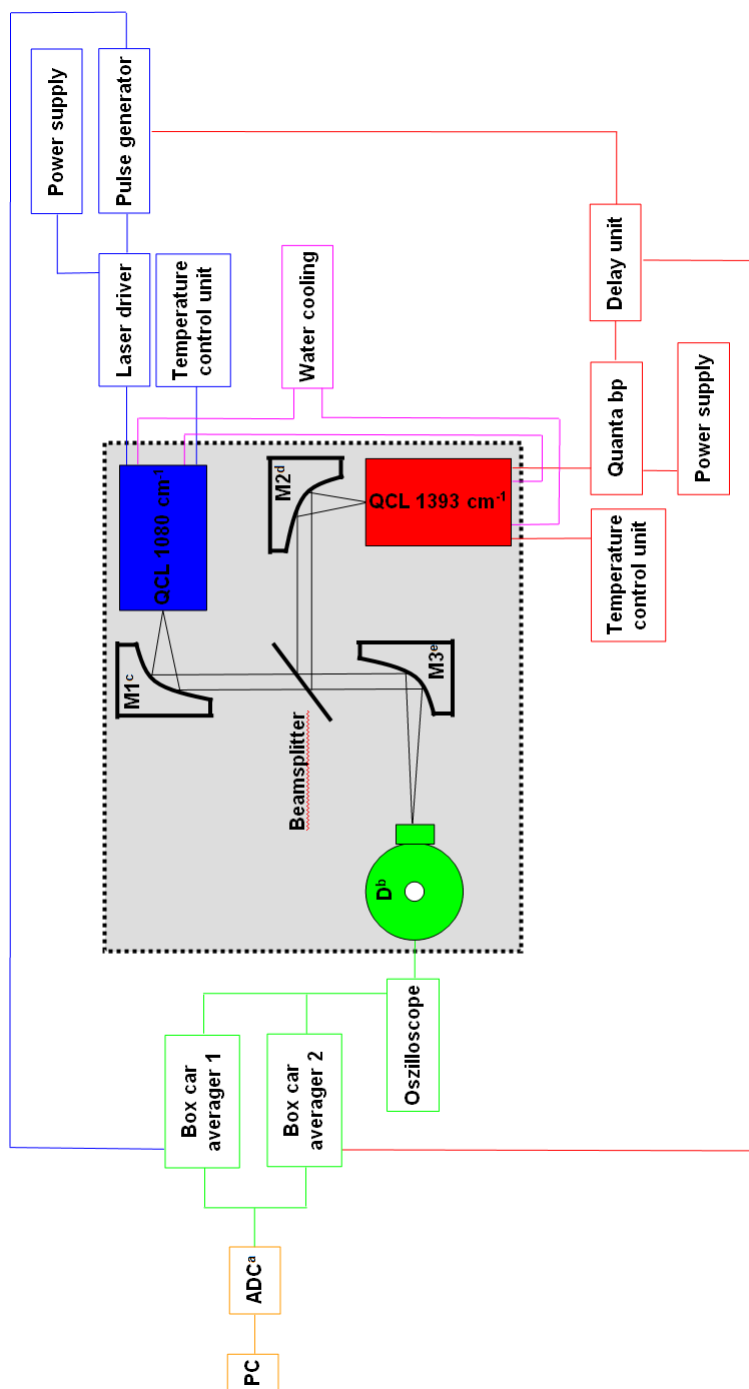


Figure 7.2.2. Experimental set-up: blue: elements connected to the QC-laser (QCL) emitting at 1080 cm⁻¹, red: elements connected to the QC-laser (QCL) emitting at 1393 cm⁻¹, pink: water cooling system for both lasers, green: analog data processing, orange: digital data processing, ADC^a stands for analog digital-converter, D^b stands for detector, M1^c, M2^d and M3^e are mirrors 1, 2 and 3; all elements are described in detail in section 7.2.2.

Quantum cascade laser operation and optical set-up

As light sources, two Fabry-Pérot (FP) lasers emitting at different wave lengths were used. Lasers and mountings were both purchased from Alpes Lasers (Neuchâtel, Switzerland). The lasers were positioned in the laser mountings which contained a silica gel pad and were purged with N₂ (g) before closing to avoid condensation on the QC-laser while cooling down. The laser mounting was also provided with Peltier elements and a compartment for air- or water-cooling. The first QC-laser emitting at 1080 cm⁻¹ (S1839a21), was operated using an Alpes Lasers starter kit, the trigger signal of a pulse generator from Alpes Lasers and an Agilent (Santa Clara, CA, USA) E 3620A 0-25V 0-1 A DC power supply. The second laser emitting at 1393 cm⁻¹ (n121b17), was operated using the QUANTA-BP laser driver from Laser Components (Olching, Germany) which was attached to the Alpes Laser mounting and controlled with a self-made power supply unit. To obtain a trigger signal with appropriate delay time with respect to the signal of the first QC-laser, the trigger signal of the pulse generator of the first laser was lead through a home-made delay unit with variable delay time before reaching the second laser driving unit. For both lasers the pulse repetition rate was set to 25 μs and the pulse amplitude to about 95% of the specified maximum. The pulse length was adjusted to 50 ns. Both lasers were cooled down to -30°C with Peltier elements controlled by two separate temperature control units from Alpes Lasers. To remove the excessive waste heat, a temperature-controlled water bath (Julabo F12) with an integrated pump (Julabo MV) was set to 18°C and connected to the water-cooling compartments of the laser mountings.

Other optical components used were two parabolic gold mirrors with a focal length of 43 mm which were employed to collimate the emitted laser light, a ZnSe beam splitter, a third parabolic gold mirror with a focal length of 69 mm which focused the laser light through the flow cell onto the sensitive element of the detector, a flow cell with CaF₂ windows and an optical pathlength of 52 μm connected to the LC system and a liquid nitrogen refrigerated photovoltaic MCT-detector (Kolmar Technologies, Newburyport, MA, USA). All components were fixed to an optical disk (hole-center distance 25 mm) using supports from Newport Spectra-Physics (CA, USA).

Data acquisition

The voltage output signal of the detector was split and processed by two box car averagers (gated integrator and box car averager, Stanford Research Systems, Sunnyvale, CA, USA). The QC-laser signals were evaluated separately setting the gates of each box car averager on one laser pulse. The box car averagers were triggered with the same trigger signals as the corresponding QC-lasers. The following settings were selected on the box car averager: external trigger signal, a gate delay of 300 ns for the first QC-laser and 200 ns for the second one, a gate width of 10 ns, a signal amplification of 0.1, DC and averaging of 100 samples. The averaged output signal was connected to an AD-Converter (NI 9239, 4 channels) mounted in an 8-slot NI CompactDAQ 9172 chassis, both from National Instruments. The digital signal was processed on a standard PC using NI LabVIEW SignalExpress (version 2.5.1, National Instruments). The signal was recorded with a sampling frequency of 2000 Hz and averaged with a frequency of 1000 Hz which resulted in a final sampling frequency of 2 data points s^{-1} . Further data evaluation and conversion into absorbance units was run under Matlab 7.0 from Mathworks (Natick, USA, 2004). OPUS 6.5 from Bruker (Ettlingen, Germany) was used for linear baseline corrections and smoothing of chromatograms (Savitzky-Golay, 9 points).

Chromatographic separation

The LC separation system consisted of a L7100 LaChrom pump (Merck-Hitachi, Tokyo, Japan) equipped with a Rheodyne 7725 injection valve and an injection loop of 50 μ l. In order to protect the analytical column (Rezex RCM Monosaccharide Ca^{2+} , 300 x 7.8 mm, Phenomenex) a Security Guard Cartridge (Carbo Ca^{2+} , 4 x 3 mm, Phenomenex) was used. The stationary phase of both, the guard and the analytical column, was an anion exchange resin with Ca^{2+} counter ion, a particle size of 8 μ m and 8% cross linkage. De-ionized water was filtered and degassed in an ultrasonic water bath for 15 minutes before using it as mobile phase. The system was run in isocratic mode at a flow rate of 0.6 $mL\ min^{-1}$. The column was thermostatted at 85°C using a modified glass tube connected to a temperature-controlled water bath (Lauda M3) with an integrated water pump (Lauda MT). All connections were made of polyetheretherketon (PEEK) tubings with an ID of 0.25 mm.

Fourier transform infrared reference measurements

A Bruker (Ettlingen, Germany) Equinox 55 FTIR spectrometer was used for the acquisition of FTIR reference spectra of the analytes. The instrument was equipped with a liquid nitrogen refrigerated mercury–cadmium–telluride (MCT) detector and a dry air purged sample compartment. The scanner of the interferometer was operated at a HeNe laser modulation frequency of 160 kHz. Spectra were recorded in the range between 4000 and 1000 cm^{-1} with a spectral resolution of 4 cm^{-1} and a zero filling factor of 2. For each spectrum 125 scans were co-added. The flow cell was built using two CaF_2 windows and a polytetrafluoroethane (PTFE) spacer. Its optical path length was determined to be 102 μm . Liquid samples were transported into the flow cell with a Gilson Minipuls 3 peristaltic pump (Gilson S.A., Villiers Le Bel, France). The OPUS software (version 6.5) from Bruker was employed for instrumental and measurement control as well as for data acquisition.

Reagents and samples

To establish external calibration lines, standard solutions of citric acid (99%, Sigma Aldrich), L(+)-tartaric acid (p.a., AppliChem), α -D-glucose (ACS reagent, Sigma Aldrich), DL-malic acid (99%, Aldrich), D(-)-fructose (min. 99%, Sigma), acetic acid (puriss p.a. ACS reagent, $\geq 99.8\%$, Fluka), glycerol (99.5+%, ACS reagent, Aldrich) and ethanol absolute (puriss, Sigma Aldrich) were prepared weighing appropriate amounts of the reagents into 25 mL volumetric flasks and filling them up to volume with de-ionized water. Red (Zweigelt variety) and white wine (Traminer, Welschriesling, Neuburger and Weissburgunder varieties) samples and two grape juices, all drawn from Austrian wineries, were analyzed by the proposed approach. If necessary, the samples were diluted with an appropriate amount of de-ionized water prior to injection. Recovery studies on the analyzed samples were carried out by spiking appropriate amounts of standard solutions of the considered analytes. Prior to injection into the chromatographic system, all standards and samples were degassed in an ultrasonic water bath for 5 minutes and filtered through a 0.2 μm nylon membrane syringe filter.

7.2.3 Results and discussion

Reference Spectra

Figure 7.2.3 shows FTIR reference spectra of all analytes included in this study at a concentration of 3 g L^{-1} . From this figure it can be clearly appreciated that organic acids show: i) a strong absorption band due to the C-O-H in-plane bending vibration of the COOH group in the region near 1400 cm^{-1} [7.35] and ii) a band due to the C-O deformation vibration of the COOH group in the region between 1280 and 1220 cm^{-1} [7.36]. Sugars show absorption bands at 1035 and 1015 cm^{-1} caused by C-O stretching vibrations [7.37] and C-C stretching vibrations [7.38], respectively. Absorption bands of alcohols and sugars show up between 1430 and 1200 cm^{-1} due to the C-O-H bending vibration and between 1210 and 1000 cm^{-1} because of the C-C-O stretching vibration of the C-OH group [7.35]. Furthermore all analytes show certain absorption due to different C-H vibrations, like for example the CH_2 scissoring vibration between 1475 and 1445 cm^{-1} , the C- CH_3 bending vibration between 1395 and 1365 cm^{-1} and the C-C stretching vibration between 1180 and 1090 cm^{-1} [7.35].

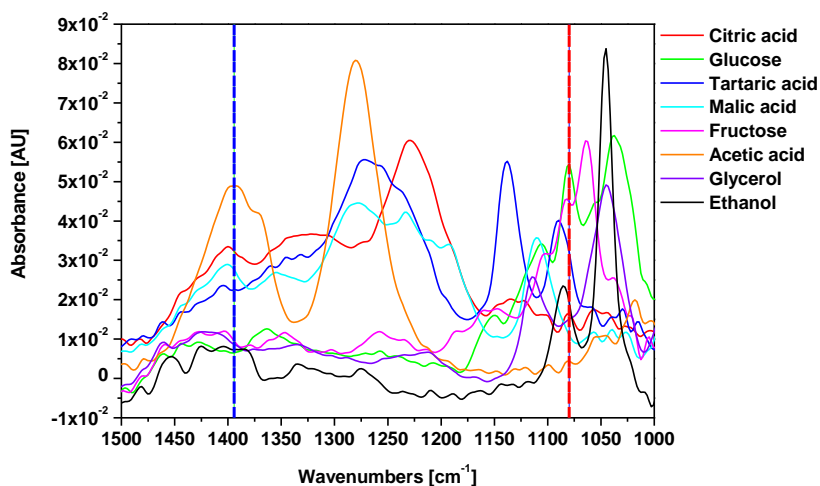


Figure 7.2.3. FTIR spectra of standard solutions at a concentration of 3 g L^{-1} ; the red and blue straight dashed lines represent the emission frequencies of the two QC-lasers emitting at 1080 and 1393 cm^{-1} , respectively.

The red and blue dashed lines in Figure 7.2.3 show the emission frequencies of the QC-lasers at 1080 and 1393 cm^{-1} , respectively. Sugars show a strong absorption band at 1080 cm^{-1} and a negligible absorption at 1393 cm^{-1} in contrast to organic acids where the absorption bands are 3 to 5 times more intense at 1393 than at 1080 cm^{-1} . Only tartaric acid shows similar absorption intensities at both wavenumbers. It can be seen that all analytes show absorption bands at least at one of the two wavenumbers emitted by the lasers.

Determination of carbohydrates, alcohol and organic acids with the on-line dual QC-laser set-up

To test the performance of the system, an external calibration with standard solutions was established. The results of the calibration experiments are summarized in Table 7.2.1. Five calibration solutions containing all the analytes listed in Table 7.2.1 at different concentration levels were prepared and injected twice. The concentration range used for each analyte is specified in Table 7.2.1. The detector output signal (volts) of the transmission measurement was recorded as a function of time. The obtained chromatograms were converted into absorbance units and smoothed and a linear baseline correction was carried out if necessary.

In Figure 7.2.4 a characteristic chromatogram showing the chromatographic separation of the eight analytes at a concentration of 5 g L^{-1} using a dual QC-laser set-up as light source for on-line infrared detection is depicted. It clearly can be seen that all eight peaks are baseline separated and have a symmetric shape. A fronted peak shape was only observed injecting citric acid and tartaric acid. Table 7.2.1 indicates which QC-laser signal was used for the quantification of each analyte. Measuring the peak heights of each analyte, a 5-point linear regression line was calculated. The obtained equations including standard deviations of slope and intercept and their corresponding regression coefficients are given in Table 7.2.1. The regression lines show high linearity ($R^2 > 0.99$), the slopes differ significantly from zero and all calibration lines pass through zero. Limits of detection (LOD) and quantification (LOQ) calculated as three and ten times the root mean square (RMS) noise of a blank injection, respectively, are also specified in Table 7.2.1.

Table 7.2.1. Calibration results of all investigated analytes.

Analyte	QC-laser ^a [cm ⁻¹]	Conc. Range [g L ⁻¹]	T _{RET} ^b [s]	Equation y=(k±s _k)x + (d±s _d)	R ²	LOD ^c [g L ⁻¹]	LOQ ^d [g L ⁻¹]
Citric Acid	1393	1.5-10	643	y = (1.66±0.05)x + (0.0±0.3)	R ² = 0.993	0.46	1.53
Glucose	1080	1.25-10	688	y = (3.50±0.04)x - (0.1±0.3)	R ² = 0.999	0.24	0.72
Tartaric Acid	1393	5-15	759	y = (1.05±0.03)x + (0.1±0.4)	R ² = 0.991	1.29	4.53
Malic Acid	1393	2-10	798	y = (2.23±0.08)x + (0.1±0.5)	R ² = 0.991	0.38	1.39
Fructose	1080	1.25-10	832	y = (3.12±0.05)x - (0.1±0.3)	R ² = 0.998	0.23	0.69
Acetic Acid	1393	1.5-10	932	y = (4.2±0.1)x - (0.1±0.6)	R ² = 0.996	0.19	0.56
Glycerol	1080	1.5-10	1007	y = (2.07±0.04)x - (0.0±0.3)	R ² = 0.997	0.28	0.92
Ethanol	1393	4.5-100	1035	y = (0.75±0.02)x + (0±1)	R ² = 0.996	1.22	4.07

Note: QC-laser^a: indicates the quantum cascade laser which was used for the quantification of the analyte; T_{RET}^b: retention time in seconds; LOD^b: limit of detection; LOQ^c: limit of quantification.

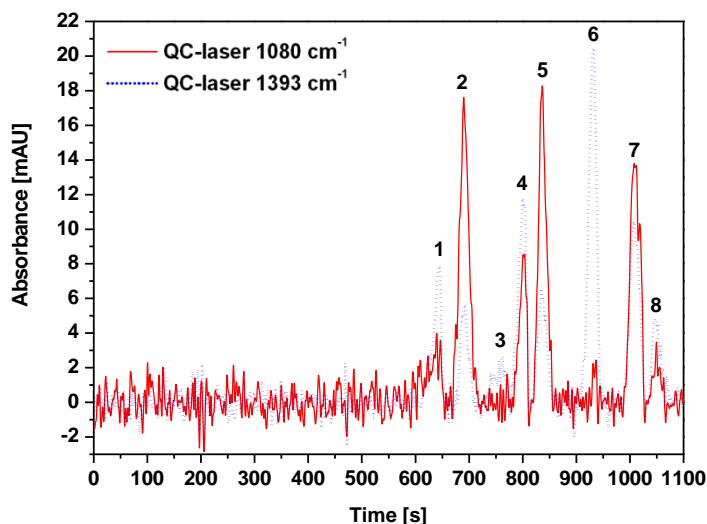


Figure 7.2.4. Chromatogram of a standard mixture containing 5 g L^{-1} of each analyte; (1) citric acid, (2) glucose, (3) tartaric acid, (4) malic acid, (5) fructose, (6) acetic acid, (7) glycerol, (8) ethanol.

Analysis of wine and grape juice samples

The performance of the developed method was tested on real samples with a complex matrix. All samples were diluted with water (1:2), if necessary, and injected three times. The retention times of the peaks in the recorded sample chromatograms were compared to the retention times of the analytes obtained from standard injections to identify the analytes contained in the samples.

Concentrations of all analytes were calculated using the corresponding equations of the previously established external calibration lines and are listed in Table 7.2.2 together with their standard deviations and relative standard deviations (RSD). The RSD lies between 0.1 and 10% in all measured samples and for all detected analytes. In Figure 7.2.5 chromatograms obtained from the injection of a white wine sample (Traminer variety) at different concentration levels are shown as an example. Chromatograms recorded with the QC-laser emitting at 1080 cm^{-1} (Figure 7.2.5, left) and with the QC-laser emitting at 1393 cm^{-1} (Figure 7.2.5, right) are shown. Resolved peaks of glucose, tartaric acid, fructose, glycerol and ethanol can be identified. Moreover, the chromatogram of the QC-laser emitting at 1080 cm^{-1} shows a badly shaped peak at about 480 s caused by an unidentified component or impurity.

Table 7.2.2. Results of the analysis of seven real samples.

Analyte	Concentration found ^a [g L ⁻¹] ± s ^b (RSD ^c [%])						
	Sample 1	Sample 2	Sample 3	Sample 4	Sample 5	Sample 6	Sample 7
	White wine	White wine	White	White wine	White wine	Red	Red wine
	Traminer	Welschriesling	grape juice	Neuburger	Weissburgunder	grape juice	Zweigelt
Citric Acid	< LOD	< LOD	< LOD	< LOD	< LOD	< LOD	< LOD
Glucose	4.5±0.1 (2.20)	< LOD	63.3±0.2 (0.35)	1.5±0.1 (8.64)	1.1±0.1 (9.99)	90.31±0.09 (0.10)	< LOD
Tartaric Acid	4.7±0.4 (8.65)	<LOQ	6.0±0.2 (3.49)	6.1±0.3 (4.48)	5.0±0.4 (8.15)	14.1±0.9 (6.21)	< LOD
Malic Acid	< LOD	<LOQ	4.2±0.1 (2.74)	< LOD	< LOD	< LOD	< LOD
Fructose	24.1±0.4 (1.55)	2.70±0.03 (1.26)	59.4±0.5 (0.87)	< LOD	1.1±0.1 (9.64)	85.7±0.9 (0.99)	< LOD
Acetic Acid	< LOD	< LOD	< LOD	< LOD	< LOD	< LOD	< LOD
Glycerol	5.7±0.3 (5.92)	3.6±0.3 (8.72)	< LOD	5.9±0.5 (8.38)	6.3±0.5 (8.55)	< LOD	7.4±0.3 (3.83)
Ethanol	109.2±3.3 (2.98)	92±2 (2.20)	< LOD	108.1±2.6 (2.37)	113.5±0.4 (0.37)	< LOD	108.5±0.8 (0.70)

Note: Concentration found^a: calculated as the average absorption signal obtained from three consecutive measurements of the same sample; s^b: standard deviation calculated from three consecutive measurements of the same sample; RSD^c: relative standard deviation calculated dividing the standard deviation by the average value and multiplied by 100.

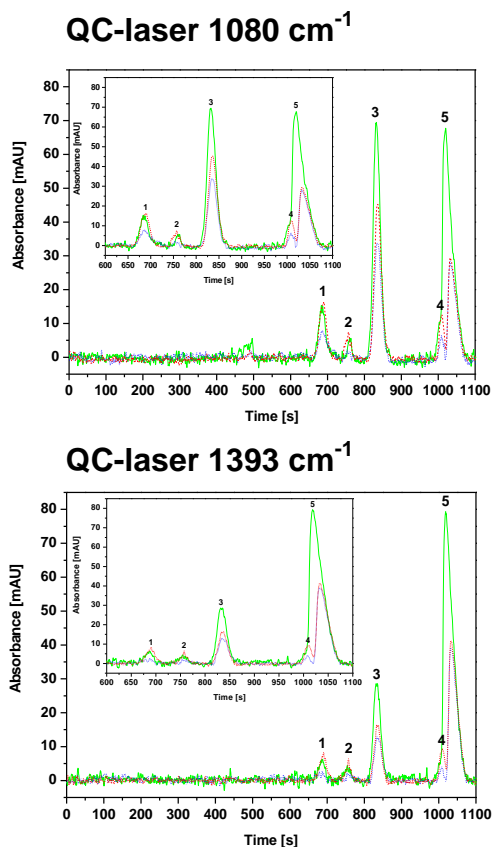


Figure 7.2.5. Chromatograms of sample 1; top: chromatograms recorded with the QC-laser emitting at 1080 cm^{-1} ; bottom: chromatograms recorded with the QC-laser emitting at 1393 cm^{-1} ; straight green line: sample 1, dotted blue line: sample 1 diluted (1:2), dashed red line: sample 1 with added standard solution containing glucose, tartaric acid, fructose, glycerol and ethanol; inserts show the region between 600 and 1100 s in detail; (1) glucose - 686 s, (2) tartaric acid - 761 s, (3) fructose - 830 s, (4) glycerol - 1006 s, (5) ethanol - 1033 s.

Finally, recovery experiments were carried out to assess the accuracy of the proposed method. Previously analyzed wine and grape juice samples were spiked with known amounts of the found analytes at two different concentration levels and analyzed two times. Calculated recovery values for the different spiked concentration levels of each compound are summarized in Table 7.2.3. The recovery values of all compounds were satisfactory and ranged between 95 and 109%. As an example, Figure 7.2.5 shows the chromatograms of a raw and a spiked sample at both wavenumbers.

Table 7.2.3. Results of the recovery experiments carried out at two increasing spiking levels on a characteristic sample.

Level 1							
Analyte	Recovery [%] ± s (added std [mg])						
	Sample 1	Sample 2	Sample 3	Sample 4	Sample 5	Sample 6	Sample 7
Glucose	96.0±0.1 (5.8)	0 (0)	97±3 (3.0)	97±4 (0.8)	104±3 (0.8)	102±1 (0.9)	0 (0)
Tartaric Acid	104±2 (9.9)	102.2±0.7 (12.3)	103±6 (10.7)	97±2 (10.1)	106±5 (10.1)	105±5 (12.4)	0 (0)
Malic Acid	0 (0)	101.0±0.5 (11.25)	105.9±0.7 (10.2)	0 (0)	0 (0)	0 (0)	0 (0)
Fructose	97.1±0.7 (5.9)	102±1 (5.8)	107±1 (2.9)	0 (0)	0 (0)	105±5 (1.0)	0 (0)
Glycerol	98±2 (7.7)	96±4 (6.5)	0 (0)	103±6 (8.5)	107.6±0.4 (8.5)	0 (0)	107.9±0.7 (5.8)
Ethanol	102±2 (3.0)	99±3 (3.0)	0 (0)	107±2 (2.8)	103.0±0.4 (2.8)	0 (0)	109±2 (3.0)
Level 2							
Analyte	Recovery [%] ± s (added std [mg])						
	Sample 1	Sample 2	Sample 3	Sample 4	Sample 5	Sample 6	Sample 7
Glucose	96.6±0.4 (2.3)	0 (0)	95±2 (1.2)	101±3 (0.3)	101±2 (0.3)	107±3 (0.4)	0 (0)
Tartaric Acid	100±4 (4.0)	101±6 (4.9)	106.5±0.6 (4.3)	97±3 (4.1)	107±2 (4.1)	100±2 (5.0)	0 (0)
Malic Acid	0 (0)	102±5 (4.5)	105±3 (4.1)	0 (0)	0 (0)	0 (0)	0 (0)
Fructose	101.9±0.5 (2.4)	103±6 (2.3)	103±2 (1.2)	0 (0)	0 (0)	101.5±0.2 (0.4)	0 (0)
Glycerol	101±2 (3.1)	101±5 (2.6)	0 (0)	106±5 (3.4)	108±2 (3.4)	0 (0)	103.1±0.1 (2.3)
Ethanol	101±4 (1.2)	101±4 (1.2)	0 (0)	100±6 (1.1)	106±2 (1.1)	0 (0)	101±2 (1.2)

7.2.4 Conclusions

This study demonstrated for the first time the feasibility of the introduced on-line coupling of a LC separation to a dual QC-laser detection system. All investigated species could be chromatographically separated, detected and quantified in complex matrices, as the analysis of seven different wine and grape juice samples showed.

Compared to the use of state-of-the-art FTIR spectrometers, the use of QC-laser based systems offers a significant advantage for the on-line detection: the on-line data acquisition frequency can be increased to up to 120 data points min^{-1} which is significantly higher than the 27 data points min^{-1} obtained using on-line FTIR detection employing a Bruker Equinox 55 FTIR spectrometer, co-adding 25 scans per spectrum and using a resolution of 8 cm^{-1} and a HeNe laser frequency of 180 kHz.

For future experiments it would be of interest to enhance the signal to noise ratio to improve the limits of detection. First, the performance of the detection system could be improved significantly modifying data acquisition. Using a lock in amplifier instead of the box car averager, the obtained noise was 15 times smaller. As the available lock in amplifier could not be used to process the signal of two QC-lasers simultaneously it was not suitable for further experiments in this set-up. Secondly it would be preferable to use more stable laser drivers to diminish noise and long-term drifts. Thirdly the chromatographic system could be adapted to meet the requirements of the detection system. Using columns with a smaller inner diameter diminishes peak broadening thereby achieving better resolution and sensitivity. An additional advantage is the lower consumption of samples and solvents.

Due to their high spectral power density, the small size and the fact that QC-lasers nowadays are available operating at room temperature, they have become of great interest in infrared detection systems. This study showed the potential of using a dual QC-laser system as light source for on-line IR detection in LC.

7.3 References for Chapter 7

- [7.1] G. Quintas, J. Kuligowski, B. Lendl, *Analytical Chemistry*, 81 (2009) 3746-3753.
- [7.2] J. Kuligowski, G. Quintas, B. Lendl, *Applied Physics B-Lasers and Optics*, 99 (2010) 833-840.
- [7.3] B.M. Patterson, N.D. Danielson, A.J. Sommer, *Analytical Chemistry*, 75 (2003) 1418-1424.
- [7.4] B.M. Patterson, N.D. Danielson, A.J. Sommer, *Analytical Chemistry*, 76 (2004) 3826-3832.
- [7.5] A. Edelmann, J. Diewok, J.R. Baena, B. Lendl, *Analytical and Bioanalytical Chemistry*, 376 (2003) 92-97.
- [7.6] G. Quintas, B. Lendl, S. Garrigues, M. de la Guardia, *Journal of Chromatography A*, 1190 (2008) 102-109.
- [7.7] R. Vonach, B. Lendl, R. Kellner, *Journal of Chromatography A*, 824 (1998) 159-167.
- [7.8] A. Edelmann, C. Ruzicka, J. Frank, B. Lendl, W. Schrenk, E. Gornik, G. Strasser, *Journal of Chromatography A*, 934 (2001) 123-128.
- [7.9] R. Vonach, B. Lendl, R. Kellner, *Analytical Chemistry*, 69 (1997) 4286-4290.
- [7.10] R. Schulte-Ladbeck, A. Edelmann, G. Quintas, B. Lendl, U. Karst, *Analytical Chemistry*, 78 (2006) 8150-8155.
- [7.11] C. Legido-Quigley, N.W. Smith, D. Mallet, *Journal of Chromatography A*, 976 (2002) 11-18.
- [7.12] M. Kranendijk, J.C.M. Waterval, G.W. Somsen, G.J. de Jong, *Journal of Separation Science*, 28 (2005) 1796-1802.
- [7.13] P.R. Griffiths, J. de Haseth, *Fourier Infrared Transform Spectroscopy*, second ed., John Wiley & Sons, New York, 2007.
- [7.14] M. Kölhed, P. Hinsmann, P. Svasek, J. Frank, B. Karlberg, B. Lendl, *Analytical Chemistry*, 74 (2002) 3843-3848.
- [7.15] S. Kulka, G. Quintas, B. Lendl, *Vibrational Spectroscopy*, 42 (2006) 392-396.
- [7.16] T. Takamuku, M. Tabata, A. Yamaguchi, J. Nishimoto, M. Kumamoto, H. Wakita, T. Yamaguchi, *Journal of Physical Chemistry B*, 102 (1998) 8880-8888.
- [7.17] J. Kuligowski, A. Breivogel, G. Quintas, S. Garrigues, M. de la Guardia, *Analytical and Bioanalytical Chemistry*, 392 (2008) 1383-1389.

- [7.18] R.F. Kazarinov, R.A. Suris, *Fizika i Tekhnika Poluprovodnikov*, 5 (1971) 797-800.
- [7.19] J. Faist, F. Capasso, D.L. Sivco, C. Sirtori, A.L. Hutchinson, A.Y. Cho, *Science*, 264 (1994) 553-556.
- [7.20] D. Weidmann, F.K. Tittel, T. Aellen, M. Beck, D. Hofstetter, J. Faist, S. Blaser, *Applied Physics B-Lasers and Optics*, 79 (2004) 907-913.
- [7.21] Q. Shi, D.D. Nelson, J.B. McManus, M.S. Zahniser, M.E. Parrish, R.E. Baren, K.H. Shafer, C.N. Harward, *Analytical Chemistry*, 75 (2003) 5180-5190.
- [7.22] M. Nagele, D. Hofstetter, J. Faist, M.W. Sigrist, *Analytical Sciences*, 17 (2001) S497-S499.
- [7.23] G. Wysocki, M. McCurdy, S. So, D. Weidmann, C. Roller, R.F. Curl, F.K. Tittel, *Applied Optics*, 43 (2004) 6040-6046.
- [7.24] B.A. Paldus, C.C. Harb, T.G. Spence, R.N. Zare, C. Gmachl, F. Capasso, D.L. Sivco, J.N. Baillargeon, A.L. Hutchinson, A.Y. Cho, *Optics Letters*, 25 (2000) 666-668.
- [7.25] H. Ganser, M. Horstjann, C.V. Suschek, P. Hering, M. Murtz, *Applied Physics B-Lasers and Optics*, 78 (2004) 513-517.
- [7.26] B. Lendl, J. Frank, R. Schindler, A. Muller, M. Beck, J. Faist, *Analytical Chemistry*, 72 (2000) 1645-1648.
- [7.27] M. Kölhed, M. Haberkorn, V. Pustogov, B. Mizaikoff, J. Frank, B. Karlberg, B. Lendl, *Vibrational Spectroscopy*, 29 (2002) 283-289.
- [7.28] S. Schaden, M. Haberkorn, J. Frank, J.R. Baena, B. Lendl, *Applied Spectroscopy*, 58 (2004) 667-670.
- [7.29] S. Schaden, A. Dominguez-Vidal, B. Lendl, *Applied Physics B-Lasers and Optics*, 86 (2007) 347-351.
- [7.30] S. Schaden, A. Dominguez-Vidal, B. Lendl, *Applied Spectroscopy*, 60 (2006) 568-571
- [7.31] S. Schaden, A. Dominguez-Vidal, B. Lendl, *Applied Physics B-Lasers and Optics*, 83 (2006) 135-139.
- [7.32] R. Bauer, H. Nieuwoudt, F.F. Bauer, J. Kossmann, K.R. Koch, K.H. Esbensen, *Analytical Chemistry*, 80 (2008) 1371-1379.
- [7.33] R. Schindler, R. Vonach, B. Lendl, R. Kellner, *Fresenius Journal of Analytical Chemistry*, 362 (1998) 130-136.

[7.34] Foss, <http://www.foss.dk/Solutions/ProductsDirect/WineScanFT120.aspx>, Denmark.

[7.35] D. Lin-Vien, N.B. Colthup, W.G. Fateley, J.G. Grasselli, *The handbook of infrared and Raman characteristic frequencies of organic molecules*, Academic Press, Inc, 1991.

[7.36] G. Quintas, E. Nuñez, M. Vellekoop, B. Lendl, *Analytical and Bioanalytical Chemistry*, 387 (2007) 287-292.

[7.37] M. Kölhed, B. Karlberg, *Analyst*, 130 (2005) 772-778.

[7.38] J.J. Max, C. Chapados, *Journal of Physical Chemistry A*, 111 (2007) 2679-2689.

CHAPTER 8. CONCLUSIONS AND OUTLOOK

Infrared spectroscopy has the potential to quickly emerge as a viable alternative to conventional detectors such as ELSD, UV or RID, combining the non-destructive and molecular specific information of IR spectrometry with the high resolution provided by liquid phase separation systems (e.g. LC). As described in the first chapter of this Thesis, IR detection presents two main drawbacks that hinder its use as on-line hyphenated detector in LC systems:

- 1) Intense spectral overlapping between the mobile phase constituents and the analytes.
- 2) Reduced sensitivity as compared to other detection systems (e.g. UV or ELSD)

This Thesis focused on the development of suitable chemometric and instrumental tools to overcome these drawbacks. The following is a summary of the partial conclusions extracted during its completion, comprised in fifteen published papers included in this Thesis.

Innovations on the field of isocratic separations

1. The developed isocratic methods showed their suitability for different applications using dichloromethane and acetonitrile:water as mobile phases. The performance of the developed methods was improved by the application of multivariate chemometric tools (SBC) for the extraction of chromatograms and by the use of the rapid scan data acquisition mode.

New chemometric methods

2. The usefulness of the developed chemometric methods developed for background correction has been evaluated and demonstrated for qualitative and quantitative

purposes employing both, isocratic and gradient conditions using acetonitrile:water, methanol:water, ethanol:water and 2-propanol:water binary systems.

The developed chemometric methods can be clustered in two groups according to the use of a reference spectra matrix (**RSM**) for background correction. Among the methods that use **RSM**, a further division in three sub-groups can be established:

- i) AR-, RW-, PLS-, and p2p-BGC-RSM are methods based on the use of identification parameters (IPs) for the selection of the optimal **RSM** spectrum for each data point (i.e. spectrum) included in the chromatogram to be corrected (**SM**).
- ii) Polyfit-BGC-RSM uses a polynomial fitting at each wavenumber of the data included in the **RSM** to predict and subtract the background contribution during the chromatogram, also using an IP.
- iii) PCA-BGC-RSM and SIMPLISMA-BGC-RSM are methods that use the information content of a **RSM** for the calculation of multivariate models to predict and correct the background absorption throughout the sample chromatogram.

The second group includes the methods that do not require the measurement of a **RSM** for background correction. The method based on the use of cubic smoothing splines (CSS), as well as SBC are included in this group.

3. The selection of the background correction method depends on different instrumental parameters and no method can be classified as optimal under all circumstances. Therefore, the user must be aware of the capabilities and limitations of both, the correction methods and the instrumental set-up (e.g. data acquisition frequency, instrument stability, etc). As an example, the type of mobile phase, the gradient slope, the IR spectra of the analytes, the detector stability or the need to perform on-the-fly background correction are parameters that determine the correction method to be used.

As a rule of thumb, simple methods are more robust and are therefore preferred over more sophisticated approaches if obtained results are comparable. In general, the methods AR-, RW-, p2p-, PLS-BGC-RSM and Polyfit-RSM only should be applied if a spectral region that is characteristic for the mobile phase composition and free from spectral interferences due to other sample constituents is available. On the other hand side, if the number of spectra and/or the distribution of the spectra in the **RSM** is not

adequate or if the instrument stability is poor, the accuracy of those methods might be affected.

The advantage of the CSS method is that there is no need to acquire a **RSM** therefore minimizing the influence of the instrument stability on the method's accuracy. Furthermore this method is easy to use as the number of parameters that have to be selected by the user is reduced. However, the background correction accuracy of this method might be influenced by the distribution of the knots which becomes critical when a high number of peaks is detected in the chromatogram and their resolution is low.

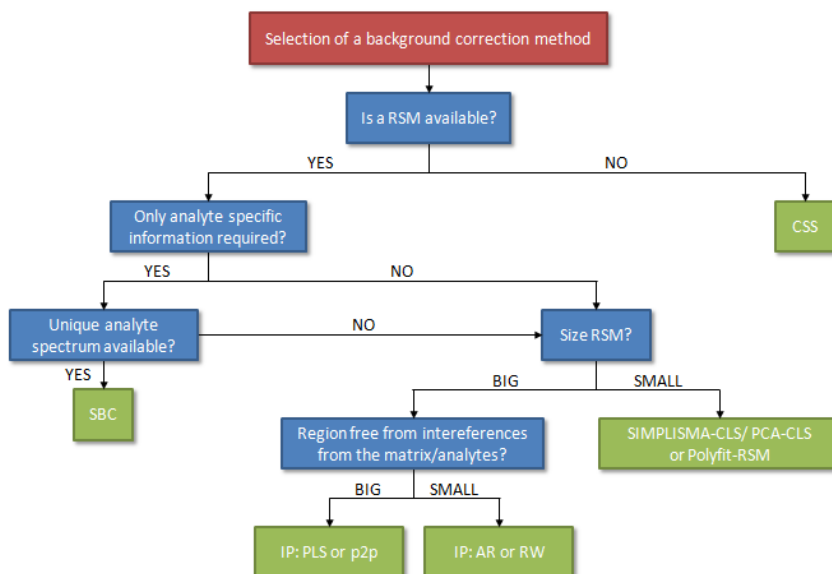


Figure 8.1. Flow diagram of the selection of the most appropriate background correction method.

In the case of the use of multivariate methods such as SIMPLISMA and PCA in combination with CLS, the importance of the **RSM** size is not as critical as in other approaches (e.g. AR-BGC-RSM). The use of these potent and well established chemometric tools facilitates background correction in difficult situation (e.g. reduced **RSM** size, co-eluting analytes), while maintaining the background correction performance.

The flow diagram shown in Figure 8.1 includes the main considerations that have to be addressed in order to select a background correction method and it also gives an overview of the different methods developed during this Thesis.

4. The use of Multivariate Curve Resolution – Alternating Least Squares (MCR-ALS) in on-line gradient LC-IR systems was facilitated when the eluent background contribution was eliminated prior to its application. When MCR-ALS was applied to background corrected spectra, improved spectral and concentration profiles of the analytes were recovered. Besides, remaining signal variation due to changing background absorption and detector drift could also be compensated.

5. The use of Science Based Calibration (SBC) in on-line LC-IR facilitated the extraction of ‘analyte specific’ chromatograms without prior background correction. This approach increases significantly both, the sensitivity and specificity of the signal in isocratic as well as gradient applications. On the other hand side, it has to be considered that the SBC approach does not compensate the eluent absorbance and therefore, in case of gradient measurements, no background corrected spectra are obtained.

Instrumental Developments

6. Employing miniaturized nL flow cells in combination with a capillary LC system demonstrated to be a viable tool to improve the sensitivity of the on-line coupling. In this Thesis an increase in mass sensitivity by a factor of approximately 30 as compared to LC systems employing a 4.6 mm column was achieved.

7. Quantum Cascade Lasers (*QC-lasers*) are capable to handle the utmost demands of on-line LC-IR coupling: high emission power, small size, fast response, room temperature working conditions and low power consumption. The use of on-line dual quantum cascade laser detection in LC facilitates the analyte detection and improves the sensitivity of the system allowing the use of flow cells with bigger optical pathlengths. In this Thesis, in spite of employing an aqueous mobile phase, the QC-laser system allowed the use of a standard flow cell with an optical pathlength of 52

μm . Considering that using Globar sources, the maximum pathlength is approximately 7-8 μm , this represents a gain in sensitivity of a factor of approximately 7. Another advantage of the QC-laser set-up is its fast response time, enabling a high data acquisition rate improving the precision in quantitative methods.

Outlook

Based on the developed state-of-the-art concerning chemometric background correction and instrumental improvements of on-line LC-IR described in this Thesis, potential future objectives can be identified.

8. In on-line LC-QC-laser systems, higher gains in sensitivity might be very likely obtained: (i) modifying data acquisition to improve the performance of the detection system; (ii) improving the stability of the laser drivers to diminish noise and long-term drifts which were observed using the set-up described in this Thesis and (iii) using modern tunable QC-lasers with higher optical power densities to enable the use of increased flow cell pathlengths and working spectral ranges. The use of tunable QC-lasers is very probably going to be of high importance, as their implementation would permit the acquisition of spectral ranges of up to several hundred wavenumbers in the fingerprint region using simple optical set-ups in comparison to the approach presented in this Thesis, therefore rising the amount of qualitative information obtained from the detection system. At the same time the number of potential sources of electronic noise, as well as the total cost of the detection system, are reduced by using only one single QC-laser. Furthermore it has to be remarked that the field of QC-laser technology is rapidly developing, steadily improving its products not only providing devices with bigger spectral tuning ranges but also with significantly higher output powers. It should be possible to directly exploit enhanced output powers in terms of achievable LODs in on-line LC-IR systems, permitting their extension to more sophisticated analytical challenges, e.g. dealing with more complex mixtures of analytes at lower concentrations as well as the implementation of on-line comprehensive 2D LC-IR systems.

In summary, as aforementioned, this Thesis presented chemometric and instrumental solutions to overcome the main limitations which hindered the use of on-line LC-IR: the low sensitivity and the need of chemometric methods for the elimination of the background eluent contribution in gradient systems. The instrumental and chemometric tools described in this Thesis could be a useful starting point for future developments as they show a great potential to be employed, for example, for the development of a system combining tunable *QC-lasers*, miniaturized flow cells, capillary LC systems and chemometric methods which could be applied to solve new exciting analytical tasks.

APPENDIX.

MATLAB® Functions

The Appendix contains some of the in-house written MATLAB functions developed during this Thesis.

- **Science Based Calibration Multivariate Approach for its use in on-line LC-IR**

This code was used for calculations included in Chapter 2 (2.2 Monitoring of polymerized triglycerides in deep-frying olive oil by on-line GPC-IR spectrometry using the Science Based Calibration multivariate approach) and Chapter 6 (Chemometric extraction of 'Analyte-Specific' chromatograms in on-line LC-IR). The MATLAB function was adapted from *R. Marbach, J. Near Infrared Spectrosc. 13, 241-254 (2005)*.

```
% SBC CALIBRATION
X=input('X=matrix of measured "noise" spectra [AU]; (mxk)
matrix= ');
g=input('g=Analyte response spectrum [AU/mg]; (kx1) vector=
');
[m,k]=size(X);

% CALIBRATION
% g=Analyte response spectrum [AU/mg]; (kx1) vector
% X=matrix of measured "noise" spectra [AU]; (mxk) matrix
% m=Number of 'noise' spectra
avgX=mean(X); % Line 1.
% Line 1 computes the mean of the 'noise' spectra [AU], the
% result is a (1xk) vector
Xmc=X-ones(m,1)*avgX; % Line 2
% Line 2 mean-centers the 'noise' spectra
Z=(Xmc'*Xmc)/(m-1); % Line 3
% Line 3 estimates the covariance matrix of the spectral
noise [AU^2], the result is a (kxk) matrix
b=pinv(Z)*g/(g'*pinv(Z)*g); % Line 4
```



```
% Line 4 computes the optimal b-vector [mg/AU] using
Matlab's pinv function for full-rank inversion

% PREDICTION
% xu=unknown spectrum to be predicted [AU]; (1xk) vector
% cavg=avg. analyte concentration of "noise" spectra [mg];
scalar
xu=input('xu=unknown spectra matrix to be predicted [AU];
(n x k) matrix= ');
cavg=input('cavg=avg. analyte concentration of "noise"
spectra [mg]; scalar= ');
[n,k]=size(xu);
for i=1:n
cu(i)=(xu(i,:)-avgX)*b+cavg; % Line 5
% Line 5 performs the prediction [mg]
end

SEPop=(g'*pinv(Z)*g)^-0.5;
plot (cu)
clear X avgX cavg g i k m n xu Z Xmc
```

- **Univariate Background Correction using a Reference Spectra Matrix and the Absorbance Ratio as Identification Parameter (AR-BGC-RSM)**

This code was used for calculations included in Chapter 3 (3.1 Determination of critical eluent conditions for polyethylene glycols using univariate chemometric background correction and 3.2 Quantification of sugars in beverages using univariate chemometric background correction).

```

%# function [SSM_Model]=ARs_UBC_RSM(RSM,SM,wn,i,j,k,KF)
%# AIM: Univariate Background Correction using a
%# Reference Spectra Matrix.
%# Identification Parameter: absorbance ratio
AR=Abs(@i)/Abs(@j)
%#
%# REFERENCE: G. Quintás et al. J. Chromatogr A, 1190
(2008), 102-109.
%#
%# INPUTS:
%# Reference Matrix = RSM (points x wavenumbers) (r,c)
%# Sample Matrix = SM (points x wavenumbers) (z,c)
%# Wavenumber = Vector of wavenumbers (self explainable)
(1,c)
%# First Wavenumber (cm-1) = i
%# Second Wavenumber (cm-1) = j
%# Wavenumber (cm-1) used for the calculation of a KF = k
(optional)
%# Correction Factor:
%# '0': No correction factor
%# '1': KF = Abs. Sample Spectrum(@k)/Abs.
Ref.Spectrum(@k)
%#
%# OUPUT: SSM_Model = Model is a structured array
% containing relevant information and results
%#
%# Example
%# [A]=ARs_UBC_RSM(RSM,SM,wn,2256.5,2252.6,0,0);
%#
%# J. Kuligowski
%# e-mail: julia.kuligowski@uv.es
%# University of Valencia

function [SSM_Model]=ARs_UBC_RSM(RSM,SM,wn,i,j,k,KF)

[Sr,c]=size(SM);
[d1,c1]=min(abs(i-wn)); % Column i
[d2,c2]=min(abs(j-wn)); % Column j
[d3,c3]=min(abs(k-wn)); % Column k
ARrsm=RSM(:,c1)./RSM(:,c2); % IP vector of the RSM
ARsm=SM(:,c1)./SM(:,c2); % IP vector of the SM

```

```
SSM=zeros(Sr,c); % Pre-allocate memory for speed
for p=1:Sr
    [m,t]=min(abs(ARrsm-ARsm(p))); % Location of the
closest spectra in the RSM acc. to the AR value
    if KF==0; % Without using KF
        KFc=1;
    else % Calculation of the correction factor
        KF=Asm(k)/Arsm(k)
        KFc=(SM(p,c3)/RSM(t,c3));
    end
    SSM(p,:)=SM(p,:)-(KFc.*(RSM(t,:)));
end
SSM_Model.RSM=RSM;
SSM_Model.SM=SM;
SSM_Model.RefWns=[i j k];
SSM_Model.KF=KF;
SSM_Model.Solution=SSM;
```

- **Background Correction using a Reference Spectra Matrix and a point-to-point matching algorithm (p2p-BGC-RSM)**

This code was used for calculations included in Chapter 3.4 Application of point-to-point matching algorithms for background correction.

```
function [CorrectedSM, p2p_Results] = p2p_UC_RSM(RefMatrix, SampleM, Wavenumber, variables, simindx);
% Spectral similarity is based on the point to point
% matching similarity indices
%
% INPUTS
% RefMatrix = RSM (points x wavenumbers) (r,c)
% SampleM = SM (points x wavenumbers) (r2,c)
% Wavenumber = Vector of wavenumbers (self explainable)
% (1,c)
% variables = Vector with the index of variables (1,
% FirstVar:LastVar]
% It is also possible to type variable intervals ex.
% variables = [1:5 25:50]
% simindx = Similarity index
% 1: 'cor' ; Correlation coefficient (mean centered)
% 2: 'dpn' ; Correlation coefficient
% 3: 'rmsd' ; Root mean squared error (difference)
% 4: 'mse' ; Mean squared error
% 5: 'mae' ; Maximum absolute error
% 6: 'mare' ; Maximum absolute relative error
% 7: 'mad' ; Mean absolute error (difference)
% 8: 'md' ; Manhattan distance
%
%# J. Kuligowski
%# e-mail: julia.kuligowski@uv.es
%# University of Valencia

Mr=size(RefMatrix,1); Sr=size(SampleM,1);
for i=1:Sr % For every spectra included in the SM
    A=SampleM(i,variables);
    mA=A-mean(A);
    enmA=sqrt(mA*mA');
    for j=1:Mr % compare every sample spectrum with every
RSM spectrum
        if simindx==1; %'cor'
            B=RefMatrix(j,variables); % Similarity indice = COR
            mB=B-mean(B);
            enmB=sqrt(mB*mB');
            r=(mB*mA')/(enmA*enmB);
            SimIndex(1,j)=999*(r+1)/2;
        elseif simindx==2; %'dpn'; % Similarity indice = DPN
            enA=sqrt(A*A');
            B=RefMatrix(j,variables);
```

```

        enB=sqrt(B*B');
        SimIndex(1,j)=999*(B*A')/(enA*enB);
    elseif simindx==4; %'mse'; % Similarity indice = mean
square error
        B=RefMatrix(j,variables);
        r=(mean(A-B).^2);
        SimIndex(1,j)=999*(1-r);
    elseif simindx==3; %'rmsd'; % Similarity indice = RMSE
root mean square error (difference)
        B=RefMatrix(j,variables);
        r=sqrt(mean(A-B).^2);
        SimIndex(1,j)=999*(1-r);
    elseif simindx==5; %'mae'; % Similarity indice = Maximum
absolute error
        B=RefMatrix(j,variables);
        SimIndex(1,j)=-max(A-B); % Data not autoscaled.
** The - sign is to find the maximum **
    elseif simindx==6; %'mare'; % Similarity indice = Mean
absolute relative error
        B=RefMatrix(j,variables);
        d=abs(A-B);
        SimIndex(1,j)=-max(abs(d./A)); % Data not
autoscaled. ** The - sign is to find the maximum **
    elseif simindx==7; %'mad'; % Similarity indice = MAD
        B=RefMatrix(j,variables);
        k=length(variables);
        m=mean(abs(A-B)); % Short-way
        SimIndex(1,j)=999*(1-m);
    else simindx==7; %'mD'; % Similarity indice = MAD
Manhattan distance
        B=RefMatrix(j,variables);
        k=length(variables);
        mD = sum(abs(A-B));
        SimIndex(1,j)=999*(1-mD);
end
end

[Y,I] = max(SimIndex(1,:));%For every spectrum locate the
RSM spectrum with the highest SimIndex
SelectedRef(i,1)=I; % Position
SelectedRef(i,2)=Y; % Value
end

for i=1:Sr; % Background correction of the SM matrix
    CorrectedSM(i,:)=SampleM(i,:)-
RefMatrix(SelectedRef(i,1),:);
End

SimIndxVals=abs(SelectedRef(:,2));
MeanSimIndxVals=mean(SimIndxVals);
% Additional matrix with every useful data to use/save
results

```

```
p2p_Results.Solution=Solution;  
p2p_Results.SelectedRef=SelectedRef;  
p2p_Results.SimIndxVals=SimIndxVals;  
p2p_Results.MeanSimIndxValue=MeanSimIndxVals;  
p2p_Results.Conditions.RSM=RefMatrix;  
p2p_Results.Conditions.SM=SampleM;  
p2p_Results.Conditions.wnVector=Wavenumber;  
p2p_Results.Conditions.interval_Vars=variables;  
p2p_Results.Conditions.CorrectionFactor=kf;  
p2p_Results.Conditions.SimilarityIndex=simindx;
```

- **Background correction based on polynomial regressions**

The following code was used for calculations included in Chapter 4.1 Background correction based on polynomial regressions.

```
% AR-Polyfit-RSM:
%
% # Calculation of the n polynomial regression curves
% # Regression: X=Absorbance at each variable j (j=1:c) for
each spectrum
% #          Y=Absorbance ratio A(Wn1)/A(Wn2) for each
spectrum
% # A series of polynomial regressions of order
op=1:OrderPoly are calculated
% # Order(op).MatrixPolynCoeff=Matrix of the regression
coefficients using order op.
% # Order(op).ErrorEstimates=Matrix of the error estimates
of the (op)polynomial regression.
% # Data INPUT
%       RSMat (r,c)= Reference Spectra Matrix ;
%       SMat (rr,cc)= Sample Matrix to be background
corrected ;
%       OrderPoly (n)= Max. Polynomial order ;
%       Wn1= Col 1 to calculate AR1/AR2 ) ;
%       Wn2= Col 2 to calculate AR1/AR2 ;
%       ImpF= Improvement factor (0<ImpF<=1)
% # Data OUTPUT
%       CorrecMatrix_adjceff (r,c) = Corrected Sample
Matrix
%       ADJR (OrderPoly+1,c) = Adjusted-R2 values
(1:OrderPoly,j) and optimal polynomial degree found for
each wn.
%       R2_results (1,c) = Values of the adjusted-R2 at the
optimal polynomial degrees
%
%# J. Kuligowski
%# e-mail: julia.kuligowski@uv.es
%# University of Valencia

function
[CorrecMatrix_adjceff,ADJR,R2_results]=AR_Polyfit_RSM(RSMat
,SMat,OrderPoly,Wn1,Wn2,ImpF)

[r,c]=size(RSMat);
[rr,cc]=size(SMat);

for op=1:OrderPoly
    clc
    disp(' ')
endfor
```

```

    disp('STEP 1: Calculation of the different polynomial
fittings ... ')
    disp('Polynomial degree: '),disp(op)
    for j=1:c;

A=polyfit(RSMat(:,Wn1)./RSMat(:,Wn2),RSMat(:,j),op);
    Order(op).MatrixPolynCoeff(j,:)=A;
    end
end
clc
disp(' ')
disp('STEP 2: Selection of the optimal polynomial degree
for each variable according to the Degrees of Freedom
Adjusted R-Square ... ')
disp('STEP 2.1 - Calculation of the theoretical background
matrices of the RSM using the calculated polynomial
models... ')

% # Selection of the most appropriate order using the stdev
of the residuals for the op. regression curves.
for op=1:OrderPoly
    for i=1:r
        for j=1:c;

OrderSelection(op).CalcBackg(i,j)=polyval(Order(op).MatrixP
olynCoeff(j,:), (RSMat(i,Wn1)./RSMat(i,Wn2)));
        end
    end
end

% # Calculation of the residuals for the op. calculated
models
for op=1:OrderPoly;
    clc
    disp(' ')
    disp('STEP 2.2 - Calculation of the residuals for the
considered polynomial degrees')
    disp('Polynomial degree: '),disp(op)
    OrderSelection(op).Residuals_Matrix=(RSMat-
OrderSelection(op).CalcBackg);
end

% # Calculation of the coefficient of efficiency (1 =
perfect fitting)
% # gf = 1 - sum(e.^2)/sum((t - mean(t)).^2); % 1 -
perfect match -
% # Degrees of Freedom Adjusted R-Square. This statistic
uses the R-square statistic defined above, and adjusts it
based on the residual degrees of freedom.
% # The residual degrees of freedom is defined as the
number of response values n minus the number of fitted

```



```

coefficients m estimated from the response values v=n-m;
n=Number of rows in RSMat and m=OrderPoly

for op=1:OrderPoly
    clc
    disp(' ')
    disp('STEP 2.3 - Calculation of the Degrees of Freedom
Adjusted R-Square values for the considered polynomial
degrees')
    disp('Polynomial degree: '),disp(op)
    for j=1:c
        cef=OrderSelection(op).Residuals_Matrix(:,j);
        Xvalt=RSMat(:,j);
        n=r;
        m=op+1;
        v=n-m;
        OrderSelection(op).AdjCoeffEff(1,j)=((n-1)/(v-
1))* (sum(cef.^2)/sum((Xvalt-mean(Xvalt)).^2));
    end
end

for op=1:OrderPoly
    for j=1:c

AdjCoeffEff_Mat(op,j)=OrderSelection(op).AdjCoeffEff(1,j);
    end
end

% Find the optimum polynomial order: That provides a
significant improvement of the normr value (higher than the
ImpF)
[r,c]=size(RSMat);
for j=1:c
    clc
    disp(' ')
    disp('STEP 2.4 - Finding the optimal polynomial degrees
for each variable')
    disp('Variable: '),disp(j)
    for i=1:(OrderPoly-2);
        if AdjCoeffEff_Mat(i,j)*ImpF<=AdjCoeffEff_Mat(i+1,j)
& AdjCoeffEff_Mat(i,j)*ImpF<=AdjCoeffEff_Mat(i+2,j);
            OrderOptimVar_adjceff(j,1)=i;
            break
        else OrderOptimVar_adjceff(j,1)=OrderPoly-1;
        end
    end
end

% Calculation of the corrected matrix using the selected
polynomial coeff.
% for each variable
[rr,cc]=size(SMat);

```

```
for i=1:rr
    clc
    disp(' ')
    disp('STEP3: Correction of the sample matrix using the
selected polynomial fittings ... ')
    disp('Correcting sample spectrum number: '),disp(i)
    for j=1:cc;

backMat_adjceff(i,j)=polyval(Order(1,(OrderOptimVar_adjceff
(j,1))).MatrixPolynCoeff(j,:), (SMat(i,Wn1)./SMat(i,Wn2)));
    end
end
ADJR=[AdjCoeffEff_Mat;OrderOptimVar_adjceff'];
for j=1:c;
    R2_results(1,j)=ADJR(ADJR(OrderPoly+1,j),j);
end
CorrecMatrix_adjceff=SMat-backMat_adjceff;
```

- **Cubic smoothing splines background correction**

This code was used for calculations included in Chapter 4.2 Cubic smoothing splines background correction.

```
function [Xbgc,Backgr]=fCSS_BGC(X,v,sf)
% Background correction using cubic smoothing splines
% Trick 1: carefull select knots
% Trick 2: CHECK the background corrected spectra
%
% INPUTS
% X = LCIR chromatogram (r x k)
% v = Knots for splines (1 x z). Make sure there is only
eluent!
% sf =Smoothing factor (if you are not sure, 50 use to work
well..)
% sf is used to calculate the 'p' value.
% As p changes from 0 to 1, the smoothing spline
changes, h
% correspondingly, from one extreme, the least squares
straight-line
% approximation to the data, to the other extreme,
% the "natural" cubic spline interpolant to the data
%
% OUTPUTS
% Xbgc = Background corrected crows.
% Bacgr = calculated (interpolated) background
%
% Refs:
% [1] csaps Matlab function:
%
http://www.mathworks.de/access/helpdesk/help/toolbox/splines/csaps.html
% [2] J. Kuligowski et al.,Journal of Chromatography A,
2010,
% DOI: 10.1016/j.chroma.2010.05.033
%
% EXAMPLE:
% [Xbgc,Backgr]=fCSS_BGC(SM_NP44,[1:10:148 174
224:10:459],1);
%
%# J. Kuligowski
%# e-mail: julia.kuligowski@uv.es
%# University of Valencia

[r,k]=size(X);
Xbgc=zeros(r,k);
Backgr=zeros(r,k);
```

```
for j=1:k; % background correction is 'univariate' (i.e.
for each wn)
    disp(j)
    x=(v);
    y=X(v,j);
    epsilon=(abs((x(end)-x(1)))/(numel(x)-1))^3/16; % Calc.
of the 'magic number'
    p=1/(1+(sf*epsilon)); % sf=Smoothing factor
(0.01<sf<100) (p=0->
    %Linear)
    %for i=1:r
    [Backgr(1:r,j),pk(1:r,j)]=csaps(x,y,p,(1:r));
    %end
end
Xbgc=X-Backgr;
```

- **Background Correction in on-line LC-IR based on PCA, SIMPLISMA, CLS and Reference Spectra Matrices**

This code was used for calculations included in Chapter 5 Background Correction in on-line LC-IR based on PCA, SIMPLISMA, CLS and Reference Spectra Matrices.

```
function
[corr_SM,corr_SM_pca,bkg,ch,sp,model,pred]=SVD_SIMPLISMA_CL
S_PCA(RSM,SM,kmax);
[rr,j]=size(RSM);
RSM_bl=RSM-(min(RSM'))'*ones(1,j); % baseline correct.
SM_bl=SM-(min(SM'))'*ones(1,j); % baseline correct.

% I: Chemical Rank selection
% 1: Using log(svd)
Sv1=svd(RSM_bl);
% 2: Venetian blinds CV (2-sets)
A=RSM_bl; A(1:2:end,:)=[];
B=RSM_bl(1:2:end,:);
[ME_b,lofb]=koptsel(A,B,kmax);
[ME_a,lofa]=koptsel(B,A,kmax);
MeanError=0.5*(ME_a+ME_b);
MeanLof=0.5*(lofa+lofb);
% 3: Plots
figure('name','SVD analysis of the RSM and effect
of the rank on the background correction accuracy')
subplot(1,3,1), plot(log(Sv1(1:kmax)),'o--');
grid on; xlabel('Chemical rank','FontWeight','bold');
ylabel('log(eigenvalues)','FontWeight','bold'), title('SVD
analysis','FontWeight','bold','FontSize',13)
subplot(1,3,2), plot
(mean(abs(MeanError),2),'ro--'); grid on; xlabel('Chemical
rank','FontWeight','bold'); ylabel('Mean correction
error','FontWeight','bold'), title('Correction
error','FontWeight','bold','FontSize',13)
subplot(1,4,4), plot(MeanLof,'ro--'); grid
on; xlabel('Chemical rank','FontWeight','bold');
ylabel('Lack of fit','FontWeight','bold'), title('Lack of
fit (%)','FontWeight','bold','FontSize',13);

rkssel=input('Select rank: ');

%II: Start correction
%using SIMPLISMA
[corr_SM,bkg,ch,sp]=koptcalc(RSM_bl, SM_bl,rkssel);
% using PCA
model = pca(RSM_bl,rkssel); %calibration step
pred = pca(SM_bl,model); %projects a new X-block
bkg_pca=pred.loads{1,1}*pred.loads{2,1}';
corr_SM_pca=SM_bl-bkg_pca;
```

```
%plot results
    figure ('name','Background corrected SM using
SIMPLISMA-CLS and PCA')
    subplot (1,2,1), plot(corr_SM'); xlabel
('Variable','FontWeight','bold'), ylabel ('Absorbance
(background corrected)','FontWeight','bold');title
('SIMPLISMA-CLS','FontWeight','bold','FontSize',13)
    subplot (1,2,2), plot (corr_SM_pca'); xlabel
('Variable','FontWeight','bold'), ylabel ('Absorbance
(background corrected)','FontWeight','bold');title
('PCA','FontWeight','bold','FontSize',13)

%# J. Kuligowski
%# e-mail: julia.kuligowski@uv.es
%# University of Valencia
```

New Instrumental and Chemometric Developments for the on-line Hyphenation of Liquid Chromatography and Infrared Spectroscopy

Julia Kuligowski

Department of Analytical Chemistry, Faculty of Chemistry, University of Valencia, Spain

Infrared (IR) spectrometric detection in liquid chromatography (LC) can provide useful information which is not amenable to other detectors. In the past, the range of real life analytical applications was limited due to the low sensitivity of IR detection and difficulties in on-line measurements arising from the dominating absorption of most of commonly used mobile phase systems. This Thesis describes instrumental developments as well as mathematical advances improving the feasibility of LC-IR on-line coupling, giving rise to exciting new possibilities for the use of vibrational detection systems in LC.

The following topics are included:

- Latest innovations on the field of on-line LC-IR under isocratic conditions, including the use of the rapid scan mode and novel chemometric approaches
- New chemometric methods for background compensation in gradient systems to remove undesired sources of variation in LC-IR hyphenated data systems
- Recent advances in instrumental developments concerning IR sources and miniaturized devices
- Different examples of applications showing the improvements and limitations of chemometric and instrumental developments